Isolation and Structure Elucidation of Secondary Metabolites from the Gliding Bacteria *Ohtaekwangia kribbensis* and *Hyalangium minutum*

Dissertation

zur Erlangung des Grades

des Doktors der Naturwissenschaften

der Naturwissenschaftlich–Technischen Fakultät III

Chemie, Pharmazie, Bio- und Werkstoffwisseschaften

der Universität des Saarlandes

von

Patrick W. S. Okanya

Saarbrücken

2012

Tag des Kolloquiums: 02. November 2012

Dekan: Prof. Dr. Wilhelm F. Maier

Berichterstatter: Prof. Dr. Rolf Müller

     Prof. Dr. Marc Stadler

Vorsitz: Prof. Dr. Rolf W. Hartmann

Akad. Mitarbeiter: Dr. Angelika Ullrich

Publications

Okanya, P. W., Mohr, K. I., Gerth, K. Jansen, R., Müller, R. (**2011**). Marinoquinolines A-F, Pyrroloquinolines from *Ohtaekwangia kribbensis* (Bacteroidetes). *J. Nat. Prod.* **74**, 603 – 608.

Okanya, P. W., Mohr, K. I., Gerth, K. Steinmetz, H., Huch, V., Jansen, R., Müller, R. (**2012**). Hyaladione, an S-Methyl Cyclohexadiene-dione from *Hyalangium minutum*. *J. Nat. Prod.* **75**, 768-770.

Okanya, P. W., Mohr, K. I., Kessler, W., Gerth, K. Jansen, R., Müller, R. (**2012**). Hyafurones and Hyapyrones: Polyketide family from *Hyalangium minutum.* (Manuscript in preparation).

Symposium contribution

HZI Graduate School Symposium, 2011, Braunschweig

Poster "Marinoquinolines A-F, Pyrroloquinolines from *Ohtaekwangia kribbensis* (Bacteroidetes)".

VAAM International Workshop "Biology and Chemistry of Antibiotic-Producing Bacteria and Fungi", 27th – 29th September 2012, Braunschweig

Poster "Isolation and Characterisation of Marinoquinolines A- F, Pyrroloquinolines from *Ohtaekwangia kribbensis"*

Acknowledgement

This dissertation would not have been possible without the contribution and support of a great number of people of whom I owe my sincere gratitude.

First, I am greatly thankful to my doctoral advisor Prof. Dr. Rolf Müller for accepting me to work in his group of Microbial Drugs. He always found time to read through my reports and gave constructive criticism. He is a team player who believes in finding solutions to even the most difficult problems. His scientific standards are admirable and I will forever cherish my graduate experience under his mentorship.

I am deeply indebted to my co-advisor Dr. Rolf Jansen. His office was always open and he would stop his other schedules to attend to my queries whenever they arose. He gave me the tips on tackling structure elucidation and allowed me the space to have an independent line of thinking. Natural products chemistry became so fascinating under his guidance, and I have undoubtedly gained a lot from his wealth of experience. I am also thankful to him for carefully reading and commenting on several revisions of this dissertation.

Special thanks to Prof. Dr. Marc Stadler for consenting to review my thesis. His insightful comments and constructive criticisms were thought-provoking that helped me focus my ideas. His experience in drug discovery from natural products is exceptional and I learned quite a lot from our discussions.

I am thankful to Dr. Klaus Gerth for providing the producer strains, Dr. Kathrin Mohr and Dipl.-Ing. Wolfgang Kessler for their valuable input in microbiology and fermentation experiments respectively and to Dres. Jutta Niggeman and Mathias Keck for providing material for characterization of hyapyrone B. I am also greatly indebted to my thesis committee members, Dr. Victor Wray and Dipl.-Ing. Heinrich Steinmetz for the foresight and valuable input in the formulation of my thesis.

My sincere thanks to all members of the work group *Microbial Drugs* for the high sense of team work. Particularly, I would like to acknowledge Dr.Wiebke Zander for her help to many technical and administrative procedures, my laboratory colleagues Kerstin Schober, Aileen Teichmann, Silke Reinecke, Dr. Enge Sudarman, Eric Kunnert and Dr. Frank Surup for their help and making the corridors of Chemistry department a memorable place to be. I also greatly appreciate the support of Diana Telkemeyer, Christiana Mollenschott, Birte

Zusammenfassung

Die Untersuchung von Sekundärmetaboliten gleitender Bakterien liefert weiterhin neue biologisch aktiver Verbindungen. Im Rahmen meiner Doktorarbeit wurden drei Substanzgruppen isoliert und mittels analytischer Methoden wie NMR-Spektroskopie, Massenspektrometrie und Röntgenkristallographie in ihrer Struktur aufgeklärt. Marinoquinolin A, ein Pyrroloquinolin, und fünf Derivate, die Marinoquinoline B - F, wurden aus dem Bacteroidetes *Ohtaekwangia kribbensis* isoliert. In einem zweiten Projekt wurden aus zwei Stämmen des Myxobakteriums *Hyalangium minutum* acht neue Verbindungen isoliert. Hyaladion, ein S-Methyl-cyclohexadien-dion und sieben Polyketide, die Hyafurone A_1-D zusammen mit den Hyapyronen A und B.

Alle Substanzen wurden auf ihre biologische Aktivität gegen pathogene Bakterien und Pilze, sowie auf Zytotoxizität und anti-parasitische Wirkung getestet. Hyaladion zeigte die besten Aktivitäten mit der Inhibierung des Methicillin-resistenten *Staphylococcus aureus* mit einer MIC von 0.83 µg/mL und einer Zytotoxizität gegen die Brustkrebs-Zelllinie MCF-7 mit einer IC_{50} von 1.23 µM, sowie Aktivität gegen den Malariaparasiten *P. falciparum* mit einer IC_{50} von 0.92 µM. Auch die Marinoquinoline B und F waren aktiv gegen *P. falciparum* mit IC_{50}-Werten von 1.8 bzw. 1.7 µM.

Summary

Investigation of secondary metabolites from gliding bacteria continues to provide new biologically active compounds. In the present thesis, three classes of compounds were isolated and their structures elucidated by analysis of NMR and HRESIMS data and by X-ray crystallography of crystalline compounds. Marinoquinoline A, a pyrroloquinoline, was isolated from the Bacteroidetes *Ohtaekwangia kribbensis* together with five analogues, marinoquinolines B - F. In a second project, eight new compounds, hyaladione, an S-methyl cylohexadiene dione, and seven polyketides, the hyafurones A_1 - D, together with the hyapyrones A and B were isolated from two strains of the myxobacterium *Hyalangium minutum.*

All compounds were evaluated for their biological activity against pathogenic bacteria and fungi, for cytotoxicity and anti-parasitic activity. Hyaladione displayed the highest activities with the inhibition of the methicillin-resistant *Staphylococcus aureus* (MR*SA*) with a MIC of 0.83 µg/mL, cytotoxicity against the breast cancer cell line MCF-7 with an IC_{50} of 1.23 µM, and activity against the malaria parasite *P. falciparum* with an IC_{50} of 0.92 µM. Marinoquinolines B and F were also active against *P. falciparum* with IC_{50} values of 1.8 and 1.7 µM, respectively.

Table of Content

List of abbreviations

Å	Angstrom
ACN	Acetonitrile
$[\alpha]_D^{RT}$	Specific optical rotation at room temperature and 589 nm (D line of sodium lamp)
APT	Attached proton test
c	Concentration [g/100 ml]
calcd	Calculated
°C	Degree Celsius
$CaCl_2 \times 2\ H_2O$	Calcium chloride dihydrate
$CDCl_3$	Deutero chloroform
CD_3OD	Deutero methanol
CF_3	Trifluoro methyl
CoA	Coenzyme A
COSY	Correlation spectroscopy
DBE	Double bond equivalence
DCC	N,N´-Dicyclohexylcarbodiimide
DCM	Dichloromethane
δ_C	^{13}C chemical shift
DEPT	Distortionless enhancement by polarization transfer
δ_H	^{1}H chemical shift
DMAP	4-(dimethylamino)-pyridine
DNA	Deoxyribonucleic acid
DNP	Dictionary of natural products
DSMZ	German Resource Centre for Biological Material
EDTA	Ethylenediaminetetraacetic acid
ESI	Electrospray ionisation
ESI-TOF-MS	Electrospray ionisation- time of flight- mass spectrometry
FR	Flow rate
g	Gram
GBF	German Centre for Biotechnology
GC	Gas chromatography

h	Hour
H_2	Hydrogen gas
HCl	Hydrochloric acid
HEPES	(4-(2-hydroxyethyl)-1-piperazineethanesulfonic acid
HETLOC	Hetero half-filtered TOCSY
HMBC	Heteronuclear multiple-bond correlation
HMQC	Heteronuclear multiple quantum coherence
H_2O	Water
HPLC	High-performance liquid chromatography
HPTLC	High performance thin layer chromatography
HRESIMS	High-resolution electron spray ionisation mass spectrum
HRMS	High resolution mass spectrometry
H_2SO_4	Sulphuric acid
HSQC	Heteronuclear single quantum coherence
HTS	High-throughput-screening
Hz	Hertz
HZI	Helmholtz Centre for Infection Research
IC_{50}	Half maximal inhibitory concentration
IR spectrum	Infrared spectrum
J	Coupling constant
KBr	Potassium bromide
KOH	Potassium hydroxide
L	Liter
LC-MS	Liquid chromatography-coupled mass spectrometry
LC-NMR	Liquid chromatography coupled NMR
LC-SPE-NMR/MS	Liquid chromatography coupled solid-phase extraction and NMR/MS
m	Multiplicity
m	Mass
M	Molar
MeOH	Methanol
mg	Milligram
MHz	Mega hertz

MIC	Minimum inhibitory concentration
min	Minute
mL	Milliliter
MM	Molecular mechanics
mp	Melting point
MPLC	Medium-pressure liquid chromatography
MRSA	Methicillin-resistant *Staphylococcus aureus*
MTPA	α-Methoxy-α-trifluorophenylacetic acid
MTPA-Cl	MTPA chloride
MTT	3-(4-5-dimethylthiazol-2-yl)-2,5-diphenyltetrazolium bromide
mM	Milli molar
nM	Nano molar
m/z	Mass-to-charge ratio
NaAc	Sodium acetate
NaCl	Sodium chloride
Na-Fe-EDTA	Sodium iron ethylenediaminetetraacetate
N_2-gas	Nitrogen gas
NH_4Ac	Ammonium acetate
$NaHCO_3$	Ammonium bicarbonate
nm	Nanometer
NMR spectroscopy	Nuclear magnetic resonance spectroscopy
NOE	Nuclear Overhauser enhancement
NOESY	Nuclear Overhauser enhancement spectroscopy
PM3	Parameterized model number 3
ppm	Parts per million
QM	Quantum mechanics
R_f	Retention factor
R_t	Retention time
R&D	Research & development
RNA	Ribonucleic acid
ROESY	Rotating frame Overhauser enhancement spectroscopy
RP-chromatography	Reversed phase chromatography

rpm	Revolutions per minute
TLC	Thin-layer chromatography
TOCSY	Total correlation spectroscopy
UDB	Universal NMR database
UHPLC -HRESIMS	Ultrahigh performance liquid chromatography coupled HRESIMS
UV/Vis spectrum	Ultraviolet-visible spectrum
VLC	Vacuum liquid chromatography
vvm	Volume gas per reaction volume per minute
μg/ μm/ μL	Microgram / micrometer / microlitre
φ	Torsion angle
λ_max	Wavelength of the most intense UV/Vis absorption
ε	Molar extinction coefficient

1 Introduction

1.1 The indisputable role of natural products in drug discovery

Natural products, especially the secondary metabolites, are chemical substances from plants, animals or microorganisms that exhibit a wide variety of biological activities. They are structurally diverse with concomitant diverse bioactivities such as antibiotic, antifungal, immunosuppressive or cytotoxic. These molecules have been used to treat human and veterinary diseases since the dawn of medicine.[1,2] Additionally, they have also been used in agriculture as pesticides or plant growth regulators. Natural products and derivatives thereof are the single most productive and successful source of drug leads[3,4] that have contributed to the doubling of our life expectancy in the 20th century.[5,6] Nearly, 50 % of the drugs in clinical use are natural products or their derivatives while more than two-thirds of all antibiotics and anticancer drugs are natural products or their semi synthetic derivatives (selected natural products are presented in Figure 1).[7,8] Undoubtedly therefore, the combinatorial chemistry of nature to craft small organic molecules replete with structural complexity and biological potency is unrivalled.[9]

1.1.1 The evolution of natural products as therapeutics

Natural products as sources of drugs have evolved since time immemorial. The Chinese traditional medicines from plant natural products have been used for millennia arguably before 3000 BC. The ancient Egyptians used bark of trees to treat inflammation, but it was until the 5th century that Hippocrates, the father of modern medicine described several plants as sources of medicine among which was the use of willow bark extracts against fever and pain.[10] Acetylsalicylic acid a derivative of the active ingredient (salicylic acid) in willow bark extract was first synthesized in 1853 and later developed into aspirin and marketed in 1899 by Bayer .[11,12] Morphine crystals isolated from opium poppy plant in 1805 was among the first pure natural products to be isolated. It is used as analgesic and the standard against which all new opioids for postoperative pain relief are compared.[13]

The search for antibiotics began in the late 19th century, after the acceptance of Louis Pasteur's 'germ theory of diseases' that linked most infectious diseases to germs, i.e. bacteria and other microbes. In 1877, Pasteur demonstrated how virulent anthrax bacilli could be rendered harmless in animals with the injection of soil bacteria.[14] It had been observed by

several scientists that the growth of bacteria was inhibited when contaminated with other microorganisms. For example, in 1897 Ernest Duchesne had shown in his dissertation the inhibition of the lethal typhoid bacilli by the fungus *Penicillium glaucum.* When more work was urged, Duschesne was unable to complete due to his commitment in the army and his work went unnoticed. It was however until 1928 that Alexander Fleming discovered in a Petri dish seeded with *Staphylococcus aureus* that a compound from the fungus *Penicillium chrysogenum* (formerly, *P. notatum)* killed the bacteria. He named this compound penicillin and the publication of his work one year later profoundly changed the course of medicine.[15]
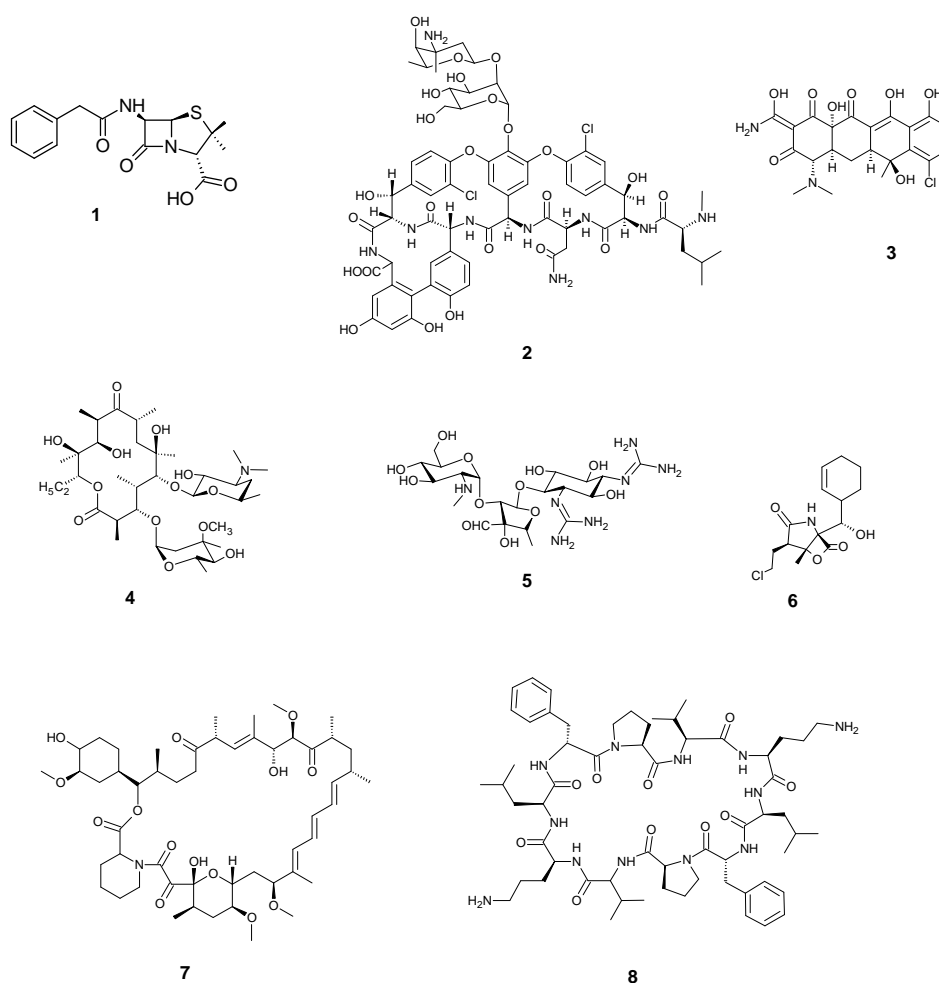
Figure 1.   Structural diversity of bioactive secondary metabolites from bacteria and fungi (activity and producing organism are given in parenthesis). penicillin G (**1**) (antibiotic*, Penicillium chrysogenum*); vancomycin (**2**) (antibiotic, *Amycolaptosis orientalis*); chlortetracycline (**3**) (antibiotic, *Streptomyces aureofaciens*); erythromycin A (**4**) (antibiotic, *Saccharopolyspora erythrea*); streptomycin (**5**) (antibiotic, *Streptomyces griseus*); salinosporamide A (**6**) (anticancer, *Salinispora tropica*); rapamycin (**7**) (immunosuppressant, *Streptomyces hygroscopicus*); gramicidin (**8**) (antibiotic, *Bacillus brevis*).

Penicillin was isolated as a yellow powder in 1939 and used as a potent antibacterial during the Second World War. The discovery and application of penicillin as an antibiotic agent marked the beginning of the antibiotic revolution. Waksman and his group at Rutger University is credited for the discovery of more than twenty antibacterial and antifungal compounds from Streptomyces (Actinobacteria) including streptomycin, neomycin, actinomycin and candicidin. The term "antibiotic" was indeed coined by Waksman. A plethora of antibiotic research using Fleming's and Waksman methods[16] ensued in the years between 1940 and 1960s leading to the discoveries of diverse antibiotic classes including tetracyclines, ß-lactams, macrolides, aminoglycosides, glycopeptides and polypeptides (Figure 2)[17] a period generally referred to as the "antibiotics golden age."[18]
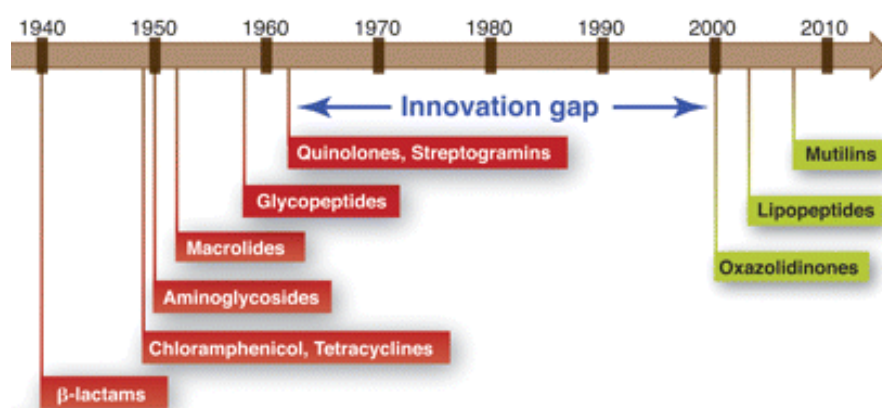
Figure 2. Major classes of antibiotics discovered in the period between 1940 and 1962 that was followed by an innovation gap of almost 40 years.[17]

It was during this period that terms like 'wonder drugs' and 'magic bullet' were coined to refer to the broad spectrum antibiotics. In fact, the battle against bacterial infections was considered won in the late 1960s. Nevertheless, it was too early to celebrate since methicillin-resistant *S. aureus* (MRSA) strains were isolated as early as 1961[19] and ten years later penicillin resistant *Klebsiella pneumoniae* strains were isolated from humans.[20] To-date, virtually all *S. aureus* isolates are resistant to ß-lactam antibiotics and to all the other antibiotic classes including vancomycin that was once daunted as the ultimate weapon against the worst hospital acquired infection.[21] The emergence of multi-drug resistant strains and of new infectious disease pathogens is alarming. Currently, infectious diseases are the second-leading cause of death worldwide and the third major cause of death in developed countries

predominated mainly by acute lower respiratory tract infections, HIV/AIDS, diarrheal diseases, tuberculosis and malaria.[22,23] The development of new drugs particularly from unexplored and scarcely investigated natural sources may be thus an important key to the solution.

Other important natural products developed into drugs include the cyclosporins and statins. Cyclosporin A is a cyclic non-ribosomal peptide that was initially isolated from the fungus *Tolypocladium inflatum* and it is widely used as an immunosuppressant.[24,25] In addition to transplants, cyclosporine A is also used in psoriasis, severe atopic dermatitis, and infrequently, in rheumatoid arthritis and related diseases. It is also being investigated for the treatment of cardiac hypertrophy.[26] Statins are a cholesterol-lowering class of drugs with a large market share. They act by inhibiting 3-hydroxy-3-methyl-glutaryl-CoA (HMG-CoA) reductase, an important enzyme in cholesterol biosynthesis. Mevastatin, a polyketide derived natural product from the fungus *P. citrinum* was the first statin to be isolated as a potent inhibitor of HMG-CoA. However, its structural analogue, lovastatin isolated from *Aspergillus terreus* was the first to be marketed.[27] Since then, several statins have been developed either as semi-synthetic derivatives or purely synthetic. They include among others, simvastatin, pravastatin, fluvastatin, rosuvastatin and atorvastatin. Atorvastatin, marketed as lipitor[®] by Pfizer has dominated the market as the best-selling drug of all time!

1.2   Gliding bacteria - a repository of novel secondary metabolites

Bacteria that move by creeping or gliding on surfaces are generally called gliding bacteria.[28] They are a diverse group of microorganisms that have adapted to different environments including the tropical rain forest, hydrothermal vents, marine shores, waste water, desert sand and the gastro-intestinal tract of man and animals. Despite their ubiquitous nature, gliding bacteria are only found in a few taxa such as Chloroflexi, Proteobacteria, Bacteroidetes and Cyanobacteria.[29,30] Other than actinomycetes, fungi, bacilli and pseudomonads which are the established sources of secondary metabolites contributing to almost 90 % of the approximately 50,000 microbial metabolites known,[31] the last three decades have seen the emergence of gliding bacteria as alternative sources for drug discovery. Of these, the most studied for their secondary metabolism are cyanobacteria[32] and myxobacteria (δ-Proteobacteria) with a slow progress in investigation of the Bacteroidetes.

1.2.1   Bacteroidetes – a promising source of novel natural products

With the growing increase in resistance of infectious-disease pathogens to established pharmaceuticals compounded with the emergence of new pathogens , new drugs are urgently needed. Bacteroidetes, previously known as the *Cytophaga-Flavobacteria-Bacteroides* (CFB)[33] are widely distributed in different habitats. They comprise a large group of heterotrophic bacteria that presently appears to be the highest growing phylum with new genera being added every month.[29] However, most Bacteroidetes genera studied show a close association with human and animal hosts, where they perform useful functions including degradation of polysaccharides and synthesis of essential vitamins.[34] They are known to be the most dominant part of the micro-flora in the human intestinal tract together with Firmicutes and Actinobacteria.[35,36]

Bacteroidetes have only been scantly investigated for their production of secondary metabolites. Examples of these metabolites are shown in Figure 3. They include the, β-lactams PB-5266 A (**9**), PB-5266 B (**10**), PB-5266-C (**11**) isolated from the gliding bacterium *Flavobacterium johnsoniae,* formerly known as *Cytophaga johnsoniae*.[37,38]Additionally, a cell growth promoting resorcinol derivative, resorcinin (**12**), also isolated from the same bacterium, *F. johnsoniae*.[39] Other compounds isolated from *Cytophaga* sp. include the katanosin peptides (**13**, **14**)[40] that exhibited activity against Gram-positive bacteria including activity against methicillin resistant *Staphylococcus aureus* (MRSA)[41] and the macrolides

YM-32890 A (**15**) and YM-32890 B (**16**) also with anti-MRSA activities.[42] Besides compounds from Cytophaga, the ß-lactams, formacidins A, (**17**), B (**18**) and C (**19**)[43] and the topoisomerase 1 inhibitors, topostins A (**20**) and B (**21**)[44] have been isolated from Flexibacter strains. The preceding compounds were all isolated during the "antibiotics golden age". In recent times, Bacteroidetes strains of the marine arctic have been investigated for the emission of volatile methyl ketones whose structures were established by retrosynthesis.[45] The most recent investigation of secondary metabolites of this phylum is the isolation of the polyketide-derived anti-Gram-positive antibiotic class, elansolids A1/A2* (**22**/**23***) macrolide atropisomers and elansolid A3 (**24**) a quinonone methide from *Flexibacter sancti*,[46,47] a species recently reclassified as *Chitinophaga sancti*.[48] Biological screening of extracts from non-myxobacterial gliding bacteria from the strain collection at the Helmholtz Centre for Infection Research (HZI) continues to show promising results for antinfectives.
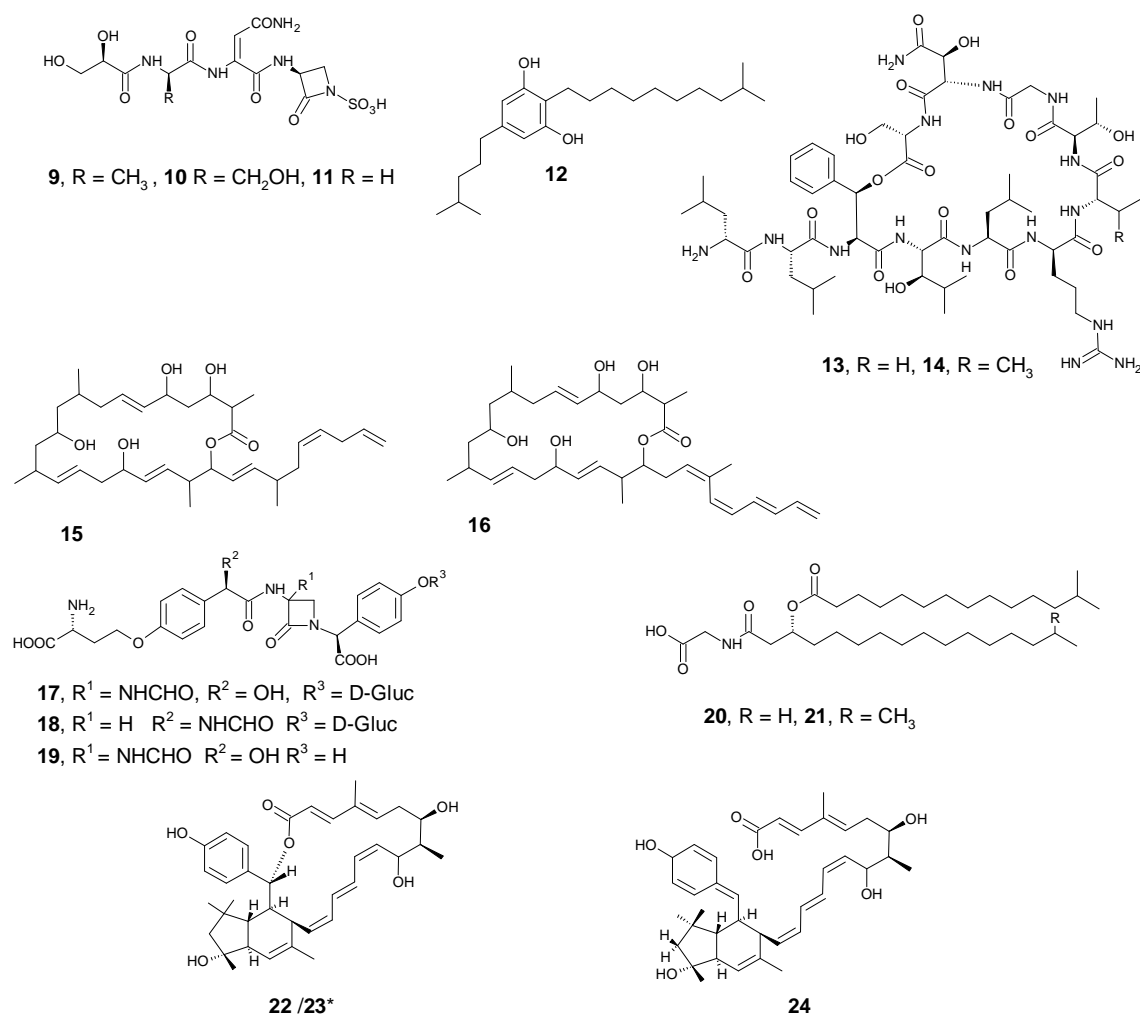
Figure 3.   Bioactive secondary metabolites from the phylum Bacteroidetes.

1.2.2 Myxobacteria – an established source of natural products

Myxobacteria are Gram-negative δ-proteobacteria characterized by their gliding motility and unusual formation of fruiting bodies upon starvation. They are found in diverse habitats including soil, bark of trees, decaying plant material, dung of herbivores and marine shores.[49,50] Their taxonomy is dependent mainly on the morphology of vegetative cells, swarms, fruiting bodies, myxospores and currently also by phylogeny of the 16S rDNA.[51] All known myxobacteria are grouped in the order *Myxococcales*, which is further divided into three suborders, *Sorangiineae*, *Cystobacteraceae* and *Nannocystineae* (Figure 4).[52]

Systematics of myxobacteria
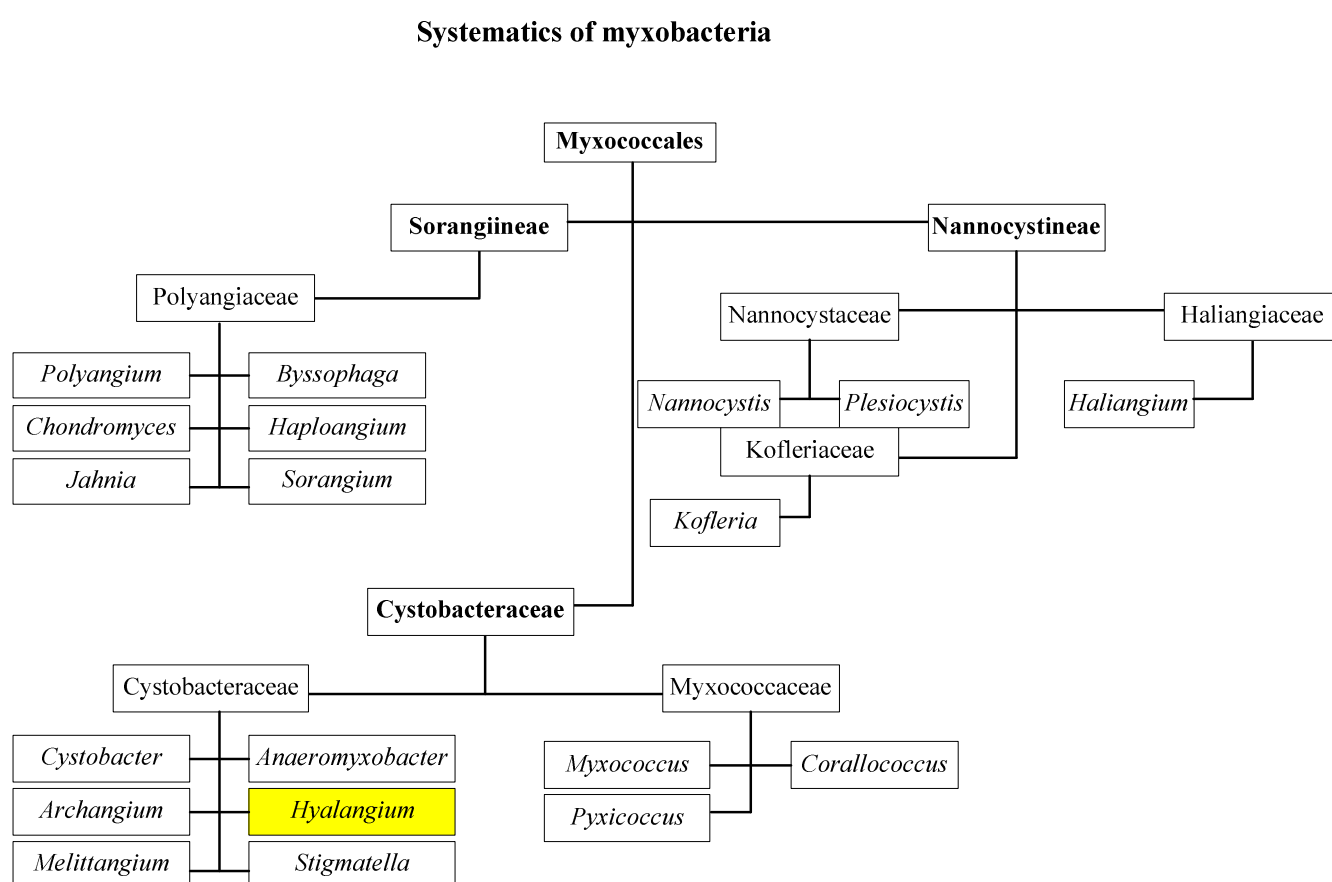
Figure 4.   Systematic of myxobacteria, adapted from Bergey's Manual of Systematic Bacteriology.[52]

After more than 30 years of research on the secondary metabolism of myxobacteria, at least 120 unique basic structures and more than 800 derivatives have been characterized. Unquestionably, myxobacteria have therefore been established as source of novel bio-actives joining the ranks of actinomycetes, *Bacillus* species, pseudomonads and fungi.[53,54] The

compounds have diverse ranges of biological activities spanning across most of the infectious pathogens including viruses, bacteria, fungi and protozoa in addition to cytotoxicities. Most of the activities are, however, against fungi and bacteria at 54 % and 29 %, respectively, supposedly due to the competitive pressure at the natural myxobacteria biotope.[55]

Many myxobacterial compounds display unique structural features that were unknown at the time of their discoveries. Additionally, the compounds often exhibit novel modes of action when compared to other microbial compounds.[53] These findings are appealing and therefore reinforce more research efforts into myxobacterial secondary metabolites for lead compounds in drug discovery. A few selected examples of structural diversity of some lead compounds are shown in Figure 5. Ixempra® (ixabepilone), a semi-synthetic amide derivative of the lactone epothilone B (**25**) is indeed in clinical use as an anti-breast cancer drug. Epothilone B (**25**) was isolated from *Sorangium cellulosum* and interacts with the cytoskeleton of eukaryotic cells by binding to ß-tubulin inducing microtubule polymerization.[56] The resulting suppression of microtubule dynamics leads to the arrest of the cell cycle at the G2/M transition that finally induces apoptosis.[57] Contrary to epothilones mode of action, tubulysin A (**26**) isolated from the myxobacterium *Archangium gephyra*, acts by depolymerizing microtubules which also induces mitotic arrest and finally leads to apoptosis.[58,59] Tubulysin A (**26**) is a potential anticancer and antiangiogenic lead structure.[60] Other potential drug leads against cancer are argyrin (**27**)[61] which is a proteasome inhibitor acting via the tumor suppressor protein p27[62] and the recent disorazol Z (**28**) a highly cytotoxic macrodilactone that is in preclinical development (AEterna Zentaris) as an agent inhibiting tubulin polymerization in cancer cell lines.[63,64]

The antifungals whose modes of action have been characterized include the quinolone aurachin (**29**)[65] and myxothiazol (**30**),[66,67] that act by inhibiting the electron flow within the mitochondrial respiratory chain and –further soraphen A (**31**), a macrolactone that exhibits a remarkable broad-spectrum of anti-fungal activity. Elucidation of the mode of action revealed that **31** inhibited the growth of yeasts and molds by selectively targeting the fungal acetyl-CoA carboxylase (ACC). Consequently, there were concerted efforts that included cooperation with Ciba-Geigy (currently Norvatis) to develop **31** as a plant protective agent.[68,69] However, further development was stopped due to teratogenic effects observed in rat experiments. Nevertheless, the novelty of the mode of action has been used in recent

studies to show that small-molecule inhibitors of human ACCs have potential in the treatment of both the metabolic syndrome[70] and cancer.[71]

Many myxobacterial compounds have been isolated that exhibit antibacterial activity. However, only few have been characterized for their modes of action as lead structures. The most recent promising lead compound is carolactone (**32**)[72] a biofilm inhibitor that acts by disturbing membrane integrity and cell division of *Streptococcus mutans* through the serine/threonine protein kinase, PknB.[73] Others include sorangicin A (**33**),[74,75] as well as myxopyronin B (**34**),[76] corallopyronin[77] and ripostatin[78] all of which bind to two different sites at the bacterial RNA polymerase (RNAP), an important target in the treatment of tuberculosis. The activity and mode of action of **33** is similar to rifampicin, though it sustains some viability against rifampicin resistant mutants. A good drug candidate should be better than the existing drug and in this case **34** is superior. A detailed binding study of **34** identified the switch region of RNAP as novel antibiotic target.[79] However, recently microbiologists at Cubist Pharmaceuticals evaluated the activity of **34** and concluded that it is not a viable starting point for antibiotic development because of a high serum protein binding and a high resistance rate by *S. aureus.*[80]
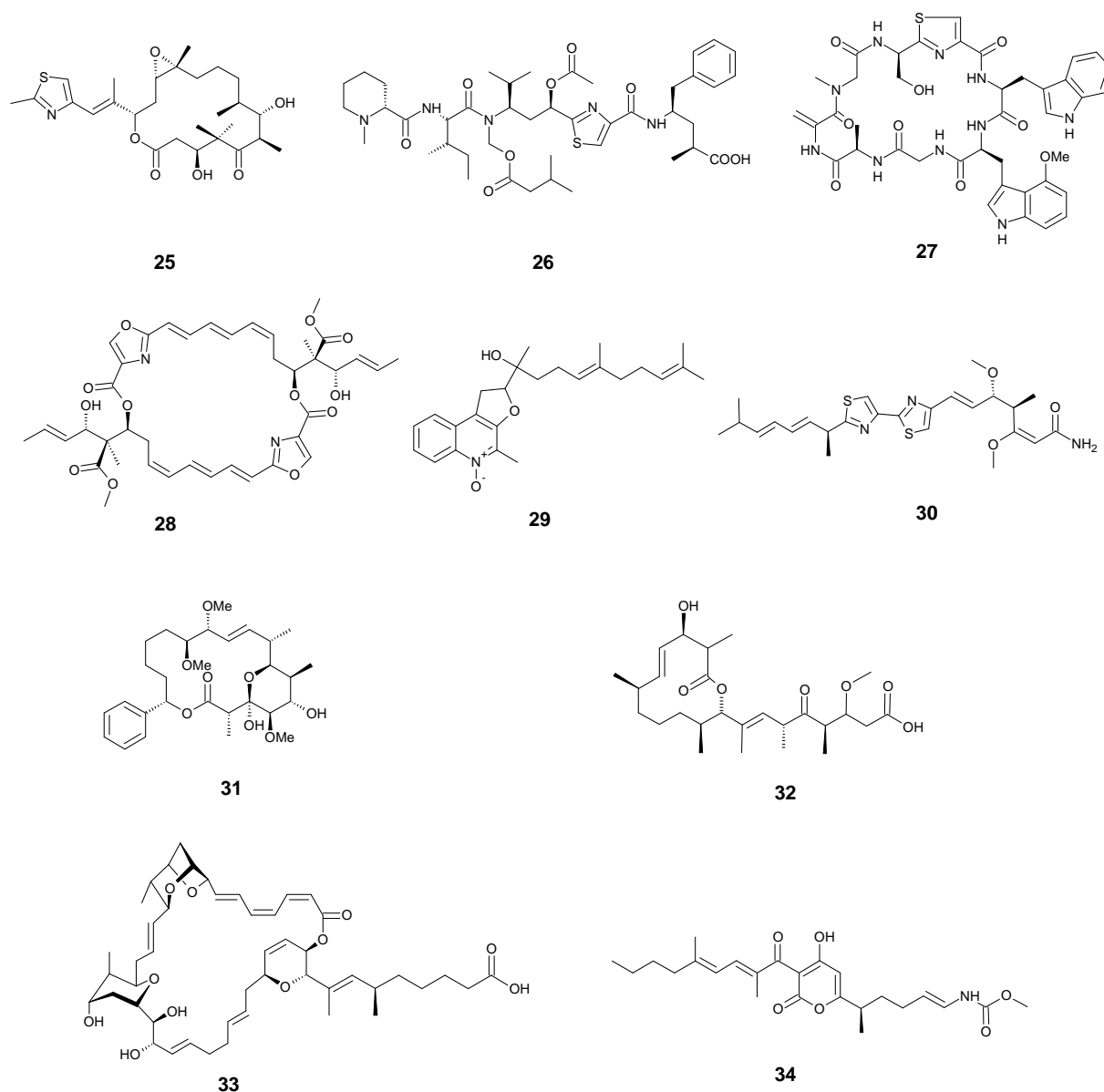
Figure 5. Epothilon B (**25**) and selected lead structures of myxobacterial secondary metabolites displaying their structural diversity.

1.3 Isolation and structure determination of organic compounds

Isolating natural products and determining their structures used to be a daunting task in earlier times. The only tools available for early chemists were purification by distillation for liquids and recrystallization for solids. In recent times, a resurgence of interest in natural product research has seen an outstanding development in the areas of separation science, spectroscopic techniques, and microplate-based ultrasensitive *in vitro* assays.[81] The new high-

10

tech chromatographic techniques make the isolation process relatively easy and faster while the modern spectroscopic techniques allow structure determination to be achieved in days to a few weeks depending on the complexity of the compound.

1.3.1 Extraction and isolation

The producer strains are cultivated under optimized conditions in shake flasks or bioreactors to produce the target secondary metabolites. The crude extracts are recovered by either liquid-liquid extraction of the fermentation broth with an organic solvent or by eluting with an organic solvent from an adsorbent resin like XAD-16 that had been used during fermentation. Most products from gliding bacteria adsorb to XAD-16 resin that is quite efficient since it eliminates the end-product inhibition. The crude extract contains a cocktail of compounds that makes it difficult to apply a single method of separation to isolate an individual compound. However, initial stages of compound enrichment would include liquid- liquid phase partitioning exploiting the polarity of target compounds. A good isolation protocol is designed based on the features of the target molecule that would include solubility, acid-base properties, charge, stability and molecular weight. Chromatographic techniques employed may include high performance liquid chromatography (HPLC), high-performance thin layer chromatography (HPTLC), silica gel flash chromatography, solid-phase extraction, size exclusion chromatography on Sephadex LH-20, medium-pressure liquid chromatography (MPLC) or vacuum liquid chromatography (VLC) among others. Compounds from highly enriched fractions can be purified by recrystallization or by use of preparative HPLC or preparative silica gel flash chromatography.

1.3.2 Mass spectrometry and NMR spectroscopy for structure elucidation

The modern hyphenated ultra-high pressure liquid chromatography high resolution electro spray ionization mass spectrometry (UHPLC-HRESIMS) allows the determination of the precise molecular mass and molecular formula as well as the UV/vis absorption spectrum of a compound. Only very small samples are injected in the instrument. In the ion source of the MS instrument the analytes are vaporized by spraying and ionized by removal or addition of a proton or buffer ion from or to each molecule under high voltage. The resulting molecular ion is recorded as a mass to charge ratio m/z when it is passed through a magnetic field. Because the charge on essentially all the ions that are recorded in the positive ionization mode is

usually +1, *m/z* is taken to be the mass (*m*) of the ion, from which e.g. the molecular mass of the analyte can be calculated.

1.3.3   Structure determination of organic compounds

Structural assignment of natural products is mainly achieved by either structural elucidation by high resolution mass spectrometry (HRMS) combined with nuclear magnetic resonance (NMR) spectroscopy or by X-ray crystallography. The latter method is the "holy grail" for absolute molecular structural details if X-ray suitable mono-crystals are obtained. This is however rare in natural product isolations and thus the most widely used method for structural characterization is the integrated HRMS/NMR spectroscopic method.

NMR spectroscopy has been an indispensable tool for the structure determination of organic molecules since the early 1960s.[82] The older spectroscopies with low field strengths were relatively insensitive performing simple experiments. Over the last couple of years, NMR technology improvement has been impressive. The current state-of-the-art NMR spectrometers have superconducting cryogenic probe-heads, superconducting cryogenic high-field magnets (up to 1000 MHz) and smaller sample volumes with enhanced sensitivity.[83] Additionally, the new NMR hardware enables liquid chromatography coupled NMR (LC-NMR) that offers the advantage of faster dereplication in high throughput screening (HTS) and structural elucidation of compounds from crude mixtures at nano-mole scale.[84,85]

Basically, NMR spectroscopy is a physical phenomenon in which atomic nuclei in a magnetic field absorb and re-emit electromagnetic radiation at a specific resonance frequency. The frequency is directly proportional to the magnetic field strength and the magnetic properties of the isotope of the atoms. The most common studied nuclei are the ^{1}H, ^{13}C and ^{15}N isotopes. The experiments involve the alignment of the atomic nuclear spins in an applied magnetic field and sequential perturbation of the aligned spins by a magnetic pulse radio frequency that causes chemical shifts recorded in Hz or parts per million (ppm).

Structural elucidation begins with the determination of the molecular formula predicted by HRESIMS. From the molecular formula, the number of double bonds and rings are calculated using the double bond equivalence (DBE) formula [DBE = $C_aH_bO_cN_d$, ½ [(2a + 2) – (b-d)]]. The functional groups are then determined from the chemical shifts of the 1D ^{1}H and ^{13}C NMR spectra in combination with the information from IR- and UV/vis spectra. Structural

parts of the compound are then assembled using information from both the 1D and the 2D NMR experiments. A systematic method would initially involve identification of each proton directly bound to carbons ($^1J_{HC}$) by using heteronuclear multiple quantum coherence (HMQC) spectroscopy or the phase sensitive heteronuclear single quantum coherence (HSQC) spectroscopy. Additionally, HSQC provides information on the multiplicity of carbons, information that can also be obtained from attached proton transfer (APT) or distortionless enhancement by polarization transfer (DEPT) experiments. The ^{1}H,^{1}H correlation spectroscopy (COSY) experiments identify structural fragments of adjacent protons by bond-coupling of vicinal, geminal or distant (up to 5 bonds) protons. A 2D TOCSY (total correlation spectroscopy) experiment is used to assign all protons within a spin system. It is mostly used in the analysis of peptides or polysaccharides where key COSY cross-peaks often are obscured. Finally, when all possible fragments have been assigned, the overall connectivity is established through a heteronuclear multiple-bond correlation (HMBC) experiment. HMBC is useful in revealing correlations through intervening heteroatoms and quarternary carbons by long-range interactions that correlate protons with more distant carbons.[86] A summary of the above NMR experiments is found in Table 1.[87]

Table 1. Overview of the basic NMR experiments used for structure elucidation.[87]

Abbreviation	Experiment	Purpose	Comment	Enhanced Experiments
APT	attached proton test	1D inverse technique for ^{13}C multiplicity	includes signals for quaternary carbons	DEPTQ
DEPT	distortionless enhancement by polarization transfer	1D inverse technique for ^{13}C multiplicity	standard	diverse
HMQC	heteronuclear multiple quantum coherence	2D inverse H,C correlation	decoupled ^{13}C NMR spectrum	diverse, better HSQC
HSQC	heteronuclear single quantum coherence	2D inverse H,C correlation	phase-sensitive gradient-selected version	gs-HSQC, E-HSQC
COSY	correlation spectroscopy	2D spin coupling nuclei	most important 2D NMR experiment: possible nuclei ^{1}H, ^{19}F, ^{31}P	Long-Range COSY, COSY-45, E.COSY
TOCSY	total correlation spectroscopy	2D correlations of protons in one spin-system	also called HOHAHA, used for peptides and oligosaccharides	gs-TOCSY, gs- SELTOCSY,
HMBC	heteronuclear multiple bond correlation	2D long-range H,C correlation	$^{2}J(C,H)$ and $^{3}J(C,H)$ coupling	gs-HMBC, ACCORD-HMBC
NOESY	nuclear Overhauser enhancement spectroscopy	2D dipolar cross-relaxation of nuclei in close spatial relationship	assignment of conformations and tertiary structures of e.g. peptides or proteins	gs-NOESY, (3D): HN-NOESY-HSQC, HC-NOESY-HSQC
ROESY	rotating frame Overhauser enhancement spectroscopy	2D dipolar cross-relaxation of nuclei in close spatial relationship	also called CAMELSPIN, shorter time compared to NOESY, also applied for molar mass of 1000-3000	
HETLOC	heteronuclear long range coupling	2D determination of long-range C,H spin coupling constants	low sensitivity, overlapping signals and coupling constants of the same spin system, enhanced versions	PS-HMBC, J-HMBC, HSQC-TOCSY, HSQMBC

1.4 Stereochemistry of natural products

1.4.1 The biological importance of chirality

Most of the drugs derived from natural products are obtained as single enantiomer rather than as a racemic mixture. This is because most of the molecules that make up plants and animals are chiral i.e all the naturally occurring 20 amino acids except glycine are left handed (L-amino acids), whereas all the natural sugars are right handed (D-sugars). The origin of biological properties relating to chirality is likened to the specificity of our hands for their respective gloves; the binding specificity for a chiral molecule at a chiral receptor is only favorable in one way. If either the molecule or the biological receptor site had the wrong handedness, the intended physiological response will not occur[88].

14

Pure natural products are usually recovered in insufficient amounts for drug development. The synthesis of sufficient analogous bioactive natural compounds or modifications thereof requires the consideration of the arrangements of atoms in space. However, until recently most pure synthetic drugs with few exceptions were prepared, sold and administered as racemic mixtures even though the desired therapeutic activity resided in only one of the enantiomers. An example is in the enantiomeric mixture of the (*R*)-ibuprofen (**35**), which is inactive and the (*S*)-ibuprofen (**36**) (Figure 6), the active ingredient of pain relief. Fortunately, the (*R*)-enantiomer (**35**) is converted *in-vivo* to the active (*S*)-form enzymatically by the isomerase, alpha-methyl CoA racemase.[89,90]

35   **36**
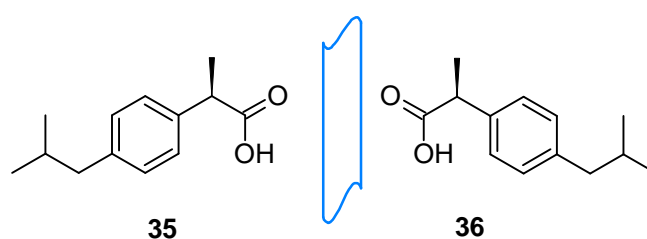
Figure 6. The mirror images of the inactive (*R*)-ibuprofen (**35**) and the active (S)-form, **36.**

A deleterious consequence of using chiral drugs as racemic mixtures is illustrated by thalidomide that was administered to alleviate the symptoms of morning sickness in pregnant women between 1958 and 1962. Teratogenic effects involving shortened or absent limbs in babies whose mothers had used the drug were observed.[91] The drug was sold in more than 40 countries and approximately 10,000 births affected.[92] The sleep-inducing properties are associated with the (*R*)-thalidomide (**37**) whereas the (*S*)-thalidomide (**38**) enantiomer (Figure 7) was teratogenic. The two enantiomers are interconvertible under physiological conditions. Although thalidomide is no longer prescribed to women who are pregnant, or who may become pregnant, it is used in the treatment of leprosy and multiple myeloma.[93,94]

37   **38**
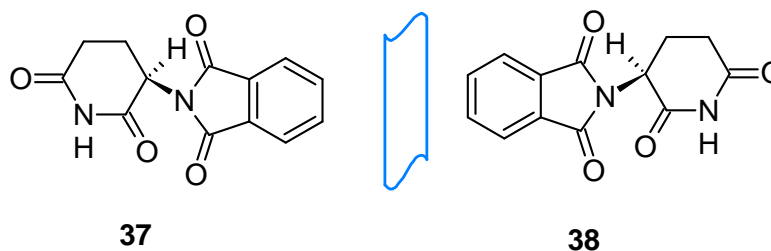
Figure 7.   The mirror images of the sleep-inducing (*R*)-thalidomide (**37**) and the teratogenic (*S*)-thalidomide (**38**).

1.4.2   Assignment of the relative and absolute stereochemistry

Determination of both the relative and absolute configuration of compounds is a pre-requisite in drug discovery. Good quality mono-crystals of a compound would be ideal for the assignment of the stereochemistry by X-ray crystallography. Sadly, they are hardly produced for natural products where yields of pure substances are mostly low. NMR therefore became a practical alternative to X-ray diffraction for both structure elucidation and determination of the 3-D conformations of natural products.

The 2D NMR experiments NOESY (nuclear Overhauser enhancement spectroscopy) and ROESY (rotating frame Overhauser enhancement spectroscopy) provide information about the dipolar cross-relaxation of protons with close spatial relationships. This is achieved by selectively irradiating certain resonances which in effect increases the intensity of spatially proximal resonances. The cross peak intensities between the two spectra are inversely proportional to the sixth power of the distance separating the interacting protons and are therefore used in the assignment of relative configurations.[95] The intensity of NOE correlations is heavily influenced by molecular weight and the choice of mixing time.[96] Conformational analysis of the direct correlation of dihedral angles of protons corresponding to their vicinal $^3J_{H,H}$ coupling constants was first described by Karplus.[97] These vicinal couplings are well suited to the identification of 1,2–stereochemical relationships in cyclohexanes, olefins, and cyclopropanes. The proton-proton coupling constants are extracted directly from the first-order multiplets. However, when the spectral overlap or strongly coupled spectra preclude direct extraction, the simplest solution is to obtain 1D ^1H NMR spectra in different solvents or to use J-resolved that additionally gives coupling constant of the overlapping signals. Another alternative would be to use 1D-TOCSY to selectively irradiate a clearly resolved proton that lies in the same spin system as an obscured one.[98]

The stereochemistry of many acyclic chains for which $^nJ_{H,H}$ and NOE measurements alone are inconclusive, proton-carbon ($^nJ_{C,H}$) coupling constants can be used. Geminal couplings ($^2J_{C,H}$) are usually negative, whereas vicinal couplings ($^3J_{C,H}$) are usually positive.[99] The ($^{2,3}J_{C,H}$) values are measured using 2D HETLOC (hetero half-filtered TOCSY) or PS-HMBC (phase sensitive HMBC) NMR pulse sequences. Additionally, the relative geometries of unknown compounds can also be found by comparing the ^1H and ^{13}C NMR chemical shifts with model compounds of defined stereochemistry.[100] However, complex structures with no close

relatives in the universal NMR database (UDB) can be analysed by molecular modeling using computer software that apply quantum mechanics in calculating NMR parameters e.g HyperChem. Briefly, the conformational search and geometry optimization of all significant conformers of each stereoisomer is carried out by empirical methods such as molecular mechanics (MM) or on the semi empirical level (PM3) followed by a quantum mechanical (QM) method for optimization. The ^{1}H and ^{13}C NMR chemical shifts are thereafter calculated for each stereoisomer and compared with the experimental data.[101]

Several approaches are employed in determining the absolute stereochemistry of natural products. A common approach is the degradation by use of chemical reactions such as ozonolysis, hydrolysis or olefin metathesis. The resulting degradation products are then compared to their corresponding enantiomers by chiral HPLC or GC chromatography, a method commonly used for the amino acid analysis after hydrolysis of peptides.[102,103] The derivatization of chiral alcohols and amines using Mosher's reagent, α-methoxy-α-trifluoromethyl-α-phenylacetic acid (MTPA) or MTPA-Cl is the most widely used method.[104,105] The compound is derivatized with both the (*R*)- and (*S*)-enantiomers of the MTPA acid or MTPA-Cl to give diastereomers. The substituents of the MTPA ester shields or deshields the NMR signals of the neighboring protons next to the MTPA ester as shown in Figure 8. The shift differences $\Delta\delta^{SR}$ of these protons in the two distereomers are calculated by subtracting the chemical shift δ_H of the (*R*)-MTPA ester derivative from the chemical shift δ_H of the (*S*)-MTPA ester derivative. The resulting $\Delta\delta^{SR}$ values (+/-) of the protons are interpreted to give the configurational assignment based on the chiral center of the auxiliary (Figure 8 c and d).[106] It is important to note that upon conversion of the MTPA acid to MTPA-acid chloride, the relative priority of the two substituents is switched, i.e. the trifluoromethyl group (CF$_3$) is higher in priority than the carboxyl group (COOH) in the acid or ester, but lower than the chloro-carbonyl group (COCl) in the acid chloride. Thus, the *R*-enantiomer of the Mosher acid chloride (*R*)-(+)-MTPA-Cl) gives rise to the (*S*)-MTPA esters and vice versa.[107]
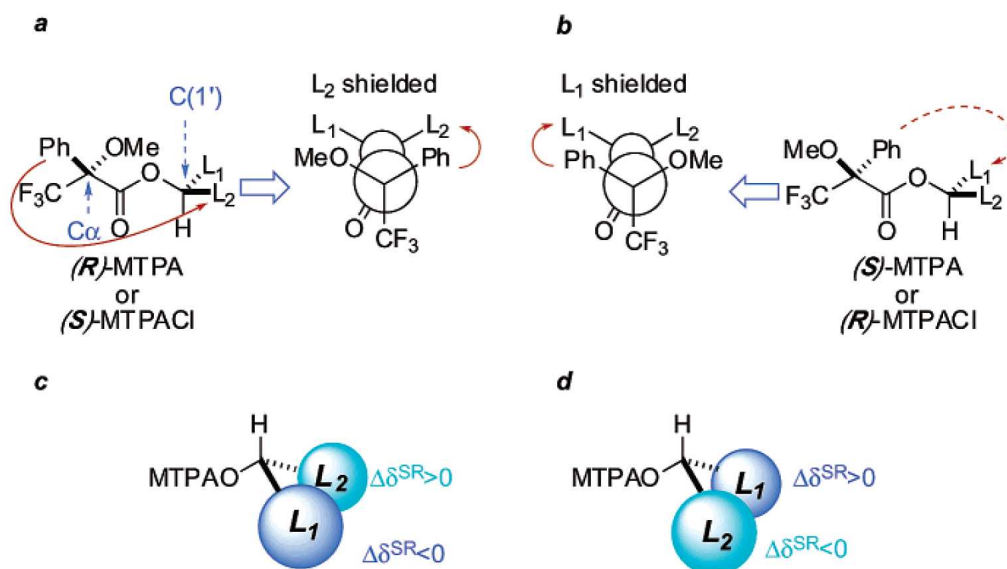
Figure 8 Mosher model of the (*R*)-MTPA ester (a) and (*S*)-MTPA ester (b) of an alcohol and the interpretation of the observed $\Delta\delta^{SR}$ values of protons for both possible configurations (c and d).[106]

1.5   Outline of this work

The overall goal of the work described in this thesis was to isolate new biologically active secondary metabolites from gliding bacteria and elucidate their structures since new bioactive compound scaffolds have the potential of becoming lead structures for drugs against infectious diseases. Screening for biological activities against a panel of pathogenic bacteria and fungi with the crude methanol extracts of the strain collection at Helmholtz Centre for Infection Research (HZI) led to the selection of the Bacteroidetes *Ohtaekwangia kribbensis* strain PWU 25 and the Myxobacteria *Hyalangium minutum* strains NOCB-2[T] and Hym 3. The raw extract of PWU 25 was found to inhibit growth of *Mucor himalis*, *Sacharomyces pombe*, *Nocardia flava, Micrococcus luteus* and *Staphylococcus aureus.* Similarly, evaluation of the crude extracts of the *H. minutum* strains exhibited bioactivities against *Chromobaterium violaceum, S. aureus* and *N. flava.*

The work in this thesis presents the processes involved in the identification of the bioactive compounds in crude bacterial extracts and their eventual isolation and characterization. The raw extracts from shake flasks cultivation were fractionated by HPLC into 96 well plates for peak-biological activity correlation and dereplication by HPLC-UV-MS for peak-UV spectrum and peak-molecular mass correlations. Since both *O. kribbensis* and *H. minutum* strains were found to produce new compounds, large scale fermentations were performed and the crude extracts eluted in methanol. Compound isolations were carried out using several separation techniques and the structures of purified compounds elucidated by a combination of the molecular formulae derived from HRESIMS correlated to the UV/Vis spectral data and NMR spectroscopic data. The relative stereochemistries of the metabolites were determined from both the proton-proton coupling constants and from ROESY spectral data whereas structures of crystalline compounds were determined by X-ray crystallography.

Finally, biological activities of the pure compounds were evaluated against pathogenic bacteria and fungi available at HZI. Additionally, where compound amounts were not limiting, cytotoxicity and anti-parasitic tests were also performed in collaboration with the laboratories of Dr. F. Sasse (HZI) and Prof. Dr. Reto Brun of the Swiss Tropical and Public Health Institute, respectively.

2   Results

2.1   Marinoquinolines A – F, pyrroloquinolines from the bacterium

2.1.1   Strain selection and isolation of marinoquinolines A –F

Strain PWU 25 was selected among other strains for the production of bioactivity against the filamentous fungus *Mucor himalis* and the fission yeast *Sacharomyces pombe*. Additionally, the crude extract exhibited activities against the Gram-positive bacteria *Nocardia flava*, *Micrococcus luteus* and *Staphylococcus aureus*.

Taxonomic studies (Dr. Kathrin Mohr) indicated strain PWU 25 cells to be Gram-negative, aerobic, non-flagellated, non-spore former and rod shaped. The cells measured 0.2 -0.5 µm in diameter and 1.5-7.0 µm long. The strain grows optimally at 30 $^{\circ}$C and pH 6.8-7.2. Colonies on agar plate appear in deep yellow colour with amorphous shape (Figure 9). A 16S rDNA analysis identified PWU 25 at 99.9 % similarity to the recently described *Ohtaekwangia kribbensis*.[108]
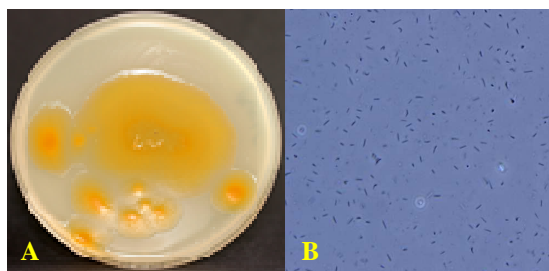
Figure 9.   Colony of PWU 25 on agar plate; panel A and the vegetative cells; panel B.

O. kribbensis, strain PWU 25 was optimized for large scale fermentation in a medium containing skimmed milk, defatted soy flour, yeast extract, starch, $MgSO_4$, Fe-EDTA, and glycerol. A 70 L batch fermentation was performed in the presence of Amberlite XAD-16 adsorber resin for production of the metabolites (fermentation details are explained in the experimental section). The resin was harvested by sieving and eluted with methanol and acetone. Subsequently, a methanol/*n*-heptane liquid-liquid partitioning was performed to enrich the active metabolites in methanol. An isolation strategy was developed that incorporated acid/base extraction, size exclusion chromatography (Sephadex LH-20), and final purification by preparative RP HPLC (Figure 10). Finally the major-compound **39** could be crystallized.
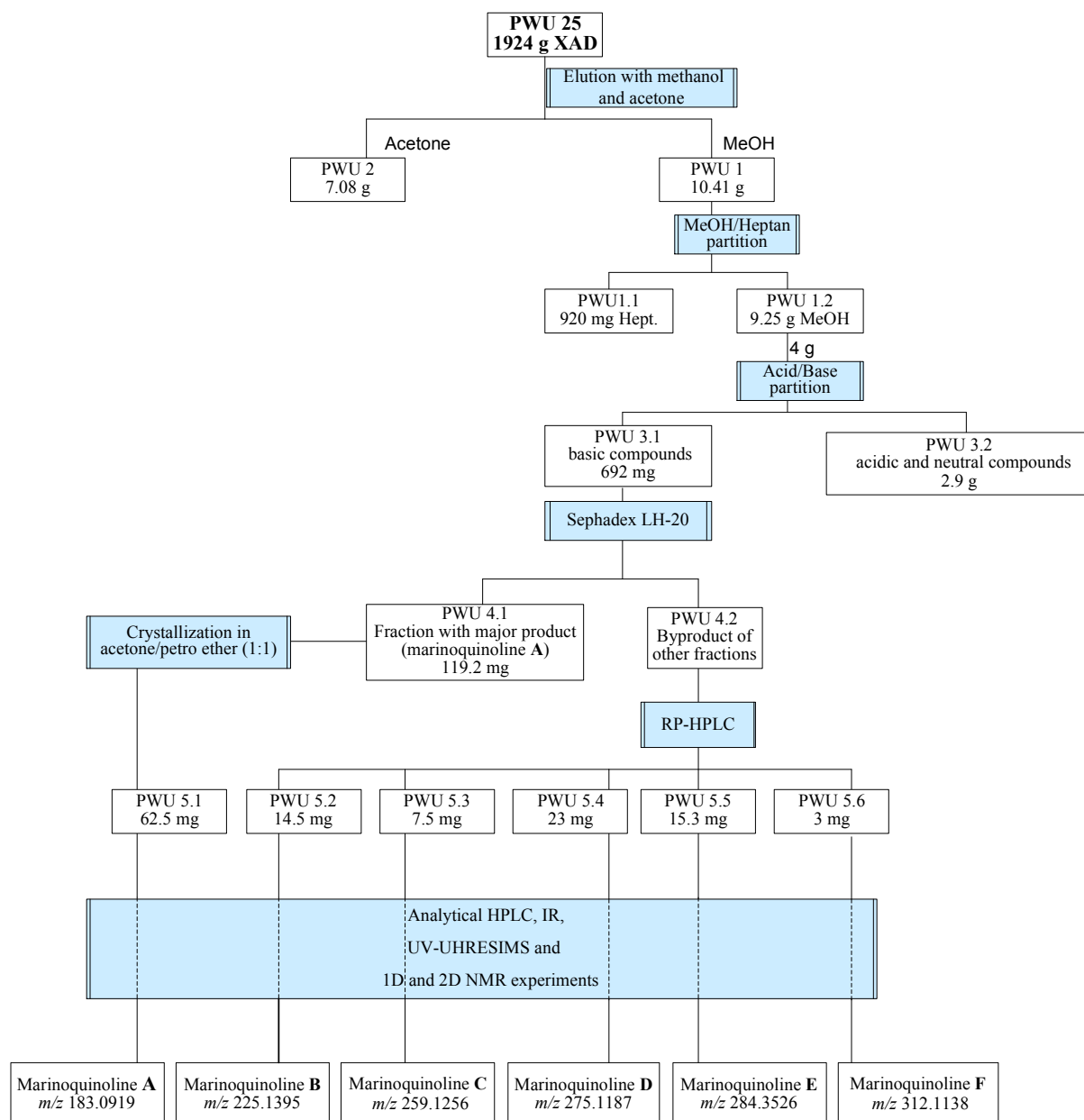
Figure 10. Isolation of marinoquinolines A – F (**39-44**) from XAD-16 adsorber resin of a 70 L fermentation of strain PWU 25.

2.1.2   Structure elucidation of marinoquinolines A – F (39-44)

The crude extract was fractionated by RP HPLC on a 96 well micro-titre plate and each fraction tested against *M. luteus.* The growth inhibitions were correlated to two peaks, a major peak **39** at R_t 8.2 with a HRESIMS molecular ion at *m/z* 183.0919 $[M + H]^+$ and a minor peak **41** at *Rt* 15.4 min with a HRESIMS molecular ion at *m/z* 259.1236 $[M + H]^+$ (Figure 11).
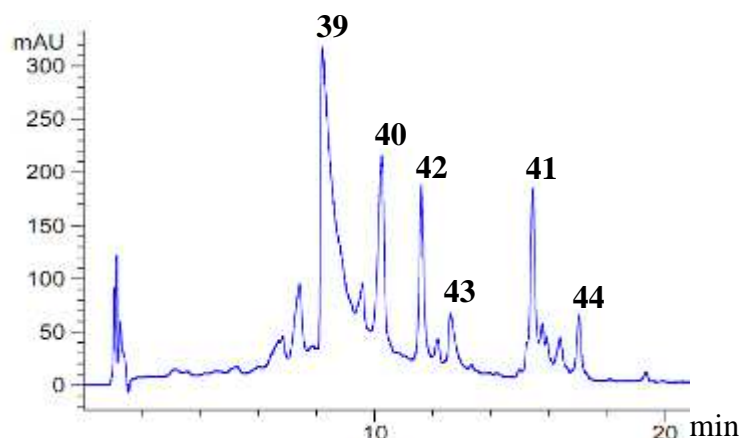
Figure 11.   HPLC fractionation of the crude extract of strain PWU 25. Peaks 39 and 41 were correlated to the growth inhibition of *M. luteus.*

HRESIMS and isotopic pattern analysis of the pseudo-molecular ion peak at *m/z* 183.0919 $[M+H]^+$ (calcd. for $C_{12}H_{10}N_2$, 183.0922) was consistent with the molecular formula $C_{12}H_{10}N_2$ for the main product **39**, which allowed the identification of two possible structures using the DNP data base, i.e. marinoquinoline A (**39**) and the pyridoindole isomer harman (**45**).[109] Since **39** has previously been isolated from the marine bacterium *Rapidithrix thailandica*[110] and characterized solely by X-ray analysis,[111] the structural details were elucidated by IR, UV and a series of 1D (^{1}H, ^{13}C, DEPT) and 2D (COSY, ROESY, HMQC, HMBC) NMR experiments in acetone-d_6 (Table 2). The presence of an NH group was deduced from the characteristic IR absorption band at v_{max} 3442 cm^{-1} in potassium bromide. The UV spectrum of **39** with λ_{max} 239, 300, 312, and 326 nm was compatible with a heteroaromatic compound, which was also suggested by the nine calculated double-bond equivalents.

The ^{13}C NMR spectrum showed signals of twelve carbon atoms and all carbon-bound proton signals were correlated with their corresponding carbon signals from an ^{1}H,^{13}C HMQC NMR spectrum. The remaining NH proton was detected as a broad singlet at δ_H = 11.12 ppm while the methyl group C-10 appeared as a singlet at δ_H = 2.83 ppm, typical of aromatic methyl

groups. The ^{1}H,^{1}H COSY NMR spectrum indicated the presence of four aromatic protons (H-6 to H-9) in an *ortho*-disubstituted ring and of a pair of aromatic protons (H-4 and H-5) , which was completed by the quaternary carbons C-9a and C-5b (Figure 12).
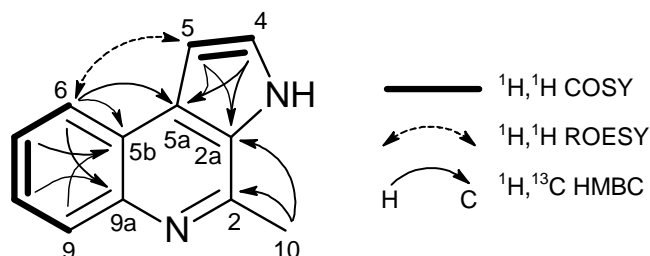
Figure 12.   Selected 2D NMR correlations of marinoquinoline A (**39**)

Carbon C-9a was identified from strong ^{1}H,^{13}C HMBC correlations with H-6 and H-8 while C-5b was assigned from HMBC correlations with H-6, -7 and -9. Similarly, the HMBC correlations of the quaternary carbon atoms C-5a and C-2a each with H-4 and H-5 allowed the assignment of the pyrrole ring in metabolite **39**. The assignment was supported by the small vicinal coupling of 2.8 Hz between H-4 and H-5 and by the observation of their direct ^{1}H,^{13}C coupling constants $^1J_{C,H}$ = 173 and 184 Hz, respectively, which are characteristic of pyrrole systems like **39**.[112]

Another HMBC correlation of C-5a with H-6 and the only NOE of **39** between H-5 and H-6 indicated the connection of the aromatic rings. A further correlation of C-2a with H-10 and the single HMBC correlation of C-2 with the methyl protons H-10 were only consistent with the position of the methyl group at C-2. In particular, the absence of any further correlations of the methyl group bearing C-2 is only compatible with the isomer marinoquinoline A (**39**). (Table 2). Finally, **39** could be crystallized from acetone/petrol ether (1:1) to give crystals suitable for the replication of the X-ray analysis of Kanjana-Opas *et al.*[111](Figure 13 and 14).
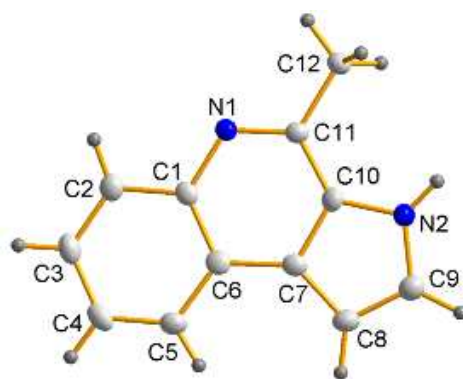
Figure 13. X-ray crystal structure of marinoquinoline A (**39**).

Crystal data:

Empirical formula $C_{12}H_{10}N_2$

Crystal size 0.37 x 0.23 x 0.13 mm^3

Formula weight 182.22

Volume 1867.79(14) Å^3

Temperature 153(2) K

Density (calculated) 1.296 Mg/m^3

Wavelength 0.71073Å

Colourless needles
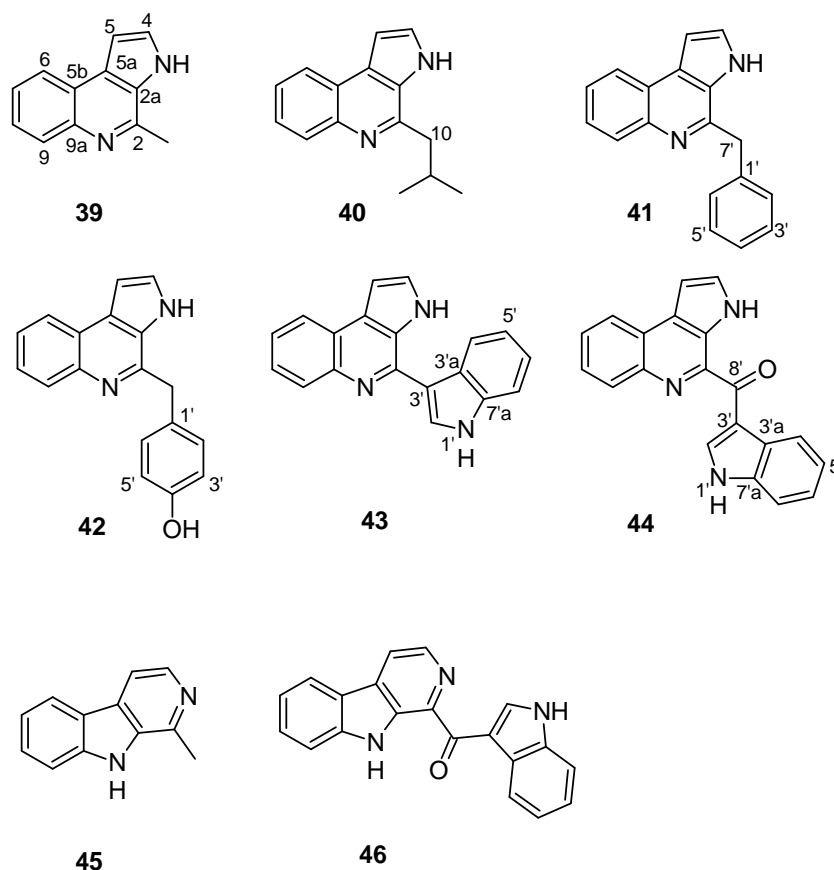
Figure 14. Marinoquinolines A – F (**39** – **44**), the isomers, harman (**45**) and pityriacitrin (**46**).

24

HRESIMS analysis of marinoquinoline B (**40**) displayed a molecular ion $[M+H]^+$ at *m/z* 225.1382 consistent with the molecular formula $C_{15}H_{16}N_2$. Similar to **39** and all further marinoquinolines the $^1H,^1H$ COSY and $^1H,^{13}C$ HMQC and HMBC correlations indicated the pyrroloquinoline core structure. Two new methyl group signals 12-H_3 and 13-H_3, overlapping as an aliphatic doublet at $\delta_H = 1.00$ ppm, and a multiplet of a methine H-11 at $\delta_H = 2.44$ ppm were observed in the ^1H NMR spectrum of **40**. According to the COSY and HMBC correlations between C-10 and H-12, H-13, and H-11 they constitute an isopropyl side chain that replaces the methyl group of **39** in marinoquinoline B (**40**). The connection of the side chain was confirmed by the HMBC correlation of C-2 with H-10 and H-11 (Table 2).

The molecular formula $C_{18}H_{14}N_2$ was indicated from the $[M+H]^+$ ion at *m/z* 259.1236 in the HRESIMS analysis of marinoquinoline C (**41**). Besides the pyrroloquinoline core structure in **41** (Table 3) all further carbon-bound proton signals in the novel phenyl ring in **41** were correlated with their corresponding carbon signals from a $^1H,^{13}C$ HMQC NMR spectrum. The additional phenyl ring was assigned from the $^1H,^1H$ COSY correlations of the aromatic protons and from the HMBC correlations observed e. g. between C-6´ and H-4´ and H-2´ or between C-1´ and H-5´ and H-3´.

Curiously, no HMBC correlations were observed with the methylene group C-7´ initially, though this remained as the only perfect link to complete structure **41**. However, during NMR measurements the protons at C-7´ had been exchanged against deuterium from the acetone-d_6 solvent. Consequently, the singlet signal of methylene group C-7´, in the beginning observed in a ^1H NMR spectrum was no longer present during later NMR experiments. The unexpected H/D exchange was verified by HRESIMS of the deuterated molecular ion $[C_{18}H_{12}N_2D_2 + H]^+$ at *m/z* 261.1351. The H/D exchange with the solvent can be explained by keto-enol tautomerism of acetone-d_6 providing deuterium ions. The enolization probably was catalyzed by the basic alkaloid **41** itself. In **41** H/D exchange at the methylene group bridging both aromatic systems was reversible. Similar H/D changes have been observed on aromatic rings during APCI LC/MS[113], and are also used as a method in probing protein conformational changes in solution[114] and for peptide identification and mapping in mass spectrometry.[115]

HRESIMS analysis of marinoquinoline D (**42**) revealed a $[M+H]^+$ ion at *m/z* 275.1180 with the elemental formula $C_{18}H_{14}N_2O$ indicating an additional oxygen atom compared to **41**. Unlike **3**, marinoquinoline D (**42**) was only poorly soluble in acetone. Hence its NMR data

were collected in methanol-d_4 (Table 3). All carbon-bound proton signals in the new *p*-phenol unit were correlated with their corresponding carbon signals from a ^{1}H,^{13}C HMQC NMR spectrum. The phenol carbon atom (C-4´) at δ_C = 157.6 ppm provided HMBC correlations with the overlapping signals of H-5´/H-3´ and H-2´/H-6´ and allowed the assignment of the phenol unit. The signal of the bridging methylene group C-7´ was detected as a singlet at δ_H = 4.60 ppm. A HMBC correlation of C-7´with H-2´ and H-6´ and the only HMBC correlation of C-2 with H-7´ in **42** indicated the direct connection to the marinoquinoline core structure. Similar to **41** a slow H/D exchange of the methylene protons H-7´ in **42** was observed.

The [M+H]$^+$ ion of marinoquinoline E (**43**) (C$_{19}$H$_{13}$N$_3$) appeared at *m/z* 284.1182 in the HRESIMS analysis. Again the NMR spectra showed the presence of the pyrroloquinoline core structure (Table 4). However, the otherwise higher order multiplet of H-7 and H-8 was separated in **43**, due to the enlarged conjugated system. The latter was assigned from the COSY correlations from H-4´ to H-7´ and the HMBC correlations observed between C-7´ and H-2´, -4´and -6´, and between C-3´a and H-2´, -5´ and -7´.

The most complex of the hitherto known *O. kribbensis* metabolites is marinoquinoline F (**44**). HRESIMS analysis of **44** revealed a molecular ion peak [M+H]$^+$ at *m/z* 312.1138 consistent with the molecular formula C$_{20}$H$_{13}$N$_3$O. Thus **44** contain an additional CO group compared to **43**. In the ^{1}H NMR spectrum several signals were overlapping and highly complex due to the second-order multiplets of H-6 to H-9 and H-4´ to H-7´, respectively. Nevertheless, the pyrroloquinoline core structure in **6** was easily recognized in the NMR data (Table 4) as well as an indole moiety from correlations, which were similar to those described above for **43**. The additional carbonyl carbon C-8´ was detected at δ_C = 189.0 ppm, a shift characteristic for a ketone. Reliable HMBC correlations of the ketone carbon were not detected. However, its only possible position was the bridge between both aromatic systems. Advantageously, in addition to the NOE between protons H-5 and H-6, which was previously observed in marinoquinoline A (**39**), a weaker correlation between H-9 and H-2´ was detected in the ROESY spectrum of marinoquinoline F (**44**). Consistent with these NOEs, the distances of H-5 to H-6 and H-9 to H-2´ were 2.50 and 3.33 Å, respectively, in a PM 3 generated model of **44** [HyperChem Ver. 8. (PM3 Optimization)] (Figure 15). Noticeably, the singlet of the 2´-H proton was shifted about 1.4 ppm down-field to δ = 9.7 ppm. This de-shielding can also be

26

explained from the nearly planar keto-indole part which brings the indole methine H-2´ into the region affected by the carbonyl anisotropy.[116]
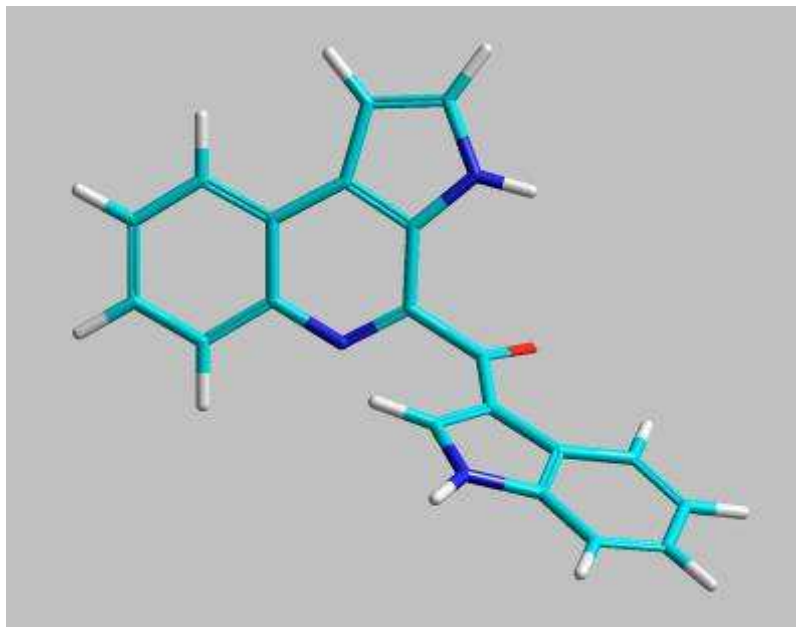
Figure 15.　　　3D model of marinoquinoline F (**44**) [HyperChem Ver. 8. (PM3 Optimization)].

Marinoquinoline F (**44**) is closely related to the isomer pityriacitrin (**46**), a potent UV filtering compound featuring a core structure derived from harman (**45**)[117,118] which was produced by the yeast *Malassezia furfur*. The indole ketone moiety was present in both. Consequently, comparison of the ^{1}H and ^{13}C NMR data of **44** and **46** in deuterated acetonitrile showed a high similarity of the indole signals (Table 5).

Table 2. NMR Data of Marinoquinoline A (**39**) and B (**40**) in acetone-d_6.

C/H	**39**[a] δ_H, m (J in Hz)	δ_C[c]	HMBC[e] ($^1J_{C,H}$ in Hz)	**40**[b] δ_H, m (J in Hz)	δ_C[c]	HMBC ($^1J_{C,H}$ in Hz)
2		146.92, qC	10		149.99, qC	10
2a		129.89, qC	4, 5, 10		129.69, qC	4, 5, 10,
NH	11.12, br. s			11.16, br. s		
4	7.57, d (2.8)	127.11, CH	5 (184 Hz)	7.57, d (2.9)	127.05, CH	5 (184 Hz)
5	7.12, d (2.8)	102.04, CH	4 (173 Hz)	7.12, d (2.9)	101.87, CH	4 (174 Hz)
5a		128.41, qC	4, 5, 6		128.64, qC	4, 6 >5
5b		124.26, qC	7, 9 >6		124.01, qC	7, 9
6	8.22, dd (7.7, 2)	123.77, CH	8 >7	8.23, d (7.7, 1.8)	123.66, CH	8
7	7.48, td (7-8, 2)[d]	125.71, CH	9 (163 Hz)	7.51, td (7-8, 2)[d]	125.63, CH	9
8	7.51, td (7-8, 2)[d]	126.11, CH	6 (163 Hz)	7.51, td (7-8, 2)[d]	126.05, CH	6
9	7.99, dd (7.7, 2)	129.98, CH	7, 6	8.04, d (7.7, 1.8)	129.87, CH	7
9a		143.89, qC	6, 8 >9		143.53, qC	6, 7/8
10	2.83, s	21.34, CH$_3$	(120 Hz)	3.08, d (7.3)	43.91, CH$_2$	12/13, >11
11				2.44, tspt (7.3, 6.8)	29.01, CH	10, 12/13
12				1.00, d (6.8)	22.96, CH$_3$	10, 13 >11
13				1.00, d (6.8)	22.96, CH$_3$	10, 12 >11

[a] ^{1}H/^{13}C 600/150 MHz; [b] ^{1}H/^{13}C 600/75 MHz; [c] ^{13}C data are given with two digits in order to discriminate between narrowly separated signals; [d] complex first-order multiplets; [e] HMBC correlations provide the observed protons for the carbons.

Table 3. NMR Data of Marinoquinoline C (**41**) and D (**42**).

C/H	**41**[a] δ$_H$, m (J [Hz])	δ$_C$[c]	HMBC	**42**[b] δ$_H$, m(J [Hz])	δ$_C$[c]	HMBC
2		148.98, qC	n.o.[d]		148.83, qC	7'
2a		129.20, qC	5		128.76, qC[e]	4, 5
NH	11.15, br. s		-	8.44, br. s		
4	7.55, d (2.9)	127.47, CH	5	7.85, d (2.8)	133.21, CH	5
5	7.12, d (2.9)	102.10, CH	4	7.30, d (3.0)	103.42, CH	4
5a		129.39, CH	4 >5, 6		132.87, qC	5, 6
5b		124.30, qC	7		124.77, qC	9, 7/8
6	8.24, d (6.2)	123.83, CH	8	8.12, d (1.0)	124.77, CH	7/8
7	7.51, td (7.3, 2.2)	126.06, CH	9	7.71, m	127.77, CH	9
8	7.54, td (8.4, 1.8)	126.33, CH	6	7.71, m	128.67, CH	6
9	8.07, dd (7.7, 1.5)	130.21, CH	7	8.39, d (9.6)	125.32, CH	7/8
9a		143.77, qC	6, 8 >9		139.30, qC	6, 7/8
1´		139.93, qC	3´, 5´		128.81, qC[e]	3´, 5´ >7´
2´	7.43, d (8.3, 1.3)	129.82, CH	4´, 6´	7.18, d (8.4)	130.60, CH	7´, 2´/6´
3´	7.24, m	129.24, CH	5´	6.74, d (8.6)	116.60, CH	5´, 2´/6´
4´	7.15, m	127.16, CH	2´, 6´	4.86, s	157.62, COH	2´/6´, 3´/5´
5´	7.24, m	129.24, CH	3´	6.74, d (8.6)	116.60, CH	3´/5´ >2´/6´
6´	7.43, d (8.3, 1.3)	129.82, CH	2´, 4´	7.18, d (8.4)	130.60, CH	7´, 2´/6´
7´	4.57, s	40.95, CH$_2$	2´, 6´	4.60, s	38.64, CH$_2$	2´/6´

[a] in acetone-d_6, ^{1}H/[13]C 600/150 MHz; [b] in methanol-d_4, ^{1}H/[13]C 300/75 MHz; [c] [13]C data are given with two digits in order to discriminate between narrowly separated signals; [d] not observed due to H/D-exchange of 7'-H$_2$; [e] interchangeable.

Table 4. NMR Data of Marinoquinoline E (**43**) and F (**44**) in acetone-d_6 (^{1}H/^{13}C 600/150 MHz).

C/H	**43** δ_H, m (*J* in Hz)	δ_C[c]	$^1J_{C,H}$ [Hz]	HMBC[d]	**44** δ_H, m (*J* in Hz)	δ_C[c]	HMBC[d] (^1J [Hz])
2		144.50, qC	-	4		143.23, qC	
2a		128.04, qC	-	4 >5		131.43, qC	4, 5
NH	10.79, br. s[a]				11.59, br. s	-	
4	7.61, d (2.9)	127.50, CH	184	5	7.79, d(2.9)	129.24, CH	5
5	7.20, d (2.9)	102.24, CH	174	4	7.25, d(2.9)	101.34, CH	4 (174 Hz)
5a		129.67, qC	-	6, 4, 5		128.95, qC	4, 5
5b		123.72, qC[e]	-	9, 7 >6[b]		125.85, qC	7, 9
6	8.27, dd (8.1, 1.5)	123.71, CH	158	8[b]	8.39, dd(7.5, 2.0)	124.08, CH	7,8
7	7.51, ddd (8.1, 6.9, 1.1)	125.62, CH	160	9	7.70, td(6.6, 1.8)	128.38, CH	9
8	7.57, ddd (8.2, 6.9, 1.5)	126.48, CH	159	6	7.68, td(7.5, 1.8)	127.02, CH	6
9	8.17, dd (8.1, 1.1)	129.94, CH	159	7	8.30, dd(7.7, 1.5)	131.58, CH	7
9a		143.94, qC	-	8, 6>9		142.40, qC	6, 8
NH	10.95, br. s[a]				11.24, br. s	-	
2´	8.25, br s	126.91, CH	-	-	9.70, s	139.19, CH	
3´		115.12, C	-	2´ >4´		115.94, qC	2´
3´a		127.83, qC	-	7´, 5´ >2´		128.71, qC	2´, 5´ 7´
4´	8.77, d (7.3 br.)	123.64, CH	164	6´ >5´	8.65, dd(6.6, 2.5)	123.31, CH	5´,6´
5´	7.21, td (7.2, 1.0 br.)	121.17, CH	159	7´ >4´	7.29, td(7.3, 1.8)	124.05, CH	4´ 7´
6´	7.25, ddd (7.8, 7.1, 0.9)	123.43, CH		4´	7.31, td(7.5, 1.4)	123.16, CH	7´
7´	7.53, d (7.8 br.)	112.33, CH	184	5´	7.60, m	112.89, CH	5´
7´a		137.93, qC	-	4´, 6´, 2´		137.14, qC	2´, 4´, 6´
8´						189.01, qC	

[a] interchangeable; [b] C-5b overlapping with C-6 was assigned from strong HMBC-correlations with H-9 and H-7 at this position, which should not be present if only carbon-6 was located there. Further there is a weak correlation with H-6 at this position, which is not possible for C-6; [c] ^{13}C data are given with two digits in order to discriminate between narrowly separated signals; [d] HMQC and HMBC spectra with enhanced ^{13}C resolution; [e] quaternary carbons were observed in an APT ^{13}C NMR spectrum.

Table 5. Comparison of the NMR Data of Marinoquinoline F (**44**) and Pityriacitrin (**46**) in acetonitrile-d_3.

	marinoquinoline F (**44**)[a]			pityriacitrin (**46**)[b]	
Atom	δ_H, m (J in Hz)	δ_C[c]	Atom	δ_H, m (J in Hz)	δ_C[c]
2		143.35	1		139.48
2a		131.67	1a		137.09
NH	11.06, br. s		3	8.58, d (4.8)	138.42
4	7.71,m	129.54	4	8.27, d (4.8)	118.87
5	7.18, d (2.2)	101.82	4a		132.15
5a		128.91	5	8.26, d (7.8)	122.68
5b		126.02	5a		121.69
6	8.34, m	124.38	6	7.32, m	121.27
7	7.68, m	128.91	7	7.62, dd (7.8,7.8)	129.92
8	7.66, t (2.8)	127.61	8	7.77, d (7.8)	113.40
9	8.32, m	131.81	8a		142.40
9a		142.64	9 NH	10.96, s	
NH	10.13, br. s		1'NH	10.06, s	
2´	9.56, d (2.9)	139.84	2'	9.40, d (2.9)	138.69
3´		115.98	3'		115.83
3´a		128.71	3'a		128.48
4´	8.58, d (6.6)	123.38	4'	8.60, d (6.7)	123.12
5´	7.32, td (7.2, 1.5)	124.61	5'	7.32, m	123.30
6´	7.34, td (7.3, 1.5)	123.76	6'	7.32, m	124.20
7´	7.59, dd (6.4, 2.0)	113.33	7'	7.57, dd (6.7,1.9)	112.94
7´a		137.33	7'a		136.93
8´		189.60	10		189.39

[a] (^{1}H/^{13}C 600/75 MHz).[b] (^{1}H/^{13}C 400/100 MHz)[8]. [c] ^{13}C data are given with two digits in order to discriminate between narrowly separated signals.
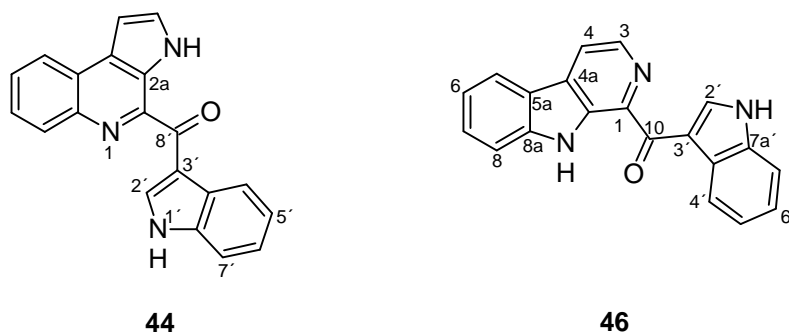
Figure 16. Marinoquinoline F (**44**) and its isomer pityriacitrin (**46**).

2.2 Biological activities of marinoquinolines A –F

2.2.1 Antibacterial and antifungal activities

Testing of marinoquinolines A - F (**39** - **44**) for antibiotic activity against a broad panel of bacteria and fungi showed weak activity with minimum inhibition concentration (MIC) of 33.5 µg/mL against some of the strains tested. The indole variant **43** showed the broadest activity inhibiting Gram-positive bacteria (*Nocardia flava* and *Micrococcus luteus*) and three fungi (*Schizosaccharomyces pombe, Mucor hiemalis* and *Rhodotorula glutinis*) followed by the phenyl derivative **41** with antifungal activity only (*S. pombe* and *R. glutinis*). Both **39** and **44** were active against Gram-negative *Escherichia coli* and *S. pombe*, respectively, while the phenyl variant **42** and isopropyl variant **40** were not active at 33.5 µg/mL. The MIC concentrations tested ranged from 33.5 to 0.052 µg/mL (Table 6).

Table 6. Antibacterial and antifungal activity of Marinoquinolines A - F (**39 - 44**) [MIC, µg/mL].

Pathogen	39	40	41	42	43	44	Ref[a]	Ref[b]
Bacteria								
Chromobacterium violeceum	>33.5	>33.5	>33.5	>33.5	>33.5	>33.5	0.21	
Escherichia coli	33.5	>33.5	>33.5	>33.5	>33.5	33.5	0.83	
Micrococcus luteus	>33.5	>33.5	>33.5	>33.5	33.5	>33.5	0.104	
Nocardia flava	>33.5	>33.5	>33.5	>33.5	33.5	>33.5	1.67	
Staphylococcus aureus	>33.5	>33.5	>33.5	>33.5	>33.5	>33.5	0.104	
Fungi and yeasts								
Candida albicans	>33.5	>33.5	>33.5	>33.5	>33.5	>33.5		1.67
Mucor hiemalis	>33.5	>33.5	>33.5	>33.5	33.5	>33.5		1.67
Pichia anomala	>33.5	>33.5	>33.5	>33.5	>33.5	>33.5		1.67
Rhodotorula glutinis	>33.5	>33.5	33.5	>33.5	33.5	>33.5		0.42
Schizosaccharomyces pombe	>33.5	>33.5	33.5	>33.5	33.5	33.5		1.67

[a] Oxytetracyclin hydrochloride, (1 mg/mL; 2µL); [b]Nystatin (1 mg/mL; 2µL).

2.2.2 Cytotoxic activities

Marinoquinolines A - F (**39** – **44)** were moderately cytotoxic when evaluated against three growing cancer cell lines, L929, MCF -7, and KB-3-1 and a primary cell line, HUVEC (Table 7). Methanol was used as a negative control. The keto-indole variant **44** was the most toxic followed by the phenyl derivatives **41** and **42**, while the isopropyl variant **40** showed the least cytotoxicity.[119]

Table 7. Cytotoxicity of Marinoquinolines A - F (**39 – 44**) (IC$_{50}$ in μg/mL).

Compound.	L929	MCF-7	KB-3-1	HUVEC
39	5.5	3.5	2.2	1.5
40	8.0	6.5	5.0	3.6
41	5.4	2.6	2.0	0.55
42	1.1	3.2	3.2	2.5
43	5.5	1.9	4.5	5.8
44	4.1	1.6	0.3	2.8

2.2.3 Antiparasitic activities

In a screening against tropical parasites (Table 8) marinoquinoline B (**40**) and F (**44**) were identified as the most active structural variants with IC$_{50}$ values of 1.8 and 1.7 μM, respectively, against *P. falciparum*. However, the IC$_{50}$ values against the cell line L6 indicated a considerable higher cytotoxicity compared to 3*H*-pyrrolo[2,3-*c*]quinoline (IC$_{50}$ 173.2 μM).[120] All the compounds were inactive when tested against *Trypanosoma brucei rhodesia*, *Trypanosoma cruzi* and *Leishmania donovani*.

Table 8. Antiprotozoal activity and cytotoxicity of marinoquinolines A–F (**39–44**) (IC$_{50,}$ μM).

Compound no.	*Trypanosoma brucei rhodesia*	*T. cruzi*	*Leishmania donovani*	*Plasmodium falciparum* (K1)	Cytotoxicity L6 cells
39	54.4	29.5	>548.8	9.8	30.6
40	45.9	53.1	86.5	1.8	58.7
41	42.2	28.3	58.8	5.5	39.1
42	61.2	27.0	119.9	15.0	66.4
43	51.5	23.6	63.9	7.6	35.6
44	39.0	21.8	16.1	1.7	12.5
Melarsoprol	0.012				
Benznidazole		1.95			
Miltefosine			0.386		
Chloroquine				0.141	
Podophyllotoxin					0.021

2.2.4 Acetylcholine esterase activity

Marinoquinoline A (**39**) has also been characterized as an inhibitor of the acetylcholine esterase.[121]

2.3 Hyaladione, an S-methyl cyclohexadiene-dione from *Hyalangium minutum*

2.3.1 Strain selection and cultivation

The myxobacterium, *Hyalangium minutum* type strain NOCB-2^T was isolated from a soil sample containing decaying plant material collected in the mountains of Izu and Manazuru in Japan as described by Reichenbach *et al.*[122,123] The strain was selected because the crude methanol extract indicated activity against the Gram-positive bacteria, *S. aureus, N. flava* and the Gram-negative bacterium *C. violaceum*. Peak activity correlations by fractionation and bioassays and subsequent initial dereplication with the chemical data of hyaladione (**47**), a UV/Vis chromophore at $\lambda_{max,}$ ca. 360 nm, HRESIMS [M+H]$^+$ at *m/z* 203.9882, and comparison of the HPLC retention time (R_t) with the in-house Myxobase as well as searches in the DNP database and Chemical Abstracts online established **47** to be novel. The strain was cultivated and maintained in liquid soybean-flour medium. The cells appear orange-brown in color on agar plates or in liquid cultures (Figure 17 panel A and B) respectively.
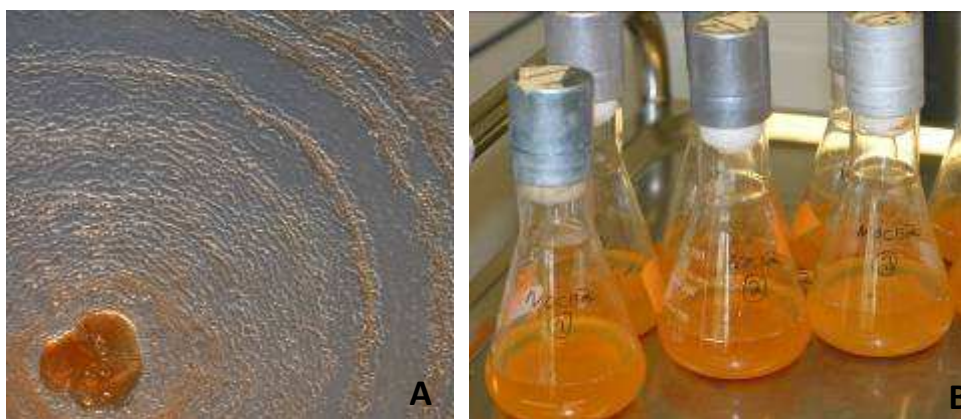
Figure 17.   **A**: Growth of *H. minutum* strain NOCB-2^T on agar plate; **B**: Cultivation in shake flasks.

Isolation of **47** was achieved by an up-scale fermentation of strain NOCB-2^T. The strain was inoculated in liquid soybean-flour medium containing 2% Amberlite XAD-16 adsorber resin and fermented in a 100 L bioreactor for 7 days. The adsorber resin was recovered from the culture broth by sieving and the crude extract was eluted from the resin with methanol. An isolation strategy was developed involving solvent-solvent partitioning, silca-gel flash chromatography, preparative RP MPLC and finally crystallization from acetone to produce pink needle shaped crystals of **47** (Figure 18).
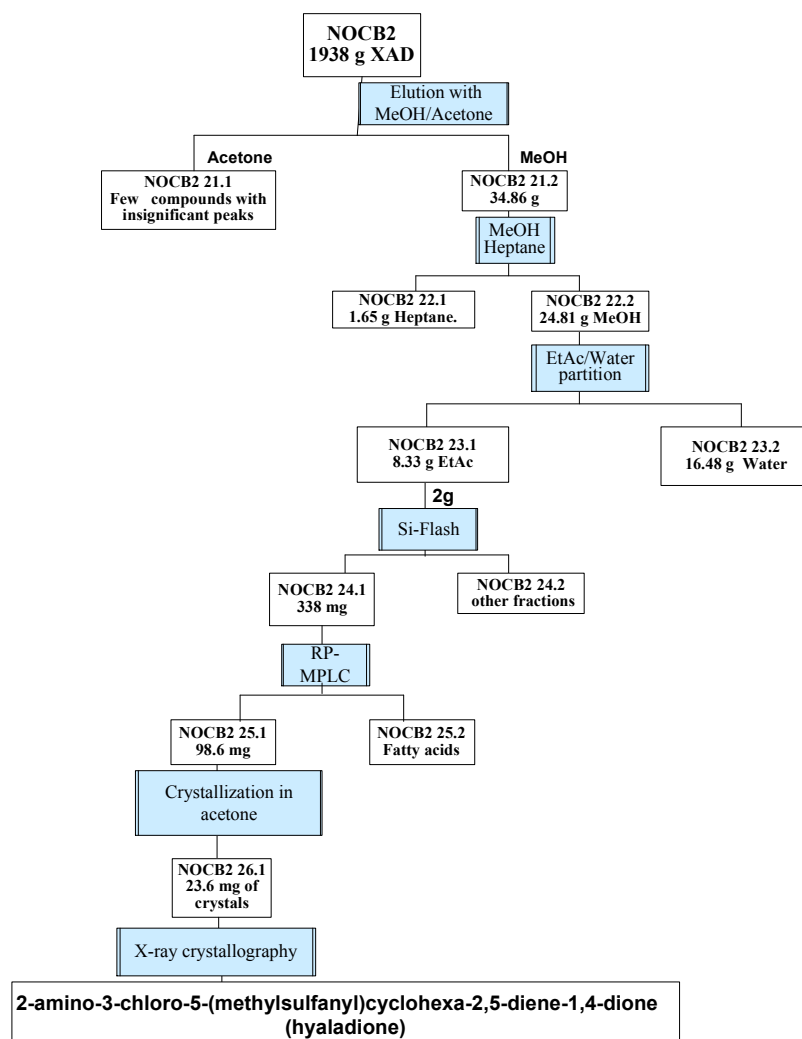
Figure 18. Isolation of hyaladione from XAD-16 resin recovered from a 100 L fermentation of strain NOCB-2^T (outlined numbers from 21.1 to 26.1 are representative of the experimental numbers).

2.3.2 Structure elucidation of hyaladione (47)

The structure of hyaladione (**47**) was established by extensive HRESIMS, NMR, and X-ray crystallographic analysis. Ultrahigh-resolution ESI-TOF MS and isotopic pattern analysis of the pseudo-molecular ion peak [M+H]$^+$ at *m/z* 203.9882 revealed the molecular formula $C_7H_6ClNO_2S$ for **47** indicating five degrees of unsaturation. Supporting the empirical formula all seven carbon atoms were present in the ^{13}C NMR spectrum of **47** in acetone-d_6. The signals of a methyl carbon and a methine carbon were found at δ_C 13.9 (C-7) and δ_C 120.3 (C-

5) respectively. Five quaternary signals of two carbonyl carbons [δ_C 177.9 (C-4), δ_C 174.9 (C-1)] and three carbon signals [δ_C 106.2 (C-2), δ_C 146.4 (C-3), δ_C 159.2 (C-6)] suggested the presence of a substituted quinone-type aromatic system. This was supported by the IR spectrum showing two strong bands of α,β-unsaturated carbonyl groups at ν_{max} 1604 and 1566 cm^{-1}. Additionally, the IR spectrum revealed two sharp bands of a primary amine at ν_{max} 3438 and 3308 cm^{-1} while the presence of UV absorption at λ_{max} 360 nm supported the presence of a conjugated chromophore.

The ^{1}H NMR spectrum of **47** in acetone-d_6 presented only three singlet signals of a methyl group (δ_H 2.41, CH_3-7), a methine proton (δ_H 6.26, H-5), and a broad singlet of an amine (δ_H 6.81) (Table 9). However, the few correlations from the COSY,[124] HMBC and ROESY spectra were insufficient for a complete structure elucidation, because the ratio of 5 quaternary carbons to 2 proton-bearing carbons was too unfavorable (Figure 19 and Table 9). Fortunately, the compound could be crystallized from acetone to obtain pink needle-shaped crystals for an unambiguous structure elucidation by X-ray analysis (Figure 20).

Table 9.   NMR Data of Hyaladione (**47**) in acetone-d_6 (^{1}H 600 MHz; ^{13}C 150 MHz).

C/H	δ_C, mult	δ_H, mult	COSY[a]	ROESY[a]	HMBC[a] ($^1J_{C,H}$ in Hz)
1	174.8, qC				5
2	106.2, qC				
3	146.4, qC				5
4	177.7, qC				
5	120.3, CH	6.26, s	7	7	5 (171), 7
6	159.2, qC				7, 5
7	13.9, CH$_3$	2.41, s	5	5	7 (142)
NH$_2$		6.79, br s			

[a] positions of correlated protons.
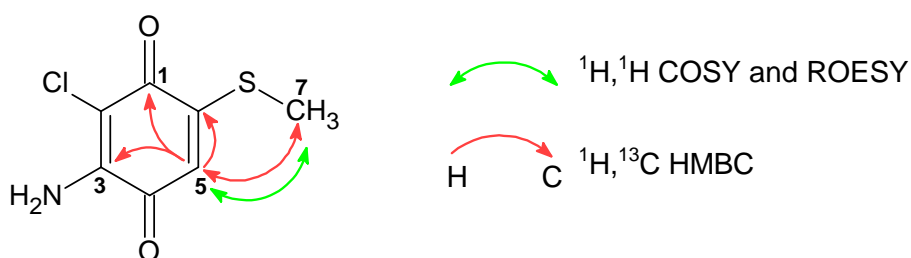
Figure 19. All ^{1}H,^{1}H COSY, ROESY, and ^{1}H,^{13}C HMBC correlations of hyaladione (**47**).
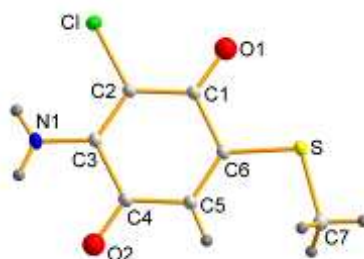
Figure 20. X-ray crystal structure of hyaladione (**47**).

2.4 Biological activities of hyaladione

2.4.1 Antibacterial and antifungal activities

Hyaladione (**47**) displayed broad but weak antibacterial and antifungal activities with the best minimum inhibition concentration (MIC) value at 0.83 µg/mL against the methicillin-resistant *Staphylococcus aureus* (Table **10**).

Table 10. In vitro antibacterial and antifungal activity of hyaladione (**47**) and two control drugs.

Pathogen	MIC [µg mL^{-1}]		
	hyaladione (**47**)	oxytetracycline hydrochloride[a]	nystatin[b]
Bacteria			
Micrococcus luteus	3.3	0.104	
Staphylococcus aureus	0.83	0.104	
Escherichia coli	33.3	0.83	
Nocardia flava	3.3	1.67	
Chromobacterium violaceum	2.1	0.21	
Pseudomonas aeruginosa	8.5		
Fungi and yeasts			
Mucor hiemalis	16.5		1.67
Schizosaccharomyces pombe	> 33.3		1.67
Rhodotorula glutinis	1.7		0.42
Pichia anomala	33.3		1.67
Candida albicans	> 33.3		1.67

[a] broad spectrum antibacterial [b] broad spectrum antifungal.

37

2.4.2 Cytotoxic activity

The cytotoxicity of **47** was evaluated against three growing cancer cell-lines and a primary cell-line using the MTT method.[9] **47** was cytotoxic against the breast cancer cell line MCF-7 (IC_{50} 1.23 µM), the mouse subcutaneous connective tissue fibroblast cell line L929 (IC_{50} 1.47 µM), the cervix carcinoma cell line KB-3-1 (IC_{50} 3.93 µM), and the non-transformed human umbilical vein endothelial cell line HUVEC (IC_{50} 2.21 µM).

2.4.3 Antiparasitic activity

Hyaladione (**47**) was moderately active against three mammalian parasites, *T. b. rhodensia*, *T. cruzi, L. donovani,* and *P. falciparum* K1 when compared with the respective reference drugs (Table 11). However, it was also cytotoxic against the rat myoblast L6 cells. The assays were performed at the Swiss Tropical and Public Health Institute, Basel Switzerland.

Table 11. *In vitro* antiparasitic activity of hyaladione (**47**) (IC_{50} µg mL^{-1}).

Test drug/compound	*T. b. rhod*.	*T. cruzi*	*L. don. axen.*	*P. falc. K1*	Cytotoxicity. L6
	IC_{50}	IC_{50}	IC_{50}	IC_{50}	IC_{50}
Hyaladione (**47**)	0.055	1.84	0.197	0.186	0.552
Melarsoprol	0.002				
Benznidazole		0.58			
Miltefosine			0.144		
Chloroquine				0.046	
Podophyllotoxin					0.005

2.5 The hyafurone family from *Hyalangium minutum*, strain NOCB-2^T

2.5.1 Identification and isolation of the hyafurones and hyapyrones

Besides hyaladione (**47**), the myxobacterium *H. minutum* strain NOCB-2^T also produced a novel family of polyketides with common typical UV spectra. Hyafurone A$_1$ (**48**) was identified as the second major compound of the extract and the main product of the polyketide family. However, in the bioassay guided fractionations of the crude extract of NOCB-2^T, **48** was inactive against the bacterial and fungal pathogens tested. Nevertheless, the activity of hyafurone B (**49**) with a UV pattern similar to **48** was correlated to *S. aureus*, *N. flava*, *C. violaceum*, and *M. hiemalis*. HRESIMS analysis of **48** displayed a molecular ion at *m/z* 547.3027 [M + Na]$^+$ revealing the molecular formula $C_{32}H_{44}O_6$. Hyafurone A$_1$ (**48**) and all its derivatives (**49**-**54**) were established to be new according to the dereplication of their high resolution masses (HRESIMS) and UV data by searches in the in-house Myxobase, Chemical Abstracts online and the DNP.

The hyafurones A$_1$ - D and hyapyrone A (**48** - **53**) were isolated from the XAD-16 resin of a 70 L large-scale fermentation of strain NOCB-2^T. The adsorber resin was recovered from the culture broth by sieving and the crude extract eluted from the resin with methanol and acetone. An isolation strategy was developed involving methanol/*n*-heptane partitioning, a subsequent partitioning of the extract in methanol layer between ethyl acetate and water, followed by silica-gel flash chromatography, preparative RP MPLC and RP HPLC to yield hyafurones A$_1$ (**48**), A$_2$ (**49**), B (**50**), C (**52**), D (**53**) and hyapyrone A (**51**) (Figure 21).

Although initially detected in smaller amounts in strain NOCB-2^T, hyapyrone B (**54**) was isolated preferably from *H. minutum* strain Hym 3, which showed a higher production. The isolation procedure was similar to the isolation of other hyafurones with the exception of the last purification step where acetonitrile, acidified with formic acid was used in the preparative RP-HPLC (Figure 22).
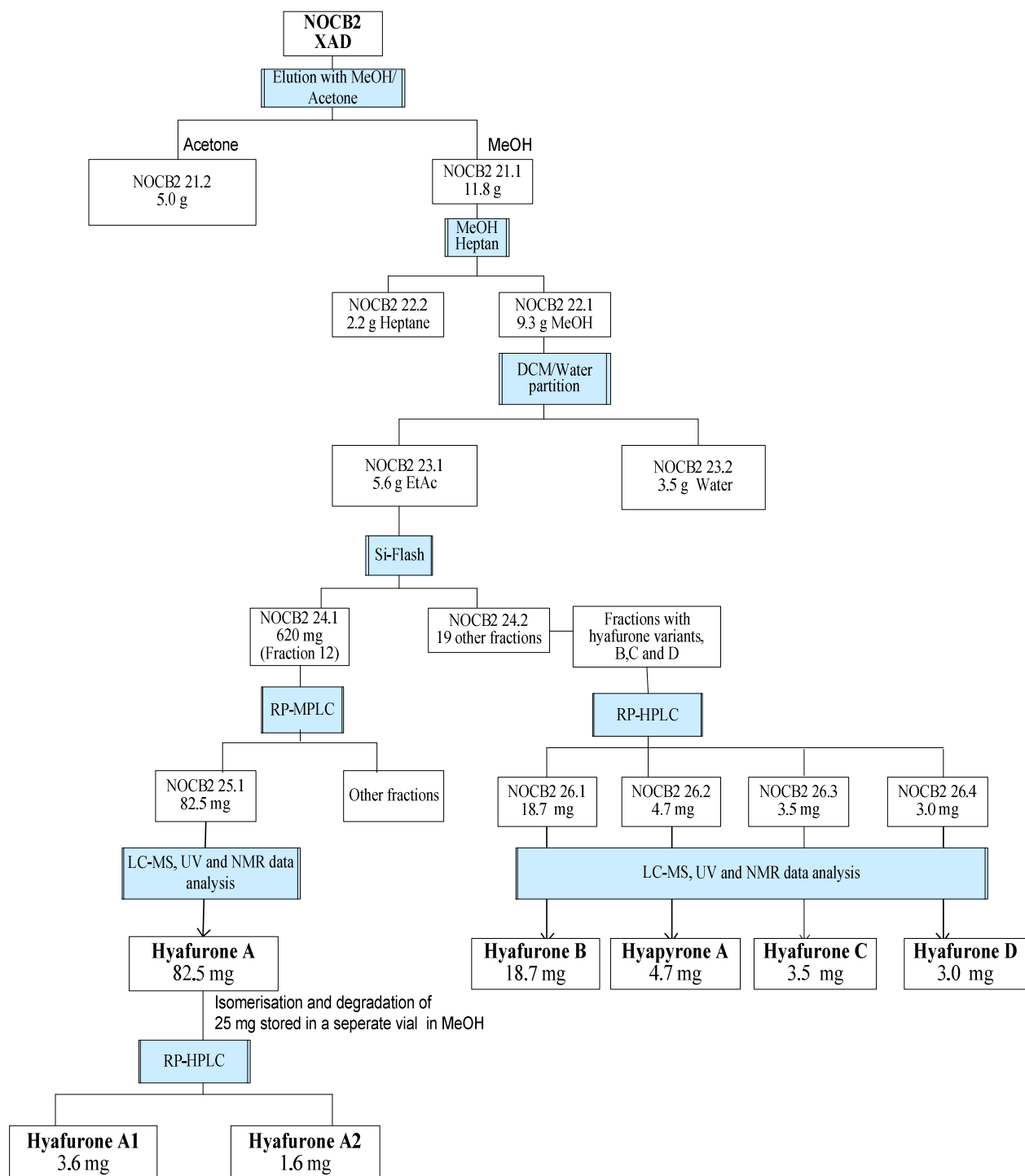
Figure 21. Isolation of hyafurones, A_1 (**48), A_2 (**49), B(**50), C(**52), D(**53) and hyapyrone, A (**51) from XAD resin of a 70 L fermentation of strain NOCB-2[T].
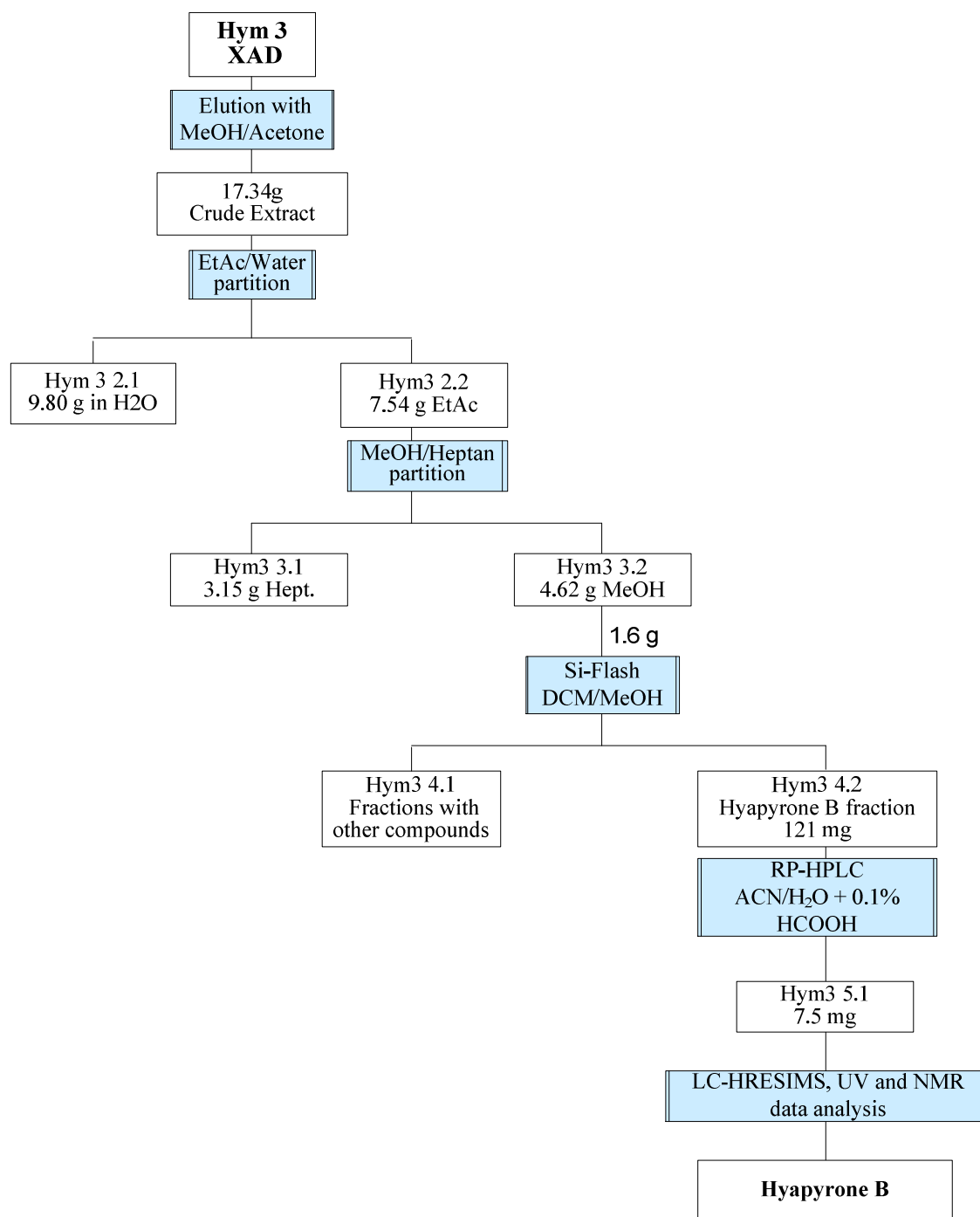
Figure 22. Isolation scheme of hyapyrone B (**54**) from XAD resin of a 70 L fermentation of strain Hym 3.

2.5.2 Structure elucidation of hyafurones and hyapyrones

Hyafurone A_1 (**48**) was isolated as yellow oil. Ultrahigh-resolution ESI MS (UHRESIMS) and isotopic pattern analysis of the molecular ion m/z 547.3027 [M + Na]$^+$ revealed the molecular formula $C_{32}H_{44}O_6$ for hyafurone A_1 (**48**). This was further verified by the presence of the molecular ion [M+H]$^+$ at m/z 525.3206 giving rise to the same molecular formula (Figure 23).
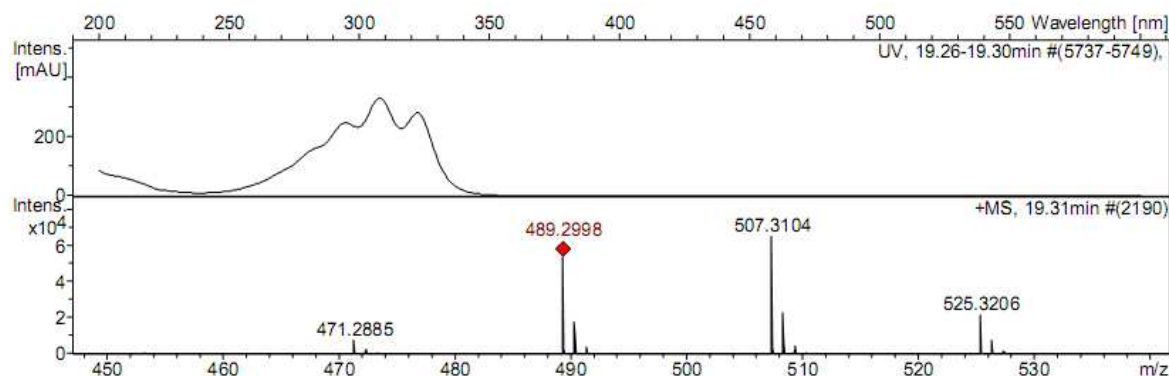
Figure 23. UV-MS of the molecular ion cluster of hyafurone A_1 (**48**) at m/z 525.3206 and three other fragment clusters from loss of water molecules m/z 507.3104, 489.2998 and 471.2885 respectively, i.e. a difference of 18 mass units between the clusters.

Additionally, the presence of a sodiated double mass ion [2M+Na]$^+$ at m/z 1071.6165 unambiguously agreed to the assigned molecular formula (Figure 24). The empirical formula indicated eleven double-bond equivalents for **48** which were also reflected by the polyene type UV spectrum, with three main bands at ν_{max} 292, 306 and 320 nm.
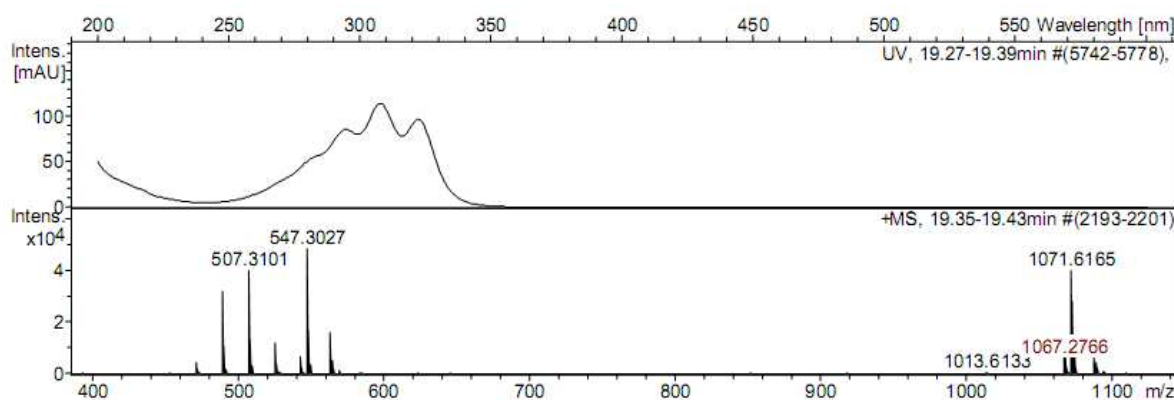
Figure 24. UV and MS of hyafurone A_1 (**48**) with the sodiated molecular ion clusters [M+Na]$^+$ at m/z 547.3027 and [2M+Na]$^+$ at m/z 1071.6165.

The skeletal structure of **48** was assigned through interpretation of both 1D and 2D NMR spectroscopic data (COSY, ROESY, HMQC, HMBC) acquired in methanol-d_4 (Table 12). The ^{1}H NMR spectrum revealed the presence of five methyl groups, four methylene and seven methine signals. The methyl signals CH_3-1(δ_H 1.71, 1.71 ppm) and CH_3-29 (δ_H 1.46, 1.47 ppm) each with equal integral values to the other three methyl protons were conspicuously split into doublets. The ^{13}C NMR spectrum showed signals for all 32 carbon atoms with 10 of them split in double signals (C-1, C-2, C-4, C-5, C-6, C-7, C-8, C-9, C-10, and C-13). All carbon-bound proton signals were correlated to their corresponding carbon signals from an ^{1}H,^{13}C HMQC NMR spectrum. Additionally, a DEPT NMR spectrum revealed the four methylene signals (C-6, C-8, C-21, and C-22) and supported the assignment of the quaternary carbons C-2, C-4, C-5, C-14, and C-23.

Analysis of the ^{1}H,^{1}H COSY NMR spectrum established three structural fragments (Figure 25). The first fragment contained the five aromatic protons (H-24 - H-28) of a phenyl residue. Construction of the second fragment chain was based on the serial correlations of six adjacent methine protons from H-15 to H-20 with an extension to CH_2-21 and CH_2-22. Additionally, correlations were observed between the sp3-hybridized methines H-18 and H-20 and the methyl group protons CH_3-31 and CH_3-32, respectively. The last fragment was derived from a series of correlations between the methylene protons CH_2-6 and the unsaturated methine proton H-13. Three hydroxyl groups were established on the basis of ^{13}C NMR chemical shift at C-7 (δ_C 68.6), C-9 (δ_C 67.5) and C-19 (δ_C 79.3).

—— ^{1}H, ^{1}H COSY

selected ^{1}H, ^{13}C HMBC
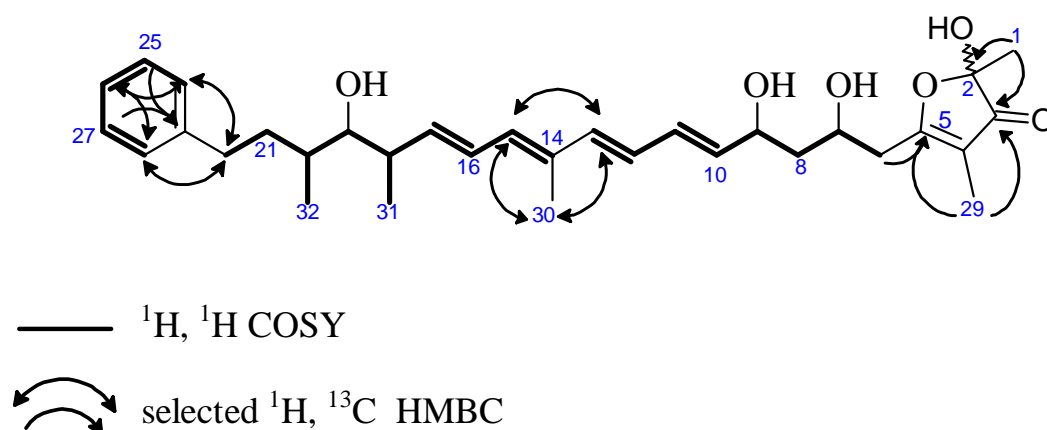
Figure 25. ^{1}H,^{1}H COSY and ^{1}H,^{13}C HMBC NMR correlations for elucidation of hyafurone A$_1$ (**48**).

43

The three main fragments were then linked using long-range HMBC correlations. The phenyl moiety was joined to the second COSY fragment from a mutual HMBC correlation between the methylene CH_2-22 with the aromatic methines CH-24 and CH-28. Similarly the second aliphatic fragment was joined to the third fragment from mutual key HMBC correlations assigned between the methyl group CH_3-30 with the methines CH-13 and CH-15 and a HMBC correlation of CH_3-30 to the olefinic quaternary carbon (C-14). Additionally, a mutual HMBC correlation was observed between the methines CH-13 and CH-15.

The furone moiety was assigned solely from the ^1H,^{13}C HMBC long-range correlations, i.e. correlations between the methyl protons CH_3-1 (δ_H 22.1) with quaternary hemiketal carbon (C-2, δ_C 104.2) and with the carbonyl carbon C-3 (δ_C 205.3), correlations between the methyl protons CH_3-29 (δ_H 1.71) with quaternary carbon C-5 (δc 186.6) and carbonyl carbon (C-3) and also with the quartenery carbon (C-4, δc 110.1). These data, and an HMBC correlation between the methylene CH_2-6 and the quaternary carbon C-5, established the five-membered ring as 2,4-dimethylfuran-4-en-3-one, connecting to the afore assigned fragment at C-5 (Figure 25).

The relative stereochemistry of hyafurone A_1 was assigned by analysis of both the vicinal proton coupling constants ($^3J_{H,H}$) and by 1D-NOE correlations. The $\Delta^{10,11}$ double- bond was assigned as *cis* (*Z*) on the basis of small vicinal coupling constant of $^3J_{10,11}$ = 11.0 Hz. Similarly, the double-bonds at $\Delta^{12,13}$ and $\Delta^{16,17}$ were assigned as *trans* (*E*) from the large vicinal coupling constants of ^3J = 15.0 Hz. Irradiation at the resonance frequency of CH_3-30 caused an NOE enhancement of the H-16 signal indicating a 14*E* double-bond geometry (Figure 26).
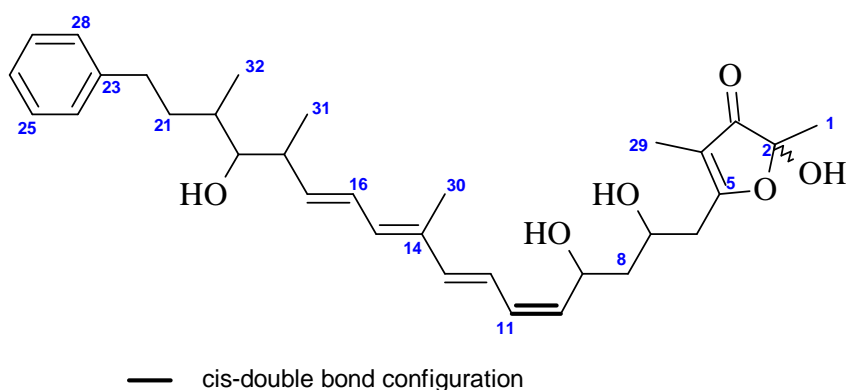
Figure 26.   Structure of hyafurone A$_1$ (**48**)

When exposed to light or stored in methanol hyafurone A$_1$ (**48**) was converted to its isomer hyafurone A$_2$ (**49**) as a degradation product, e.g. 30 % of **48** was found to have isomerized to **49** after a while. Re-purification of **48** additionally led to isolation of **49**. HRESIMS analysis of **49** displayed a molecular ion [M+Na]$^+$ at *m/z* 547.3040 consistent with the molecular formula $C_{32}H_{44}O_6$. ^{1}H and ^{13}C NMR spectra (Table 13) were near identical to hyafurone A$_1$ (**48**) except for the overlap of three olefinic proton signals H-11, H-12 and H-13. The *trans* (*E*) double bond configuration at methines C-10 and C-11 in **49** was assigned from the proton coupling constant $^3J_{10,11}$ = 14.0 Hz. Additionally, strong NOEs (Figure 27) between H-9 and H-11 and the methine protons H-10 and H-12 were observed. All the other 2D NMR correlations were identical to those observed in **48** thus establishing **49** as a stereoisomer (Figure 27).
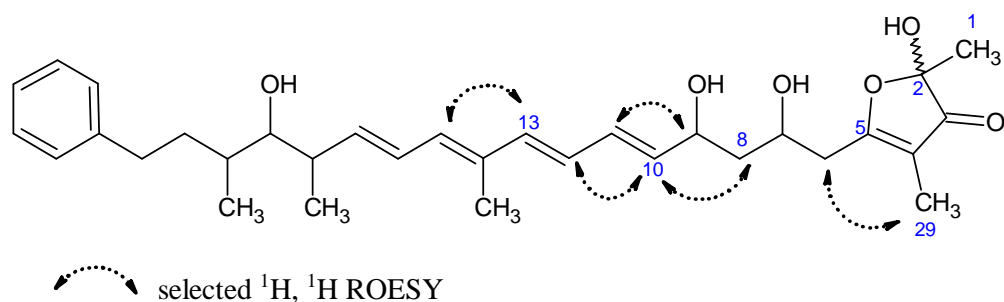
Figure 27.   Selected NOE correlations of hyafurone A$_2$ (**49**).
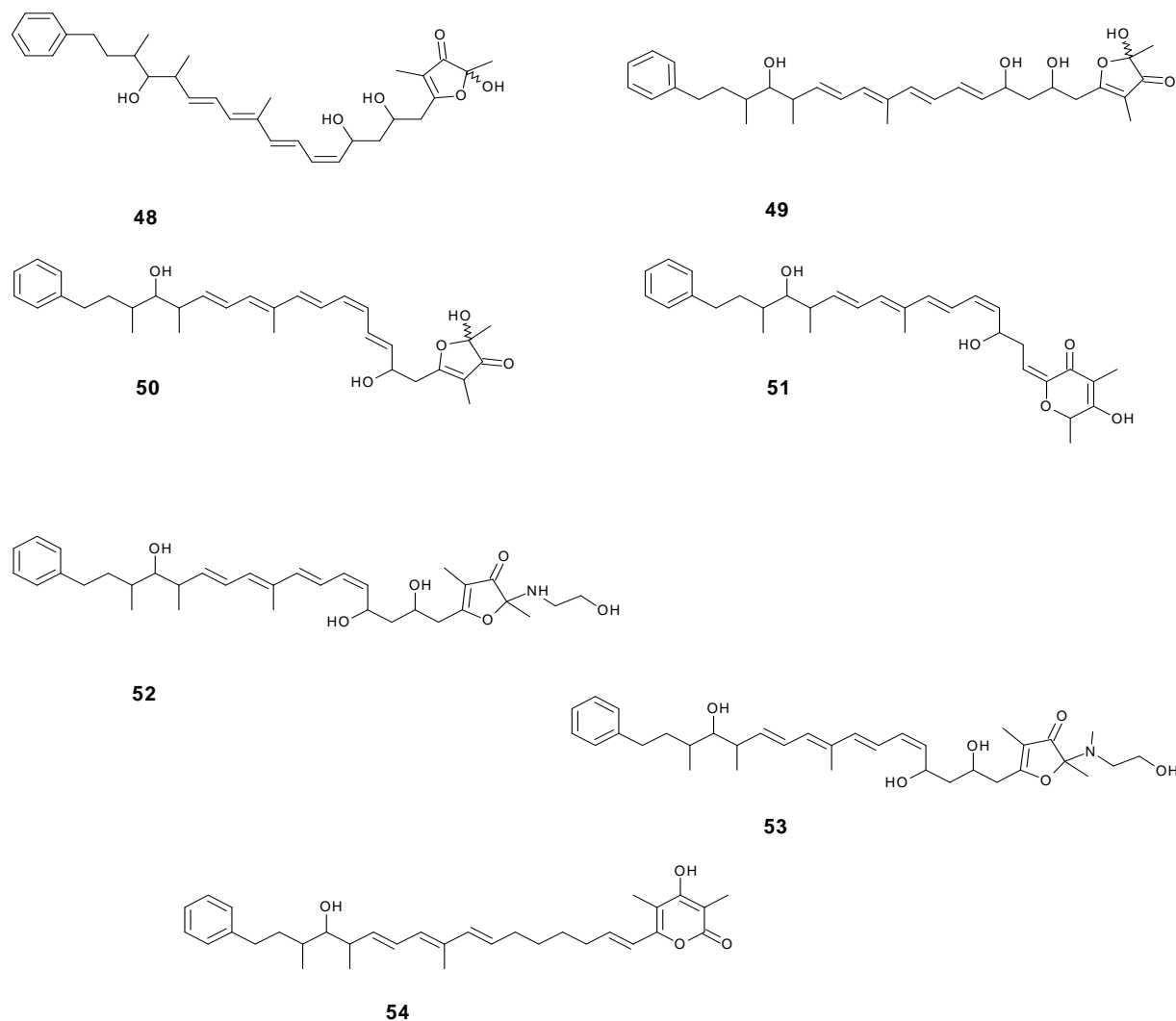
Figure 28. Structures of hyafurones; A$_1$ (**48**), A$_2$ (**49**), B (**50**), C (**52**), D (**53**), and hyapyrones; A (**51**), B (**54**).

Hyafurone B (**50**) was the second major compound of the hyafurones in the extract. Unlike hyafurone A$_1$ (**48**), **50** was identified in the methanol crude extract of strain NOCB-2^T as possessing activity against *S. aureus*, *N. flava, C. violaceum*, and *M. hiemalis* after fractionations with bioassays. The molecular formula $C_{32}H_{42}O_5$ was established from the HRESIMS and isotopic pattern analysis of the molecular ion at *m/z* 507.3099 [M+H]$^+$ and the sodiated ion [M+Na]$^+$ at *m/z* 529.2923. Similar to **48**, the ion clusters at *m/z* 489.2996, 471.2885, 453.2772 (Figure 29) displayed sequential losses of water molecules from the

compound. The molecular ion at *m/z* 507.3099 had been identified as a fragment ion of **48** from elimination of water.
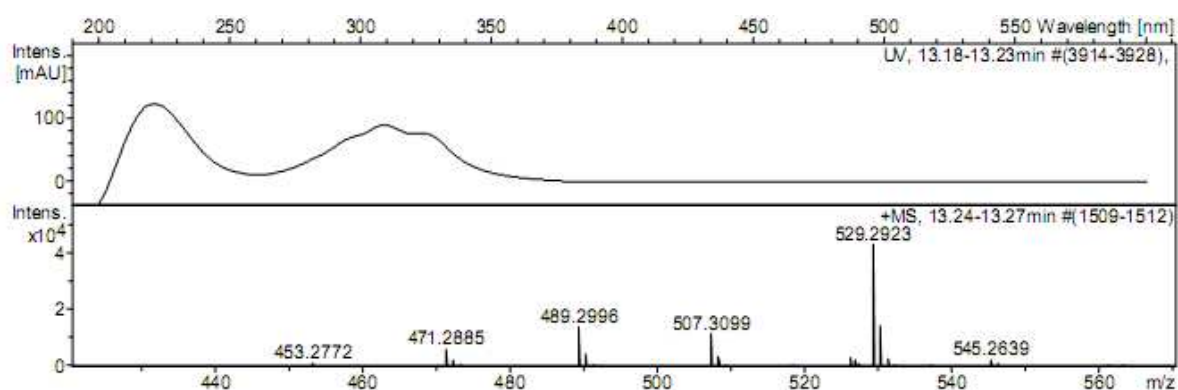
Figure 29. UV-MS of hyafurone B (**50**) with a λ_{max} 306 nm and various molecular ion clusters. The base peak at *m/z* 529.2923 is the sodiated molecular ion cluster [M+Na]$^+$ while the ion clusters at *m/z* 489.2996, 471.2885 and 453.2772 represented sequential loss of water from the actual [M+H]$^+$ ion *m/z* 507.3099.

The ^{1}H and ^{13}C NMR spectra of **50** in CD$_3$OD were similar to **48**. The only differences were found in the methylene CH$_2$-8 ($\delta_{H,C}$ 1.69, 1.91/45.2) and methine CH-9 ($\delta_{H,C}$ 4.92/66.5) of **48** (Table 12) which were shifted to the unsaturated methines $\delta_{H,C}$ 6.61/121.1 and $\delta_{H,C}$ 6.89/141.1 in hyafurone B (**50**) (Table 14), respectively, showing the extension of the polyene by a formal elimination of water. The relative *trans* configuration of the new $\Delta^{8,9}$ double bond was assigned from the large vicinal proton coupling constant $^3J_{8,9}$ = 15.3 Hz , while the *cis* configuration of the $\Delta^{10,11}$ double bond (Figure 30) was assigned from a small vicinal coupling constant of $^3J_{10,11}$ = 11.1 Hz together with strong NOE correlations between the methyl protons CH$_3$-30 (δ_H 1.93) and CH-12 (δ_H 6.58) and between the methines CH-8 (δ_H 6.61) and CH-10 (δ_H 5.43).

47
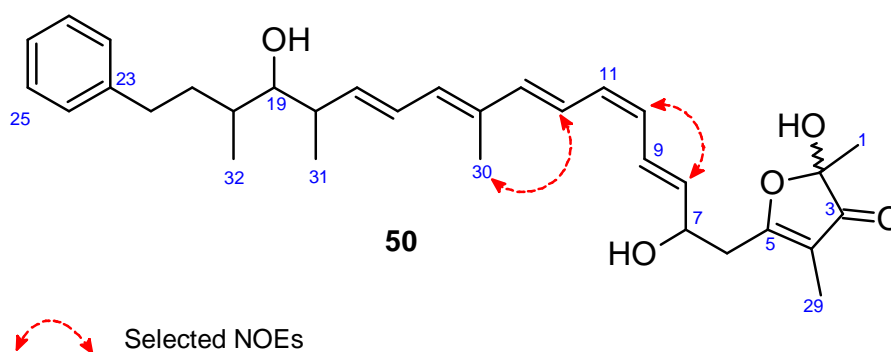
Figure 30. A small vicinal proton coupling constant of $^3J_{10,11}$ = 11.1 Hz together with strong NOEs of neighbouring groups supported the assignment of a *cis* configuration.

Hyapyrone A (**51**) an isomer of hyafurone B (**50**) was isolated independently as a minor compound of the strain NOCB-2[T]. HRESIMS of **51** displayed an [M+H]$^+$ peak at *m/z* 507.3103 consistent with the molecular formula $C_{32}H_{42}O_5$. 1D and 2D NMR data of **51** acquired in CD_3OD exhibited many similarities to those observed with hyafurone B (**50**) (Tables 14 and 15). The structural assignment of the western fragment from the phenyl moiety to the methine group CH-9 (δ_H 5.43, δ_C 132.8) of **51** was identical to the similar fragment of **50**. Notable differences in the ^{1}H NMR spectrum of **51** were a methine quartet at δ_H 4.89 (H-4), a methine triplet at δ_H 6.17 (H-6) and shifts of two methyl signals H-28 and H-29 (δ_H 1.84, s and δ_H 1.52, d, *J* = 6.6) compared to similar methyl signals H-1 and H-29 (δ_H 1.45, s and δ_H 1.76, s) in **50**. The assignment of the eastern fragment of the structure was derived by COSY and long-range HMBC correlations. The short fragment from H-6 to H-9 was assigned from the adjacent ^{1}H,^{1}H COSY cross peaks in the chain. Another COSY correlation was observed between the methine H-4 and methyl H-29 protons. The pyranone ring and its connection to the rest of the molecule were assigned from HMBC correlations shown in Figure 31.

————— Selected ^{1}H, ^{1}H COSY

⌒⟶ Selected ^{1}H, ^{13}C HMBC
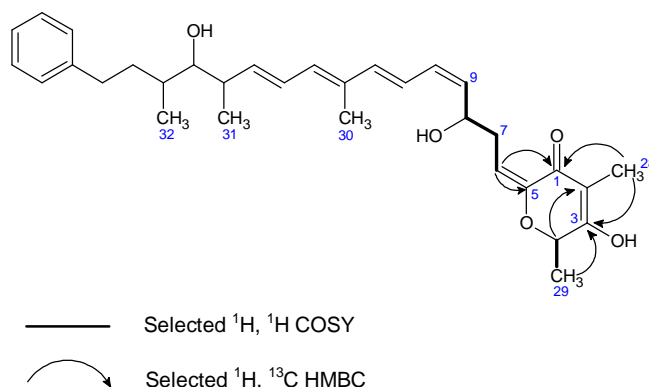
Figure 31.   Selected ^{1}H,^{1}H COSY and ^{1}H, ^{13}C HMBC correlations of hyapyrone B (**51**).

Hyafurone C (**52**) was the third member of the polyketide family to be isolated. HRESIMS analysis of **52** showed a molecular ion [M+H]$^+$ at m/z 568.3634 indicating an empirical formula of $C_{34}H_{49}NO_6$ with eleven degrees of unsaturation (Figure 32). The ion cluster at m/z 550.3538 represents the loss of a water molecule. Additionally present was the sodiated ion [M+Na]$^+$ at m/z 590.3450 which supported the assigned molecular formula unambiguously.

Two additional carbons, five protons, and nitrogen (C_2H_5N) were calculated from the elemental formulae in addition to the composition of the main component hyafurone A$_1$ (**48**). The structure of hyafurone C (**52**) was elucidated from 1D and 2D NMR spectroscopic data in CD$_3$OD (Table 16). In the NMR spectra the major part i.e. from the phenyl moiety to the furanone ring quaternary carbon at C-7 was similar to the same positions in **48**. The latter **52** was only substituted at the hydroxyl group of the furanone ring.
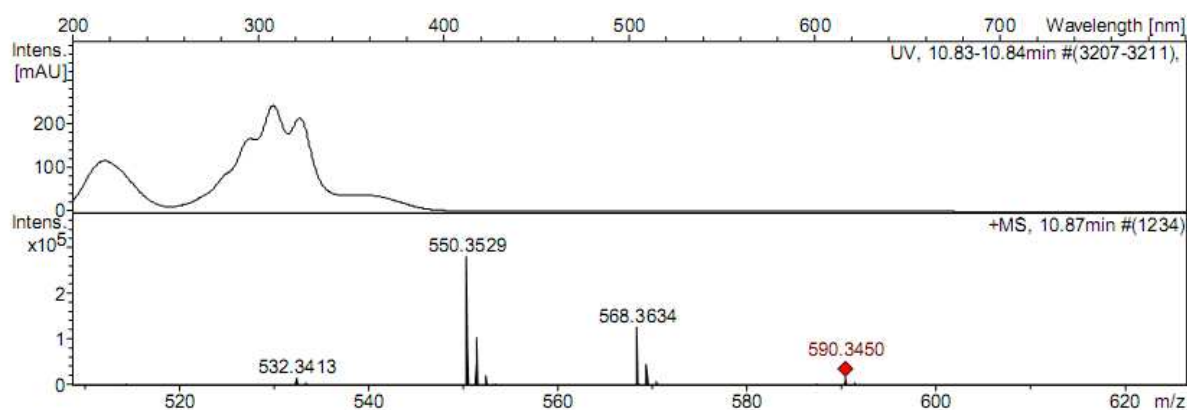
Figure 32.   UV-MS of hyafurone C (**15**), with a UV λ_{max} at 307 nm and the molecular ion [M+H]$^+$ at m/z 568.3634. The sodiated ion cluster at m/z 590.3450 [M+Na]$^+$ and two fragment ion clusters of sequential loss of water at m/z 550.3529 and 532.3413 are also indicated.

49

The nitrogen atom was observed as an amino group represented by a slowly exchanging broad singlet in the ^{1}H NMR spectrum at δ_H 8.60. COSY cross peaks observed between the new methylene protons H-1 and H-2 together with corresponding HMBC correlations unambiguously indicated that CH_2-1 and CH_2-2 were adjacent to each other. Since oxygen is more electronegative compared to nitrogen, the hydroxyl group was assigned to C-1 (δ_C 62.5) with a higher chemical shift compared to δ_C 45.0 of C-2 which was left as the only possible link to the NH group. A HMBC correlation between CH_2-2 (δ_H 3.52, 3.85) and the quaternary carbon C-4 (δ_C 89.5) indicated the connection of the ethanolamine residue to the hyafurone core structure. Hyafurone C (**52**) thus is the first compound with a nitrogen-linked ethanolamine at the furanone ring.
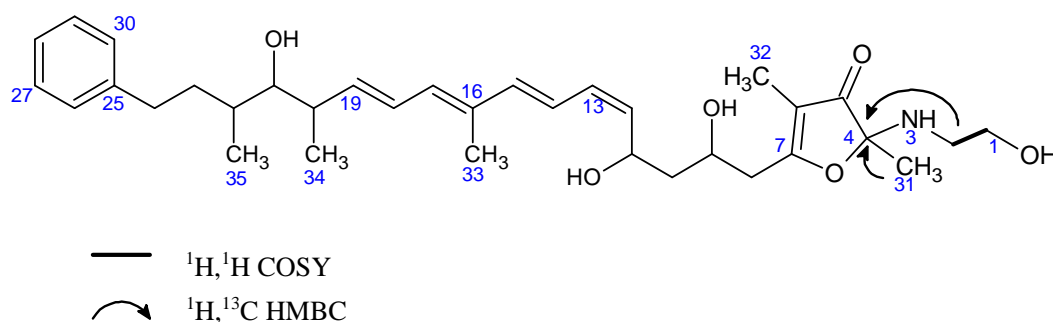
Figure 33. Selected COSY and HMBC correlations indicating the extension of the furanone ring in hyafurone C (**52**).

Like the preceding polyketides, hyafurone D (**53**) was also isolated from the strain NOCB-2^T. The structure of **53** was elucidated from the molecular formula $C_{35}H_{51}NO_6$, indicating eleven degrees of unsaturation which was established by HRESIMS analysis of the molecular ion peak [M+H]$^+$ at *m/z* 582.3788 (Figure 34). Compared to the empirical formula of hyafurone **52**, a formal addition of CH_2 was calculated.
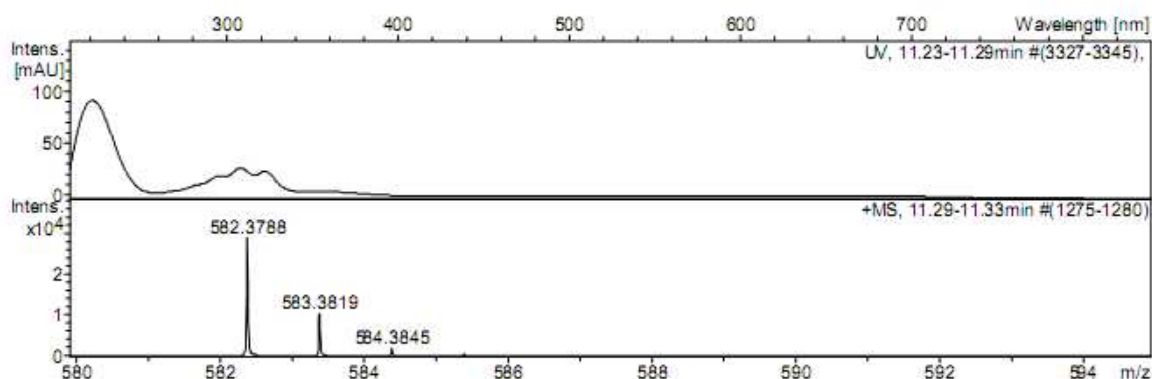
Figure 34. UV-MS of **16** showing the molecular ion cluster at *m/z* 582.3788 [M+H]⁺.

Structure elucidation was done by analysis of 1D and 2D NMR spectroscopic data acquired in CD$_3$OD. The NMR data of hyafurone **53** were near identical to **52** (Table 16). However, for **53** the NMR spectra presented an additional methyl group CH$_3$-36 with typical chemical shifts of a N-methyl group (δ_H 2.98, δ_C 52.2). A HMBC correlation was observed between the new methyl protons and the quaternary carbon C-4 (δ_C 93.7) supporting a methyl substitution at the amino group (Figure 35). Additionally, NOE's were observed between these methyl protons (CH$_3$-36, δ_H 2.98, s) and methylene protons (CH$_2$-2) at δ_H 3.53 and δ_H 3.71 together with CH$_3$-31 (δ_H 1.35, s) unambiguously indicating the position of the new N-methyl group.
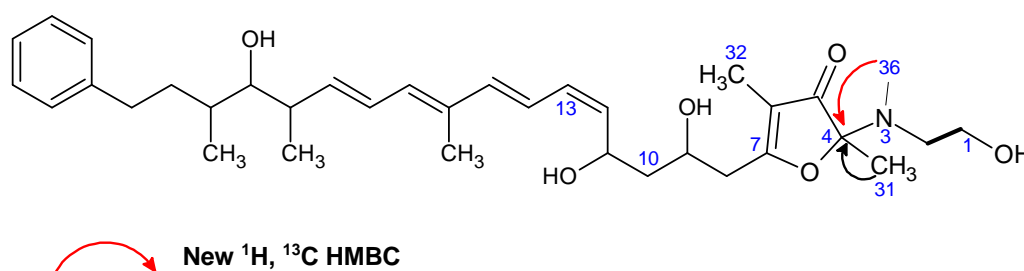
New ¹H, ¹³C HMBC

Figure 35. The new ¹H, ¹³C HMBC correlation between the methyl group (CH$_3$-36) and the quaternary carbon at C-4 in hyafurone D (**53**).

Hyapyrone B (**54**) was isolated from a 70 L large scale fermentation of *H. minutum* strain Hym 3. The molecular formula of **54** was determined as C$_{33}$H$_{44}$O$_4$ from the HRESIMS analysis showing a molecular ion [M+H]⁺ at *m/z* 505.3323 with 12 degrees of unsaturation. The structure elucidation was achieved by analyzing both 1D and 2D NMR spectroscopic data in CD$_3$OD (Table 17). The western fragment from the phenyl moiety to the aliphatic

group at CH-12 including the three methyl groups C*H*$_3$-31 to C*H*$_3$-33 and the hydroxyl group 19-OH was assigned from identical correlations observed in the 2D NMR spectra of the other hyafurones. The remaining structural parts of **54** were elucidated by joining a fragment derived from COSY cross peaks (CH-6 to CH$_2$-11) to a pyranone moiety elucidated from long range HMBC correlations (Figure. 36). The new pyranone moiety was assigned solely from the HMBC correlations observed between the methyl protons CH$_3$-29 and carbonyl C-1 (δ_C 167.8) and the enol carbon C-3 (δ_C 168.8) and from the correlations between methyl protons CH$_3$-30 (δ_H 2.04) and C-3 and C-4 (δ_C 109.3). The chemical shifts of these methyl groups CH$_3$-29 (δ_H 1.97, δ_C 9.0) and CH$_3$-30 (δ_H 2.04, δ_C 9.5) were similar to those observed for the pyranone moiety of the three polypropionates aglajne-3, -5, and -6, and dehydroaglajne-3 at equivalent positions[125,126] supporting our assignment and leaving the quaternary carbon C-5 (δ_C 153.5) as the only possible link to the remaining part of the molecule, which was supported by a small HMBC correlation between the olefin proton H-6 (δ_H 6.42) and C-5.

     —————   Selected ^{1}H,^{1}H COSY

     ⌒→   Selected ^{1}H, ^{13}C HMBC
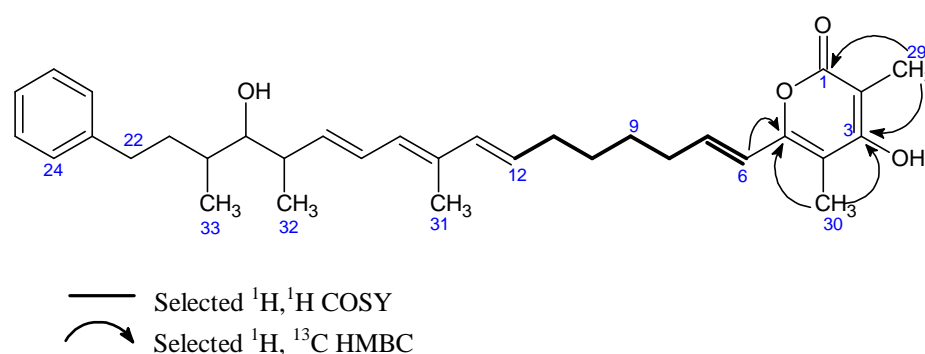
Figure 36. Selected ^{1}H,^{1}H COSY and ^{1}H,^{13}C HMBC NMR correlations of hyapyrone B (**54**).

Table 12. NMR data of hyafurone A$_1$ (**48**) in CD$_3$OD (^{1}H 600 MHz, ^{13}C 150 MHz).

No.	δ$_{H,}$ m (*J* in Hz)	COSY	ROESY	δ$_C$	HMBC ($^1J_{C,H}$ [Hz])
1	1.46, br.s			22.1, CH$_3$	1 (130)
2				104.2, qC	1
3				205.3, qC	1, 29
4				110.1, qC	6a/b, 29
5				186.6, qC	6a/b, 29
6a	2.74,dd (13.9, 7.3)	6b, 7	7, 29	38.6, CH$_2$	8a/b
6b	2.79, dd (7, 5.5)	6a, 7	7, 29		
7	4.10, m	6b, 8a/b	6a/b, 9, 29	68.0, CH-OH	6a/b, 9
8a	1.91, m	7, 8b, 9	8b, 9	45.2, CH$_2$	6a/b, 9, 10
8b	1.69, m	7, 8a, 9			
9	4.92, q (7.6)	8a/b, 10	12, 7, 8a >8b	66.5, CH-OH	8a/b, 11
10	5.36, q (9.7)	9, 11	7, 8b>8a, 11	133.4, CH	8a/b, 13
11	6.21, t (11.0)	10, 12	10, 13	132.0, CH	12, 13,
12	6.68, dd (15.0, 11.4)	11, 13	9, 30	123.8, CH	10, 11
13	6.36, d (15.0)	12	11, 15	140.6, CH	11, 15, 30
14				134.5, qC	12, 16, 30
15	6.14, d (11.4)	16	13, 17	134.0, CH	16, 17
16	6.48, dd (14.9, 11.2)	15, 17	18, 30, 31	128.3, CH	15, 18
17	5.80, dd (15.1, 8.4)	16, 18	15, 19, 31	140.0, CH	15, 19, 31
18	2.49, dquin (8.4, 6.7)	17, 19, 31	16, 20, 31, 32	42.1, CH	16, 17, 19, 31
19	3.28, t (5.9)	18, 20	17, 21a/b, 31,32	79.3, CH-OH	17, 21a/b, 31, 32
20	1.63, m	19, 21a/b, 32	18, 21a/b, 22a/b	36.3, CH	21a/b, 32
21a	1.83, ddd(13.8, 9.4, 5.7)	20, 21b, 22a/b	19, 22a/b, 32	36.8, CH2	19, 22a/b, 32
21b	1.52, ddd (13.6, 9.0, 5.5)	20, 21a, 22a/b	19, 22a/b, 32		
22a	2.71, ddd (13.8, 9.4 5.7)	21a/b, 22b,	19, 20	34.3, CH$_2$	20, 21a/b, 24, 28
22b	2.62, ddd (13.7, 9.3, 6.8)	21a/b, 22a	19, 20		
23				144.0 qC	25, 27
25	7.20, d (7.0)			129.4, qC	22a/b, 26, 28
24	7.26, t (7.3)			129.3, qC	23, 27
26	7.16, t (7.3)			126.6, qC	24, 28
28	7.26, t (7.3)			129.3, qC	23, 25,
27	7.20, d (7.0)			129.4, qC	22a/b, 24, 26
29	1.71, m	-	6a/b	5.8, qC	29 (129)
30	1.94, s	15	12, 16	12.8, qC	13, 15, 30 (125)
31	1.03, d (6.6)	18	16, 17, 19	18.3, qC	16, 17, 19, 31 (126)
32	1.00, d (6.6)	20	18, 21b , 22a/b	14.2, qC	19, 21a/b, 32 (125)

Table 13. NMR data of hyafurone A$_2$ (**49**) in CD$_3$OD (^{1}H 600 MHz, ^{13}C 150 MHz).

No	δ$_H$, m (*J* in Hz)	COSY	ROESY	δ$_C$	HMBC ($^1J_{C,H}$ in Hz)
1	1.47, br. s			22.2, CH$_3$	1(128)
2				104.2, qC	
3				205.3, qC	1, 29
4				110.2, qC	6a/b, 29
5				186.6, qC	
6a	2.75, m	6b, 7	8a/b, 29 >9	38.4, CH$_2$	8a/b
6b	2.79, dd (13.9, 7.3)	6a, 7	8a/b, 29 >9		8a/b
7	4.14, br. s	6a/b, 8a/b	8a/b, 9, >10, 12	68.0, CH-OH	6a/b, 9, 8a/b
8a	1.87, ddd (14.0, 7.0, 2.2)	7, 8b, 9	6a/b, 10	45.2, CH$_2$	6a/b, 9, 10
8b	1.74, m	7, 8a, 9	6a/b, 10		
9	4.39, q (7.0)	8a/b, 10	6a/b, 8a/b, 11	71.5, CH-OH	8a/8b, 10, 11
10	5.73, dd (14.1, 6.8)	9, 11	8a/b, 12	135.8, CH	8a/b, 9, 10 (152)
11	6.37 , ddd (14.0, 5.9, 2.6)	10, 12	9 >7	132.9, CH	
12	6.33, m[a]	11,13	10, 30	128.1, CH	10, 12(152), 13, 15
13	6.35, m[a]	12	15	139.1, CH	13, 16, 30
14				134.3, qC	
15	6.11, d (11.0)	16, 30[b]	13, 17	133.4, CH	13, 14, 15(151), 17
16	6.47, dd (15.0, 11.4)	15, 17	18, 30, 31	128.3, CH	16(150), 18
17	5.78, dd (15.0, 8.4)	16, 18	15, 19, 31	139.6, CH	15, 17(151) 19, 31
18	2.49, dquin (8.4, 6.7)	17, 19, 31	16, 20, 31, 32	42.1, CH	16, 17, 19, 31
19	3.28, t (5.7)	18, 20	17, 21a/b, 31, 32	79.3, CH-OH	17, 19 (139), 21a/b, 31, 32
20	1.63, m	19, 21a/b, 32	18, 22a/b, 32	36.3, CH	21a/b
21a	1.83, ddd (13.2, 9,9, 5.1)	20, 21b, 22a/b,	19, 22a/b, 32	36.8, CH$_2$	19, 20, 22a/b, 32
21b	1.52, ddd (13.6, 9.0, 5.5)	20, 21a, 22a/b	19, 22a/b		
22a	2.71, ddd (13.8, 9.4, 5.7)	21a/b, 22b	19, 20, 32	34.3, CH$_2$	20, 21a/b, 24, 28
22b	2.62, ddd (13.7, 9.3, 6.8)	21a/b, 22a	19, 20, 32		
23				143.9 qC	21a/b, 25, 27
24	7.20, d (7.0)	25		129.4, qC	26, 28
25	7.26, t (7.3)	24, 26		129.3, qC	27
26	7.16, t (7.3)	25,27		126.6, qC	24, 26(162), 28
27	7.26, t (7.3)	26, 28		129.3, qC	23, 25
28	7.20, d (7.0)	27		129.4, qC	24, 26
29	1.71, s		6a/b	5.8, qC	29(128)
30	1.91, s	15[b]	12, 16,	12.7, qC	12, 15, 30 (126)
31	1.03, d (7.0)	18	16, 17, 19	18.3, qC	16, 17, 19, 31 (127)
32	1.00, d (6.6)	20	18, 21a/b, 22a/b	14.2, qC	19, 21a/b,26, 32 (125)

[a]overlapping signals, [b] 4-bond COSY correlations.

Table 14. NMR Data of Hyafurone B (**50**) in CD$_3$OD (^{1}H/^{13}C 600/150 MHz).

No.	δ$_H$, m (*J* in Hz)	COSY	ROESY	δ$_C$	HMBC ($^1J_{C,H}$ in Hz)
1	1.45, s			22.3, CH$_3$	1 (128)
2				103.8, qC	1
3				204.9, qC	1, 29
4				108.4, qC	29
5				178.3, qC	29, 8
6a	2.63, m	6b, 7	8, 9 >10	42.5, CH$_2$	8, >9, 4, 5
6b	2.55, m	6a, 7	8, 9 >10		
7	4.81, m	6a/b, 8	9, >10	67.8, CH	6, 9,>>11
8	6.61, m[a]	9	6a/b, 9, 10	121.1, CH	6,10
9	6.89, ddt (15.3, 13.5,7.4)	8, 10	6a/b, 7, 8	141.1, CH	6, 7
10	5.43, m	9, 11	6a/b, 8, 11	133.0, CH	8 >6
11	6.20, td (11.1, 9.8)	10, 12	10, 13	131.7, CH	12, 13
12	6.58, m[a]	11, 13	30	123.4, CH	11
13	6.36, d (15.0)	12	11, 15, 30	140.8, CH	11, 30
14				134.4, qC	12,30
15	6.14, d (11.0)	16, 30[b]	13, 17	134.2, CH	16, 17, 30
16	6.47, dd (15.0,11.1)	15, 17	18, 30, 31	128.2, CH	15, 18
17	5.80, dd (15.0, 8.8)	16, 18	15, 19, 31	140.2, CH	15, 19, 31
18	2.48, m	17, 19, 31	16, 20, 31, 32	42.1, CH	16, 20, 31
19	3.28, t (5.7)	18, 20	17, 21a/b, 31, 32	79.2, CH	17, 21, 31, 32
20	1.63, m	19, 21a/b, 32	18, 22a/b, 32	36.3, CH	19, 32
21a	1.51, m	20, 21b, 22a/b,	19, 22a/b, 32	36.8, CH$_2$	19, 22, 32
21b	1.82, m	20, 21a, 22a/b	19, 22a/b		
22a	2.63, m	21a/b, 22b	19, 20, 32	34.3, CH$_2$	20, 21, 24, 28
22b	2.71, m	21a/b, 22a	19, 20, 32		
23				143.9, qC	
24	7.20, d (7.0)	25		129.4, CH	22, 26, 28
25	7.26, t (7.0)	24, 26		129.3, CH	23, 27, 28
26	7.16, t (7.0)	25,27		126.6, CH	24, 28
27	7.26, t (7.0)	26, 28		129.3, CH	23,25
28	7.20, d (7.0)	27		129.4, CH	22, 24, 26
29	1.76, s			5.4, CH$_3$	29 (128)
30	1.93, s	15[b]	12, 16,	12.8, CH$_3$	13, 15
31	1.03, d (6.6)	18	16, 17, 19	18.3, CH$_3$	31(127), 17, 18
32	1.00, d (6.6)	20	18, 21a/b, 22a/b	14.2, CH$_3$	32(127),19, 22

[a] overlapping signals [b] 4-bond COSY correlations.

Table 15.   NMR Data of Hyapyrone A (**51**) in CD$_3$OD (^{1}H/^{13}C 600/150 MHz).

C/H	δ$_H$, m (J [Hz])	COSY	ROESY	δ$_C$	HMBC ($^1J_{C,H}$ in Hz)
1	-			189.8 qC	6, 28
2	-			113.4 qC	28 >4
3	-			181.0 qC	28, 29 >4
4	4.89, q (6.6)	29	28	64.5 CH	29
5				150.0 qC	6, 7a/7b
6	6.17, t (8.1)	7a/7b	7a/7b	114.8 CH	7a/7b, 8
7a	2.73, ddd (14.7, 8.1, 7.0)	6, 7b, 8	9	35.0 CH$_2$	9 >8
7b	2.63, m	6, 7a, 8	9		
8	4.82, m	7a/b, 9	6, 7a/b, 9, 11	67.6 CH	7a/7b, 10
9	5.43, dd (10.6, 9.2 br.)	8, 10	6, 7a/b, 10	132.8 CH	7a/7b, 11
10	6.19, t (11.0 br.)	9, 11	9, 12	131.9 CH	8, 11, 12,
11	6.57, dd (15.2, 11.6)	10, 12	8, 30	123.3 CH	9, 10
12	6.35, d (15.2)	11	10, 14, 30	140.9 CH	10, 30
13	-			134.4 qC	
14	6.14, d (11.4)	15, 30	12, 16	134.2 CH	11, 12, 15, 16, 30,
15	6.48, dd (14.9, 11.2)	14, 16	17, 30	128.3 CH	14, 17
16	5.80, dd (15.0, 8.8)	15, 17	14, 18, 31	140.2 CH	14, 17, 18, 31
17	2.49, dt (8.8, 6.6)	16, 18, 31	15, 19, 20a/b, 32	42.1 CH	15, 16, 18, 31
18	3.28, t (5.9)	17, 19	16, 20a/b, 21a/b, 31	79.2 CH	16, 17, 20a/b, 31, 32,
19	1.62, m	18, 20a/b, 32	17, 21a/b, 31	36.3 CH	32
20a	1.52, m	20b, 21a/b, 19	17, 18, 32 >31	36.8 CH$_2$	18, 19, 21a/b, 32
20b	1.84, m	20a, 21a/b, 19	17, 18, 32 >31		
21a	2.63, m	21b, 20a/b	23, 27	34.3 CH$_2$	19, 20a/b, 23, 27
21b	2.70, dd (9.5, 5.9)	21a, 20a/b	23, 27		
22	-			143.9 qC	20a/b, 21a/b, 24, 26
23	7.20, d (6.6)	24	21a/b	129.4 CH	
24	7.26, t (7.3)	23, 25		129.3 CH	
25	7.16, t (7.4)	24, 26		126.6 CH	23, 27
26	7.26, t (7.3)	25, 27		129.3 CH	21a/b, 24, 25, 27
27	7.20, d (6.6)	26	21a/b	129.4 CH	21a/b
28	1.84, s		29	5.3 CH$_3$	(128 Hz)
29	1.52, d (6.6)	4	28	20.6 CH$_3$	(129 Hz),4
30	1.92, s	14	11, 12, 15, 30	12.8 CH$_3$	(127 Hz), 12, 14
31	1.04, d (7.0)	17	15, 16, 18, 19	18.3 CH$_3$	(127 Hz) 16, 17, 18
32	1.00, d (6.6)	19	20a/b, 21a/b	14.2 CH$_3$	(125 Hz),18, 19, 20a/b

Table 16. NMR Data of Hyafurone C (**52**) and Hyafurone D (**53**) in CD$_3$OD (^{1}H/^{13}C 600/150 MHz).

C/H	Hyafurone C δ_H, m (*J* in Hz)	δ_C	HMBC ($^1J_{C,H}$ in Hz)	Hyafurone D δ_H, m (*J* in Hz)	δ_C	HMBC ($^1J_{C,H}$ in Hz)
1a	3.66, m	62.5, CH$_2$	2a/2b	3.72, m	62.0, CH$_2$	2
1b	3.74, m			3.74, m		
2a	3.52, dt (15,1, 5,9)	45.0, CH$_2$	1a/b	3.53, m	44.9, CH$_2$	1
2b	3.85, dt (15,1, 5,9)			3.71, m		
NH	8.60, br, s			8.57, br. s		
4		89.5, qC	31, 2a/2b		93.7, qC	2, 31, 36
5		201.1, qC	31, 32		199.0, qC	31, 32
6		102.0, qC	8, 32		104.6, qC	8, 32
7		178.2, qC	8, 32 >2a/2b		180.6, qC	2, 8, 32
8	2.90, m	36.2, CH$_2$	10	2.94, m	36.3, CH$_2$	10
9	4.03, m	68.6, CH	8, 10, 11	4.04, m	68.5, CH	8, 10, 11
10a	1.96, m	45.7, CH$_2$		1.94, m	46.2, CH$_2$	8, 11
10b	1.69, m			1.69, m		
11	4.92, quin (7.7)	66.6, CH	13	4.88,	66.6, CH	13
12	5.36, ddd (14.3, 11.4, 2.2)	133.3, CH	10	5.33	133.4, CH	10
13	6.22, td (11.0, 4.03)	132.1, CH	11, 15	6.17, td (11.0, 4.03)	131.9, CH	11, 15
14	6.67, dd (15.0 11.4)	123.6, CH	12,13	6.63, dd (15.0, 11.4)	123.6, CH	12,13
15	6.36, d (15.0)	140.7, CH	13, 17, 18, 33	6.32, dd (15.0, 2.2)	140.6, CH	13, 17, 18, 33
16		134.5, qC	14, 33		134.4, qC	14, 33
17	6.14, d (11.0)	134.0, CH	15, 19	6.10, d (11.0)	133.9, CH	17 (150.8), 15, 18
18	6.48, dd (14.9, 11.2)	128.3, CH	17, 20	6.43, dd (15.0, 11.4)	128.2, CH	18 (150.9), 17
19	5.80, dd (15.0, 8.4)	140.0, CH	17, 34	5.76, dd (15.0, 8.8)	140.0, CH	19 (150.8), 21, 34
20	2.49, dquin (8.1, 6.6 br)	42.1, CH	18, 21, 34	2.45, m	42.1, CH	18, 21, 34
21	3.28, t (5.7)	79.2, CH	19, 23, 34, 35	3.24, t (5.7)	79.2, CH	21(142.8), 34, 35
22	1.61, m	36.3, CH	35	1.59, dt (12.9, 6.2)	36.3, CH	35
23a	1.50, m	36.7, CH$_2$	21, 22, 24, 35,	1.48, m	36.7, CH$_2$	21, 22, 24, 35,
23b	1.83, m			1.79, m		
24a	2.71, ddd (14.7, 9.5, 5.5)	34.3, CH$_2$	23, 26, 30	2.67, ddd (14.7, 9.5, 5.5)	34.3, CH$_2$	23, 26, 30
24b	2.62, ddd (13.7, 9.5, 6.6)			2.58, ddd (13.7, 9.4)		
25	-	143.9, qC	23, 24, 27, 29		143.8, qC	23, 24, 27, 29
26	7.20, d (7.3)	129.4, CH	24, 28, 30	7.16, d (7.3)	129.4, CH	24, 28, 30
27	7.25, t (7.3)	129.3, CH	29, 25	7.22, t (7.3)	129.2, CH	29, 25
28	7.15, t (7.3)	126.6, CH	26, 30	7.12, t (7.3)	126.6, CH	26, 30
29	7.25, t (7.3)	129.3, CH	24, 27	7.22, t (7.3)	129.2, CH	24, 27
30	7.20, d (7.3)	129.4, CH	24, 26, 28	7.16, d (7.3)	129.4, CH	24, 26, 28
31	1.39, s	22.2, CH$_3$	31 (129.6)	1.35, s	22.0, CH$_3$	31 (129.9)
32	1.71, s	6.8, CH$_3$	32 (127.9)	1.69, s	6.5, CH$_3$	32 (127.9)
33	1.93, s	12.8, CH$_3$	15, 17	1.89, s	12.7, CH$_3$	33 (127.9) 15, 17
34	1.03, d (7.0)	18.3, CH$_3$	19, 21	0.99, d (6.6)	18.3, CH$_3$	34 (127.1) 19, 21
35	1.00, d (6.6)	14.2, CH$_3$	35 (125.8), 21	0.96, d (7.0)	14.2, CH$_3$	35 (125.8), 21
36				2.98, s	52.2, CH$_3$	4

Table 17. NMR Data of Hyapyrone B (**54**) in CD_3OD (^1H 600 MHz, ^{13}C 150 MHz).

No.	δ_H, m (J inHz)	COSY	ROESY	δ_C	HMBC ($^1J_{C,H}$ in Hz)
1				167.8, qC	29
2				99.8, qC	29
3				168.8, C-OH	29, 30
4				109.3, qC	30
5				153.5, qC	6, 7, 30
6	6.42, t (5.5)	7, 8	8, 30	120.3, CH	8
7	6.64, quin (7.6)	6, 8	9	139.2, CH	8, 9
8	2.33, q (6.9)	6, 7, 9	6, 10	33.8, CH_2	6, 7, 10
9	1.53, m	8	6, 7, 11, 12,	29.6, CH_2	7, 11
10	1.53, m	11	8, 12	30.3, CH_2	8, 9, 11,
11	2.21, q (6.7)	10, 12, 13	9, 12, 31	33.8, CH_2	9, 12, 13,
12	6.13, d (15.4)	11, 13	10, 15, 31	136.5, CH	11, 14, 15, 31
13	5.72, m	11, 12	11, 15, 31	129.7, CH	11, 14, 15, 31
14				134.2, qC	12, 13, 16, 31
15	5.97, d (11.0)	16, 31	13, 17,18, 31	130.8, CH	12, 13, 16, 31
16	6.45, t (5.5)	15, 17	18, 31, 32	128.3, CH	15, 18
17	5.72, m	16, 18	15, 19, 20, 32	138.1, CH	15, 18, 32
18	2.46, m	17, 19, 32	16, 20, 21, 33	42.0, CH	16, 17, 19, 32
19	3.27, t (5.9)	18, 20	17, 21a/b, 32, 33	79.3, CH-OH	17, 21a/b, 32, 33
20	1.62, m	19, 33	18, 22a/b,	36.3, CH	19, 21a/b, 33
21a	1.53, m	21b, 22a/b	18, 19,24, 28, 33	36.7, CH_2	19, 22a/b, 33
21b	1.82, m	21a, 22a/b	18, 19,24, 28, 33		
22a	2.71, ddd (13.6, 9.5, 6.4)	21a/b, 22b	19, 20, 24, 28, 33	34.3, CH_2	21a/b, 24, 28
22b	2.62, ddd (13.6, 9.5, 6.6)	21a/b, 22a	19, 20, 24, 28, 33		
23				143.9, qC	21a/b, 25, 27
24	7.20, d (7.3)	25	22a/b	129.4, CH	
25	7.25, t (7.3)	24, 26		129.3, CH	
26	7.15, t (7.3)	25, 27		126.6, CH	24, 28
27	7.25, t (7.3)	26, 28		129.3, CH	25
28	7.20, d (7.3)	27	22a/b	129.4, CH	22a/b, 24, 26
29	1.97, s			9.1, CH_3	29 (130)
30	2.04, s		6	9.5, CH_3	30 (129)
31	1.87, s	15	12, 13, 15, 16	12.9, CH_3	12, 15, 31 (129)
32	1.02, d (7.0)	18	16, 17, 18, 19	18.4, CH_3	17, 19, 18, 32(127)
33	1.00, d (7.0)	20	18, 19, 21a/b, 22a/b	14.2, CH_3	19, 21a/b, 33 (125)

2.6   Biological activities of hyafurones and hyapyrones

2.6.1   Antibacterial and antifungal activities

Antibacterial and antifungal testing of the polyketide family showed no significant biological activity at MIC concentrations between 67 and 0.52 µg/mL (Table 18). However, hyafurone B (**50**) displayed the highest activity with a MIC of 8.3 µg/mL against *N. flava*. Hyafurone D (**53**) was not active at 67 µg/mL in all the tests performed.

Table 18.   Minimum inhibition concentrations (MIC) of hyafurone A–F against selected bacterial and fungal pathogens in µg/mL.

Test organisms	MIC [µg/mL] of hyafurones/hyapyrones						
	48	**49**	**50**	**51**	**52**	**53**	**54**
Bacteria							
Micrococcus luteus	>67	>67	>67	>67	>67	>67	>67
Staphylococcus aureus	>67	>67	67	67	67	>67	>67
Escherichia coli TolC	>67	>67	>67	>67	67	>67	>67
Nocardia flava	67	>67	8.3	33.3	67	>67	16.6
Chromobacterium violaceum	67	67	33.3	67	>67	>67	67
Pseudomonas aeruginosa	>67	>67	>67	>67	>67	>67	67
Mycobacterium phlei	>67	67	>67	>67	67	>67	>67
Fungi and yeasts							
Mucor hiemalis	>67	67	67	>67	67	>67	33.3
Schizosaccharomyces pombe	>67	>67	>67	>67	>67	>67	>67
Rhodotorula glutinis	>67	>67	>67	>67	>67	>67	>67
Pichia anomala	>67	>67	>67	>67	>67	>67	>67
Candida albicans	>67	>67	>67	>67	>67	>67	>67

2.6.2   Cytotoxic activities

Cytotoxicity tests against four mammalian cell lines are shown in Table 19. Hyafurone A_1 (**48**) was cytotoxic against the primary cell line HUVEC with an IC_{50} of 1.4 µg/mL.

Table 19.   Cytotoxicity of hyafurones (IC_{50} μg/mL) against four mammalian cell lines. Only hyafurone A_1 (**48**) was tested against all the four cell lines.

Compound	L929	MCF-7	KB-3-1	HUVEC
48	14	2.2	3	1.4
50	>33.3	nt[a]	nt	nt
52	>33.3	nt	nt	nt
53	>33.3	nt	nt	nt
54	11	nt	nt	nt

[a] nt = not tested

2.6.3   Antiparasitic activity of hyafurone A$_1$ (48)

Only the major compound of the polyenes, hyafurone A$_1$ (**48**) was evaluated for anti-parasitic activity and was found to be in-active (Table 20). The assays were performed at the Swiss Tropical and Public Health Institute, Basel.

Table 20.   *In vitro* anti-parasitic activity of hyafurone A$_1$ (**48**) (IC$_{50}$ µg mL^{-1}).

Test drug/compound	*T. b. rhod.*	*T. cruzi*	*L. don. axen.*	*P. falc. K1*	Cytotoxicity L6
	IC$_{50}$	IC$_{50}$	IC$_{50}$	IC$_{50}$	IC$_{50}$
48	7.54	18.6	5.75	2.13	12.25
Melarsoprol	0.002				
Benznidazole		0.58			
Miltefosine			0.144		
Chloroquine				0.046	
Podophyllotoxin					0.005

3 Discussion

3.1 General scope of this work

The current thesis deals with isolation and structure elucidation of secondary metabolites from three strains of gliding bacteria, *Ohtaekwangia kribbensis* strain PWU 25 (a Bacteroidetes) and two strains from the myxobacterium *Hyalangium minutum*, strains NOCB-2[T] and Hym 3. Initially active extracts were dereplicated by analytical HPLC fractionation into 96-well plates. Following biological testing of each well with the target microorganism provided the peak-activity correlation. Similarly the active extract was analyzed by HPLC-UV-MS for peak-UV spectrum and peak-molecular mass or peak-elemental formula correlation. The data obtained were then used to recognize possibly known compounds in data bases, i.e. Dictionary of Natural Products on CD-Rom (DNP) (Chapman & Hall), the in-house Myxobase, and/or Chemical Abstracts (online).

Dereplication of the extract of *O. kribbensis* strain PWU 25 indicated one known and five novel compounds. An isolation strategy was developed that led to the isolation of six pyrroloquinoline metabolites, marinoquinoline A (**39**) previously isolated but solely characterized by X–ray crystallography[111] and five new derivatives (**40**-**44**). All structures were elucidated by detailed NMR analyses. When screened for biological activities, these pyrroloquinolines showed weak antibacterial and antifungal activities and moderate cytotoxicity against four growing mammalian cell lines. Additionally, they were also active when tested against *Plasmodium falciparum*, the parasite causing human malaria.

In a second project, a complex isolation scheme was developed for the metabolites of *H. minutum*, strain NOCB-2[T]. The major compound, hyaladione (**47**) an S-methyl cyclohexadiene-dione was finally purified by crystallization and its structure elucidated by X-ray analysis. Dereplication studies identified several other novel compounds in the crude extract of this strain. Consequently, six metabolites were isolated as members of a family, hyafurones and hyapyrones (**48** -**54**). Hyafurone A_2 (**49**) was isolated as a degraded isomer of hyafurone A_1 (**48**) but not directly from the isolate. In both hyapyrone A (**51**) and hyapyrone B (**54**) a pyranone moiety replaced the furanone while the aliphatic chain and the phenyl moiety were similar to the other hyafurones. Hyapyrone B (**54**), though identified in strain NOCB-2[T] was isolated from *H. minutum* strain Hym 3. Their structures were elucidated from

61

detailed HRESIMS and NMR data analyses. Comparison of the biological activity indicated **47** to be the most active compound of *H. minutum* displaying a broad spectrum of anti-bacterial, anti-fungal, cytotoxic and anti-parasitic activities.

3.2   Marinoquinolines A – F (39 - 44) from *O. kribbensis*

O. kribbensis strain PWU 25 was found to produce secondary metabolites, mainly marinoquinoline A (**39**), which had been identified previously from the marine microorganism   *Rapidithrix thailandica* as an acetylcholine esterase inhibiting agent.[121] The strain further produced five novel metabolites related to **39**. Since the main component, marinoquinoline A (**39**) was a pyrroloquinoline,[111] an isolation strategy utilizing the basic properties of alkaloids was employed by an acid/base extraction technique. A further size exclusion chromatography on Sephadex LH-20 enriched the main product, **39** finally enabling the crystallization from acetone/petroleum ether (1:1). Purification of the other marinoquinolines B-F (**40-44**) by RP HPLC was improved by acidification of the methanol/water solvent system with formic acid. The resulting salt solution of pyrroloquinolines was stable in the solvent and offered highly resolved peaks for efficient isolation.

Only marinoquinoline A (**39**) could be crystallized and its X-ray crystallographic analysis was replicated and compared with the analysis by the Kanjana group.[111] However, all other spectroscopic data had not been reported. All 1D and 2D NMR data recorded in deuterated methanol were analysed and correlated to the structure of **39**. Additionally, further physical characteristics including melting point, the UV- and IR-spectra were measured. The stretching vibration of the secondary amine in **39** was confirmed by a broad IR absorption band at v_{max} 3442 cm^{-1} in potassium bromide. Structures of all the other marinoquinoline derivatives (**40 - 44**) were elucidated by analyses of their molecular formulae generated from HRESIMS together with 1D and 2D NMR data. The 1D ^{13}C NMR signals in most spectra of the marinoquinolines were narrowly separated and therefore reported in two decimal places contrary to the conventional one decimal place. Additionally, special ^{13}C APT NMR experiments were performed to indicate the presence of some quaternary carbons that were otherwise observed as overlapping signals in the normal ^{13}C NMR spectrum and could not be observed in DEPT spectrum. This was particularly useful in differentiating between methine C-5b (δ_C 123.71) and the quaternary C-6 (APT δ_C 123. 72) of marinoquinoline E (**43**).

Prior to isolation, the crude extract of strain PWU 25 had displayed growth inhibition of various microorganisms tested as described in chapter 2.1.1. Since compounds with antibiotic activity often have been known to possess further activities, marinoquinolines A-F (**39-44**) also were tested for cytotoxicity. But they showed only moderate activity when evaluated with three growing cancer cell lines and a primary cell line (Table 7). The keto-indole variant **44** was the most toxic followed by the phenyl derivatives marinoquinolines C (**41**) and D (**42**), while the isopropyl variant 40 showed the least cytotoxicity.

The WHO malaria world report[127] showed that nearly a million people died from malaria in 2006 alone and that the resistance of the causative parasite, *Plasmodium falciparum* continues to increase against the available drugs. This situation necessitates the screening of diverse sources for new lead compounds against *P. falciparum* and other tropical parasites. Marinoquinoline related compounds have previously been screened against malaria. For example nostocarboline hydroiodide (**55**) (Figure 37), which can be seen as a halogenated isomer of marinoquinoline A (**39**), was isolated from the cyanobacterium, *Nostoc* 78-12A[128] and showed selective activity against *P. falciparum* K1 with an IC_{50} of 0.194 µM.[129] The IC_{50} value of 3*H*-pyrrolo[2,3-c]quinoline (**56**), the core alkaloid part of the marinoquinolines, was determined as 6.4 µM.[120] Other analogues include the plant alkaloid isoneocryptolepine (**57**) with an IC_{50} of 0.23 µM against *P. falciparum* K1 cells[130] and the spiroindolone NITD609 (**58**), an improved lead candidate in the fight against malaria. Mice infected with the highly virulent *Plasmodium berghei* were completely cured with a single oral dose (100 mg per kg) of NITD609, an effect that was not seen with similar doses of the current standard antimalarial drugs artesunate, artemether, chloroquine or mefloquine.[131,132]

In a screening against tropical parasites (Table 8) marinoquinolines B (**40**) and F (**44**) were identified as the most active structural variants with IC_{50} values of 1.8 and 1.7 µM, respectively. Based on their biological activities and particularly the anti *P. falciparum* activities, marinoquinolines have aroused interest of medicinal chemists with the total syntheses of marinoquinolines A-C (**39-41**) already accomplished.[133] Equally, another group from Australia has shown interest in the synthesis of marinoquinolines also because of their antiplasmodial activities.[134]
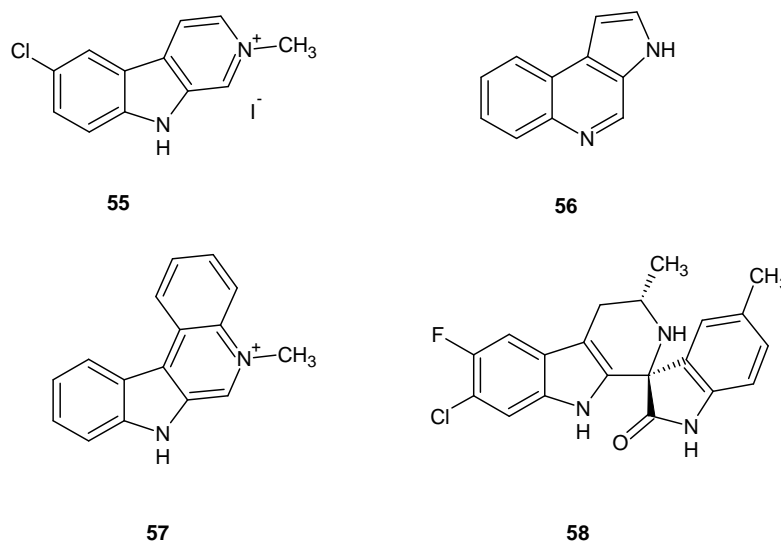
Figure 37. Structural analoques of mariquinolines active gainst *P. falciparum;* nostocarboline hydroiodide (**55**), 3*H*-pyrrolo[2,3-c]quinoline (**56**), isoneocryptolepine (**57**) and spiroindolone NITD609 (**58**).

Although feeding experiments were not done to establish the amino acid precursors of these pyrrolloquinolines, a good guess would suggest leucine as an amino acid precursor in the biosynthesis of the isopropyl side chain of marinoquinoline B (**40**). Similarly, phenyl alanine and tyrosine may be seen as precursors of the side chains of marinoquinolines **41** and **42**, respectively, whereas tryptophan might provide the indole moieties in marinoquinolines **43** and **44**.

3.3 Hyaladione an S-methyl cyclohexadiene dione from *H. minutum*

Hyalangium minutum strain NOCB-2[T] is an especially 'talented' organism producing structurally diverse metabolite families. Hyaladione (**47**) is the major and smallest compound to be isolated from this strain. It is a fairly polar compound eluting early at about six minutes in an ammonium acetate buffered acetonitrile/water gradient increasing the organic solvent from 10 % to 100 % in 40 minutes. It is a heteroatom-rich small-molecule with the elemental formula $C_7H_6ClNO_2S$. Despite its small size, it was impossible to elucidate the structure from 1D and 2D NMR spectra. Only three singlet signals were observed in the ^{1}H NMR spectrum which only provided a limited number of correlations in COSY, HMQC, HMBC and ROESY 2D spectra. Due to the low number of different protons, only one rare four-bond COSY cross peak correlation was observed between the S-methyl protons and the only methine proton at

C-7. The only NOE of the molecule was observed for the same proton pair (Figure 38). This long-range COSY correlation is not completely unusual, since it has been observed in thiopalymyrone, a cyanobacterial metabolite exhibiting molluscidal activity.[135] Other than the HMBC correlation identical to the only COSY crosspeaks, additional HMBC correlations were observed between the methine proton H-5 and the quaternary carbons at C-1, C-3, and C-6.

Finally, **47** could be crystallized from acetone to obtain pink needle shaped crystals that enabled a complete structure elucidation by X-ray diffraction analysis to give a 2-amino-3-chloro-5-(methyl sulfanyl)cyclohexa-2,5-diene-1,4-dione (hyaladione). There are no similar or related S-methyl cyclohexadiene diketones in the DNP or the Chemical abstracts-online database. Therefore, **47** with its unique structural elements represent a novel class of natural products.
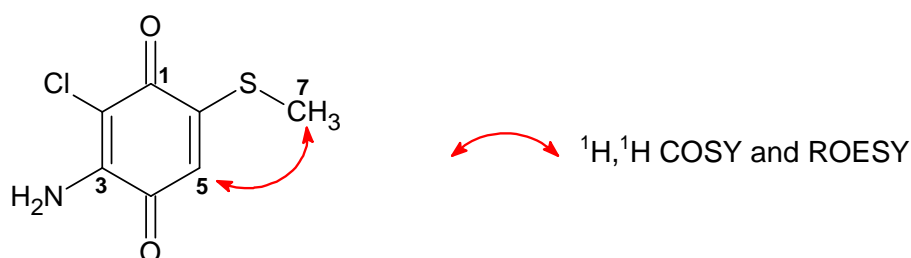
Figure 38.   The only ^{1}H, ^{1}H COSY and ROESY correlations of hyaladione (**47**).

The best activity of **47** was observed against *S. aureus* with a MIC of 0.83 µgmL^{-1}. *S. aureus* belong to the pathogens that are responsible for nosocomial infections. Methicillin-resistant *S. aureus* (MRSA) is the most dangerous strain which has developed resistance to most beta-lactam antibiotics particularly cephalosporins and penicillins (e.g. methicillin, that gave rise to the prefix "methicillin resistant"). MRSA was initially associated with hospitals (hospital-acquired [HA MRSA]), but has increasingly become prevalent in community-acquired (CA MRSA).[136] Despite the efficacy of linezolid (**59**) (Figure 39) against both HA MRSA and CA MRSA it is prized as the most expensive antibiotic, limiting its use to a smaller population. The prices will however change as the first patents will run out in 2015. Already linezolid (**59**) resistant *S. aureus* (LRSA) strains have been identified recently,[137] and alternative antibiotics against the ever emerging resistance are urgently needed.

59
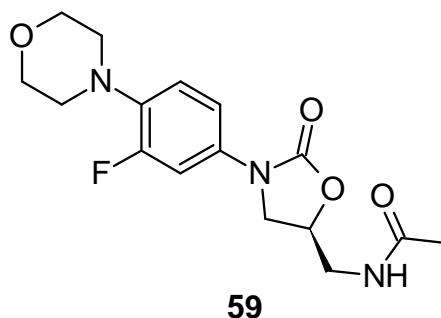
Figure 39. Linezolid (**59**), with efficacy against MRSA.

Biofilm formation of some bacteria species has contributed to the increased antibiotic resistance. The Gram-negative bacteria *C. violeceum* and *P. aeruginosa* are examples of bacteria forming biofims and are therefore prevalently used as models for the analyses of quorum sensing activity. Hyaladione (**47**) was found to be moderately active against these pathogens (Table 20). The mode of activity, though not investigated in the current thesis, might unravel new ideas that could help to fight biofilms of human pathogens.

Anti-parasitic testing of **47** was done at the Swiss Tropical and Public Health Institute in Basel. Hyaladione is reported to be active against *P. falciparum* with an IC_{50} value of 0.186 µg mL^{-1} and also cytotoxic to the rat myoblast L6 cells with an IC_{50} value of 0.552 µg mL^{-1}. However, its antimalarial activity was reported as unspecific.

The successful isolation and characterisation of **47** provides a new small and complex natural product that may find application in drug discovery programs, either as a tool to investigate the mode of action or as lead structure for derivatization in drug development. Its name hyaladione, was derived by merging the name of the producer strain ***Hya**langium minutum* with the diketo-functional group name "dione".

3.4   The hyafurones and hyapyrones

In the screening program of myxobacteria at the Helmholtz Centre for Infection Research (HZI), ten strains of *H. minutum* were shown to produce hyafurones and the two hyapyrones in different proportions, as identified by HPLC-DAD-HRESIMS analyses. *H. minutum* strain NOCB-2^T was the best producer both in amounts and variety of the derivatives. Besides these polyketides, the strain also produced hyaladione and hyaboron (Dr. J. Niggemann, unpublished result). The isolation of the light sensitive polyenes was achieved successfully by

use of amber glass ware or foiling of the sample bottles with aluminium. The first sample of hyafurone A_1 (**48**) was completely degraded when exposed to light together for some time in DCM. Further degradations were circumvented by use of methanol as a softer solvent and keeping the compounds dry under nitrogen atmosphere and storing at freezing temperatures.

Hyafurone A_1 (**48**), the major compound of the family of polyketides was separated from the others by silica gel flash chromatography and subsequent purification by RP MPLC. Detailed analyses of its molecular ions in the HRESIMS in both negative and positive modes were in agreement with its empirical formula $C_{32}H_{44}O_6$. Careful analyses of the NMR data in deuterated methanol together with the molecular formula led to structure **48** for hyafurone A_1. The experimental ^{1}H and ^{13}C NMR data corroborated with their calculated values for hyafurone A_1 (**48**) using the ACD NMR Predictor software. An unusual doubling of signals in the ^{13}C NMR spectrum was observed for CH_3-1, and the quarternary carbons C-2, C-4, and C-5. However, this was not completely unique as it had been observed in other compounds that contain a similar furanone moiety.[138,139,140] The doubling of peaks in these compounds results from the instable stereochemistry of the hemi-ketal group in the furanone ring. These compounds exist as a 1:1 mixture of epimers (respectively diastereomers) at the hemiketal stereocentre.

Despite the similarity of the furanone ring system of hyafurone A_1 (**48**) to other compounds, the producing organisms were completely diverse. For example, aglajne 2 (**60**) (Figure 40) was isolated from the mollusc *Bulla striata* and its prey *Aglaja depicta*,[125] aurafurone A (**61**) and B from the myxobacteria *Stigmatella aurantiaca* and *Archangium gephyra*,[139] 5-alkenyl-3,3(2H)-furanones from *Streptomyces aculeolatus*[141] and actinofuranones A (**62**) and B from Streptomyces of a marine actinomycete.[138] The detection of structurally related compounds from a variety of sources may be attributed to various reasons, e.g. diet and or symbiotic relationships between different organism,[142] horizontal gene transfer, or simply a coincidence of co-evolution of the biosynthetic pathways in response to a similar environmental stress. In all cases the ^{1}H and ^{13}C chemical shifts in the furanone systems were near identical.
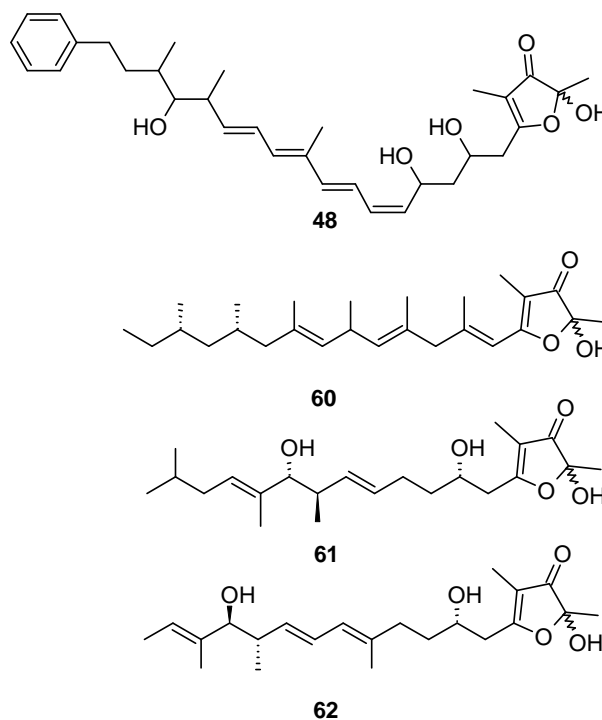
Figure 40.   Identical furanone moieties in hyafurone A$_1$ (**48**), Aglajne 2 (**60**), aurafurone A (**61**) and actinofuranone A (**62**).

The ^{1}H NMR spectra of hyafurone A$_1$ (**48**) and hyafurone A$_2$ (**49**) were superficially similar. However, a closer examination of the latter spectrum revealed slight chemical shifts of proton resonances of methylene C-9 to methines C-12 (δ_H 4.92, 5.36, 6.21, 6.68) in the former spectrum shifted to δ_H 4.39, 5.73, 6.37 and 6.33, respectively. The most apparent difference was observed in the multiplicity and vicinal proton-proton coupling constant of the olefinic proton H-11 where a triplet and a coupling constant of $^3J_{10,11}$ = 11.0 Hz was observed for **48** compared to the proton-proton coupling constants of $^3J_{10,11}$ = 14.0 Hz for the identical pair in **49**. This large coupling constant was decisive in the assignment of the *trans* configuration for the $\Delta^{10,11}$ bond in **49**.

The structure of hyafurone B (**50**) indicates an elimination of a water molecule from **48**, a process that can be envisioned *in vitro* (Figure 41). The hydroxyl group at C-9 is protonated to $-OH_2^+$, a good leaving group, and eliminated as a water molecule resulting in 12 degrees of unsaturation for **50**.
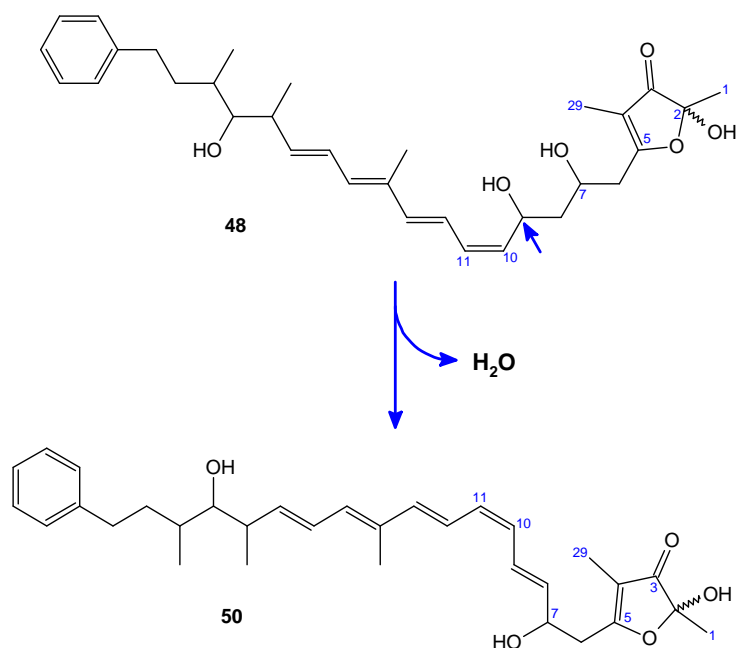
Figure 41.   Elimination of water from hyafurone A$_1$ (**48**) to give hyafurone B (**50**).

The new olefenic protons in hyafurone B (**50**) were displayed in the ^{1}H NMR spectrum at δ_H 6.61 (H-8) and δ_H 6.89 (H-9) compared to identical positions in hyafurone A$_1$ (**48**) at δ_H 1.69, δ_H 1.91 (C-8) and δ_H 4.92 (C-9). Indeed, this was the sole difference in the NMR spectra data of the two compounds (Tables 12 and 14). Molecular ion clusters in HRESIMS analysis of **48** indicated elimination of water molecules from the parent cluster. However, the experience of handling the two compounds separately indicated **50** to be more stable and biologically more active compared to **48** in the tests performed. Hyafurone B (**50)** is the biologically most active member of the polyketide family when tested against a range of pathogenic bacteria and fungi with its best activity at 8.3 µg mL^{-1}(MIC) against the Gram-positive *N. flava* (Chapter 2 Table 18).

Hyapyrone A (**51**), was isolated as an isomer of **50**. However, unlike **50**, where the hydroxyl group at C-9 (δ_C 66.5) of **48** was eliminated as water, the dehydration has occurred at the OH group at C-7 (δ_C 68.0) and the formation of pyranone moiety in place of the furanone moiety, hence the name hyapyrone for **51**. The biological activity of the two isomers was completely different, emphasizing the importance of structure-activity relationship with **50** being more active than **51**.

Hyafurone C (**52**) and hyafurone D (**53**) are the first members of this polyketide group to have a nitrogen substituent on the furanone ring. The N atom was observed as an amino group represented by a slowly exchanging broad singlet in the proton NMR spectra for both compounds (Table 16). However, these metabolites were less active when screened against the common bacterial and fungal pathogens.

Hyapyrone B (**54**), though produced by strain NOCB-2[T] was isolated from *H. minutum* strain Hym23 due to its relatively higher productivity of **54**. Compared to the hyafurones (A -D) the furanone moiety was replaced by a pyranone moiety in **54** like in **51**. Polypropionate compounds with a pyranone moiety have previously been isolated in marine molluscs. The compounds include aglajne-3,[125] pectinatone,[143] norpectinatone,[144] and diemenensin A.[145] Like other members of the family, no significant biological activity was observed for hyapyrone B (**54**). The best antibiotic and cytotoxic activities were observed against the Gram-positive bacteria *N. flava* and the mouse fibroblast cell line L929 with MIC value of 16.6 µg/mL and IC_{50} value of 11 µg/mL, respectively. Hyapyrone B (**54**) is considered a relative of hyafurones because of the similarities in structure of the western fragment from the phenyl moiety to the methine C-12 (Figure 36).

Determination of absolute configuration of natural product compounds is vital especially if they are to be developed into drugs as exemplified in the case of thalidomide in chapter one where the (*S*)-enantiomer was teratogenic. Substantial effort were made to determine the absolute configuration of **48** starting with the derivatization of the four chiral alcohols using the advanced Mosher method.[107] Two derivatization methods were applied; first a reaction involving the MTPA-Cl (α-methoxy-α-trifluoromethylphenylacetyl chloride), which seemed to work over 24 hours period according to TLC analysis. However the compound degraded during subsequent efforts to purify it. A second attempt with a MTPA-acid and 1,3-dicyclohexyldiimide (DCC) in the presence of 4-(dimethylamino)-pyridine (DMAP) as catalyst also resulted in a degradation of the product. Finally, the remaining minute amount of the unstable **48** precluded further characterization of its stereochemistry, since the biggest challenge initially was the purification of enough material for these experiments and for detailed NMR analysis.

The doubling of peaks in the ^{13}C NMR spectra was not observed for the two hyapyrones, A and B (**51** and **54**) due to the absence of the hemiketal making them more stable than their

relative hyafurones counterparts. However, after biological activity screening, the minute amounts left forestalled any further characterization for the determination of their absolute configuration.

Although feeding experiments were not performed to establish the biosynthetic precursors of the polyenes from *H. minutum*, structure of hyafurone A_1 (**48**) closely resembles a combination of structural elements of aurafurone A (**61**) and phenalamide A_1 (**63**), microbial metabolites of which the biosynthetic precursors have been elucidated as shown in Figure 42. [146,147]
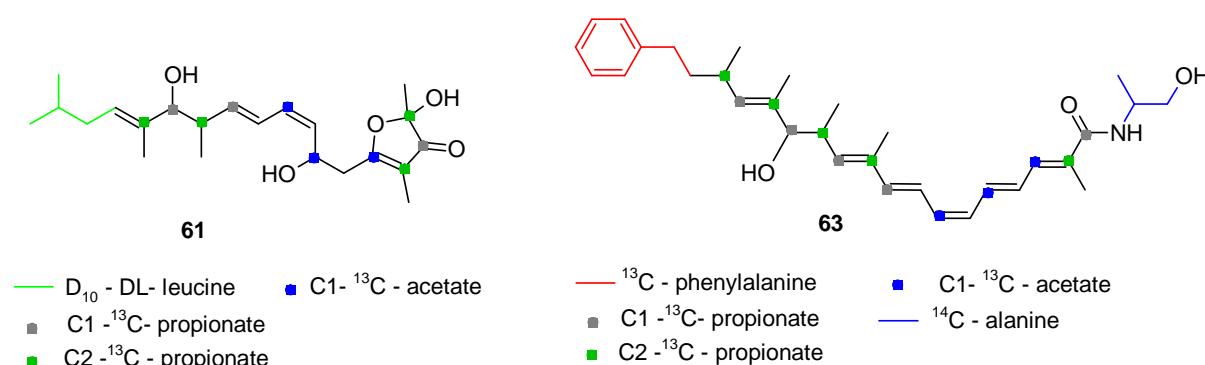
Figure 42.   Incorporation of labeled biosynthetic precursors into aurafurone A (**61**)[147] and phenalamide A_1 (**63**).[146]

Based on this information, it is feasible to predict that hyafurone A_1 (**48**) is a biosynthetic product of the condensation of the amino acid phenylalanine, propionate and acetate. The decarboxylation and deamination of phenylalanine provides the phenyl moiety as a starter unit while five propionate-derived methylmalonyl-CoA and five acetate-derived malonyl-CoA extender units are incorporated during the biosynthesis sequentially as shown in Figure 43. The furanone moiety should be identical to aurafurone A requiring the condensation of two propionates and an acetate. However, the C1 carbon derived from incorporation of the last propionate unit in this furanone moiety is lost, presumably due to a decarboxylation step.[147]

Propionates as precursors for the methyl moieties have also been shown in the biosynthesis of polypropionates in the marine *Siphonaria denticulata.*[148]
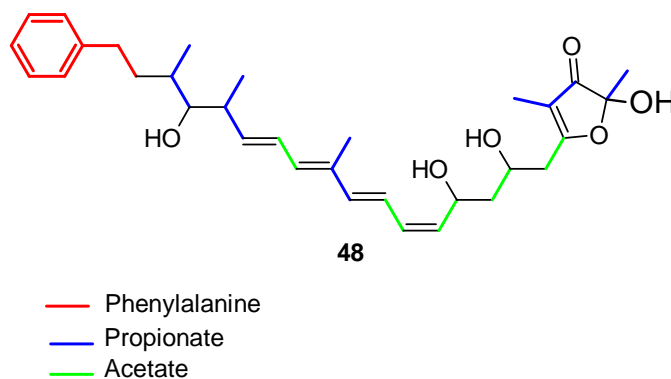
Figure 43. Hypothetical incorporation of biosynthetic precursors into hyafurone A₁ (**48**).

3.5 Conclusion and future aspects

With the growing escalation of pathogenic resistance to the available drugs and the emergency of new pathogens, expansion in drug discovery programs remains the corner stone to improvement in human health. Natural products continue to play an important role in providing new chemical entities with diverse biological activities. In the current thesis, 13 novel and one known compounds [marinoquinoline A, (**39**)] were isolated, their structures elucidated and subsequently screened for biological activities. Marinoquinolines A-F (**39-44**) were isolated from the gliding bacterium *Ohtaekwangia kribbensis* a bacteroidetes while hyaladione (**47**), hyapyrone **A,** (**51**), hyapyrone B (**54**) and five hyafurones (**48-53** except **49,** which is a degradation product of **48**) were isolated from *Hyalangium minutum* (myxobacteria). Marinoquinolines A-F (**39-44**), a family of six pyrroloquinolines exhibited a broad range of antibiotic, antifungal, cytotoxic and also anti-plasmodial activity. Marinoquinolines B (**40**) and F (**44**) exhibited good anti-plasmodial activities with IC_{50} values of 1.8 and 1.7 µM, respectively, and have generated great interest among the synthetic chemists leading to the total synthesis of marinoquinolines A –C (**39** -**41**) and E (**43**).[133,149]

Hyaladione (**47**), a small metabolite whose structure could not be resolved by NMR spectroscopy but by X-ray crystallography, re-emphasizes the power of X-ray diffraction as the undisputable technique in structure determination. It showed a range of biological activities including antibiotic activity against MRSA with a MIC value of 0.83 µg/mL and anti-parasitic activity against *P*. *falciparum* K1 cells with an IC_{50} value of 0.186 µg mL^{-1}.

Hyafurone-like metabolites with furanone or pyranone moieties have previously been isolated.[125,139] Hyafurone C (**52**) and D (**53**), however, represent the first hyafurones with an N-substitution of the hydroxyl group of the furanone ring. Their biosynthetic pathways have equally not been investigated and determination of their absolute configuration would definitely be of interest.

Gliding bacteria and particularly the myxobacteria continue to excite with amazing discoveries of new and structurally diverse compounds.[53,54] To date, the largest bacterium genome sequenced belongs to the myxobacterium *Sorangium cellulosum* with 13.0 Mbp[150] which together with *Myxococcus xanthus* (strain DK1622) with a genome of 9.1 Mbp reveal a great diversity of putative secondary metabolites.[151,152] Natural product drug discovery programs have progressed tremendously over the last few years due to improvement in culture techniques to isolate and culture the "unculturables",[51] high throughput screening in dereplication and biological activity profiling, ultra-sensitive detectors and automated purification equipment, ultra-high LC-HRESIMS and state of the art NMR facilities. Failure to get enough new lead compounds from rational drug design and combinatorial chemistry and the ever increasing multi-drug resistance pathogens as well as the emergency of new pathogens is alarming. Despite the closure of natural product R & D departments by the big pharma industries, there is a renewed effort from the governmental public funds to support natural product programs at the universities and small biotech companies. This is evidenced by the over 5,000 natural products discovered per annum, and the improvement of the journal impact factors in the field. There is no doubt therefore that natural product research has been re-launched and attention of many researchers attracted.

4 Experimental

4.1 Materials

4.1.1 General Chemicals

Table 21. Chemicals used and their corresponding suppliers

Chemical	Supplier
Acetone Calcium chloride ($CaCl_2$ x 2 H_2O) Glycerine (87 %) Methanol (technical grade) Methanol (Uvasol) Magnesium sulphate x 7 H_2O Potassium hydroxide Sodium acetate Toluene	Merck
Acetonitrile Dichloromethane Diethyl ether Ethanol Ethyl acetate Methanol Water (HPLC)	J.T. Baker
Sodium-Fe-EDTA Dimethylaminopyridine (DMAP) Sodium hydrogen carbonate Pyridine-p-toluenesulfonic acid Sephadex LH-20	Fluka
Acetic acid Aluminium oxide Ammonium acetate Formic acid *n*-Heptane	Roth

Table 21 **continued**

Chemical	Supplier
Sodium sulphate Sodium chloride Sulphuric acid HEPES	Roth
Soyabean flour Starch 12018	Cargill
Ammonia solution	Riedel-de Haen
Milli-Q-Water	Millipore
Casitone	BD
Glucose	Cerestar
Amberlite XAD -16	Rohm and Haas
Skim milk Sulphuric acid	AppliChem
Yeast extract	Ohly
Tegosipon antifoam	Evonik
Acetone-d_6 Methanol-d_4 Chloroform-d_1 Acetonitrile-d_3	Deutero GmbH

4.2 General equipment and procedures

4.2.1 Analytical reversed phase high performance liquid chromatography (RP-HPLC)

The standard RP-HPLC and fractionations into well-plates were carried out using an Agilent 1260 infinity series system equipped with two pumps, a fraction collector, an injection system, column chamber and a UV diode-array detector (DAD) [Agilent Technologies]. Additionally, the system was coupled to a corona ultra-detector (Dionex GmbH). The standard conditions for screening were: column 125×2 mm, Nucleodur 120 EC, 5 µm, C_{18}, (Macherey-Nagel); temperature 40°C; solvent A: H_2O/ACN (95/5), 5 mmol NH_4Ac, 0.04 mL/L acetic acid; solvent B: H_2O/ACN (5/95), 5 mmol NH_4Ac, 0.04 mL/L acetic acid, gradient: 10 % B increasing to 100 % B in 30 min, maintained at 100 % B for 10 min; and finally to 10 % B post-run for 10 min, flow rate 0.3 mL/min; UV detection 200-450 nm.

4.2.2 Thin Layer Chromatography (TLC)

Analytical TLC was carried out on TLC aluminum sheets, silica-gel 60 F_{254} (Merck 5554). The standard TLC analyses of crude extracts and pure compounds were done by applying approximately 5 µL solution (20mg/mL of crude extract and 2mg/mL of pure compounds) to silica gel TLC plates which were developed with DCM/MeOH (9/1; v/v) under solvent vapor saturation condition. Visualization under UV light at 254 or 366 nm (Camag) and by spraying with vanillin-sulfuric acid reagent (15g vanillin in 250 mL ethanol and 2.5 mL conc. sulfuric acid). The TLC plate was then heated to 120 °C.

4.2.3 Preparative reversed phase high pressure liquid chromatography (pRP-HPLC)

Two preparative RP-HPLC systems were used: an automated Agilent 1100 series system equipped with injection system, fraction collector, two pumps and DAD detector (Agilent Technologies) and the second system equipped with a manual injection port (Rheodyne), preparative K-1800 pump and a solvent mixing chamber (Knauer) connected to a UV-detector (Techlab). In both systems the column was a C_{18} Nucleodur 250×21 mm, 100–10 EC column (Machery-Nagel).

4.2.4 Preparative reversed phase medium pressure liquid chromatography (RP-MPLC)

RP-MPLC was carried out using a Büchi chromatography system equipped with two pumps C-605, a fraction collector C-660, a UV photometer C-635, and a control unit C-620 connected to a Kronlab RP-column (480×30 mm).

4.2.5 Silica-gel flash chromatography systems

Silica gel flash chromatography was carried out either using a manual Si-gel flash chromatography system from Biotage and Si 40 cartridges (Chromabond®) or an automated flash chromatography system (Reveleris) equipped with UV and ELSD detectors and a fraction collector. The software and the cartidges were supplied by Grace Davison Discovery Sciences.

4.2.6 Size exclusion chromatography

Size exclusion chromatography was performed on a Sephadex LH-20 column connected to a minipuls-3 pump (Gilson), a fraction collector, UV detector and a plotter (Pharmacia Biotech.) with methanol as solvent.

4.2.7 HPLC-Ultrahigh resolution mass spectrometry (HPLC-HRESIMS)

HRESIMS data were recorded on a Maxis ESI-TOF-MS spectrometer (Bruker) coupled to an Agilent 1200 series RP-HPLC system. HPLC-HRESIMS conditions: column 50×2.1 mm, Acquity UPLC BEH C-18, 1.7 µm (Waters), solvent A: 0.1 % formic acid in water; solvent B: 0.1 % formic acid in ACN, gradient 5 % B for 0.5 min, increasing to 100 % B in 19.5 min and continued at 100 % B for 5 min, flow rate 0.6 mL/min; or NH_4Ac-buffer gradient: column 100×2.1 mm, XBridge™ C18 3.5 µm (Waters), solvent A: H_2O/ACN (95/5) + 5 mM/L of NH_4Ac + 40 µL/L of acetic acid; solvent B: H_2O/ACN (5/95) + 5 mM/L of NH_4Ac + 40 µL/L of acetic acid, gradient from 10 % B increasing to 100 % B in 30 min and continued at 100 % B for 10 min, flow rate 0.3 mL/min, UV detection 200-450 nm. The molecular formulae were identified by including the isotopic pattern in the calculation using the SmartFormula algorithm of the Bruker software.

4.2.8 NMR spectroscopy

^{1}H NMR and ^{13}C NMR spectra of extracts and pure compounds for purity check and structure elucidation were recorded on Bruker FT-NMR DPX-300 (^{1}H 300 MHz, ^{13}C 75 MHz), ARX-400 (^{1}H 400 MHz, ^{13}C 100 MHz), or Bruker AVANCE DMX-600 (^{1}H 600 MHz, ^{13}C 150 MHz) spectrometers. The instruments were calibrated using deuterium solvent signals as standards (CD$_3$OD, δ_c 49.0, δ_H 3.35, 4.87 ppm; CD$_3$COCD$_3$, δ_c 29.9, δ_H 2.05 ppm; CDCl$_3$, δ_c 77.2, δ_H 7.26 ppm; CD$_3$CN, δ_C 1.6 and 118.6, δ_H 1.93 ppm). Multiplicity of ^{13}C signals were deduced from DEPT and/or APT experiments; s = C, d = CH, t = CH$_2$, q = CH$_3$. For complete structural assignment of new compounds, 1D (^{1}H, ^{13}C, DEPT, ROESY) and 2D [^{1}H-^{1}H COSY, ^{1}H-^{13}C direct correlation (HMQC), ^{1}H, ^{13}C long-range correlation (HMBC)] NMR spectra were recorded. Data acquisition, processing and spectral analyses were performed with standard Bruker software and ACD/NMRWorkbook. The chemical shifts are given in parts per million (ppm) and coupling constants in Hz.

4.2.9 Centrifugation

Centrifugation was carried out with Centifuge-5416 (Eppendorf) or/and Varifuge 20RS (Heraeus Sepatech).

4.2.10 Evaporation

Vacuum rota-evaporation of organic solvents was perfomed on a Rotavapor R-200 system coupled to a heating bath B-490 (Büchi) and a PC 600 series vacuum pump (Vacuubrand).

4.2.11 Optical rotation

Optical rotations were measured using a Perkin-Elmer 241 MC polarimeter equipped with a 1 mL cell, cell length 10 cm.

4.2.12 UV spectra

UV spectra were recorded on a Shimadzu UV/Vis-2450 spectrophotometer using 1 cm quartz cells.

4.2.13 IR spectra

Infra-red (IR) spectra were recorded on a Bruker IR Tensor 27 spectrophotometer.

4.2.14 Melting points

The melting points were measured on a Büchi-510 melting point apparatus.

4.2.15 Large-scale fermentations

Large-scale fermentations were carried out in 100 and 130 L bioreactors (B. Braun) with culture volumes of 70 L or 100 L in the presence of 2 % Amberlite XAD-16 (Rohm and Haas), respectively.

4.2.16 Milli-pore water

Milli-Q water was purified by a Millipore purification system (Millipore).

4.2.17 Microplate-shaker

The 96-well bioassay culture plates were incubated at 30 ^{0}C on a microplate-shaker (Heidolph Titramax 1000).

4.2.18 X-ray crystallography

X-ray data set for marinoquinoline A (**39**) and hyaladione (**47**) was measured at 122 K on a X8-Apex Bruker-AXS diffractometer (Mo Kα radiation), collecting 18376 reflections (independent 5432 R$_{(int)}$ = 0.031). The monoclinic space group *P2₁/n* with a unit cell of a = 3.8875(8) Å, b = 14.180(3) Å, c = 14.518(3) Å, β = 94.81(1)° was determined and the structure solved by direct methods.[153] Full matrix least-squares refinement against F_o^2 with anisotropic thermal parameters and free refinement of the hydrogen positions (133 parameter) were used, resulting in RI = 0.031 and wR2 = 0.074 with I > 2σ$_I$. This was done by Dr. V. Huch, Department of Inorganic Chemistry, Saarland University.

4.3 Fermentation of PWU 25 and Isolation of Marinoquinolines A-F

4.3.1 Isolation, identification and culture of strain PWU 25

Strain PWU 25 was isolated from a soil sample with plant residues collected at Kukrail Reserve Forest and Crocodile Research Centre, Uttar Pradesh, India in March 1995. The strain was identified as *Ohtaekwangia kribbensis* by 16S rDNA analysis (Dr. K. Mohr, HZI). The strain was isolated using procedures described for isolation of myxobacteria.[154] For maintenance it was grown on VY/2 agar plate [yeast 0.5 %, $CaCl_2$. 2 H_2O 0.1 %, cyanocobalamine 0.5 µg/ml, agar 1.5 %, pH 7.2]. Liquid batch cultures (100 mL) of the strain were cultivated in 250 mL Erlenmeyer flasks in a medium containing 0.4 % skimmed milk, 0.4 % defatted soy flour, 0.2 % yeast extract, 1.0 % starch, 0.1 % $MgSO_4 \times 7$ H_2O, 50 mM HEPES (11.9 g/L), 8 mg/L Fe–EDTA, 0.5 % glycerin and 2 % of Amberlite XAD-16 resin (E-medium) and incubated at 30 °C on a gyratory shaker at 160 rpm for 3 days. Aliquots of stock cultures in eppendorf tubes were stored at -80 °C.

4.3.2 Large-Scale fermentation of strain PWU 25

A 3 L pre-culture of *O. kribbensis* strain PWU performed in shaking flasks and cultivated for 3 days were inoculated to 70 L of E-medium (without HEPES) in a 100 L bioreactor supplemented with 1.4 kg of Amberlite XAD -16 resin. The culture was kept at 30 °C, aerated with oxygen at 0.05 vvm per minute, pH regulated at 7.4 with 10 % KOH and 5 % H_2SO_4 solutions, and agitated with a flat-blade turbine stirrer at 100 rpm. Foam formation was suppressed by addition of 100 mL of 30 % tegosipon. Fermentation was terminated after three days and XAD-16 adsorber resin and the cell mass (4.3 kg) were collected by sieving and centrifugation, respectively.

4.3.3 Isolation of marinoquinolines A-F

The adsorber resin was washed with distilled water and packed in a glass column (70×8 cm). Compounds were extracted by a three step process; first, polar compounds were extracted with 50 % aqueous methanol (4 L) followed by extraction with methanol (4 L) and a final elution with acetone (4 L), each at a flow rate of 2 L per hour. The eluent from 50 % aqueous methanol was discarded while methanol and acetone eluents were vacuo-evaporated to yield 10.41 g and 7.08 g of crude extract, respectively. Lipophilic compounds in the methanol

extract were removed by partitioning with *n*-heptane to yield 9.25 g accumulated in the methanol layer. The compounds were further enriched by acid-base partitioning. First, they were partitioned under acidic conditions between water containing 2 % formic acid (pH 2) and ethyl acetate. Acidic and neutral compounds accumulated in the acidic layer of ethyl acetate weighed 2.5 g. The pH of the water layer was shifted to 11 by addition of ammonia, and subsequent partitioning and extraction with ethyl acetate yielded 692 mg of a basic extract. This was separated by Sephadex LH-20 (1000×50 mm) column chromatography with methanol as solvent and a UV detector set at 227 nm. The fraction containing the major compound **39** (marinoquinoline A) was evaporated and subjected to crystallization and recrystallization in acetone-petrol ether (1:1) yielding 62.5 mg of colorless needle-shaped single crystals whose X-ray crystallography data were identical to those described for 4-methyl-3*H*-pyrrolo[2,3-c]quinolone.[111] The byproducts were further purified by preparative RP HPLC [column 250×21 mm Nucleodur C_{18} (Macherey Nagel), solvent A: 0.5 % HCOOH in 80 % H_2O and solvent B: 0.5 % HCOOH in 50 % CH_3OH; gradient 7 % B, 60 min to 83 % B, 30 min 100 % CH_3OH; flow rate 20 mL/min, UV detection at 240 nm] affording **40** (16.5 mg), **41** (7.5 mg), **42** (23 mg), **43** (15.3 mg) and **44** (3 mg). All pure fractions of **39** were pooled to give a final yield of 232 mg.

Marinoquinoline A (**39**): colorless needles; mp 236-237 °C; UV (MeOH): λ_{max} (log ε) 239 (4.561), 300 (4.034), 312 (3.959), 326 (3.792) nm; IR (KBr): ν_{max} 3442, 2924, 2854, 1631, 1587, 1441, 1366, 1125, 1026 cm^{-1}; NMR data see Table 2; HRESIMS *m/z* 183.0919 [M + H]$^+$ (calcd for $C_{12}H_{10}N_2$, 183.0922).

Marinoquinoline B (**40**): colorless amorphous solid; UV (MeOH): λ_{max} (log ε) 226 (4.651), 240 (4.678), 301 (4.093), 314 (4.028), 327 (3.867) nm; NMR data see Table 2; HRESIMS *m/z* 225.1382 [M + H]$^+$ (calcd for $C_{15}H_{16}N_2$, 225.1386).

Marinoquinoline C (**41**): colorless amorphous solid; UV (MeOH): λ_{max} (log ε) 228 (4.755), 239 (4.751) 302 (4.154), 314 (4.101), 329 (3.959) nm; NMR data see Table 3; HRESIMS *m/z* 259.1236 [M + H]$^+$ (calcd for $C_{18}H_{14}N_2$, 259.1230).

*Marinoquinoline D (***42**): colorless amorphous solid; UV (MeOH): λ_{max} (log ε) 227 (4.823), 240 (4.816), 302 (4.233), 315 (4.186), 329 (4.032) nm; NMR data see Table 3; HRESIMS *m/z* 275.1181 [M + H]$^+$ (calcd for $C_{18}H_{14}N_2O$, 275.1179).

Marinoquinoline E (**43**): yellow amorphous solid; UV (MeOH): λ$_{max}$ (log ε) 225 (4.563), 242 (4.451) 306 (4.018), 315 (4.009), 339 (4.009) nm; NMR data see Table 4; HRESIMS *m/z* 284.1182 [M + H]$^+$ (calcd for C$_{19}$H$_{13}$N$_3$, 284.1182).

Marinoquinoline F (**44**): yellow oil; UV (MeOH): λ$_{max}$ (log ε) 210 (4.638), 222 (4.602, sh), 271 (4.050, sh), 328 (3.866), 361 (3.739) nm; for NMR data in methanol-*d*$_4$ see Table 4; ^{1}H NMR (600 MHz, CD$_3$CN): δ [ppm] 11.06 (1H, br s, H-3), 7.71 (1H, m, H-4), 7.18 (1H, t, *J* = 2.2 Hz, H-5), 8.34 (1H, m, H-6), 7.68 (1H, m, H-7), 7.66 (1H, t, *J* = 2.8 Hz, H-8), 8.32 (1H, m, H-9), 10.13 (1H, br s, H-1´) 9.56 (1H, d, *J* = 2.9 Hz, H-2´), 8.58 (1H, dd, *J*=6.6, 1.8 Hz, H-4´), 7.32 (1H, td, *J* = 7.2, 1.5 Hz, H-5´) 7.34 (1H, td, *J* = 7.3, 1.5 Hz, H-6´) 7.59 (1H, dd, *J* = 6.4, 2.0 Hz, H-7´); HRESIMS m/z 312.1138 [M + H]+ (calcd for C$_{20}$H$_{13}$N$_3$O, 312.1131).

4.4 Biological testing

4.4.1 Determination of the minimum inhibition concentration (MIC)

The MIC values of marinoquinoline A-F were determined against the Gram-positive bacteria Staphylococcus *aureus*, *Nocardia flava*, and *Micrococcus luteus*, and the Gram-negative bacteria *Escherichia coli* and *Chromobacterium violaceum*. In addition, the fungi *Mucor hiemali*s, the yeasts *Candida albicans*, *Rhodotorula glutinis*, *Pichia anomala* and the fission yeast *Schizosaccharomyces pombe* were tested. MIC assays were conducted in 96 well microtiter well plates in a serial dilution in EBS-medium [0.5 % casein pepton, 0.5 % glucose, 0.1 % beef extract, 0.1 % yeast extract, 50 mM HEPES (11.9 g/L) at pH 7] for bacteria pathogens and MYC-medium [1 % phytone peptone, 1 % glucose and 50 mM HEPES (11.9 g/L) at pH 7] for yeasts and fungi pathogens. First, 10 µL aliquots of each of the marinoquinolines A-F at 1 mg/mL in MeOH and 2 µL for the reference drugs (broad spectrum antibacterial oxytetracycline hydrochloride (sigma) at 1 mg/mL in Millipore water and antifungal nystatin (sigma) at 1 mg/mL in MeOH) were pipetted to the first row (A) of the plate. Negative control wells were left blank. After the solvents were dried, 150 µL of a mixture of the test pathogen and the culture medium in the ratio of 1:100, respectively, was dispensed in all rows using a multichannel pipet. To the first row, an additional 150 µL of the pathogen-medium mixture was added and mixed by repeated pipetting, before transferring the same amount to the second row. A 1:1 serial dilution was done in the subsequent rows, and 150 µL discarded after the last row (H). The micro-titre plates were incubated on a micro-plate- shaker with 600 rpm at 30 ^{o}C for 24 - 48 hours. The lowest concentration of the drug

preventing visible growth of the pathogen was taken as the MIC. The concentrations tested ranged from 33.5 to 0.052 µg/mL.

4.4.2 Cytotoxicity assay

In vitro cytotoxicity (IC_{50}) was determined against a panel of mammalian cell lines including the breast cancer cell line MCF-7, the cervix carcinoma cell line KB-3-1, the established mouse fibroblast cell line L929 and the non-transformed human umbilical vein endothelial cell line (HUVEC). KB-3-1 and L929 were cultured in DMEM (Lonza), HUVEC in EBM-2 (Lonza), and MCF-7 in RPMI (Lonza) media, all supplemented with 10 % of fetal bovine serum (Gibco) under 10 % CO_2 at 37 ^{o}C. The cytotoxicity assay was performed according to the MTT (3-(4,5-dimethylthiazol-2-yl)-2,5-diphenyltetrazolium bromide) method in 96-well micro-plates.[155] Briefly, 60 µL aliquots of serial dilutions from an initial stock of 1 mg/mL in MeOH of the test compounds were added to 120 µL aliquots of a cell suspension (50,000/mL) in 96-well micro-plates. Methanol was used as a negative control. After 5 days incubation at 37 ^{o}C and 10 % CO_2, the MTT assay was performed, and the absorbance measured at 590 nm using an ELISA plate reader (Victor). The concentration at which the growth of cells was inhibited to 50 % of the control (IC_{50}) was obtained from the dose-response curves in µg/mL.

4.4.3 Antiplasmodial activity

Antiprotozoal activity of the pure compounds was determined at the Swiss Tropical and Public Health Institute (Swiss TPH) by Prof. R. Brun and M. Kaiser. Antimalarial activity was tested by a variation of the semiautomated microdilution assay against intraerythrocytic forms of *Plasmodium falciparum* derived from asynchronous stock cultures.[156] The reference strain used was K1 (Thailand; resistant to chloroquine and pyrimethamine). Activity against hemoflagellates which cause human sleeping sickness (*Trypanosoma brucei* subsp. *Rhodesia*) and Chagas disease (*Trypanasoma cruzi*) and also activity against rat skeletal muscle myoblast (L-6) cells were assessed as described by Kaminsky and Brun[157]

4.5 Fermentation and Isolation of hyaladione from strain NOCB-2^T

4.5.1 Isolation of strain NOCB-2^T

Strain NOCB-2^T was isolated in 1992 and characterized as belonging to the myxobacteria *Hyalangium minutum* by Prof. Dr. Reichenbach of the former German Centre for

Biotechnology (GBF) currently HZI and deposited at the German Resource Centre for Biological Material (DSMZ) as a type strain with accession number DSM 14724^T.

4.5.2 Large scale fermentation of strain NOCB-2^T

Large-scale fermentation of *H. minutum* strain NOCB-2^T was performed in a medium containing 0.2 % soya meal, 0.2 % glucose, 0.2 % yeast extract, 0.8 % starch, 0.1 % $CaCl_2$, 0.1 % $MgSO_4$ x 7 H_2O, 8 mg/L Fe-EDTA (H-medium) and 2 % of Amberlite XAD-16 resin in a 70 L bioreactor that was inoculated with a 6 L of shake-flask cultures grown for 7 days in the same medium. The bioreactor was kept at 30 °C, aerated at 0.05 vvm per minute, pH regulated at 7.4 with 2.5 % H_2SO_4 or 2.5 % KOH solution and agitated with a flat-blade turbine stirrer at 100 rpm.

4.5.3 Extraction and isolation of hyaladione (47)

The fermentation was terminated after 7 days and the adsorber resin collected by sieving and extracted sequentially in a glass column (70 × 8 cm) with methanol (7 L) and with acetone (4 L) at a flow rate of 2 L per hour. The combined solutions were evaporated to yield 34 g of extract. Enrichment of **47** was achieved by eliminating lipophilic compounds by partitioning between methanol and *n*-heptane to give 24 g of an enriched crude methanol extract. A further solvent-solvent partitioning with EtOAc/water resulted in 8.4 g residue from the EtOAc layer. 2 g of this extract (8.4 g) were separated by silica gel flash chromatography (Biotage Flash+) with a gradient of 2 % to 10 % methanol in DCM resulting in 330 mg of enriched hyaladione (**47**) according to TLC and HPLC analyses (R_f = 0.7, DCM/MeOH (24/1) and R_t = 6.4 min, respectively). Further enrichment was performed by reverse phase preparative Medium Pressure Liquid Chromatography (RP-MPLC) on a Kronlab ODS-AQ 120/16 column (97 x 4 cm) connected to a Büchi chromatography system with a gradient of 25 % B to 35 % B (solvent A: MeOH/H_2O 1/1, solvent B: MeOH) in 30 min. at a flow rate of 30 mL/min and UV detection at 360 nm. Hyaladione (**47**) eluted at a retention time of 9.5 minutes. The fraction containing **47** was evaporated to eliminate MeOH and the compound recovered from the water layer by extraction with EtOAc to yield 98 mg of **47**. Crystallization in acetone at room temperature yielded 23 mg of pink hyaladione (**47**) crystals that allowed structure determination by X-ray crystallography.

Hyaladione (**47**): pink needles; mp 235-236 ^{o}C; UV (methanol): λ_{max} (log ε) = 353 (3.743) nm; IR (KBr): ν_{max} 3438, 3308, 3056, 1673, 1662, 1638, 1604, 1566, 1394, 1335, 1318, 1261,

1246, 1088, 1039, 952, 877 cm^{-1}; ^{1}H NMR and ^{13}C NMR data are presented in Table 9; HRESIMS m/z 203.9882 [M+H]$^+$ (calcd for $C_7H_6ClNO_2S$ [M+H]$^+$, 203.9880).

4.6 Extraction and isolation of hyafurones

4.6.1 General remark

The hyafurones with a polyene type UV chromophore were protected against light by use of amber glassware and stored in methanol solution supplemented with nitrogen gas at -20 $^\circ$C.

4.6.2 Isolation of hyafurones A$_1$-D and hyapyrone A

A second 100 L large-scale fermentation of strain NOCB-2^T was performed in H-medium under conditions similar to the first fermentation. 2 kg of XAD were recovered. Upon washing with distilled water, the resin was packed in a column, washed again with 50 % aqueous methanol (4 L), extracted with 9 L of methanol and finally eluted with 6 L acetone. The methanol extract was evaporated to yield 11.8 g of crude extract. Partitioning in 90 % aqueous methanol/n-heptane resulted in 9.3 g accumulation in the methanol layer. Further partitioning in DCM/water resulted in 5.6 g of enriched compounds in methylene chloride layer. This residue was loaded to a 80 g silica gel flash cartridge and run on the automated flash chromatography system (Reveleris) with a gradient of 20 % to 30 % acetone in DCM for 73 minutes. 20 fractions were collected according to analytical TLC und UV-absorption. The fraction containing hyafurone A$_1$ (**48**) (689 mg) was purified by MPLC with a gradient of 70 % to 80 % aqueous methanol to yield 82 mg of pure **48**. Hyafurone A$_2$ (**49**) was isolated from an isomerization of 25 mg of **48**. The purification was performed by preparative HPLC on a C$_{18}$ Nucleodur column, 250 x 21 mm with a gradient of 60 % to 72.5 % aqueous methanol and a flow rate of 20 mL/min to obtain 1.6 mg of **49**. All subsequent hyafurone derivatives were purified by preparative HPLC using the same column but different gradients in aqueous methanol. Hyafurone B (**50**) was purified from a fraction containing 143 mg with a gradient of 72.5 % to 85 % aqueous methanol to yield 8 mg of pure hyafurone B (**50**). Hyapyrone A (**51**) was purified from a fraction containing 154 mg on the same column with a gradient of 75 % to 85 % aqueous methanol to yield 4.7 mg of **51**. For hyafurone C (**52**), a fraction containing 33 mg was purified with a gradient of 70 % to 80 % aqueous methanol to yield 3.5 mg of **52**, whereas hyafurone D (**53**) was purified from a fraction containing 79 mg with a gradient of 72.5 % to 80 % aqueous methanol to yield 3 mg of **53**.

4.6.3 Fermentation of strain Hym 3 and isolation of hyapyrone B

Although hyapyrone (**54**) was detected in *H. minutum* strain NOCB-2[T], its low production of less than 0.3 mg/L was insufficient for isolation. Luckily, other strains of *H. minutum* were also found to produce the hyafurones and hyapyrones in varying proportions. The strains include NOCB-10, Hym 3 and Hym 23. Of these, Hym 3 was found to be the best producer of **54** with a production of ca. 0.5 mg/L. A 70 L fermenter was run in a medium containing 3 % probion, 3 % starch, 2 % $MgSO_4$ and 0.5 % $CaCl_2$ (Pol-medium) in the presence of 2 % of XAD-16 adsorber resin. The extract was eluted from the resin with methanol and acetone to obtain 17 g of crude extract. An ethyl acetate water partitioning resulted in 7.5 g of crude material accumulated in the ethyl acetate phase. Further enrichment was done by partitioning between MeOH/*n*-Heptane with 4.6 g raw extract accumulated in the MeOH layer. Fractionation by silica gel flash chromatography of 1.6 g of the extract with a gradient from 2 % to 5 % MeOH in DCM yielded 297 mg of an enriched fraction. Several runs of preparative RP-HPLC with 75 % of acetonitrile in water in the presence of 0.1 % formic acid were run to obtain 7 mg of **54**.

Hyafurone A₁ (**48**): yellow amorphous oil; $[\alpha]^{22}_D = -49.6$ ($c = 0.52$, CH_3OH); UV (MeOH): λ_{max} (log ε) 280 (4.404, sh), 293 (4.498), 307 (4.563), 321 (4.498) nm; ^{1}H, ^{13}C, and 2D NMR data, see Table 12; HRESIMS *m/z* [M +Na]⁺ 547.3027 (calcd for $C_{32}H_{44}O_6Na$, 547.3030).

Hyafurone A₂ (**49**): yellow amorphous oil; $[\alpha]^{22}_D = -11.8$ ($c = 0.16$, MeOH); UV(MeOH): λ_{max} (log e) 279 (4.687, sh), 291 (4.799), 305 (4.862), 319 (4.792) nm; ^{1}H, ^{13}C and 2D NMR data, see Table 13; HRESIMS *m/z* [M +Na]⁺ 547.3040 (calcd for $C_{32}H_{44}O_6Na$, 547.3030).

Hyafurone B (**50**): yellow amorphous oil; $[\alpha]^{22}_D = -31.8$ ($c = 1$, MeOH); UV (MeOH): λ_{max} (log ε) 294 (4.856, sh), 308 (4.948), 322 (4.879) nm; ^{1}H, ^{13}C, and 2D NMR data, see Table 14; HRESIMS *m/z* [M +Na]⁺ 529.2923 (calcd for $C_{32}H_{42}O_5Na$, 529.2924).

Hyapyrone A (**51**): yellow amorphous solid; $[\alpha]^{22}_D = -69.1$ ($c = 0.43$, MeOH); UV (MeOH): λ_{max} (log ε) 294 (4.656 sh) 308 (4.774) 321 (4.700) nm; ^{1}H, ^{13}C, and 2D NMR data, see Table 15; HRESIMS *m/z* [M +Na]⁺ 529.2923 (calcd for $C_{32}H_{42}O_5Na$, 529.2924).

Hyafurone C (**52**): deep yellow oil; $[\alpha]^{22}_D = -54.2$ ($c = 0.24$, MeOH); UV (MeOH): λ_{max} (log ε) 294 (4.821), 307 (4.973), 321 (4.920) nm; ^1H, ^{13}C, and 2D NMR data, see Table 16; HRESIMS m/z [M +H]$^+$ 568.3634 (calcd for $C_{34}H_{50}NO_6$, 568.3633).

Hyafurone D (**53**): yellow oil; $[\alpha]^{22}_D = -22.8$ ($c = 0.25$, MeOH); UV (MeOH): λ_{max} (log ε) 294 (4.340), 307 (4.462), 321(4.412) nm; ^1H, ^{13}C, and 2D NMR data, see Table 16; HRESIMS m/z [M +H]$^+$ 582.3788 (calcd for $C_{35}H_{52}NO_6$, 582.3789).

Hyapyrone B (**54**): yellow oil $[\alpha]^{22}_D = +10.8$ ($c = 0.65$, MeOH); UV (MeOH): λ_{max} (log ε) 265 (4.943), 274 (4.978), 284 (4.907) nm; ^1H, ^{13}C, and 2D NMR data, see Table 17; HRESIMS m/z [M +H]$^+$ 505.3306 (calcd for $C_{33}H_{45}O_4$, 505.3312).

4.6.4   Determination of absolute configuration of hyafurone A$_1$ (48)

Two attempts were made to determine the absolute configuration of hyafurone A$_1$ (**48**) using the advanced Mosher method.[107] The first involved the reaction of MTPA-Cl for the derivatization of the chiral hydroxy groups. Vacuum dried hyafurone A$_1$ (**48**) [5 mg, 9.5 µmol] was transferred to a dry 5 mL amber glass vial with a Teflon-coated magnetic stir bar. 500 µl of anhydrous CH_2Cl_2, 200 µl of pyridine and 15 µl of (*R*)–MTPA-Cl (Fluka) were dispensed into the vial. The reaction mixture was stirred at room temperature (ca. 22 ^{o}C) and was monitored after 4 hours by TLC analysis [dichloromethane/ethyl acetate/ petroleum ether (18:2:1)]. Additional 15 µl of (*R*)-MTPA-Cl were added. After 20 hours the reaction mixture had changed from colourless to orange-yellow and was quenched by addition of 3 mL of 1 % $NaHCO_3$ and extracted three times with DCM in a 3:1 ratio (DCM:$H_2$0). 15.7 mg raw product was recovered after rota-evaporation of the DCM layer and a further TLC analysis showed two bands for the products. However, preparative purification on a 20 x 20 cm preparative silica gel glass plate (5 mm) eluted with the same solvent mixture as used above was unsuccessful.

In a second attempt, Mosher acid was used. Dry hyafurone A$_1$ (**48**) [7.3 mg, 13.9 µmol] in 300 µl of anhydrous dichloromethane was stirred with (*R*)-MTPA-OH [14.7 mg, 62.7 µmol, 4.5 equiv.], 1,3-dicyclohexylcarbodiimide (DCC) [12.9 mg, 62.7 µmol, 4.5 equiv.], and 4-dimethylaminopyridine (DMAP) [7.6 mg, 62.7 µmol, 4.5 equiv.] at ambient temperature. The reaction was monitored by TLC analysis as above. After 24 hours, all hyafurone A$_1$ (**48**) had been used up, unfortunately the products were clearly degraded as only smears were observed.

The quenching was done as described above and vacuo-evaporation of the DCM extraction afforded 25.6 mg of degraded product.

5.   References

[1]   Demain, A. L. *J. Ind. Microbiol. Biotechnol.* **2006**, *33*, 486-495.

[2]   Koehn F. E.; Carter, G. T. *Nat. Rev. Drug Discovery* **2005**, *4*, 206-220.

[3]   Harvey, A. *Drug Discovery Today* **2000,** *5*, 294-300.

[4]   Gullo, V. P.; McAlpine, J.; Lam, K. S.; Baker, D.; Peterson, F. *J. Ind. Microbiol. Biotechnol.* **2006**, *33*, 523-531.

[5]   Demain, A. L. *Med. Res. Rev*. **2009**, *29*, 821-842.

[6]   Li, J. –H.; Vederas, J. C. *Science* **2009,** *325*, 161-165.

[7]   Demain, A. L. *Appl. Microbiol. Biotechnol*. **1999**, *52*, 455-463.

[8]   Newman, D. J.; Cragg, G. M. *J. Nat. Prod.* **2007**, *70*, 461–477.

[9]   Verdine, G. L. *Nature*, **1996**, 384, 11-13.

[10]   Andermann, A. A. J. *McGill J. Med*. **1996**, *2*, 115-120.

[11]   Gerhadt, Ch., *Eur. J. Org. Chem*. **2006**, *87*, 57-84.

[12]   Sneader, W. *British Med. J*. **2000**, *321*, 23-30.

[13]   Hamilton, G, R.; Baskett, T. F. *Can, J. Anesth.* **2000**. *47*, 367-374.

[14]   Fitzgerald, J. G. *California. J. Med.***1923**, *21*, 101-103.

[15]   Fleming A. *Br. J. Exp. Path*. **1929**, *10*, 3-13.

[16]   Demain, A. L.; Sanchez, S. *J. Antibiot.* **2009**, *62*, 5-16.

[17]   Fischbach, M. A.; Walsh, C. T. *Science* **2009**, *325*, 1089-1093.

[18]   Davies. J. *Can. J. Infect. Dis. Med. Microbiol*. **2006**, *17*, 287-290.

[19]   Boyce, J. M.; Cookson, B.; Christiansen, K.; Hori, S.; Vuopio-Varkila, J.; Kocagöz, S.; Öztop, A. Y.; Vandenbrouke-Grauls, C. M . J. E.; Harbath, S.; Pittet, D.; *Lancet Infect. Dis.* **2005**, *5*, 653 -663.

[20]   Hansman, D.; Glasgow, H.; Sturt, J.; Devitt, L.; Douglas, R. *N. Eng. J. Med.* **1971**, *284*, 175-177.

[21]   Leeb, M. *Nature*. **2004**, *431*, 892-893.

[22]   Nathan, C. *Nature*, **2004**, *431*, 899-902.

[23]   Fauci, A. S. *Clin. Infect. Dis*. **2001**, *32*, 675-685.

[24]   Borel, J. F.; Feurer, C.; Gubler, H. U.; Stähelin, H. *Agents Actions*. **1976**, *6,* 468 -475.

[25]   Laupacis, A.; Keown, P.A.; Ulan, R. A.; McKenzie, N.; Stiller, C. R. *Can. Med. Assoc. J.* **1982**, *126,* 1041 -1046.

[26]   Mott, J. L.; Zhang, D. ; Freeman, J. C.; Mikolajczak, P.; Chang, S. W.; Zassenhaus, H. P. *Biochem. Biophys. Res. Commun*. **2004**, *319*, 1210-1215.

[27]   Endo, A. *Atherosclerosis Supplements*. **2004**, *5*, 125 -130.

[28]   Reichenbach, H. *Annu. Rev. Microbiol.* **1981**, 35, 339-364.

[29]   Nett, M.; König G. M. *Nat. Prod. Rep*, **2007**, *24*, 1245-1261.

[30]   McBride, M. J. *Annu. Rev. Microbiol*, **2001**, *55*, 49-75.

[31]   Berdy, J. *J. Antibiot.* **2005**, *58*, 1-26.

[32]   Singh, R. K.; Tiwari, S. P.; Rai, A. K.; Mohapatra, T. M. *J. Antibiot*. **2011**, *64*, 401-412.

[33]   Ludwig, W.; Klenk, H. P. *In Bergey's Manual of Systematic Bacteriology*' Eds. Boone, D.R.; Castenholz, R. W. *Springer Verlag, New York* **2000**, 40-65.

[34]   Karlsson, F. H.; Ussery, D. W.; Nielsen, J.; Nookaew, I. *Microb. Ecol*. **2011**, *61*, 473-485.

[35]   Rajilic`-Stojanovic`, M.; Smidt, H.; De vos, W. M. *Environ. Microbiol. **2007**, *9,* 2125-2136.

[36]   Bäckhed, F.; Ley, R.E.; Sonnenburg, J.L.; Peterson, D. A.; Gordon, J. I. *Science,* **2005**, *307*, 1915-1920.

[37] Kato, T.; Hinoo, H.; Shoji, J.; Matsumoto, K.; Tanimoto, T.; Hattori, T.; Hirooka, K. Kondo, E. *J. Antibiot*. **1987**, *40*, 135-138.

[38] Kato, T.; Hinoo, H.; Terui, Y.; Nishikawa, J.; Nakagawa, Y.; Ikenishi, Y.; Shoji. J. *J. Antibiot*. **1987**, *40*, 139-144.

[39] Imai, S.; Fujioka, K.; Furihata, K.; Fudo, R.; Yamanaka, S., Seto, H. *J. Antibiotic*. **1987**, *46*, 1319-131322.

[40] Shoji, J.; Hinoo, H.; Matsumoto, K.; Hattori, T.; Yoshida, T.; Matsuura, S.; Kondo, E. *J. Antibiot*. **1988**, *41*, 713-718.

[41] Maki, H.; Miura, K.; Yamano, Y. *Antimicrob. Agents Chemother*. **2001**, *45*, 1823-1827.

[42] Kamigiri, K.; Tokunaga, T. Sugawara, T.; Nagai, K.; Shibazaki, M.; Setiawan, B.; Rantiamodjo, R. M.; Morioka, M.; Suzuki, K. *J. Antibiot*. **1997**,*50*, 556- 561.

[43] Katayama, N.; Nozaki, Y.; Okonogi, K.; Ono, H.; Harada, S.; Okazaki, H. *J. Antibiot*. **1985**, *38*, 1117-1127.

[44] Nemoto, T.; Ojika, M.; Yakahata, Y.; Andoh, T.; Sakagami, Y. *Tetrahedron* **1998**, *54*, 2683- 2690

[45] Dickschat, J. S.; Helmke, E.; Schulz, S. *Chem. Biodiv*. **2005**, *2*, 318 – 352.

[46] Steinmetz, H.; Gerth, K.; Jansen, R.; Schläger, N.; Dehn, R.; Reinecke, S.; Kirschning, A.; Müller, R. *Angew. Chem. Int. Ed.* **2011**, *50*, 532 -536.

[47] Jansen, R.; Gerth, K.; Steinmetz, H.; Reinecke, S.; Kessler, W.; Kirschning, A.; Müller, R. *Chem. Eur. J.* **2011**, *17*, 7739 -7744.

[48] Kämpfer, P.; Young, C. C.; Sridhar, K. R.; Arun, A. B.; Lai, W. A.; Shen, F. T.; Rekha, P. D. *Int. J. Syst. Evol. Microbiol*. **2006**, *56*, 2223 -2228 .

[49] Reichenbach, H. *Environ. Microbiol*. **1999**, *1*, 15 -21.

[50] Garcia, R. O.; Krug, D.; Müller, R. *Methods Enzymol.* **2009**, *458*, 59 -91.

[51] Garcia, R.; Gerth, K.; Stadler, M.; Dogma Jr., I. J.; Müller, R. *Molec. Phylogenet. Evol.* **2010**, *57*, 878 -887.

[52] Reichenbach, H. *In Bergey´s Manual of Systematic Bacteriology*, Eds, Brenner, D. J.; Krieg, N. R.; Staley, J. T. *Springer,* **2005**, *2*, 1059 – 1144.

[53] Weissman, K. J.; Müller, R. *Nat. Prod. Rep*. **2010**, *27*, 1276 -1295.

[54]   Wenzel, S. C.; Müller, R. *Curr. Opin. Drug Discov. Devel.* **2009**, *12*, 220 - 230

[55]   Gerth, K.; Pradella, S.; Perlova, O.; Beyer, S.; Müller, R. *J. Biotechnol.* **2003**, *106*, 233 -253.

[56]   Goodin, S.; Kane, M. P.; Rubin, E. H.; *J. Clin. Oncol.* **2004**, *22*, 2015 -2025.

[57]   Bollag, D. M.; McQueney, P. A.; Zhu, J.; Hensens, O,; Koupal, L.; Liesch, J.; Goetz, M.; Lazarides, E.; Woods, M.; *Cancer Res* **1995**, *55*, 2325 -2333.

[58]   Sasse, F.; Steinmetz, H.; Heil, J; Höfle, G.; Reichenbach, H. *J. Antibiot.* **2000**, 53, 879 -885.

[59]   Khalil, M. W.; Sasse, F.; Lunsdorf, H.; Elnakady, Y. A.; Reichenbach, H.; *ChemBioChem.* **2006**, *7*, 678 -683.

[60]   Kaur, G.; Hollingshead, M.; Holbeck, S.; Schauer-Vukasinovic, V.; Camalier, R. F.; Dömling, A.; Agarwal, S. *Biochem. J.* **2006**, *396*, 235 – 242.

[61]   Vollbrecht, L.; Steinmetz, H.; Höfle, G. *J. Antibiot.* **2002**, *55*, 715 -721.

[62]   Nickeleit, I.; Zender, S.; Sasse, F.; Geffers, R.; Brandes, G.; Sörensen, I.; Steinmetz, H.; Kubicka, S.; Carlomagno, T.; Menche, D.; Gütgemann, I.; Buer, J.; Gossler, A.; Manns, M.P.; Kalesse, M.; Frank, R.; Malek, N. P. *Cancer Cell.* **2008**, *14*, 23 – 35.

[63]   Jansen, R.; Irschik, H.; Reichenbach, H.; Wray, V.; Höfle, G. *Liebigs Ann. Chem.* **1994**, *59*, 759 -773.

[64]   Aicher, B.; Hirschfelder, K.; Jansen, R.; Irschik, H.; Schmidt, P.; Engel, J.; Guenther, E.; Müller, R.; Teifel, M.; *Mol. Cancer Ther.* **2011**, 10, Abstract nr. 214.

[65]   Kunze, B.; Höfle G.; Reichenbach, H. *J. Antibiot.* **1987**, *40*, 258 -265.

[66]   Gerth, K.; Irschik, H.; Reichenbach, H.; Trowitzsch, W. *J. Antibiot.* **1980**, *33*, 1474 – 1479.

[67]   Thierbach, G.; Reichebach, H. *Biochem. Biophys. Acta. Bioenerg.* **1981**, *638*, 282 - 289.

[68]   Höfle, G.; Bedorf, N.; Schomburg, D.; Gerth, K.; Reichenbach, H. *Liebigs Ann. Chem*, **1993**, *54*, 1017 -1021.

[69]   Reichenbach, H.; Höfle, G.; *in Scientific Annual Report, Gessellschaft für Biotechnogische Forschung , Braunschweig*, **1994**, 5 -22.

[70]   Schreurs, M.; van Dijk, T. H.; Gerding, A.; Havinga, R.; Reijngoud, D. J.; Kuipers, F. *Diabetes, Obes. Metab*. **2009**, *11*, 987-991.

[71]   Beckers, A.; Organe, S.; Tinunermans, L.; Scheys, K.; Peters, A.; Brusselmans, K.; Verhoeven, G.; Swinnen, J.V. *Cancer Res*. **2007**, *67*, 8180 -8187.

[72]   Jansen, R.; Irschik, H.; Huch, V.; Schummer, D.; Steinmetz, H.; Bock, M.; Schmidt, T.; Kirschning A.; Müller, R. *Chem. Eur. J.* . **2010**,*7*, 1284 -1289.

[73]   Reck, M.; Rutz, K.; Kunze, B.; Tomasch, J.; Surapaneni, S. K.; Schulz S.; Wagner-Döbler, I. *J. Bacteriol*. **2011**, *193*, 5692 – 5706.

[74]   Irschik, H.; Jansen, R.; Gerth, K.; Höfle, G Reichenbach, H. *J. Antibiot*. **1986***, 40,* 7 - 13.

[75]   Jansen, R.; Wray, V.; Irschik, H.; Reichenbach, H.; Höfle, G. *Tetrahedron Lett*. **1985***, 26,* 603- 6034.

[76]   Irschik, H.; Gerth, K.; Höfle, G.; Kohl, W.; Reichenbach, H. *J. Antibiot*. **1983**, *36*, 1651 – 1658.

[77]   Irschik, H.; Jansen, R.; Höfle, G.; Gerth, K.; Reichenbach, H. *J. Antibiot*. **1985**, *38*, 145 – 152.

[78]   Irschik, H.; Augustiniak, K.; Gerth, K.; Höfle, G.; Reichenbach, H. *J. Antibiot*. **1995**, *48*, 787 – 792.

[79]   Mukhopadhyay, J.; Das, K.; Ismail, S.; Koppstein, D.; Jang, M.; Hudson, B.; Sarafianos, S.; Tuske, S.; Patel, J.; Jansen, R.; Irschik, H.; Arnold, E.; Ebright, R. H. *Cell*. **2008**, *135*, 295 -307.

[80]   Moy, T. I.; Daniel, A.; Hardy, C.; Jackson, A.; Rehrauer, O.; Hwang, Y. S.; Zou, D.; Nguyen, K.; Silverman, J. A.; Li, Q.; Murphy, C. *FEMS Microbiol. Lett*. **2011**, *319*, 176 -179.

[81]   Sarker, S. D.; Latif, Z.; Gray, A. I. *In Natural Products Isolation: Methods in Biotechnol*. 2nd ed. Editors Sarker, S. D.; Latif, Z.; Gray, A. I. *Humana Press Inc., Totowa, NJ.* **2005**, *20*, 1-25.

[82]   Kwan, E. E.; Huang, S. G. *Eur. J. Org. Chem*. **2008**, *2008*, 2671 – 2688.

[83]   Molinski, T. F. *Nat. Prod. Rep*. **2010**, *27*, 321- 329.

[84]   Molinski, T. F. *Curr. Opin*. *Biotechnol*. **2010**, *21*, 819- 826.

[85]   Murata, M.; Oishi, T.; Yoshida, M. *Progress in Molecular and Subcellular Biolog:Marine Molecular Biotechnology* Eds. Fusetani, N.; Clare, A. S. *Springer-Verlag, Heidelberg.* **2006**, *42***,** 203 -220.

[86]   Fukushi, E. *Biosci. Biotechnol. Biochem.* **2006**, *70*, 1803 -1812.

[87]   Berger, S.; Braun, S. *In 200 and more NMR experiments.* 1st ed.; WILEY-VCH: Weinheim; **2004**.

[88]   Carey, F. A. *In Organic Chemistry, 4th Edition, International Edition, McGraw- hill* **2000**, pp 259 -290.

[89]   Chen, C. S.; Shieh, W. R.; Lu, P. H.; Harriman, S.; Chen, C. Y. *Biochim. Biophys. Acta.* **1991**, *1078*, 411 – 417.

[90]   Tracy, T. S.; Hall, S. D. *Drug. Metab. Dispos.* **1992**, *20*, 322 -327.

[91]   McBride, W. G. *Lancet*, **1961**, *2,* 1358

[92]   Knobloch, J.; Rüther, U. *Cell Cycle* **2008**, *7*, 1121- 1127.

[93]   Sheskin, J. *Clin. Pharmacol. Ther.* **1965**, *6*, 303 -306.

[94]   Singhal, S.; Mehta, J.; Deskan, R.; Ayers, D.; Roberson, P.; Eddlemon, P.; Munshi, N.; Anaissie, E.; Wilson, C.; Dhodapkar, M.; Zeldis, J.; Barlogie, B. *N. Engl. J. Med.* **1999**, *341*, 1565 -1571.

[95]   Butts, C. P.; Jones, C. R.; Towers, E. C.; Flynn, J. L.; Appleby, L.; Barron, N. J. *Org. Biomol. Chem.* **2011***, 9*, 177 – 184.

[96]   Claridge, T. D. W. *in Tetrahedron Organic Chemistry Series: High- Resolution NMR Techniques in Organic Chemistry* (Eds.: J. E Baldwin, R. M. Williams), Elsevier, oxford, **1999**, *19*,117 -118.

[97]   Karplus, M. *J. Am. Chem. Soc.* **1963**, *85*, 2870-2871.

[98]   Duncan, S.J.; Lewis, R.; Bernstein, M. A.; Sandor, P. *Magn. Reson. Chem.* **2007**, *45*, 283 -288.

[99]   M. Karplus, *J Am. Chem. Soc.* **1962**, *84*, 2458-2460.

[100] Hoye, T. R.; Suhadolnik, J. C. *J. Am. Chem. Soc.* **1987**, *109*, 4402-4403.

[101] Di Micco, S.; Chini, M. G.; Riccio, R.; Bifulco, G. *Eur. J. Org. Chem.* **2010**, *2010*, 1411 -1434.

[102] Jundt, L.; Steinmetz, H.; Luger, P.; Weber, M.; Kunze , B.; Reichenbach, H.; Höfle, G. *Eur. J. Org. Chem.* **2006**, *2006*, 5036 -5044.

[103] Perez, L. J.; Faulkner, D. J. *J. Nat. Prod.* **2003**, *66*, 247-250.

[104] Dale, J. A.; Dull, D. L.; Mosher, H.S. *J. Org. Chem.* **1969**, *34*, 2543 -2549.

[105] Sullivan, G. R.; Dale, J. A.; Mosher, H. S. *J. Org. Chem.* **1973**, *38*, 2143 -2147.

[106] Seco, J. M.; Quiñoá, E.; Riguera, R. *Chem. Rev.* **2004**, *104*, 17-118.

[107] Hoye, T.R.; Jeffrey, C.S.; Shao, F. *Nature Protocols* **2007**, 2, 2451-2458.

[108] Yoon, J. H.; Kang, S. J.; Lee, S. Y.; Lee, J. S.; Park, S. *Int. J. Syst. Evol. Microbiol.* **2011**, *61*, 1066–1072.

[109] *Dictionary of Natural products on DVD*, Ver. 19.1, **2010**, CRC Press, London, UK.

[110] Srisukchayakul, P.; Suwanachart, C.; Sangnoi, Y.; Kanjana-Opas, A.; Hosoya, S.; Yokota, A.; Arunpairojana, V. *Int. J. Syst. Evol. Microbiol.* **2007**, 57, 2275–2279.

[111] Kanjana-opas, A.; Panphon, S.; Fun, H.; Chantrapromma, S. *Acta Cryst.* **2006**, *E62*, 2728–2730.

[112] In a pyridine type ring vicinal coupling of about 5.5 Hz would be expected. In a simple pyridine ring the direct C,H coupling of methine 5 would be expected near 163 Hz compared to 168 Hz for a corresponding pyrrole.

[113] Davies, N. W.; Smith, J. A.; Molesworth, P. P.; Ross, J. J. *Rapid Commun. Mass Spectrom.* **2010**, *24*, 1105 -1110.

[114] Katta, V.; Chait, B. T. *J. Am. Chem. Soc.* **1993**, *115*, 6317 – 6321.

[115] Garcia, R. A.; Pantazatos, D.; Villarreal, F. J. *Assay Drug Dev. Technol.* **2004**, *2*, 81 - 91.

[116] Abraham, R. J; Mobli, M.; Smith, R. J. *Magn. Reson. Chem.* **2003**, *41*, 26–36.

[117] Mayser, P.; Schäfer, U.; Krämer, H-J.; Irlinger , B.; Steglich, W. *Dermatol. Res.* **2002**, *294*, 131–134.

[118] Machowinski, A.; Krämer, H-J.; Hort, W.; Mayser, P. *Mycoses*, **2006**, *49*, 388 – 392.

[119] Mosmann, T. *J. Immunol. Methods.* **1983**, *65*, 56–63.

[120] Van Baelen, G.; Hostyn, S.; Dhooghe, L.; Tapolcsanyi, P.; Matyus, P.; Lemiere, G.; Dommisse, R.; Kaiser, M.; Brun, R.; Cos, P.; Maes, L.; Hajos, G.; Riedl, Z.; Nagy, I.; Maes, B. U. W.; Pieters, L. *Biorg. Med. Chem.* **2009**, *17*, 7209 – 7217.

[121] Sangnoi, Y.; Sakulkeo, O.; Yuenyongsawad, S.; Kanjana-opas, A.; Ingkaninan, K.; Plubrukarn, A.; Suwanborirux, K. *Mar. Drugs* **2008**, *6*, 578–586.

[122] Reichenbach, H. *Bergey's manual of systematic Bacteriology*.Springer*, New York.2*[nd] *Edition,* **2005**, 1059–1144.

[123] Shimkets, L. J.; Dworkin, M.; Reichenbach, H. *The myxobacteria*. *In The Prokaryotes: A Handbook on the Biology of Bacteria*, Dworkin, M.; Falkow, S.; Rosenberg, E.; Schleifer K. H.; Stackebrandt E. Eds.; Springer: New York, **2006**, *7*, 31-115.

[124] Pereira, A. R.; Etzbach, L.; Engene, N.; Müller, R.; Gerick, W. H. *J. Nat. Prod.* **2011**, 74,1175-1181 [a more than three-bond COSY coupling correlation was observed in hyaladione, which is not unusual, as it has been observed in thiopalymyrone, a cyanobacterial metabolite exhibiting molluscicidal activity].

[125] Cimino, G.; Sodano, G.; Spinella, A.; *J. Org. Chem.* **1987,** *52*, 5326 – 5331.

[126] Spinella, A.; Alvarez, A. L.; Cimino, G. *Tetrahedron*. **1993**, *49*, 3203–3210.

[127] WHO *World Malaria Report*, **2008**.

[128] Becher, P. G.; Beuchat, J.; Gademann, K.; Jüttner, F. *J. Nat. Prod.* **2005**, *68*, 1793-1795

[129] Bonazzi, S.; Barbaras, D.; Patiny, L.; Scopelliti, R.; Schneider, P.; Cole S. T.; Kaiser, M.; Brun, R.; Gademann, K. *Biorg. Med. Chem.* **2010**, *18*, 1464 – 1476.

[130] Miert, S. V.; Hostyn, S.; Maes, B. U. W.; Cimanga, K.; Brun, R.; Kaiser, M.; Matyus, P.; Dommisse, R.; Lemiere, G.; Vlietinck, A.; Pieters, L. *J. Nat. Prod.* **2005**, *68*, 674-677.

[131] Rottmann, M.; McNamara, C.; Yeung, B. K. S.; Lee, M. C. S.; Zou, B.; Russell, B.; Seitz, P.; Plouffe, D. M.; Dharia, N. V.; Tan, J.; Cohen, S. B.; Spencer, K. R.; González-Páez, G. E.; Lakshminarayana, S. B.; Suwanarusk, A. G. R.; Jegla, T.; Schmitt, E. K.; Hans-Peter Beck, H. P.; Brun, R.; Nosten, F.; Renia, L.; Dartois, V.; Keller, T. H.; Fidock, D. A.; Winzeler, E. A.; Diagana, T. T.; *Science* **2010**, 329 1175 –1180.

[132] Tse, M. T.; *Nature Rev. Drug Discov.* **2010**, *9*, 842.

[133] Ni, L.; Li, Z.; Wu, F.; Xu, J.; Wu, X.; Kong, L.; Yao, H.; *Tetrahedron. Lett*. **2012**, *53*, 1271–1274.

[134] Banwell, M. G.; Jones, M. T.; Reekie, T. A. *Chem. N. Z.* **2011,** *75*, 122 -127.

[135]   Pereira, A. R.; Etzbach, L.; Engene, N.; Müller, R.; Gerick, W. H. *J. Nat. Prod.* **2011**, *74*, 1175-1181.

[136]   Nicolle, L. *Can. Med. Ass. J.,* **2006,** *175*, 145 -146.

[137]   García, M. S.; De la Torre, M. A.; Morales, G.; Peláez, B.; Tolon, M. J.; Domingo, S.; Candel, F. J.; Andrade, R.; Arribi, A.; García, N.; Sagasti, F. M.; Fereres, J.; Picazo, J. *J. Amer. Med. Ass.* **2010**, *303*, 2260 – 2264.

[138]   Cho, Y. J.; Kwon, C. H.; Williams, G. P.; Kauffman, A. C.; Jensen, R. P.; Fenical, W. *J. Nat. Prod.* **2006**, *69*, 425 -428.

[139]   Kunze, B.; Reichenbach, H.; Müller, R.; Höfle, G. *J. Antibiotic*. **2005**, *58*, 244 -251.

[140]   Beukes, D. R.; Davies-Coleman, M.T. *Tetrahedron*. **1999**, *55*, 4051 – 4056.

[141]   Banskota, A. H.; McAlpine, J. B.; Sørensen, D.; Aouidate, M.; Piraee, M.; Alarco, A. M; Omura, S.; Shiomi, K.; Farnet, C. M.; Zazopoulos, E. *J. Antibiotic.* **2006,** *59***,** 168–176.

[142]   Haygood, G. M.; Schmidt, W. E.; Davidson K. S.; Faulkner, D. J. *J. Molec. Microbiol. Biotechnol*. **1999**, *1*, 33- 43.

[143]   Biskupiak, J. E; Ireland, C. M. *Tetrahedron Lett*. **1983**, *24*, 3055- 3058.

[144]   Capon R. J.; Faulkaner, D. J. *J. Org. Chem*. **1984**, *49*, 2506 – 2508

[145]   Hochlowski, J. E.; Faulkaner, D. J. *Tetrehedron Lett*. **1983**, *24*, 1917-1920.

[146]   Trowitzsch-K, W.; Forche, E.; Wray, V.; Reichenbach, H.; Jurkiewicz, E.; Hunsmann, G.; Höfle, G. *Liebigs Ann. Chem* **1992**, *7*, 659 -664.

[147]   Frank, B.; Wenzel, S. C.; Bode, H. B.; Scharfe, M.; Blöcker, H.; Müller, R. *J. Mol. Biol.* **2007**, *374*, 24 – 38.

[148]   Manker, D. C.; Garson, M. J.; Faulkner, D. *J. Chem. Comm*. **1988**, *16*, 1061 -1062.

[149]   Schwalm,   C.   S.;   Correia,   C.   R.   D.   *Tetrahedron   Lett.*   **2012**, http://dx.doi.org/10.1016/j.tetlet.2012.06.115.

[150] Schneiker, S.; Pavlova, O.; Kaiser, O.; Gerth, K.; Alici, A.; Altmeyer, M. O.; Bartels, D.; Bekel, T.; Beyer, S.; Bode, E.; Bode, H. B.; Bolten, C. J.; Choudhuri, J. V.; Doss, S.; Elnakady, Y. A.; Frank, B.; Gaigalat, L.; Goesmann, A.; Groeger, C.; Gross, F.; Jelsbak, L.; Jelsbak, L.; Kalinowski, J.; Kegler, C.; Knauber, T.; Konietzny, S.; Kopp, M.; Krause, L.; Krug, D.; Linke, B.; Mahmud, T.; Martinez-Arias, R.; McHardy, A. C.; Merai, M.; Meyer, F.; Mormann, S.; Muñoz-Dorado, J.; Perez, J.; Pradella, S.; Rachid, S.; Raddatz, G.; Rosenau, F.; Rückert, C.; Sasse, F.; Scharfe, M.; Schuster, S. C.; Suen, G.; Treuner-Lange, A.; Velicer, G. J.; Vorhölter, F.-J.; Weissman, K. J.;

Welch, R. D.; Wenzel, S. C.; Whitworth, D. E.; Wilhelm, S.; Wittmann, C.; Blöcker, H.; Pühler, A.; Müller, R. *Nat. Biotechnol.* **2007**, *25*, 1281-1289..

[151]   Goldman, B. S.; Nierman, W.C.; Kaiser, D.; Slater, S. C.; Durkin, A. S.; Eisen, J. A.; Ronning, C. M.; Barbazuk, W.B.; Blanchard, M.; Field, C.;Halling, C.; Hinkle, G.; Iarchuk, O.; Kim, H. S.; Mackenzie, C.;Madupu, R.; Miller, N.; Shvartsbeyn, A.; Sullivan, S. A.; Vaudin, M.; Wiegand, R.; Kaplan, H. B. *Proc. Natl. Acad. Sci. USA.* **2006**, *103*, 15200 -15205.

[152]   Krug, D.; Zurek, G.; Revermann, O.; Vos, M.; Velicer, G. J.; Müller, R. *Appl. Environ. Microbiol.***2008**, *74*, 3058 -3068.

[153]   Sheldrick, G. M. *Acta Cryst.* **2008**, *A64*, 112 -122

[154]   Shimkets, L J.; Dworkin, M.; Reichenbach, H. *In the prokaryotes : A handbook on the biology of bacteria;* Dworkin, M.; Falkow, S.; Rosenberg, E.; Scheifer, K. H., Stackebrandt, E., *Springer: New York*, **2006**, *7*, 31 -115.

[155]   Mosmann, T. J. *Immunol. Methods* **1983**, *65*, 56 -63.

[156]   Desjardins, R. E.; Canfield C. J.; Haynes, J. D.; Chulay, J. D. *Antimicrob. Agents Chemother*. **1979**, *16*, 710 -718.

[157]   Kaminsky, R.; Brun, R. *Antimicrob. Agents Chemother.* **1998**, *42*, 2858-2862.

6 Appendix

6.1 Author's effort in publications

Marinoquinolines A-F, Pyrroloquinolines from *Ohtaekwangia kribbensis* (Bacteroidetes)
Dereplication screening experiments were performed by the author in consultation with Dr. R. Jansen. Medium optimizations, antibacterial and antifungal activity testing were performed by Dr. K. Mohr. The author monitored secondary metabolite production during large-scale fermentation. Anti-parasitic assays were performed at the Swiss Tropical and Pubic Health Institute. The author performed the isolation of all the marinoquinolines and elucidated their structures with the help of Dr. R. Jansen and participated in the cytotoxicity assays in Dr. F. Sasse's laboratory. The author wrote the manuscript.

Hyaladione, an S-Methyl Cyclohexadiene-dione from *Hyalangium minutum*
The producer strain was selected by Dipl.-Ing. H. Steinmetz. The author participated in antibacterial and antifungal activity testing, and performed the isolation and all the spectroscopic analyses of the compound. X-ray crystallography analysis was performed by Dr.V. Huch. The author wrote the manuscript.

6.2 Spectra and X-ray data tables of marinoquinolines A - F

6.2.1 Spectra of marinoquinoline A (39)
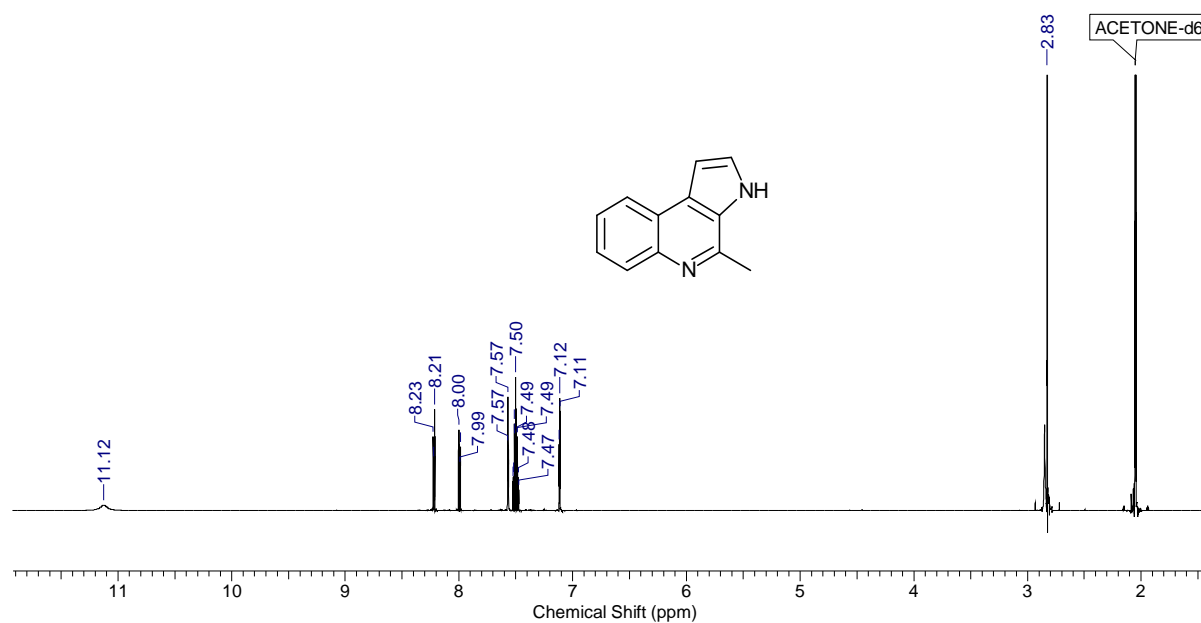
Spectrum 1: ^{1}H NMR spectrum of marinoquinoline A (**39**) (^{1}H 600 MHz, acetone-d_6).
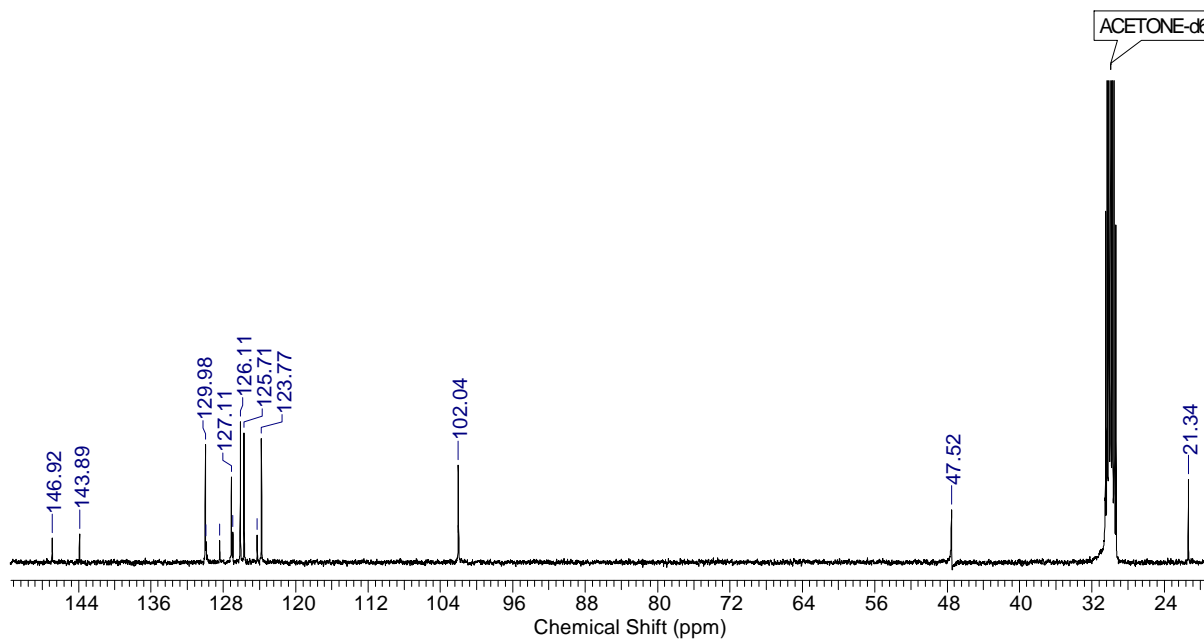
Spectrum 2: ^{13}C NMR spectrum of marinoquinoline A (**39**) (^{13}C 150 MHz, acetone-d_6).
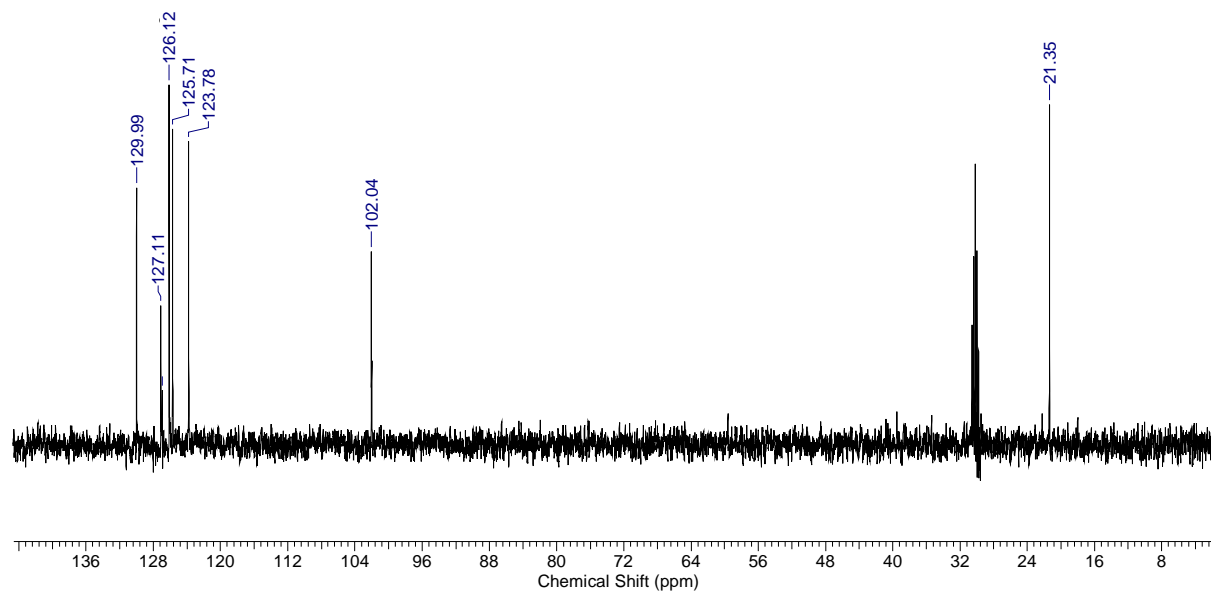
Spectrum 3: ^{13}C DEPT spectrum of marinoquinoline A (**39**) (^{13}C 150 MHz, acetone-d_6).
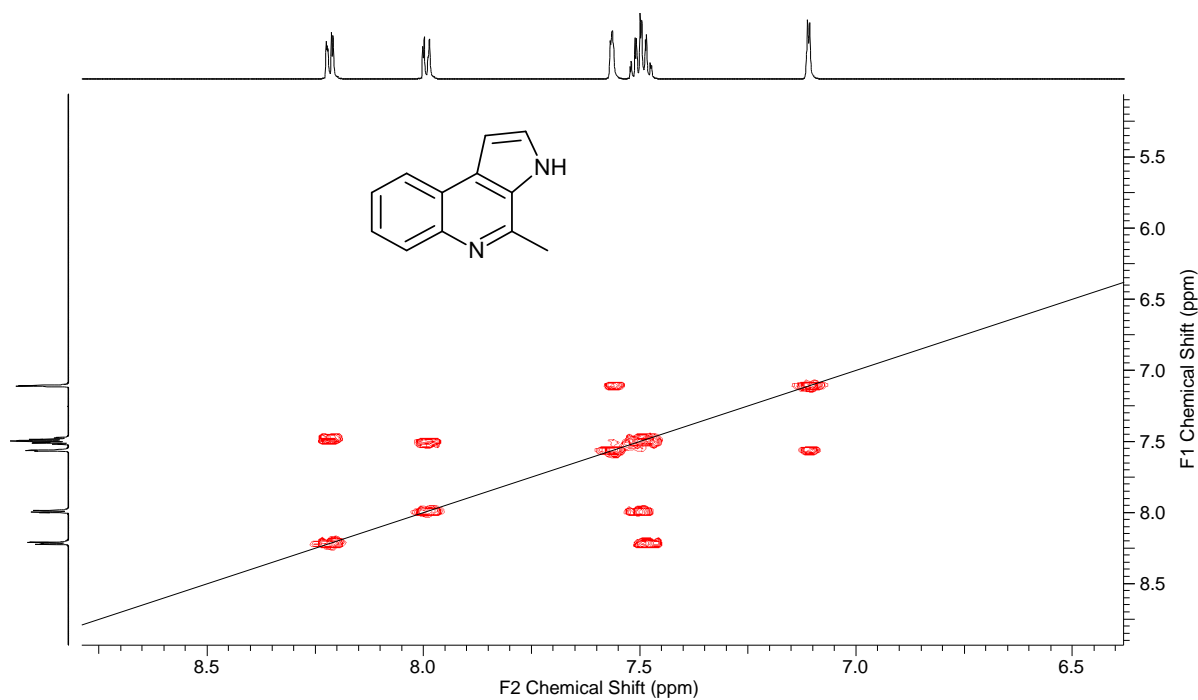
Spectrum 4: ^{1}H, ^{1}H COSY NMR spectrum of marinoquinoline A (**39**) (^{1}H 600 MHz, acetone-d_6).

101
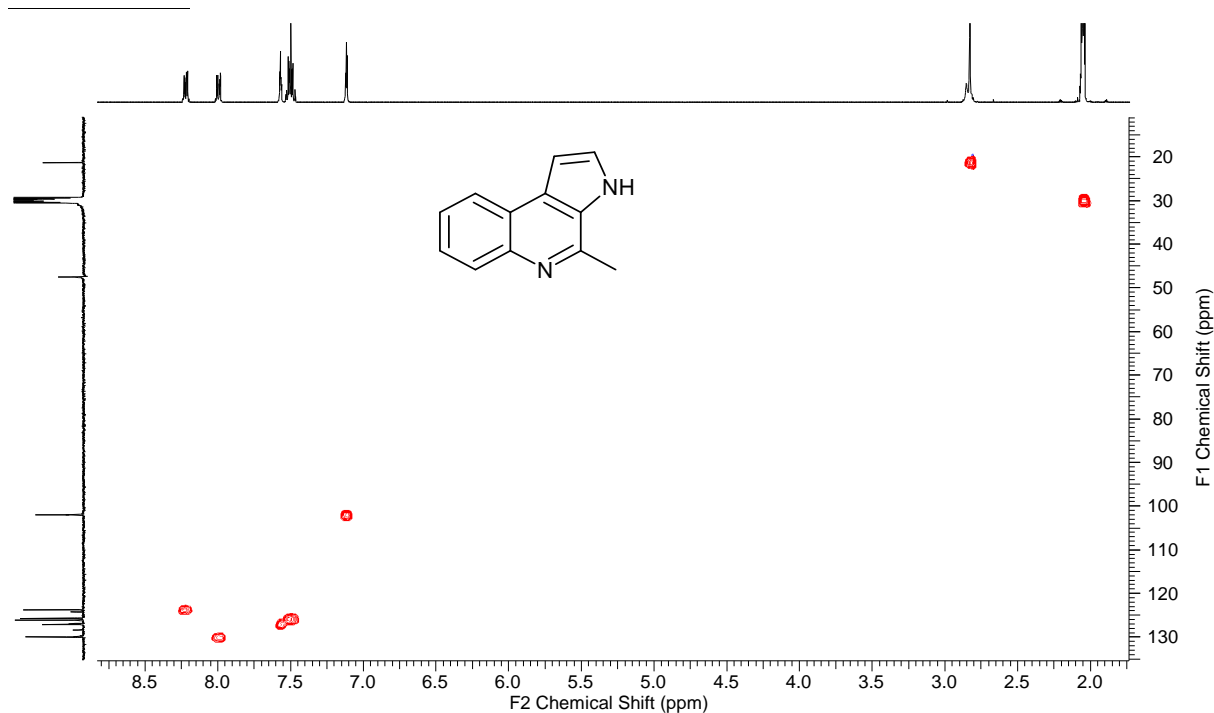
Spectrum 5: ^{1}H,^{13}C HMQC NMR spectrum of marinoquinoline A (**39**) (^{1}H 600 MHz, ^{13}C 150 MHz, acetone-d_6).
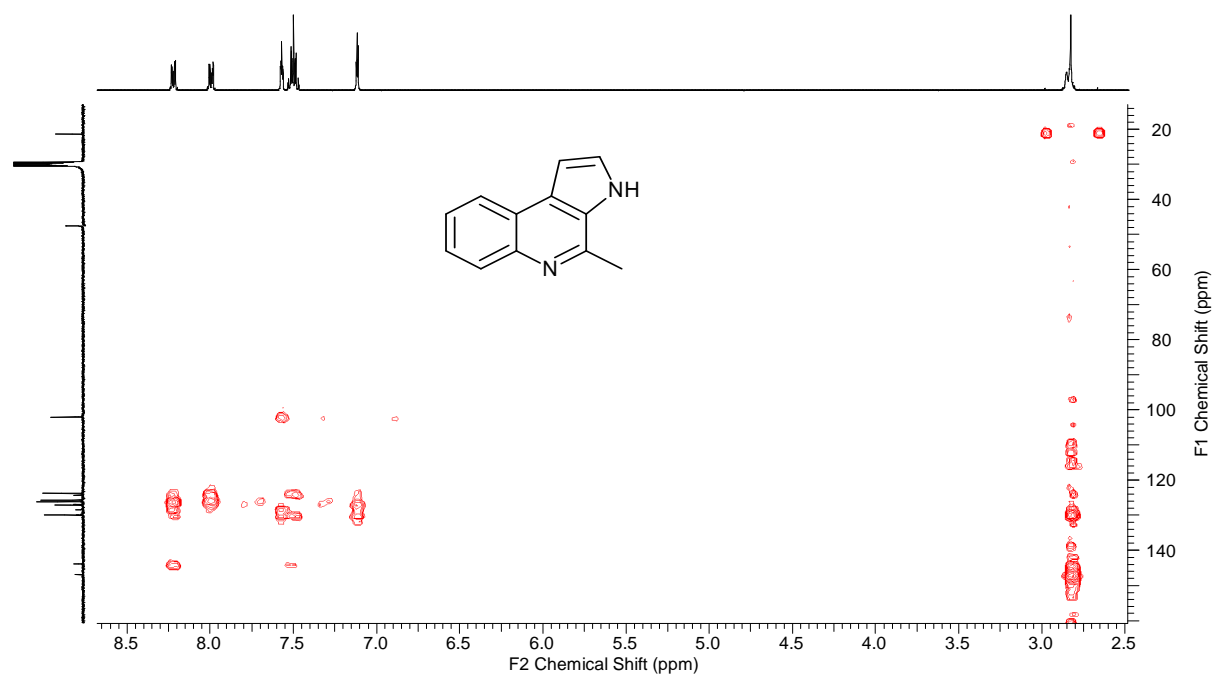
Spectrum 6: ^{1}H,^{13}C HMBC NMR spectrum of marinoquinoline A (**39**) (^{1}H 600 MHz, ^{13}C 150 MHz, acetone-d_6).
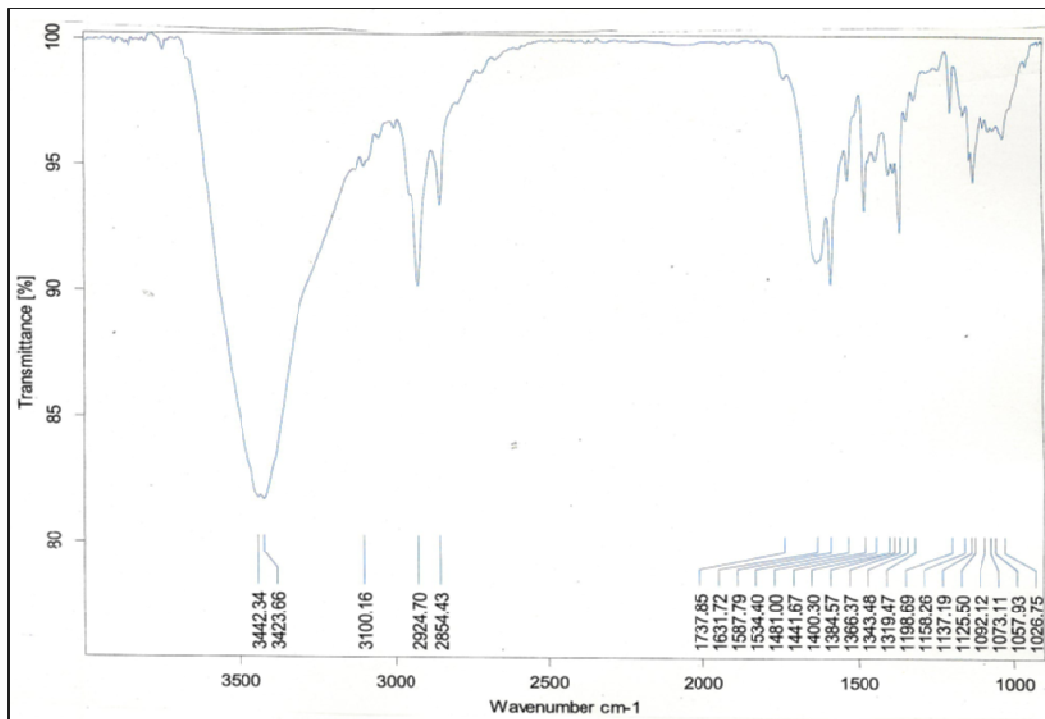
Spectrum 7: IR Spectrum of marinoquinoline A (**39**) (1 mg, 160 mg KBR).

Table 1: Crystal data and structure refinement of marinoquinoline A (**39**).

Empirical formula	$C_{12} H_{10} N_2$	
Formula weight	182.22	
Temperature	153(2) K	
Wavelength	0.71073 Å	
Crystal system	Orthorhombic	
Space group	P2(1)2(1)2	
Unit cell dimensions	a = 18.0708(8) Å	$\alpha = 90°$.
	b = 20.2174(10) Å	$\beta = 90°$.
	c = 5.1124(2) Å	$\sigma = 90°$.
Volume	1867.79(14) $Å^3$	
Z	8	
Density (calculated)	1.296 Mg/m^3	
Absorption coefficient	0.079 mm^{-1}	
F(000)	768	
Crystal size	0.37 x 0.23 x 0.13 mm^3	
Theta range for data collection	1.51 to 27.10°.	
Index ranges	-22<=h<=23, -25<=k<=25, -6<=l<=6	
Reflections collected	12803	
Independent reflections	4110 [R(int) = 0.0811]	
Completeness to theta = 27.10°	99.8 %	
Absorption correction	None	
Max. and min. transmission	0.9895 and 0.9715	
Refinement method	Full-matrix least-squares on F^2	
Data / restraints / parameters	4110 / 0 / 333	
Goodness-of-fit on F^2	1.298	
Final R indices [I>2sigma(I)]	R1 = 0.0629, wR2 = 0.1539	
R indices (all data)	R1 = 0.0723, wR2 = 0.1594	
Absolute structure parameter	1(3)	
Largest diff. peak and hole	0.332 and -0.313 e.$Å^{-3}$	

Table 2: Atomic coordinates (x 10^4) and equivalent isotropic displacement parameters ($Å^2$x 10^3) of marinoquinoline A (**39**) U(eq) is defined as one third of the trace of the orthogonalized U^{ij} tensor.

	x	y	z	U(eq)
N(1)	9805(1)	3020(1)	2487(4)	18(1)
N(2)	8105(1)	3890(1)	477(4)	20(1)
C(1)	9734(1)	2494(1)	746(5)	18(1)
C(2)	10283(1)	1998(1)	825(5)	22(1)
C(3)	10248(1)	1469(1)	-876(6)	25(1)
C(4)	9677(1)	1416(1)	-2715(5)	24(1)
C(5)	9138(1)	1894(1)	-2799(5)	22(1)
C(6)	9149(1)	2436(1)	-1073(5)	19(1)
C(7)	8598(1)	2941(1)	-1007(5)	19(1)
C(8)	7940(1)	3068(1)	-2416(5)	23(1)
C(9)	7662(1)	3649(1)	-1462(5)	24(1)
C(10)	8686(1)	3457(1)	809(5)	18(1)
C(11)	9290(1)	3485(1)	2544(5)	17(1)
C(12)	9360(1)	4033(1)	4517(5)	21(1)
N(3)	2818(1)	9814(1)	7453(4)	18(1)
N(4)	3752(1)	8278(1)	5380(4)	20(1)
C(13)	2236(1)	9772(1)	5715(5)	18(1)
C(14)	1698(1)	10281(1)	5780(5)	22(1)
C(15)	1113(1)	10276(1)	4050(6)	25(1)
C(16)	1038(1)	9765(1)	2208(5)	24(1)
C(17)	1546(1)	9261(1)	2130(5)	22(1)
C(18)	2151(1)	9251(1)	3871(5)	17(1)
C(19)	2701(1)	8744(1)	3931(5)	18(1)
C(20)	2828(1)	8158(1)	2472(5)	22(1)
C(21)	3472(1)	7895(1)	3416(5)	22(1)
C(22)	3279(1)	8804(1)	5723(5)	17(1)
C(23)	3329(1)	9345(1)	7501(5)	17(1)
C(24)	3941(1)	9397(1)	9452(5)	22(1)

Table 3: Bond lengths [Å] and angles [°] of marinoquinoline A (**39**). Symmetry transformations used to generate equivalent atoms.

N(1)-C(11)	1.323(3)
N(1)-C(1)	1.392(3)
N(2)-C(9)	1.364(3)
N(2)-C(10)	1.377(3)
C(1)-C(2)	1.412(3)
C(1)-C(6)	1.413(3)
C(2)-C(3)	1.379(4)
C(3)-C(4)	1.400(4)
C(4)-C(5)	1.374(3)
C(5)-C(6)	1.406(3)
C(6)-C(7)	1.428(3)
C(7)-C(10)	1.406(3)
C(7)-C(8)	1.413(3)
C(8)-C(9)	1.367(3)
C(10)-C(11)	1.408(3)
C(11)-C(12)	1.505(3)
N(3)-C(23)	1.324(3)
N(3)-C(13)	1.379(3)
N(4)-C(21)	1.365(3)
N(4)-C(22)	1.376(3)
C(13)-C(14)	1.417(3)
C(13)-C(18)	1.422(3)
C(14)-C(15)	1.379(4)
C(15)-C(16)	1.405(4)
C(16)-C(17)	1.371(3)
C(17)-C(18)	1.410(3)
C(18)-C(19)	1.428(3)
C(19)-C(22)	1.394(3)
C(19)-C(20)	1.418(3)
C(20)-C(21)	1.368(3)
C(22)-C(23)	1.425(3)
C(23)-C(24)	1.493(3)
C(11)-N(1)-C(1)	119.49(19)
C(9)-N(2)-C(10)	108.1(2)
N(1)-C(1)-C(2)	117.4(2)
N(1)-C(1)-C(6)	123.60(19)
C(2)-C(1)-C(6)	119.0(2)
C(3)-C(2)-C(1)	120.0(2)
C(2)-C(3)-C(4)	121.1(2)
C(5)-C(4)-C(3)	119.3(2)
C(4)-C(5)-C(6)	121.2(2)
C(5)-C(6)-C(1)	119.3(2)
C(5)-C(6)-C(7)	124.2(2)
C(1)-C(6)-C(7)	116.5(2)
C(10)-C(7)-C(8)	107.3(2)
C(10)-C(7)-C(6)	117.9(2)
C(8)-C(7)-C(6)	134.8(2)
C(9)-C(8)-C(7)	106.5(2)

N(2)-C(9)-C(8)	110.4(2)
N(2)-C(10)-C(7)	107.6(2)
N(2)-C(10)-C(11)	130.1(2)
C(7)-C(10)-C(11)	122.3(2)
N(1)-C(11)-C(10)	120.2(2)
N(1)-C(11)-C(12)	118.7(2)
C(10)-C(11)-C(12)	121.1(2)
C(23)-N(3)-C(13)	119.93(19)
C(21)-N(4)-C(22)	107.6(2)
N(3)-C(13)-C(14)	117.6(2)
N(3)-C(13)-C(18)	123.79(19)
C(14)-C(13)-C(18)	118.6(2)
C(15)-C(14)-C(13)	120.4(2)
C(14)-C(15)-C(16)	120.6(2)
C(17)-C(16)-C(15)	120.1(2)
C(16)-C(17)-C(18)	120.7(2)
C(17)-C(18)-C(13)	119.5(2)
C(17)-C(18)-C(19)	124.3(2)
C(13)-C(18)-C(19)	116.2(2)
C(22)-C(19)-C(20)	107.3(2)
C(22)-C(19)-C(18)	118.2(2)
C(20)-C(19)-C(18)	134.4(2)
C(21)-C(20)-C(19)	106.1(2)
N(4)-C(21)-C(20)	110.7(2)
N(4)-C(22)-C(19)	108.3(2)
N(4)-C(22)-C(23)	129.4(2)
C(19)-C(22)-C(23)	122.26(19)
N(3)-C(23)-C(22)	119.6(2)
N(3)-C(23)-C(24)	118.6(2)
C(22)-C(23)-C(24)	121.8(2)

Table 4: Anisotropic displacement parameters (Å^2x 10^3) of marinoquinoline A (**39**). The anisotropic displacement factor exponent takes the form: $-2\pi^2[\ h^2\ a^{*2}U^{11} + ... + 2\ h\ k\ a^*\ b^*\ U^{12}\ ]$.

	U^{11}	U^{22}	U^{33}	U^{23}	U^{13}	U^{12}
N(1)	16(1)	18(1)	19(1)	-2(1)	2(1)	-1(1)
N(2)	19(1)	19(1)	22(1)	-2(1)	-2(1)	2(1)
C(1)	20(1)	15(1)	18(1)	2(1)	6(1)	-3(1)
C(2)	21(1)	23(1)	24(1)	3(1)	4(1)	0(1)
C(3)	27(1)	18(1)	30(1)	2(1)	8(1)	4(1)
C(4)	28(1)	20(1)	25(1)	-4(1)	9(1)	-3(1)
C(5)	25(1)	23(1)	18(1)	1(1)	0(1)	-4(1)
C(6)	19(1)	18(1)	19(1)	3(1)	5(1)	-5(1)
C(7)	21(1)	20(1)	16(1)	2(1)	1(1)	-4(1)
C(8)	23(1)	25(1)	21(1)	-1(1)	-3(1)	-3(1)
C(9)	23(1)	26(1)	22(1)	1(1)	-1(1)	0(1)
C(10)	15(1)	20(1)	19(1)	2(1)	4(1)	0(1)
C(11)	18(1)	18(1)	15(1)	1(1)	1(1)	-3(1)
C(12)	22(1)	20(1)	22(1)	-4(1)	0(1)	-1(1)
N(3)	18(1)	19(1)	18(1)	0(1)	0(1)	-1(1)
N(4)	20(1)	18(1)	22(1)	0(1)	1(1)	1(1)
C(13)	13(1)	22(1)	19(1)	2(1)	4(1)	-1(1)
C(14)	22(1)	21(1)	23(1)	2(1)	1(1)	0(1)
C(15)	17(1)	25(1)	32(2)	6(1)	3(1)	4(1)
C(16)	14(1)	35(1)	23(1)	6(1)	-4(1)	-2(1)
C(17)	21(1)	29(1)	17(1)	1(1)	0(1)	-3(1)
C(18)	14(1)	21(1)	17(1)	5(1)	1(1)	-2(1)
C(19)	17(1)	18(1)	20(1)	2(1)	4(1)	-2(1)
C(20)	22(1)	24(1)	20(1)	-2(1)	3(1)	-4(1)
C(21)	23(1)	20(1)	23(1)	0(1)	4(1)	-1(1)
C(22)	13(1)	19(1)	20(1)	4(1)	3(1)	1(1)
C(23)	15(1)	18(1)	18(1)	4(1)	3(1)	-2(1)
C(24)	22(1)	24(1)	21(1)	-1(1)	-4(1)	-3(1)

Table 5: Hydrogen coordinates (x 10^4) and isotropic displacement parameters ($\mathring{A}^2$x 10^3) of marinoquinoline A (**39**).

	x	y	z	U(eq)
H(1)	10677(18)	2088(15)	2010(70)	44(9)
H(2)	10639(14)	1148(13)	-920(60)	24(7)
H(3)	9655(16)	1029(15)	-3710(70)	41(9)
H(4)	8744(15)	1915(12)	-3950(60)	24(7)
H(5)	7685(15)	2801(12)	-3740(60)	25(7)
H(6)	7191(13)	3878(11)	-2040(50)	12(6)
H(7)	8077(16)	4276(15)	1310(70)	42(9)
H(8)	9429(16)	4464(16)	3840(70)	44(9)
H(9)	9828(15)	4016(11)	5510(60)	18(6)
H(10)	8900(20)	4064(17)	5630(80)	64(11)
H(11)	1789(13)	10628(12)	7200(50)	16(6)
H(12)	745(14)	10640(12)	4000(60)	23(7)
H(13)	681(15)	9752(12)	1100(60)	22(7)
H(14)	1484(15)	8930(13)	680(60)	31(8)
H(15)	2546(15)	7971(12)	970(60)	28(7)
H(16)	3725(13)	7513(12)	2910(50)	19(6)
H(17)	4260(20)	8193(15)	6170(70)	47(9)
H(18)	3809(19)	9801(17)	10460(70)	58(10)
H(19)	3996(16)	9004(13)	10510(60)	31(8)
H(20)	4446(18)	9497(14)	8380(60)	43(9)

6.2.2 Spectra of marinoquinoline B (40)
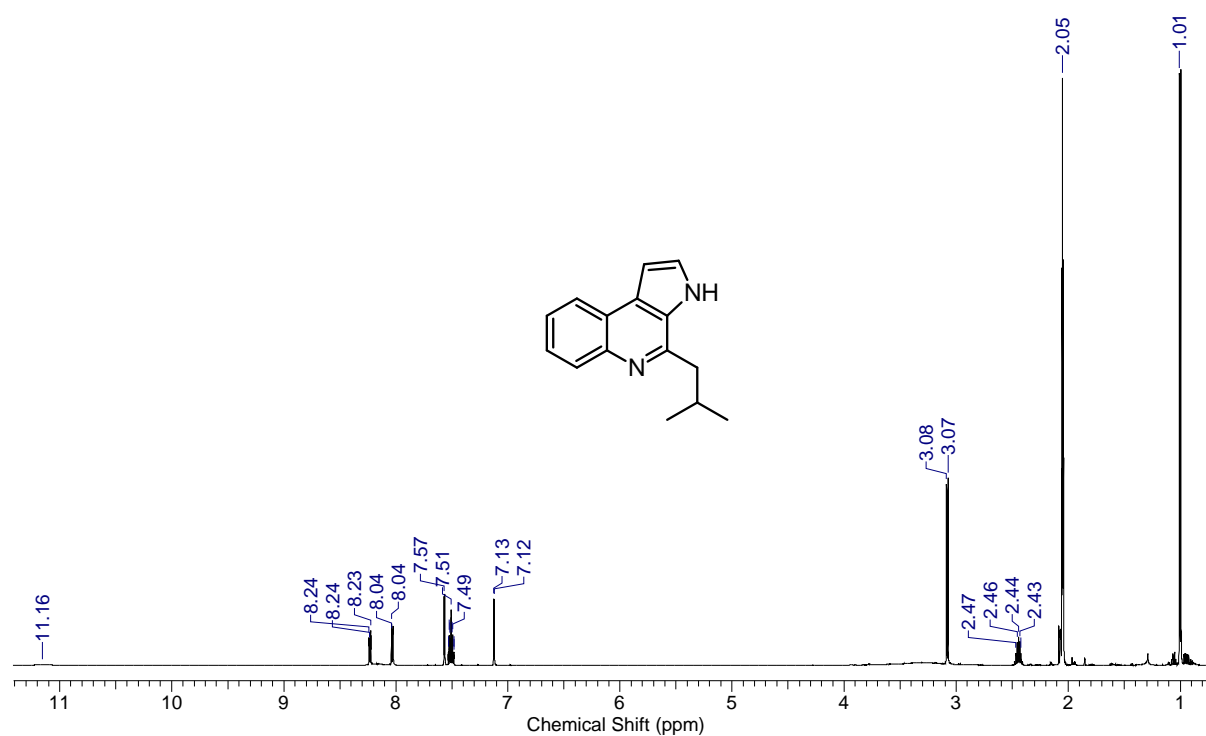
Spectrum 8: ^{1}H NMR spectrum of marinoquinoline B (**40**) (^{1}H 600 MHz, acetone-d_6).
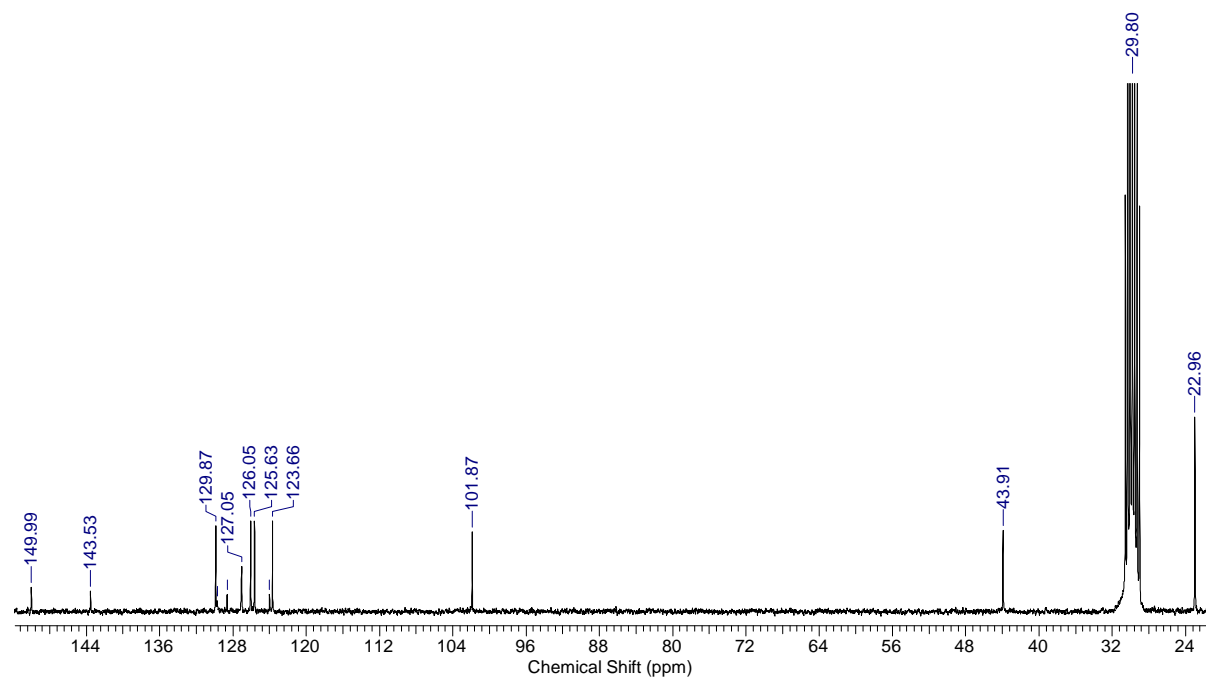
Spectrum 9: ^{13}C NMR spectrum of marinoquinoline B (**40**) (^{13}C 150 MHz, acetone-d_6).
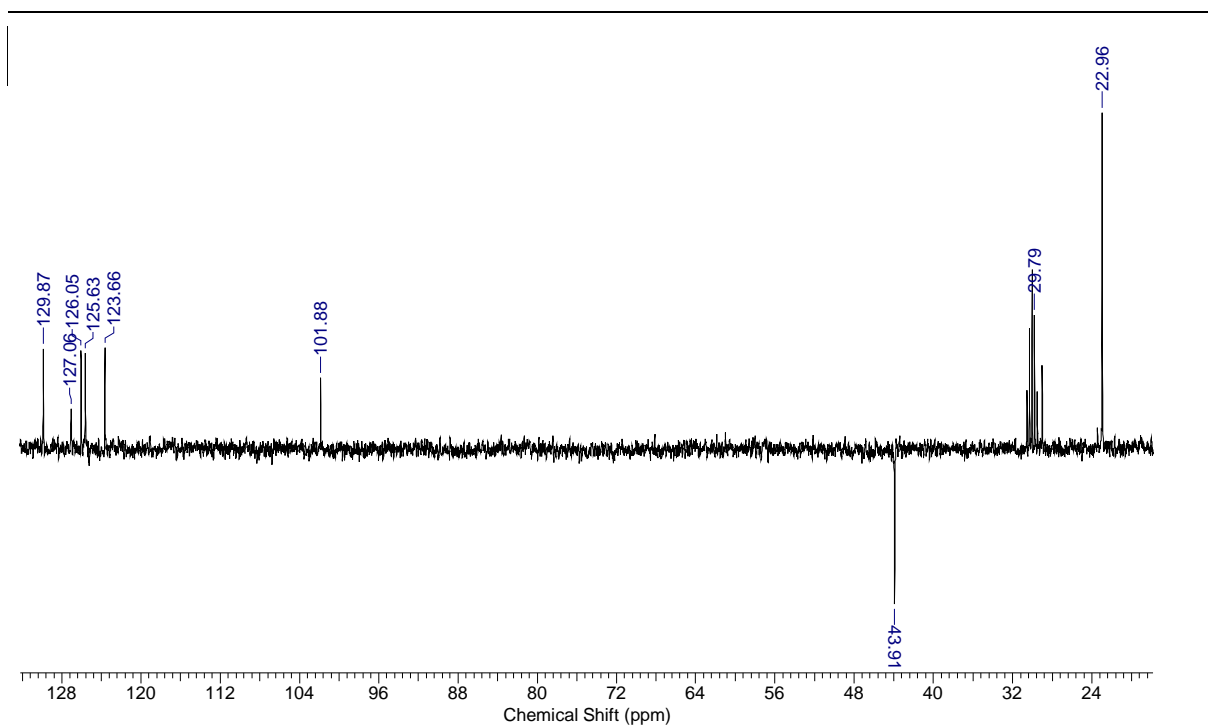
Spectrum 10: ^{13}C DEPT NMR spectrum of marinoquinoline B (**40**) (^{13}C 150 MHz, acetone-d_6).
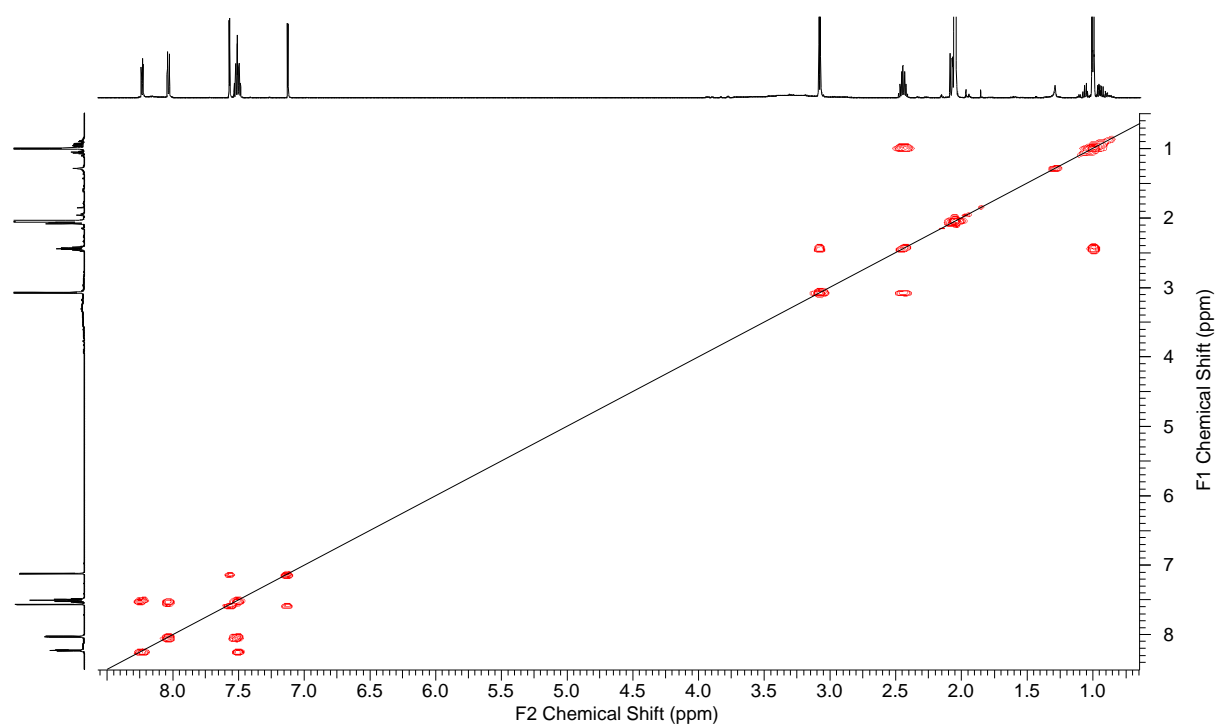
Spectrum 11: ^{1}H,^{1}H COSY NMR spectrum of marinoquinoline B (**40**) (^{1}H 600 MHz, acetone-d_6).
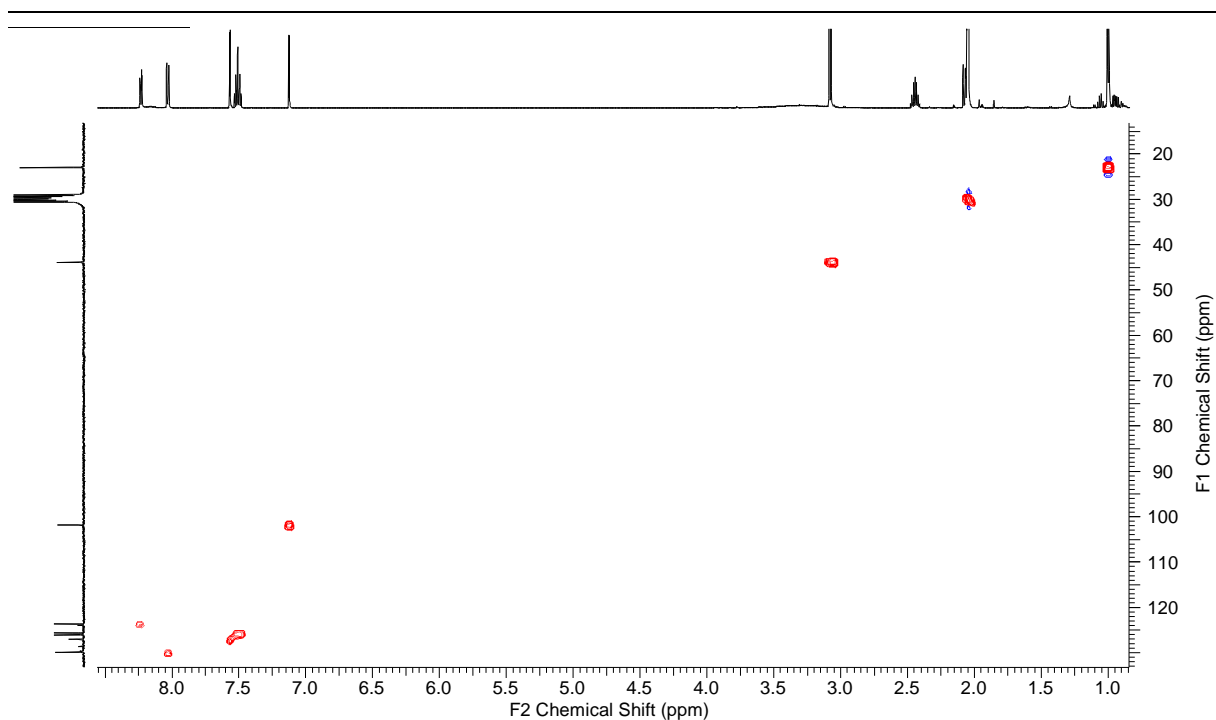
Spectrum 12: ^{1}H,^{13}C HMQC NMR spectrum of marinoquinoline B (**40**) (^{1}H 600 MHz, ^{13}C 150 MHz, acetone-d_6).
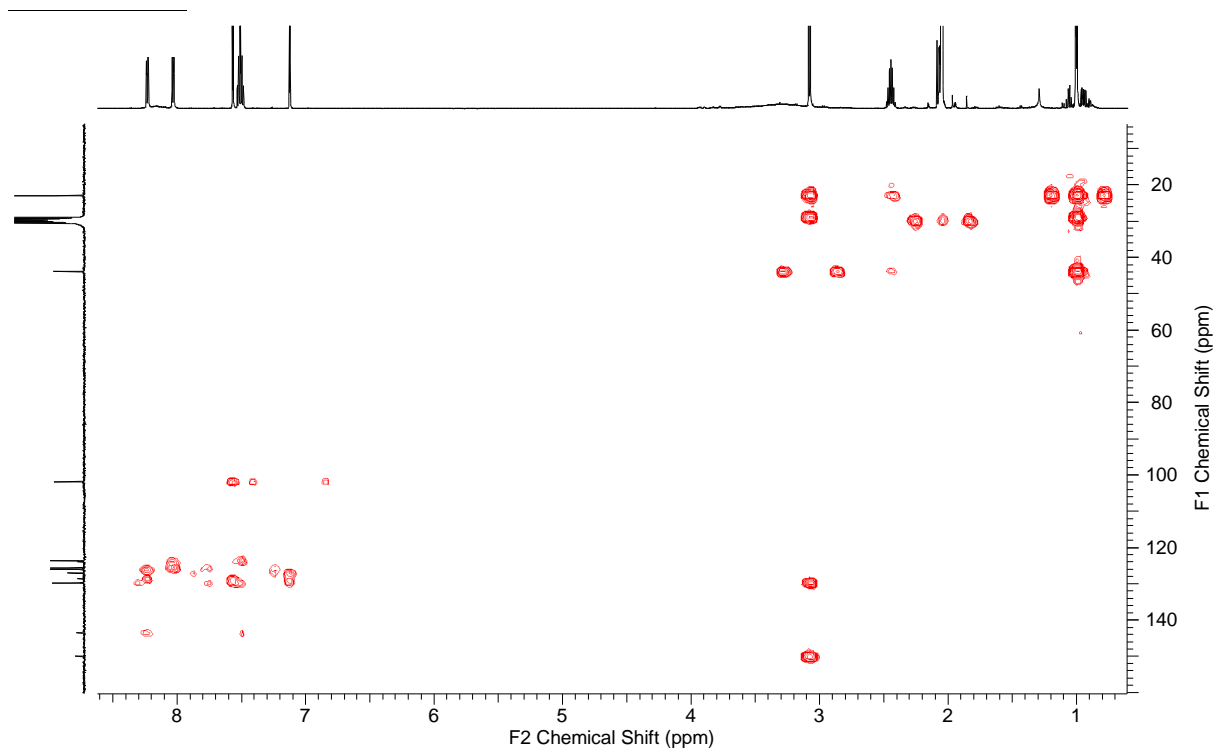
Spetrum 13: ^{1}H,^{13}C HMBC NMR spectrum of marinoquinoline B (**40**) (^{1}H 600 MHz, ^{13}C 150 MHz, acetone-d_6).

6.2.3 Spectra of marinoquinoline C (41)
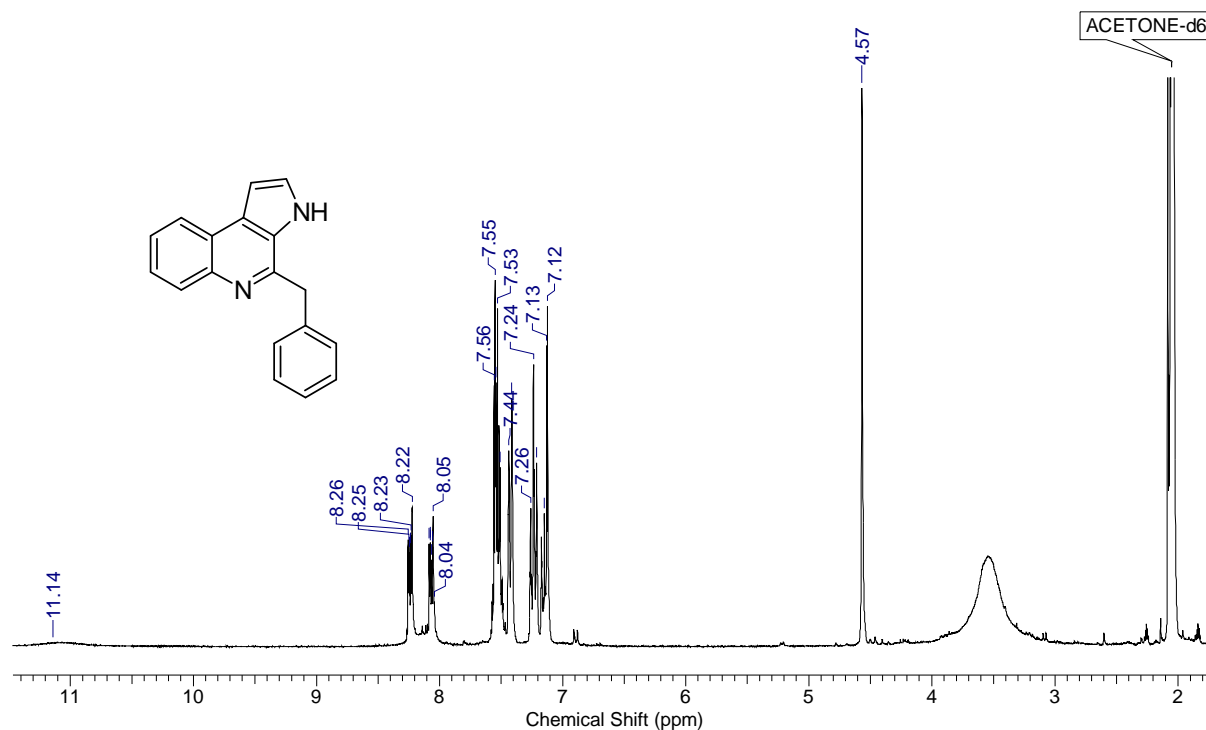
Spectrum 14: ^{1}H NMR spectrum of marinoquinoline C (**41**) (^{1}H 600 MHz, acetone-d_6).
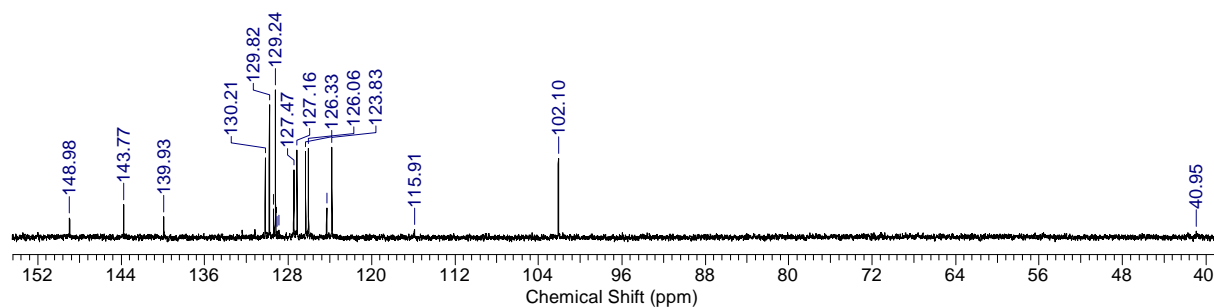
Spectrum 15: ^{13}C NMR spectrum of marinoquinoline C (**41**) (^{13}C 150 MHz, acetone-d_6).
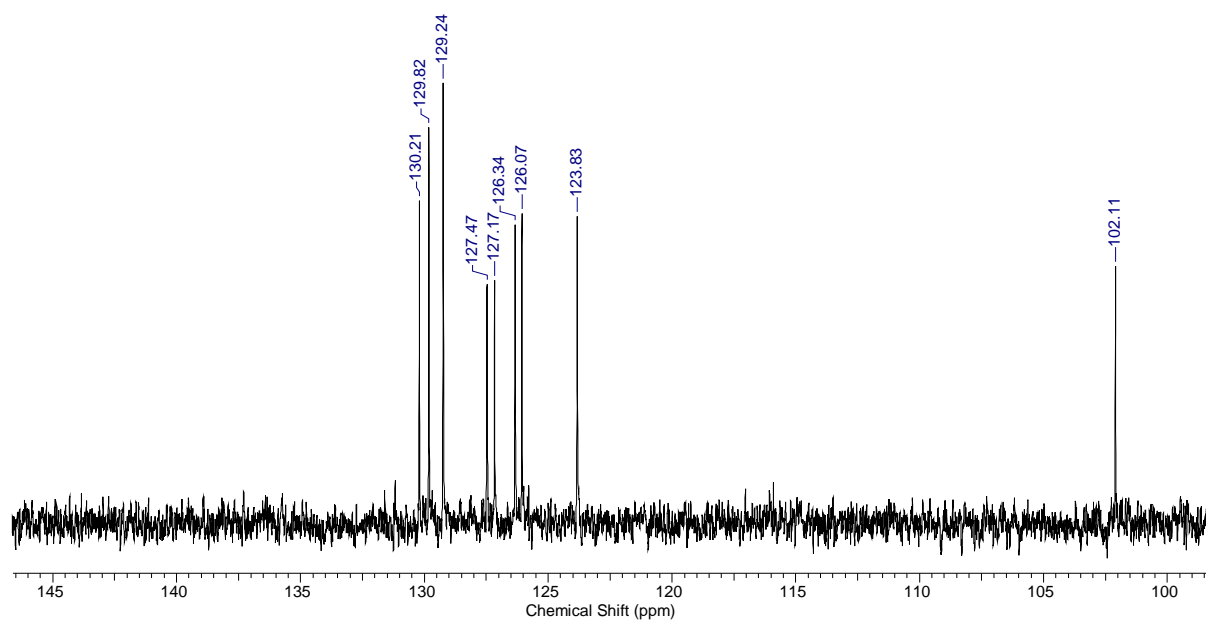
Spectrum 16: 13C DEPT NMR spectrum of marinoquinoline C(**41**) (^{13}C 150 MHz, acetone-d_6).
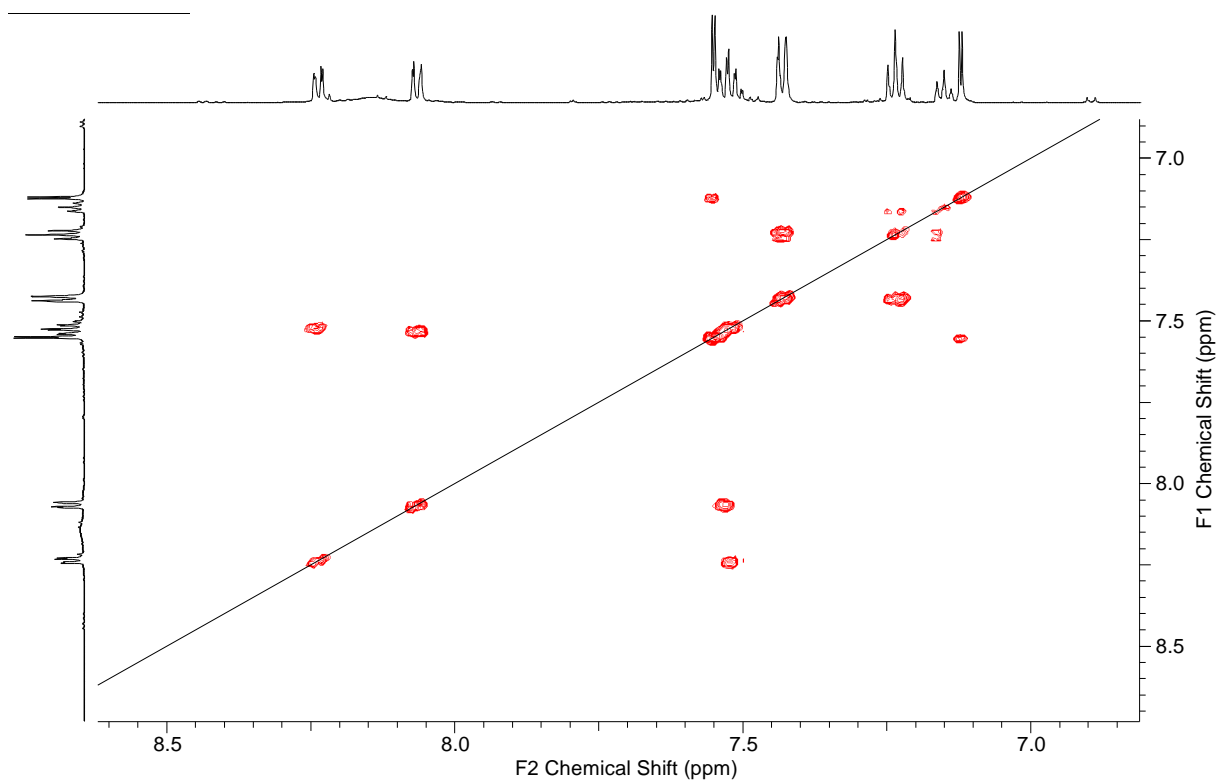
Spectrum 17: ^{1}H,^{1}H COSY NMR spectrum of marinoquinoline C (**41**) (^{1}H 600 MHz, acetone-d_6).
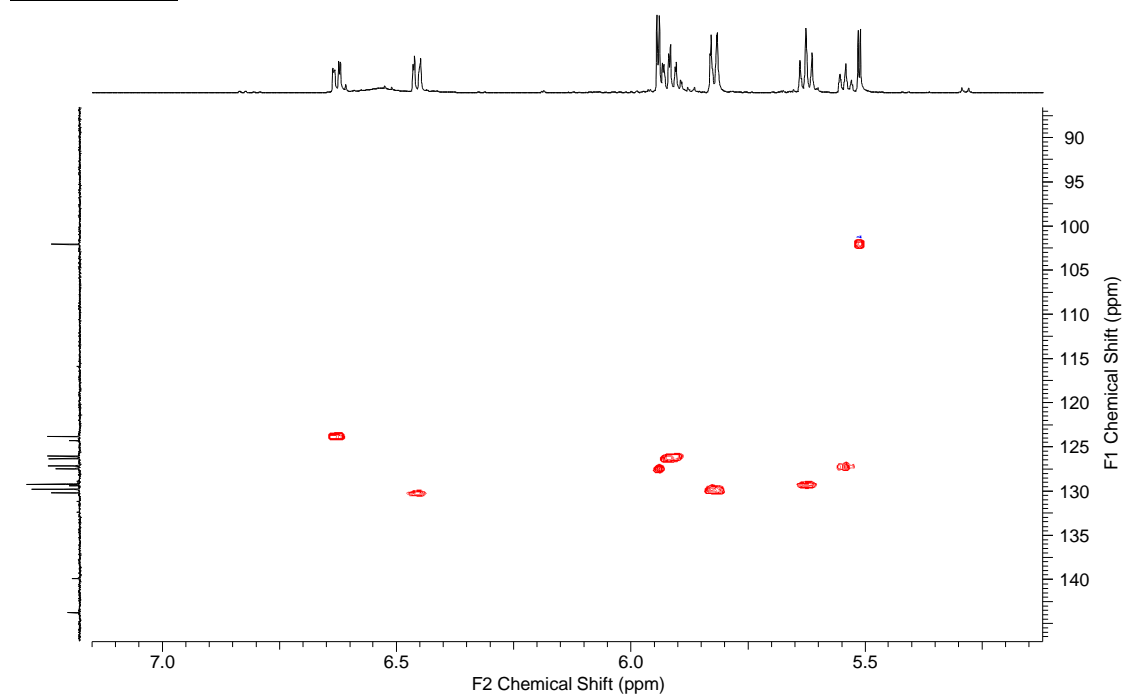
Spectrum 18: ^{1}H,^{13}C HMQC NMR spectrum of marinoquinoline C (**41**) (^{1}H 600 MHz, ^{13}C 150 MHz, acetone-d_6).
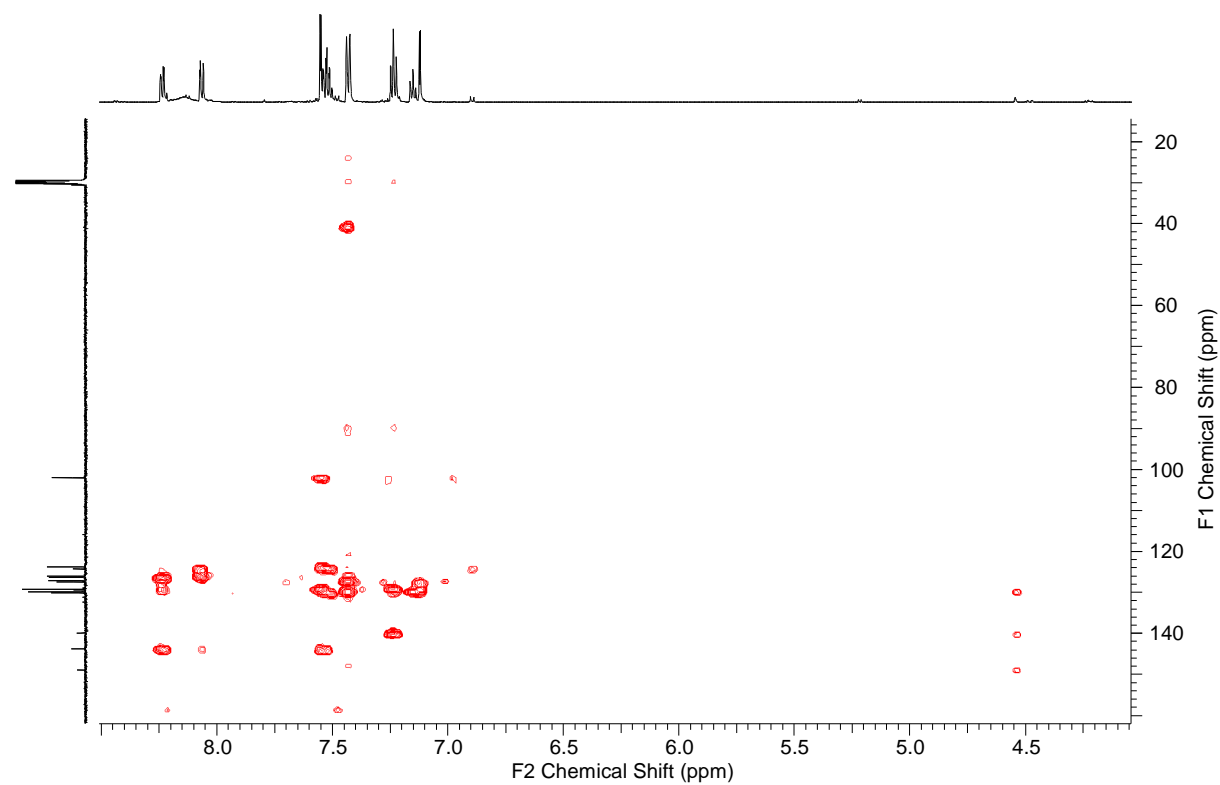
Spectrum 19: ^{1}H,^{13}C HMBC NMR spectrum of marinoquinoline C (**41**) (^{1}H 600 MHz, ^{13}C 150 MHz, acetone-d_6).

6.2.4 Spectra of marinoquinoline D (42)

METHANOL-d4

8.44
8.39
8.38
8.13
8.12
8.11
7.85
7.85
7.71
7.70
7.69
7.30
7.29
7.19
7.18
6.75
6.74
4.60
4.58
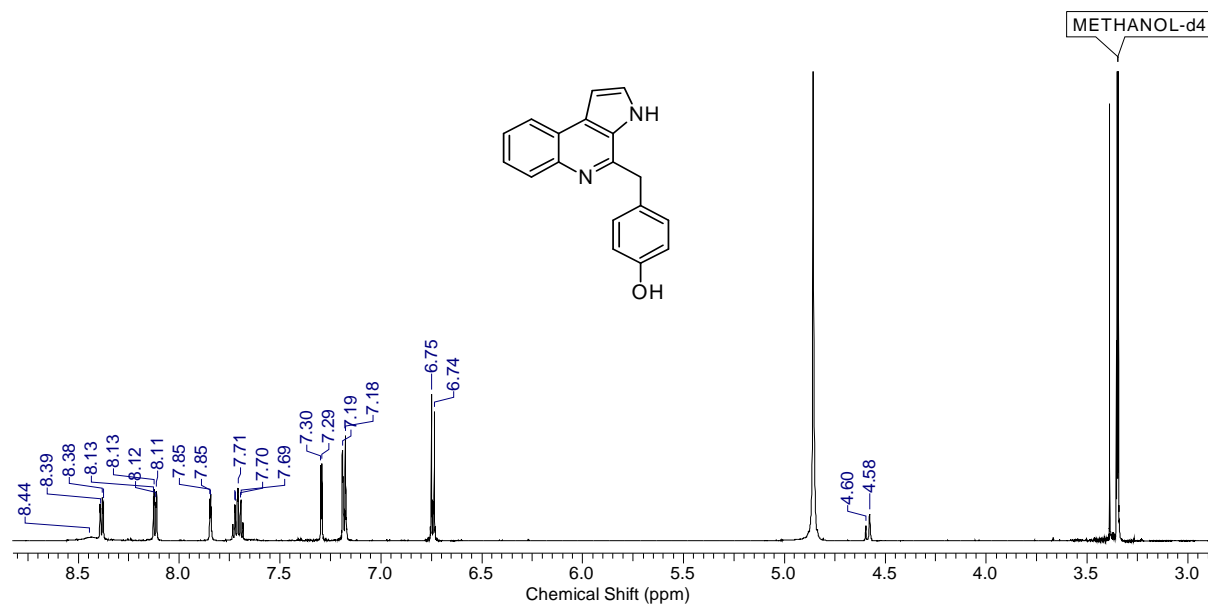
Spectrum 20: ^{1}H NMR spectrum of marinoquinoline D (**42**) (^{1}H 300 MHz, CD$_3$OD).

49.56
49.28
49.00
48.72
48.44

157.62
148.83
139.30
133.21
130.60
128.67
127.77
124.77
123.90
116.60
103.42
38.64
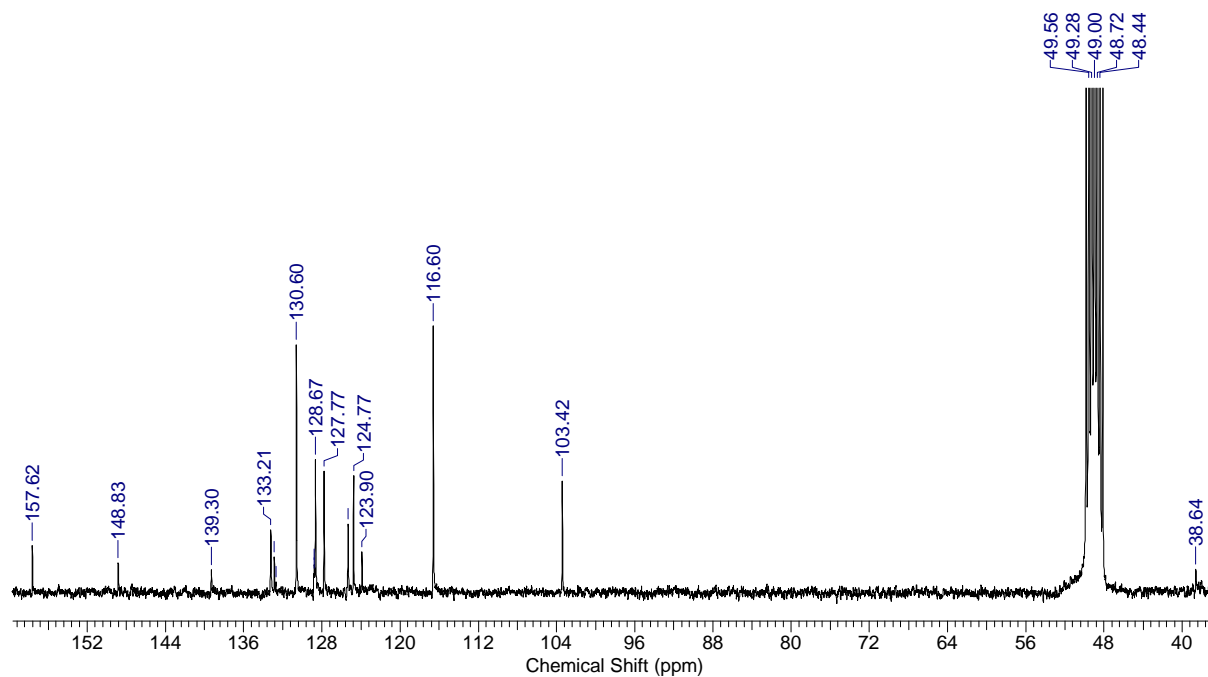
Spectrum 21: ^{13}C NMR spectrum of marinoquinoline D (**42**) (^{13}C 75 MHz, CD$_3$OD).

116
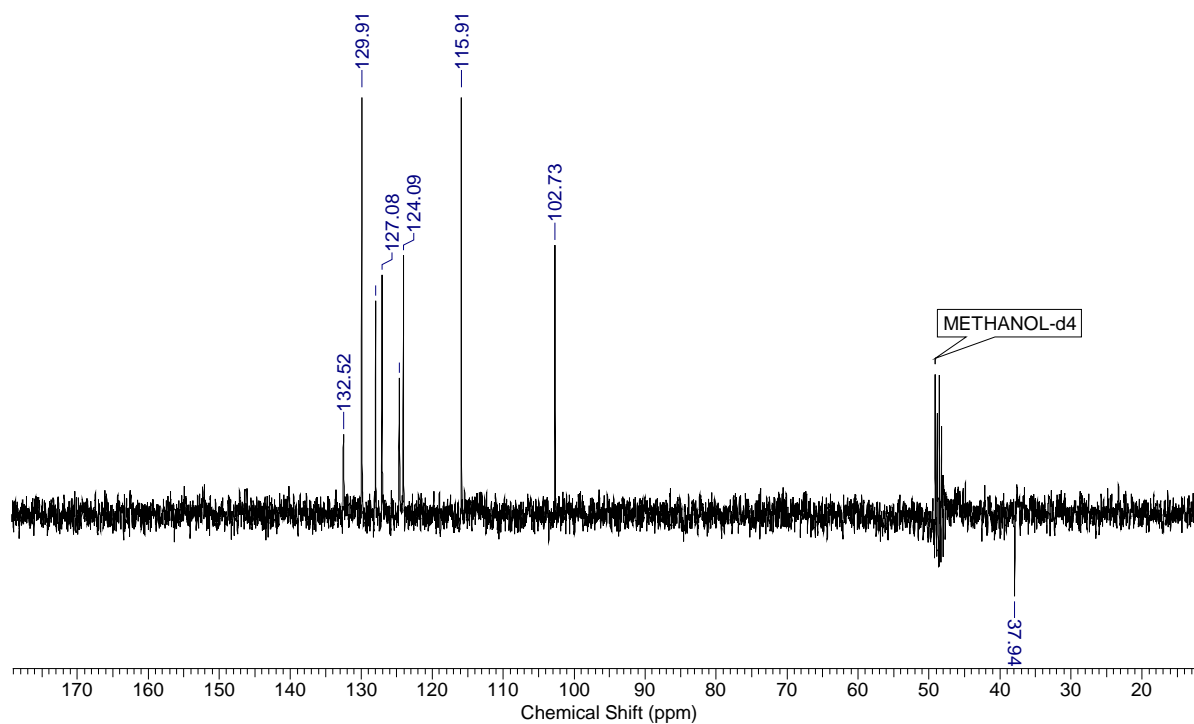
Spectrum 22: ^{13}C DEPT NMR spectrum of marinoquinoline D (**42**) ([13]C 75 MHz, CD$_3$OD).
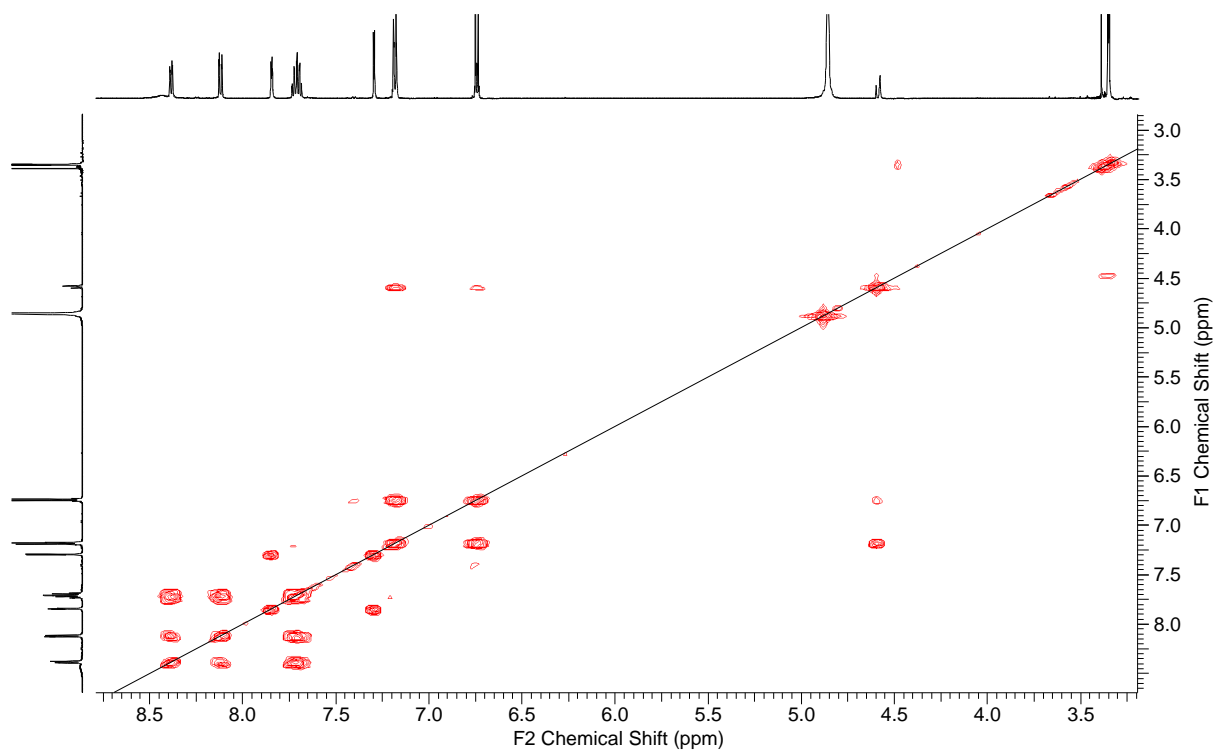
Spectrum 23: ^{1}H,^{1}H COSY NMR spectrum of marinoquinoline D(**42**) ([1]H 300 MHz, CD$_3$OD).
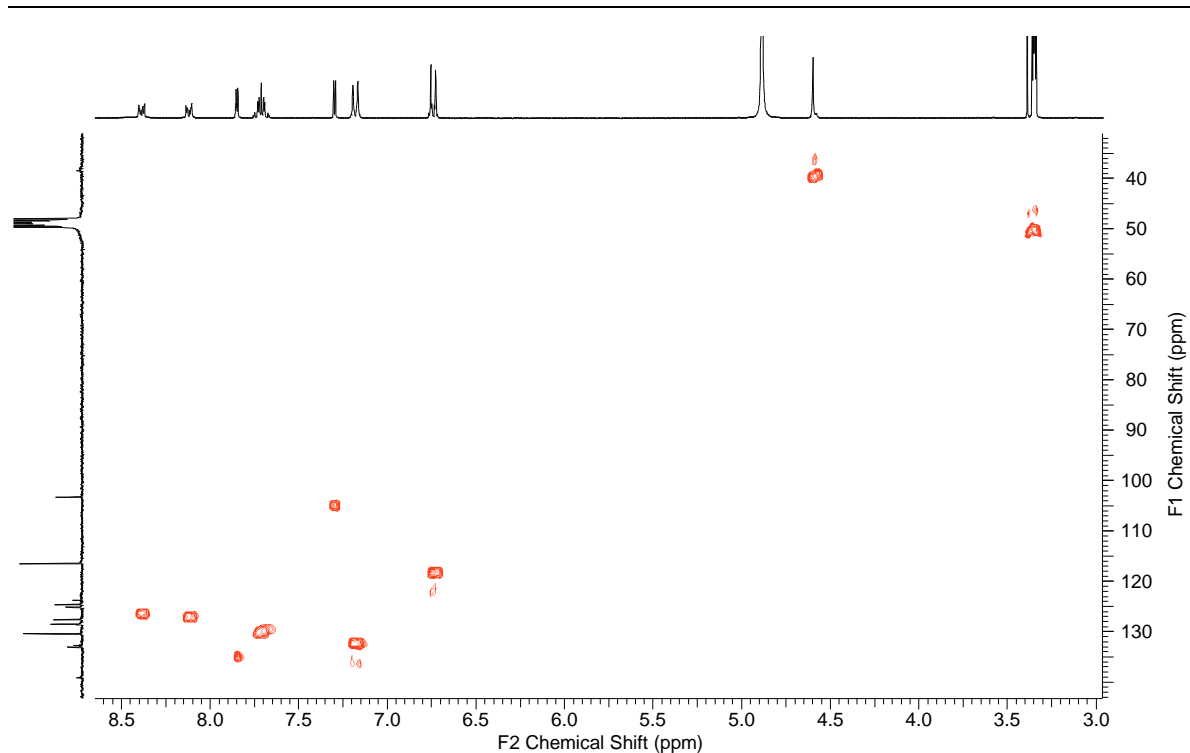
Spectrum 24: ^{1}H,^{13}C HMQC NMR spectrum of marinoquinoline D(**42**) (^{1}H 300 MHz,^{13}C 75 MHz, CD$_3$OD).
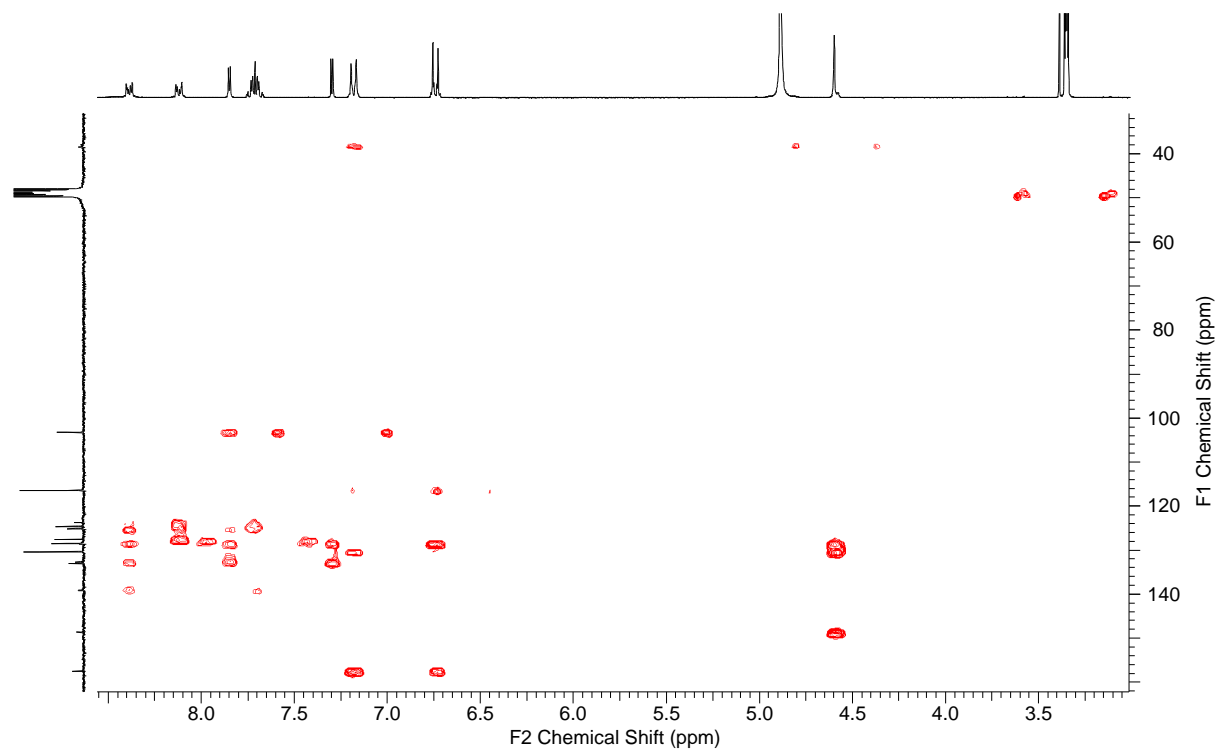
Spectrum 25: ^{1}H,^{13}C HMBC spectrum of marinoquinoline D (**42**) (^{1}H 300 MHz,^{13}C 75 MHz, CD$_3$OD).

118

6.2.5 Spectra of marinoquinoline E (43)
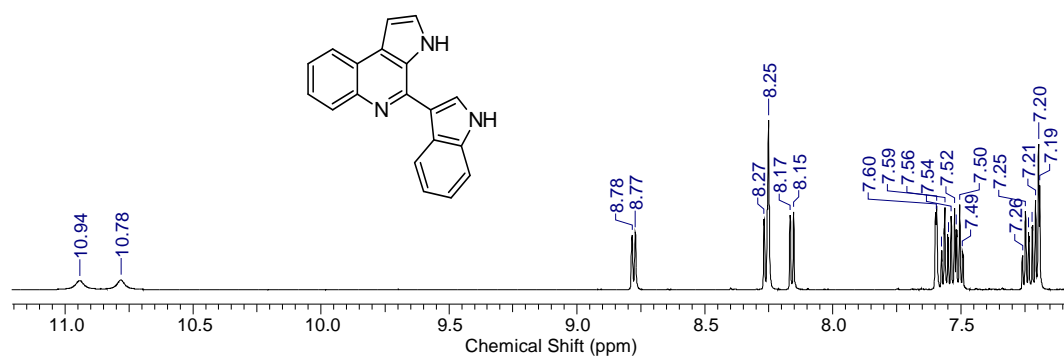
Spectrum 26: ^{1}H NMR spectrum of marinoquinoline E (**43**) (^{1}H 600 MHz, acetone-d_6).
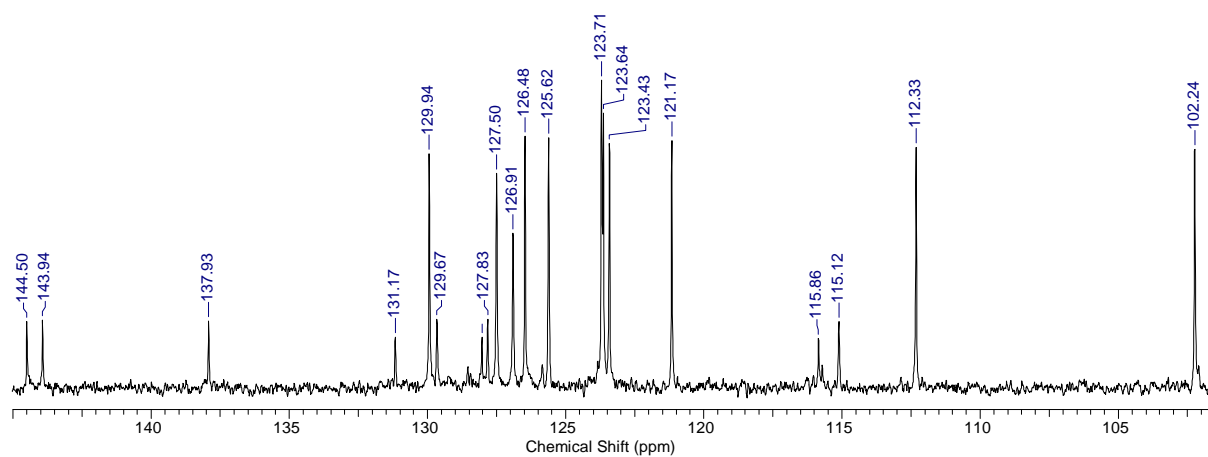
Spectrum 27: ^{13}C NMR spectrum of marinoquinoline E (**43**) (^{13}C 150 MHz, acetone-d_6).

119
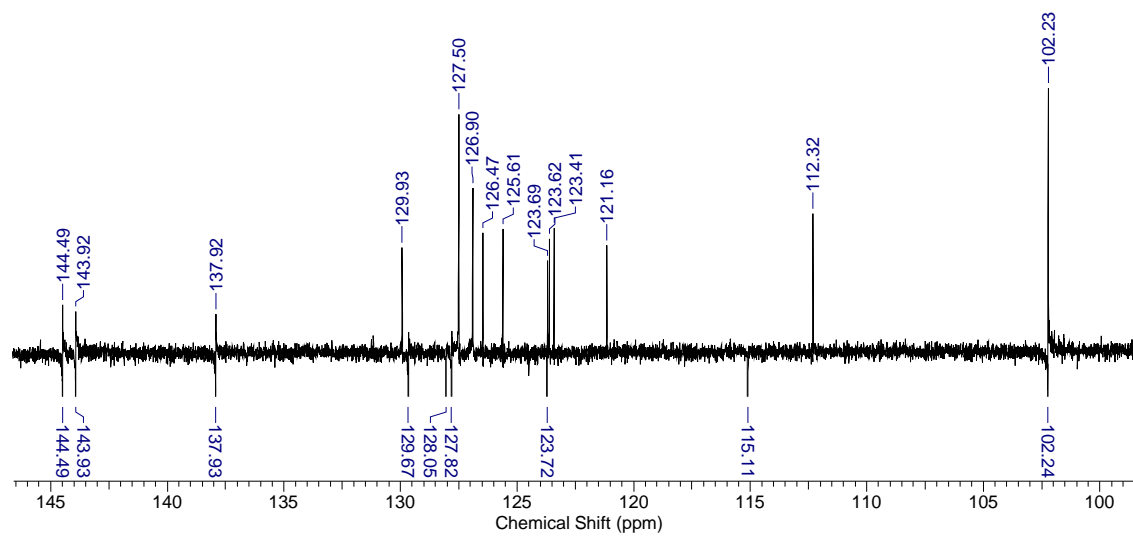
Spectrum 28: ^{13}C APT NMR spectrum of marinoquinoline E (**43**) (^{13}C 150 MHz, acetone-d_6).
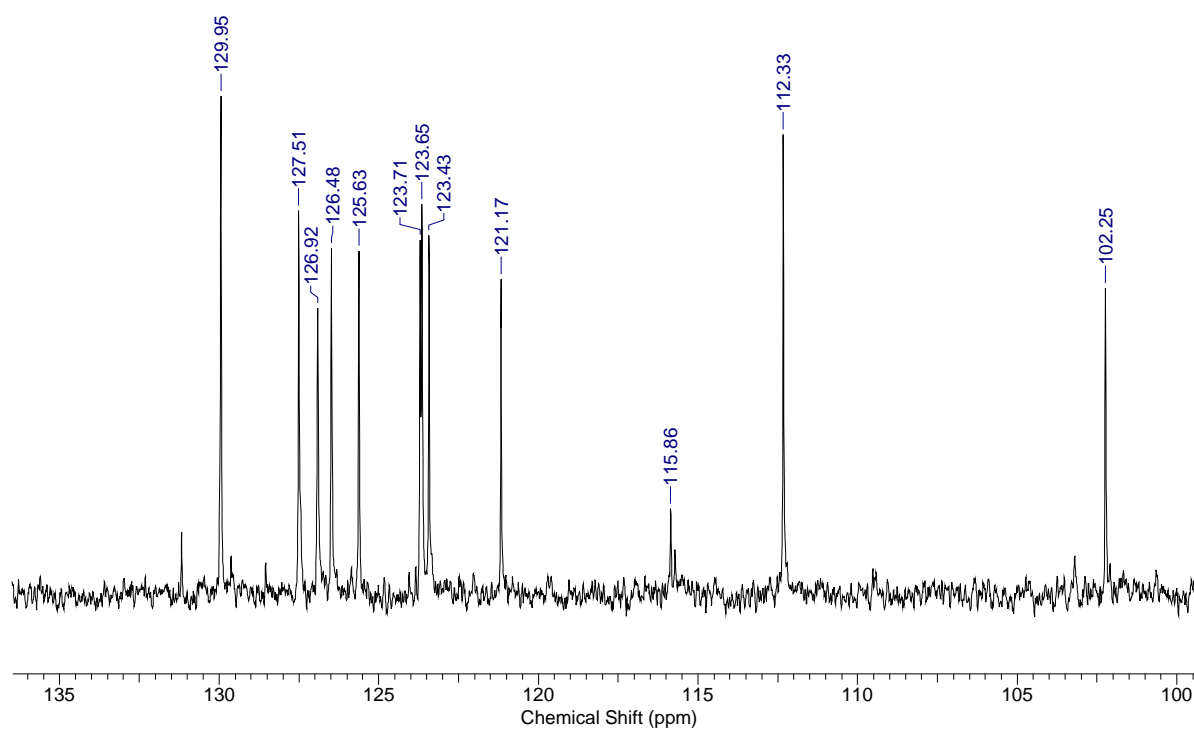
Spectrum 29: ^{13}C DEPT NMR spectrum of marinoquinoline E (**43**) (^{13}C 150 MHz, acetone-d_6).

120
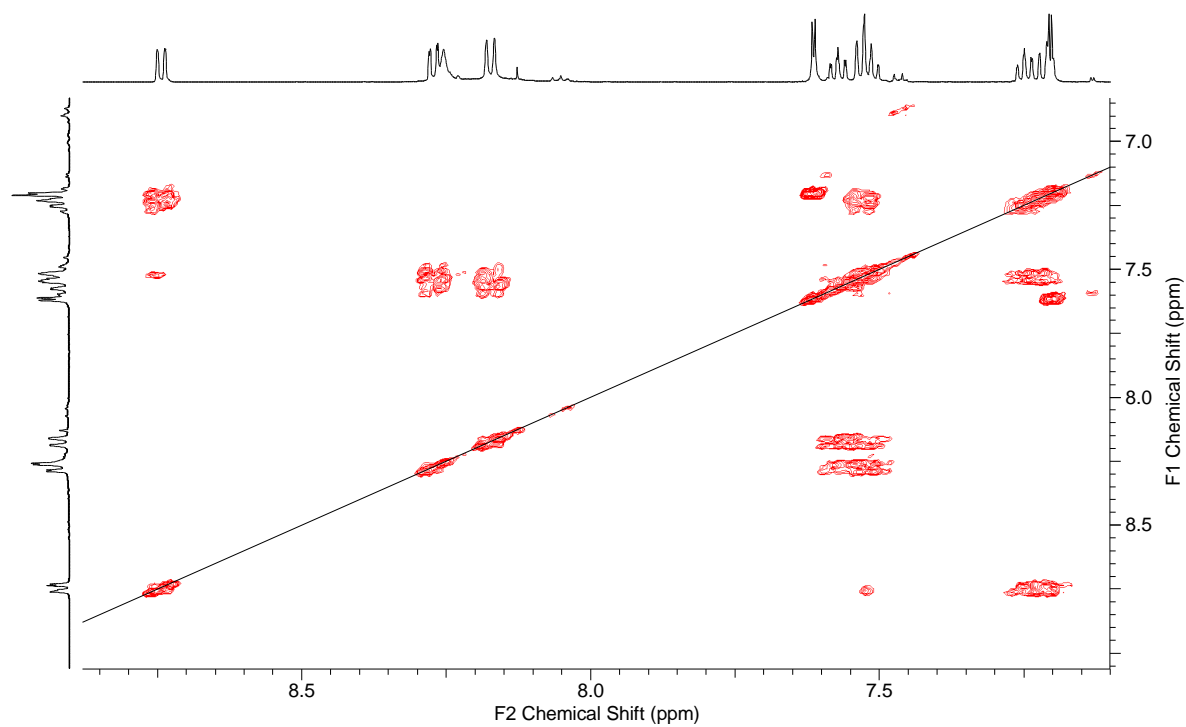
Spectrum 30: ^{1}H,^{1}H COSY NMR spectrum of marinoquinoline E (**43**) (^{1}H 600 MHz, acetone-d_6).
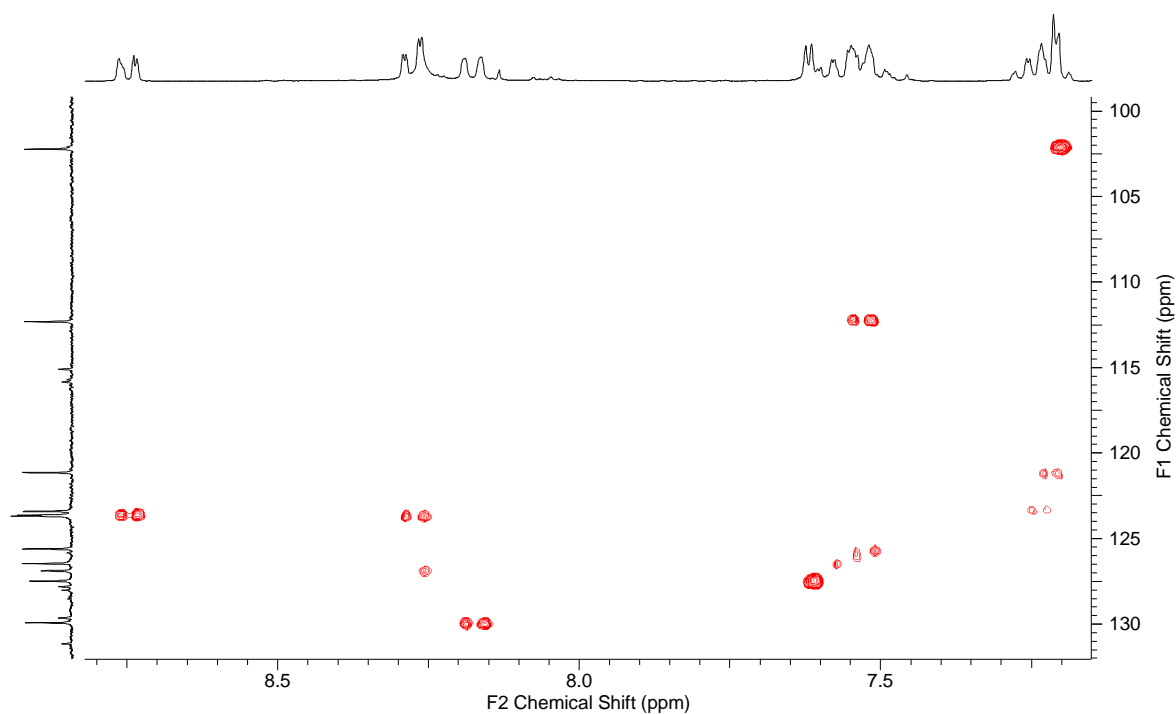
Spectrum 31: ^{1}H,^{13}C HMQC NMR spectrum of marinoquinoline E(**43**) (^{1}H 600 MHz, ^{13}C 150 MHz, acetone-d_6).
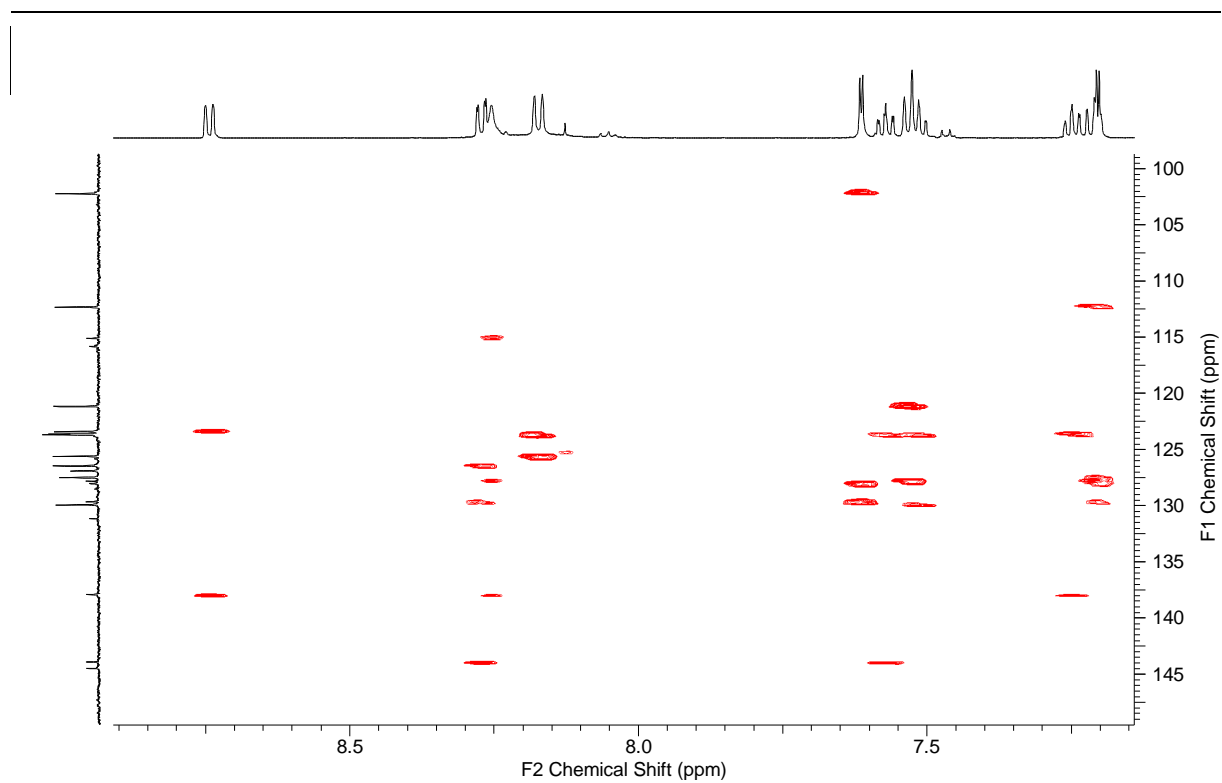
Spectrum 32: ^{1}H,^{13}C HMBC NMR spectrum of marinoquinoline E (**43**) (^{1}H 600 MHz,^{13}C 150 MHz, acetone-d_6).

6.2.6 Spectra of marinoquinoline F (44)
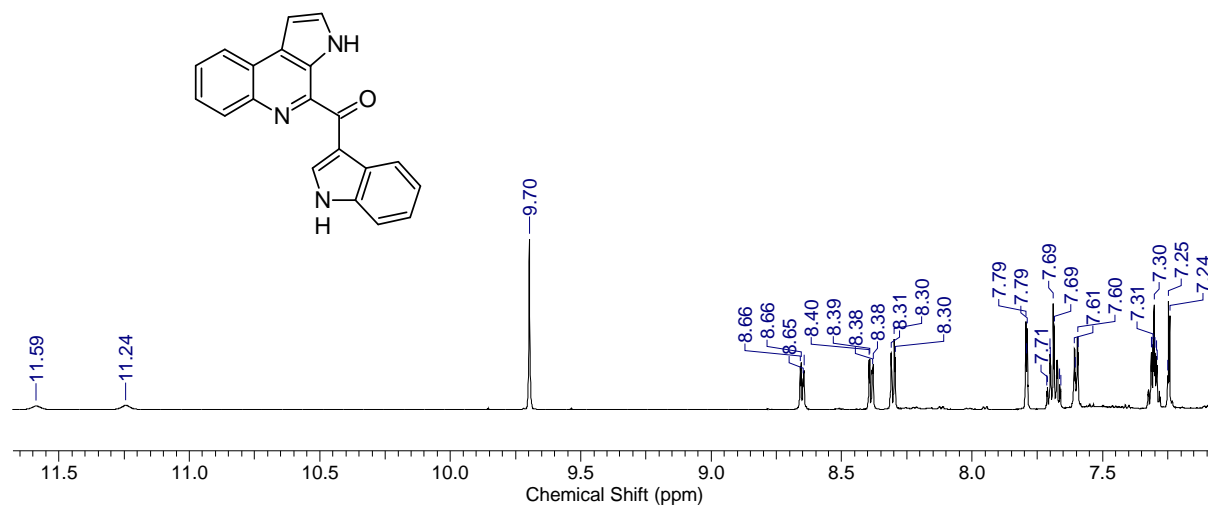
Spectrum 33: ^{1}H NMR spectrum of marinoquinoline F (**44**) (^{1}H 600 MHz, acetone-d_6).
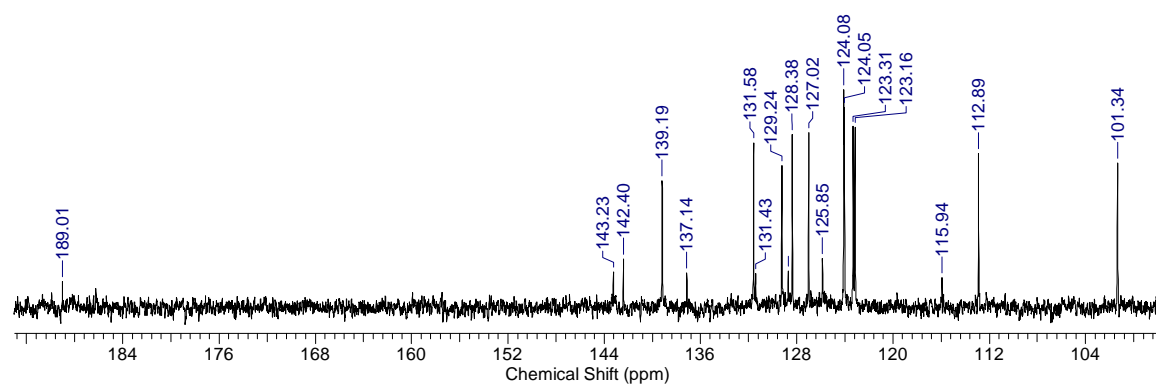
Spectrum 34: ^{13}C NMR spectrum of marinoquinoline F (**44**) (^{13}C 150 MHz, acetone-d_6).
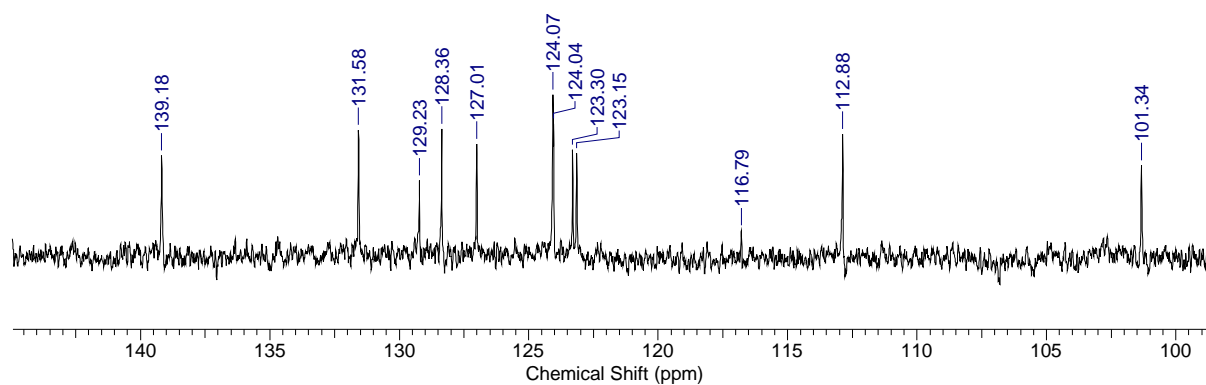
Spectrum 35: ^{13}C DEPT NMR spectrum of marinoquinoline F (**44**) (^{13}C 150 MHz, acetone-d_6).
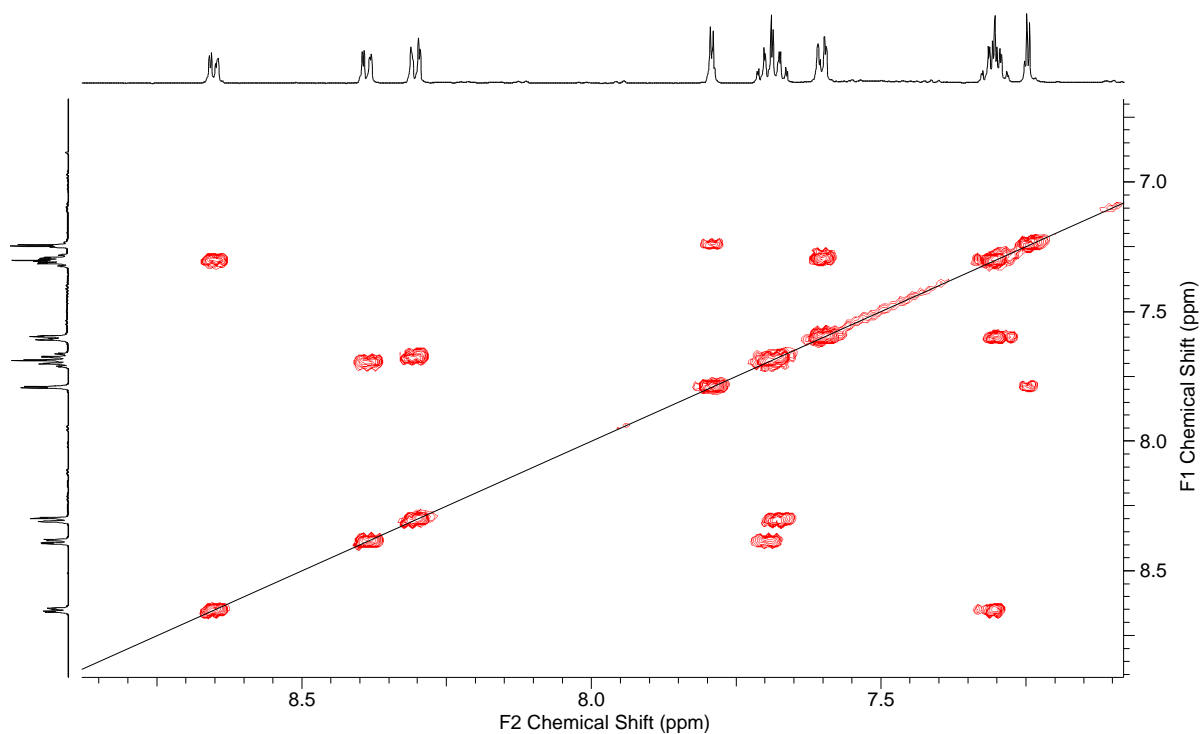
Spectrum 36: ^{1}H,^{1}H COSY NMR spectrum of marinoquinoline F(**44**) (^{1}H 600 MHz, acetone-d_6).
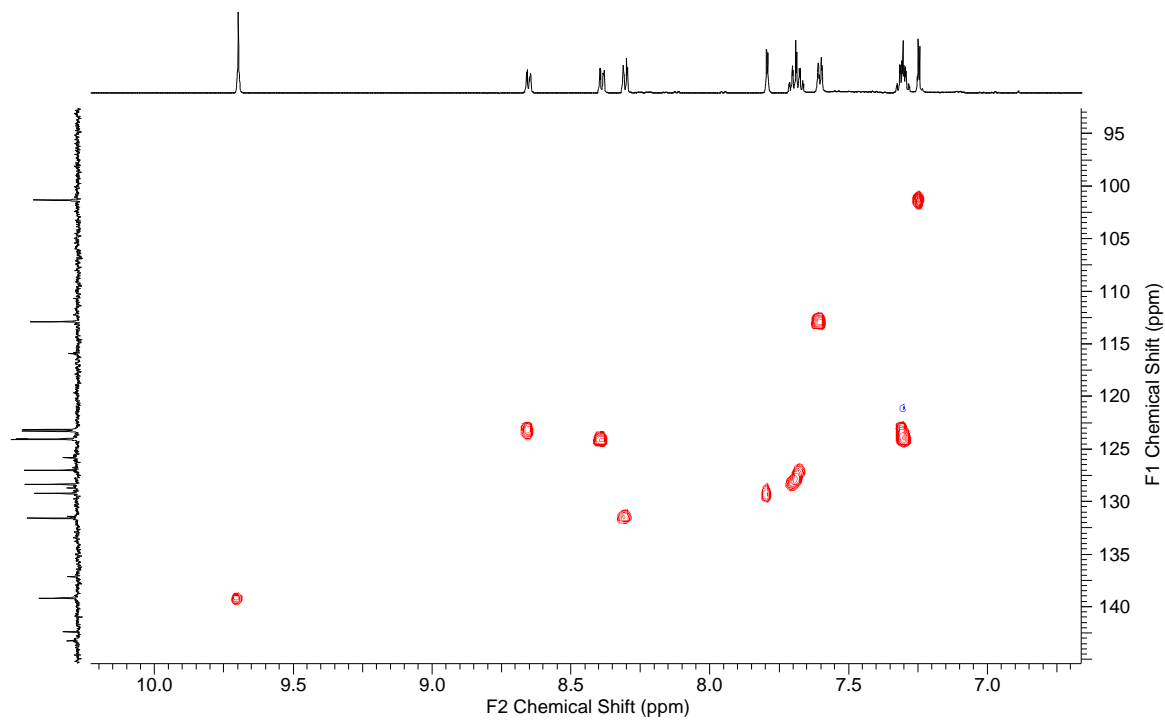
Spectrum 37: ^{1}H,^{13}C HMQC NMR spectrum of marinoquinoline F(**44**) (^{1}H 600 MHz, ^{13}C 150 MHz, acetone-d_6).
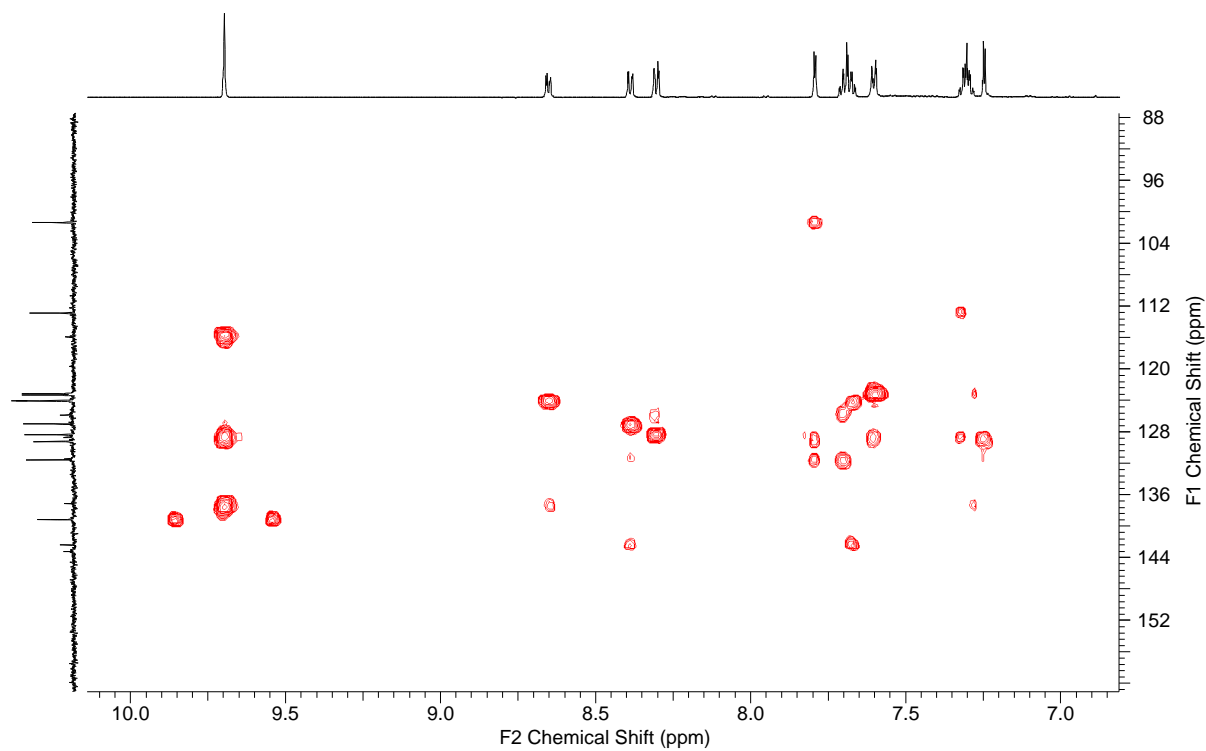
Spectrum 38: ^{1}H,^{13}C HMBC NMR spectrum of marinoquinoline F(**44**) (^{1}H 600 MHz, ^{13}C 150 MHz, acetone-d_6).

6.3 Spectra and X-ray data of hyaladione (47)

6.3.1 Spectra of hyaladione (47)
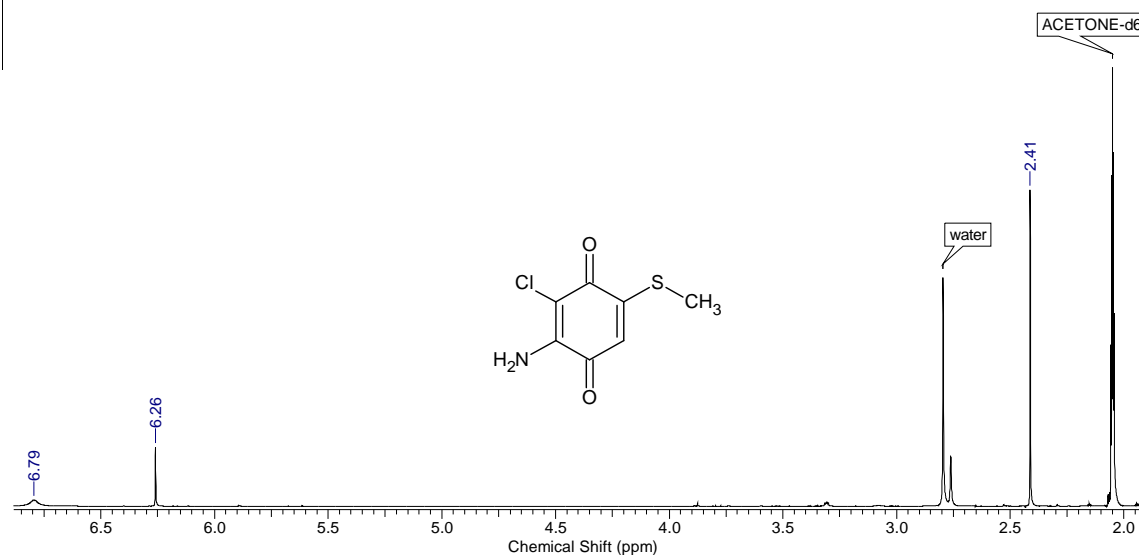
Spectrum 39: ^{1}H NMR spectrum of hyaladione (**47**) (^{1}H 600 MHz, acetone-d_6).
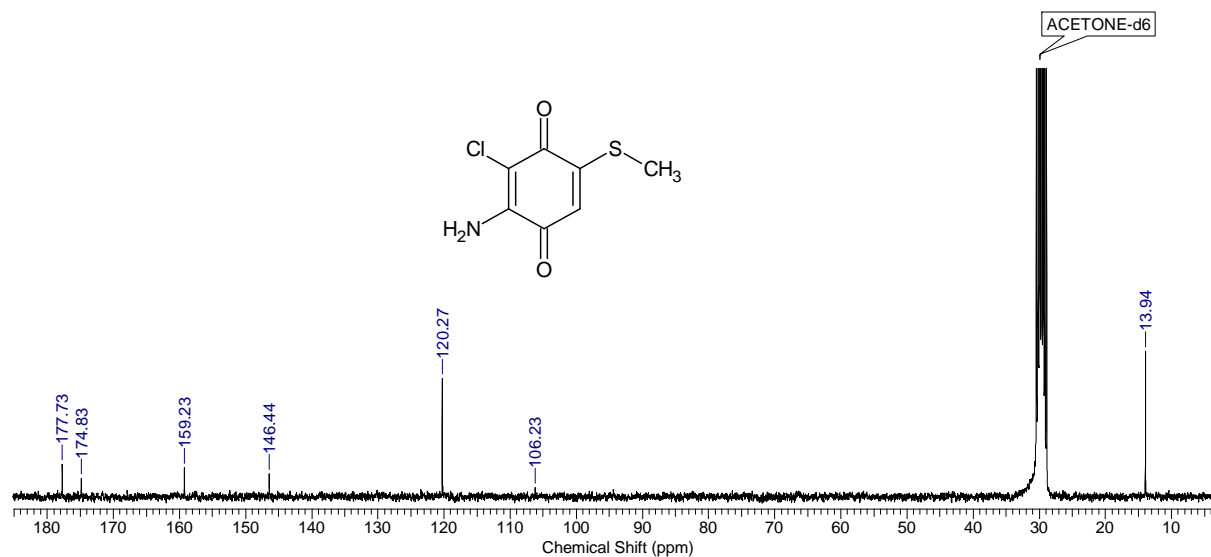
Spectrum 40: ^{13}C NMR spectrum of hyaladione (**47**) (^{13}C 150 MHz, acetone-d_6).

126
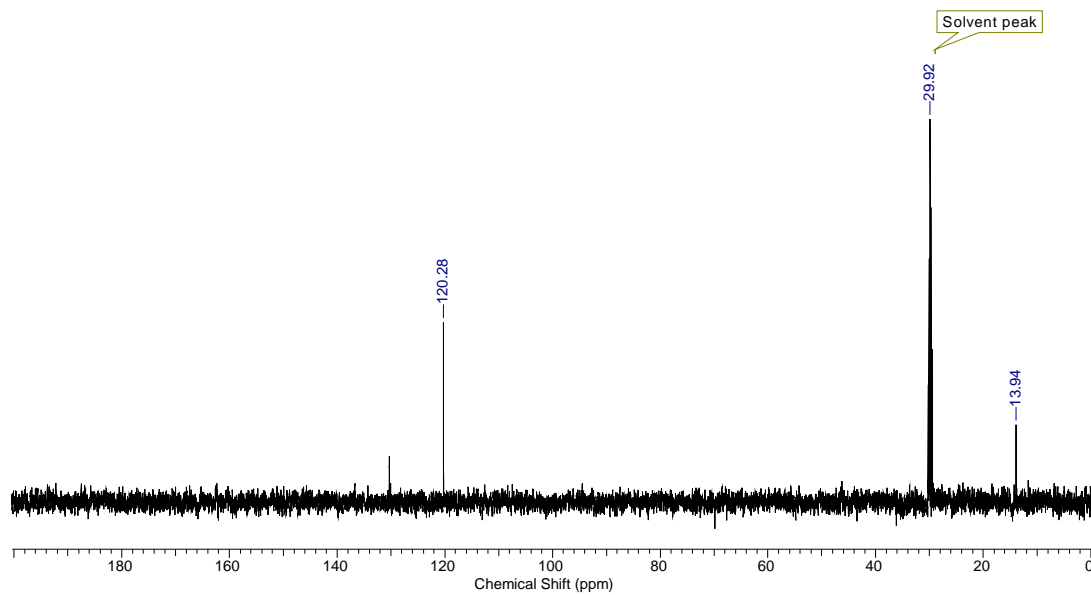
Spectrum 41: ^{13}C DEPT NMR spectrum of hyaladione (**47**) (^{13}C 150 MHz, acetone-d_6).
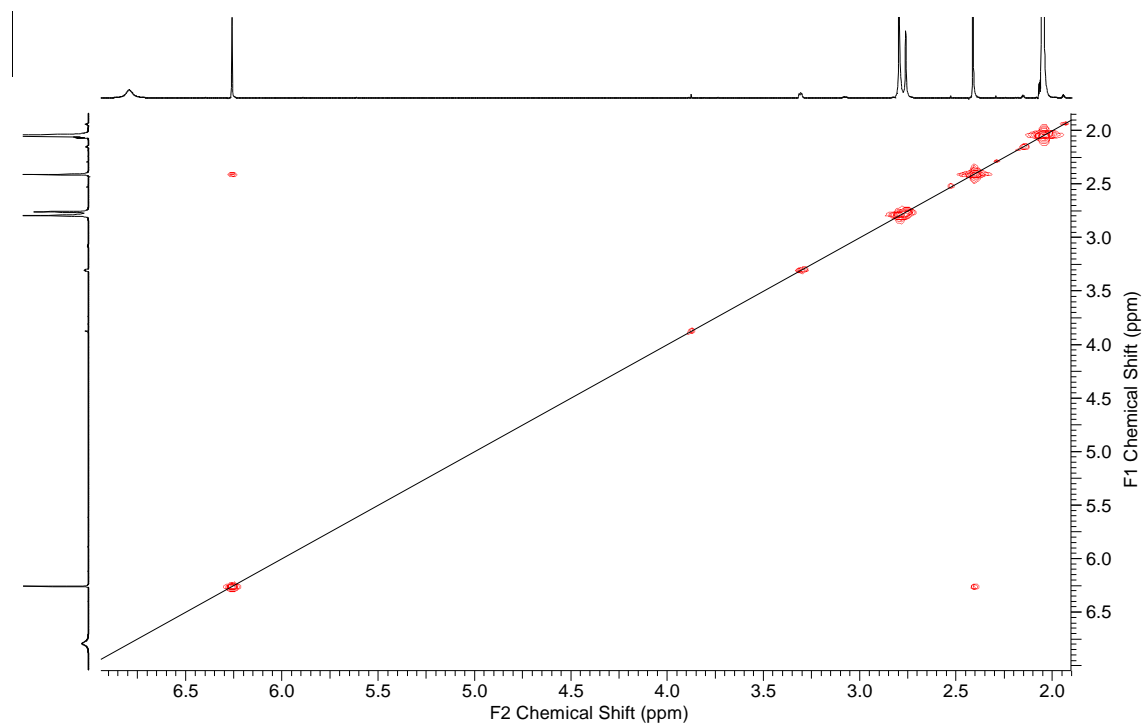
Spectrum 42: ^{1}H,^{1}H COSY NMR spectrum of hyaladione (**47**) (^{1}H 600 MHz, acetone-d_6).
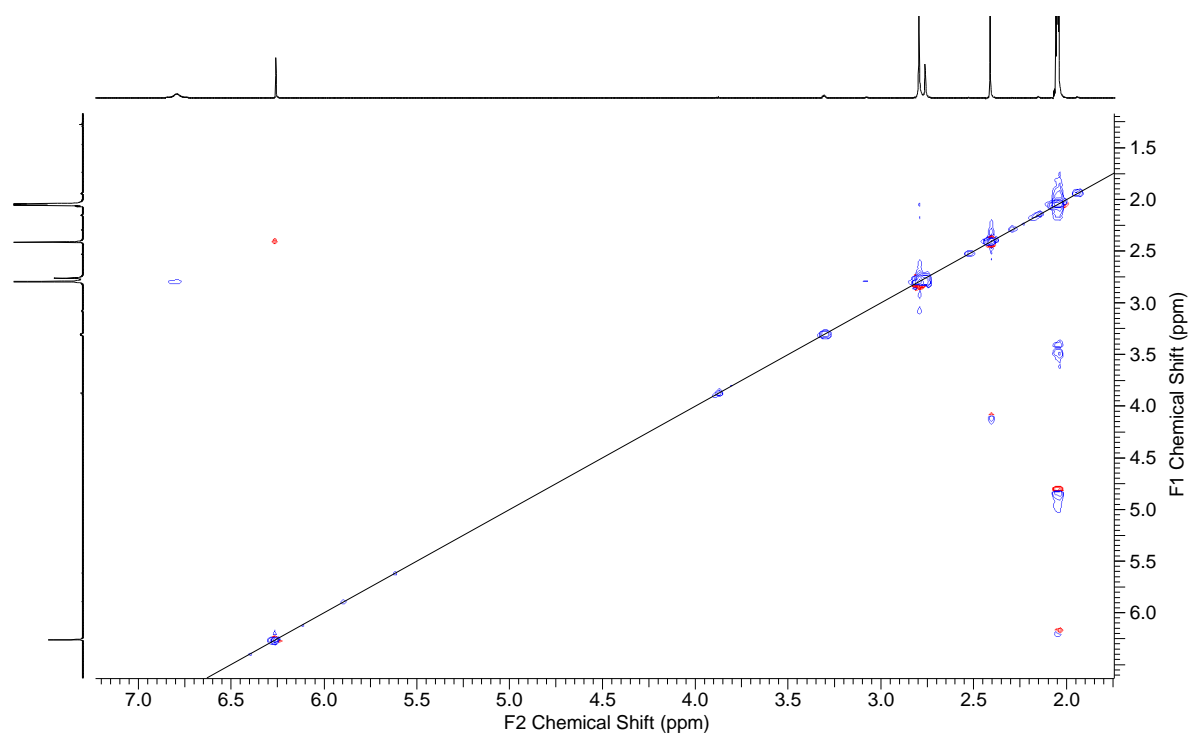
Spectrum 42: ^{1}H,^{1}H ROESY NMR spectrum of hyaladione (**47**) (^{1}H 600 MHz, acetone-d_6).
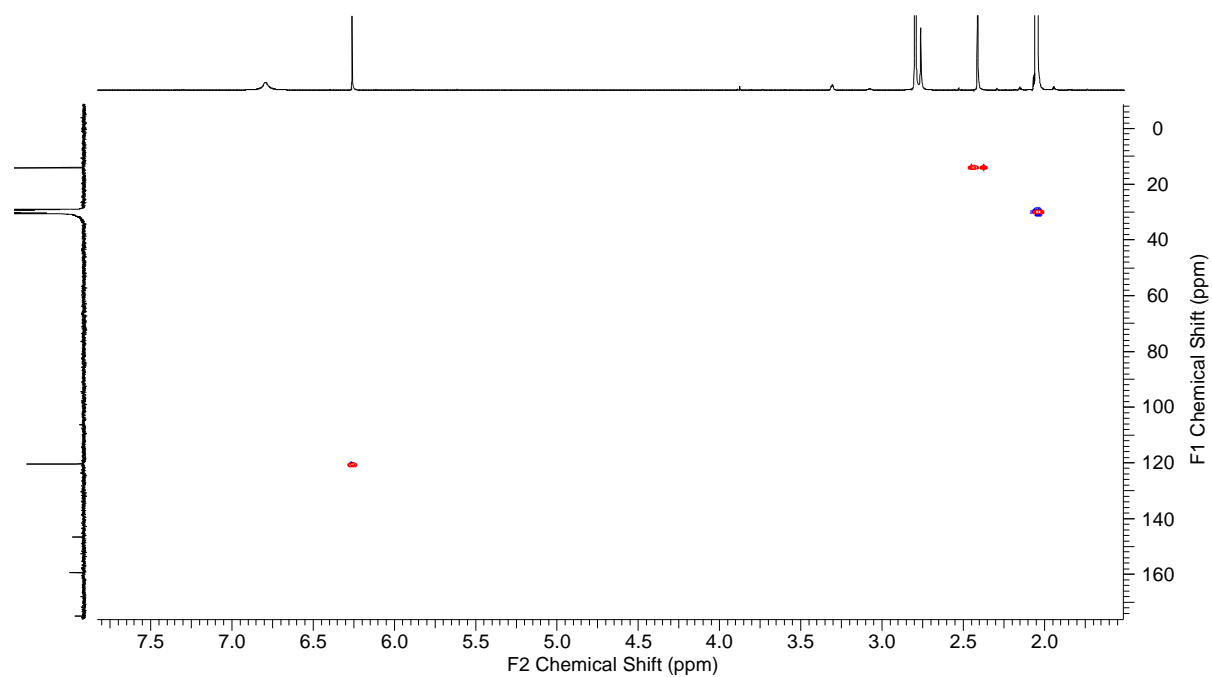
Spectrum 43: ^{1}H,^{13}C HMQC NMR spectrum of hyaladione (**47**) (^{1}H 600 MHz, ^{13}C 150 MHz, acetone-d_6).
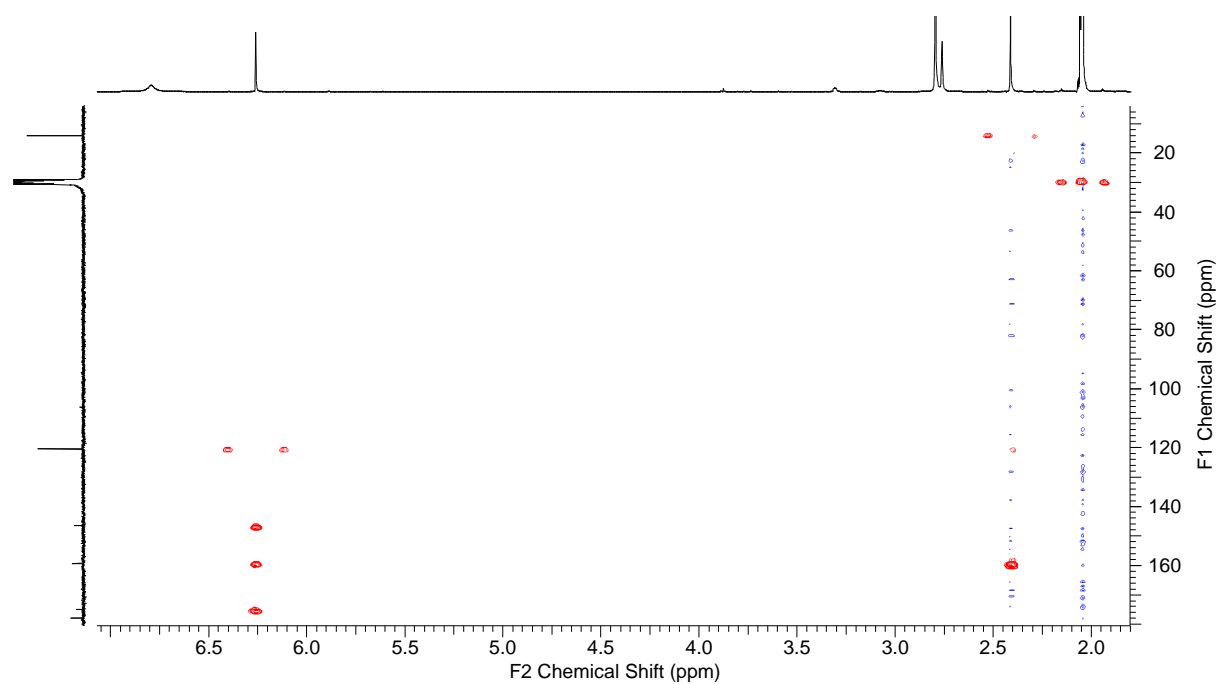
Spectrum 44: ^{1}H,^{13}C HMBC NMR spectrum of hyaladione (**47**) (^{1}H 600 MHz, ^{13}C 150 MHz, acetone-d_6).
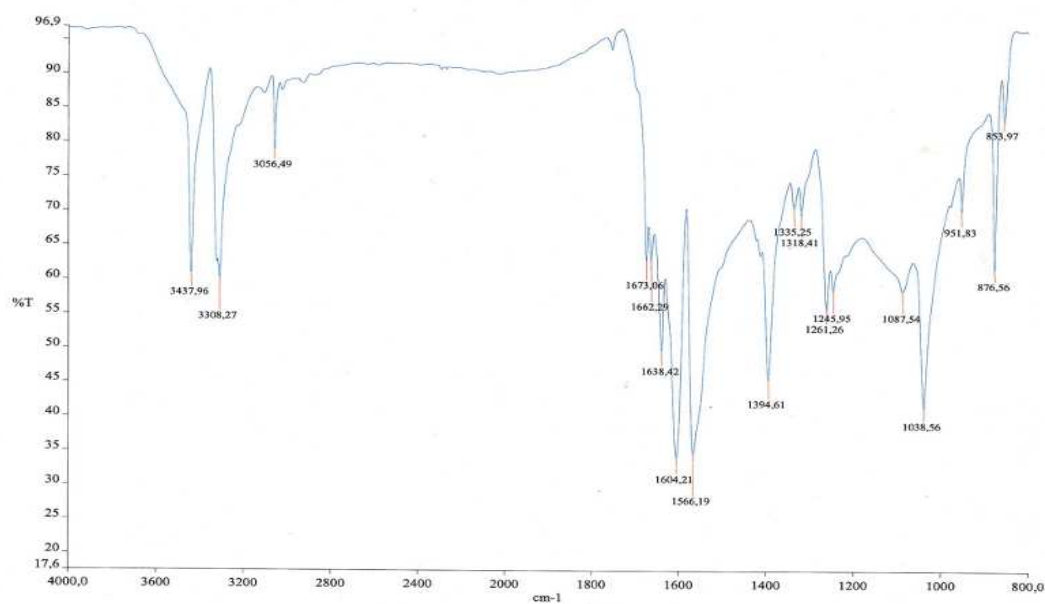
Spectrum 45: IR spectrum of hyaladione (**47**) (1 mg, 160 mg KBR).

129
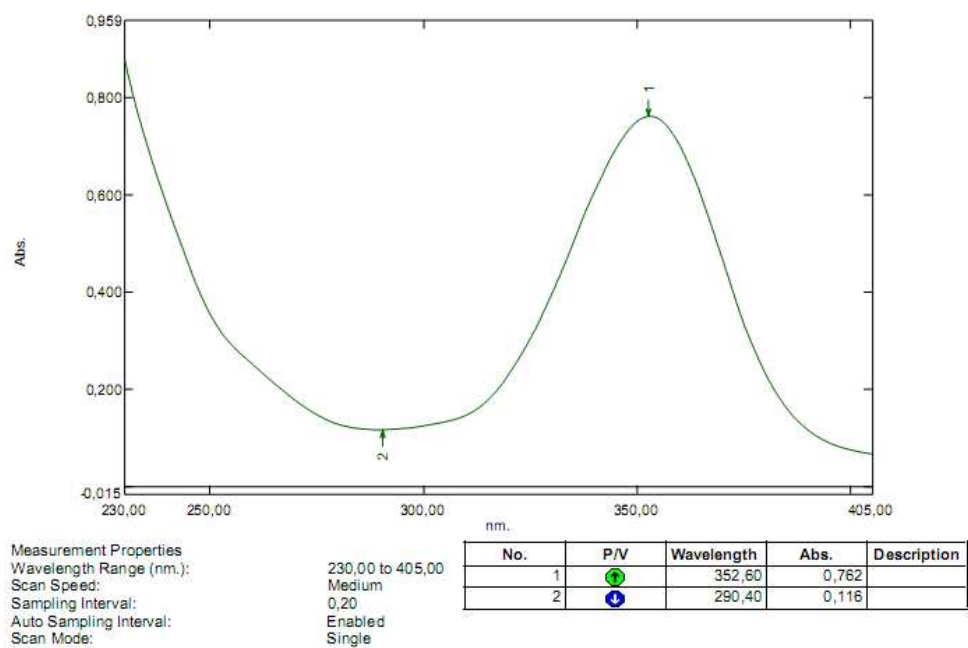
Spectrum 46: UV/vis spectrum of hyaladione (**47**) in Uvasol methanol (c = 0.5 mg/100 mL).

6.3.2 X-ray data of hyaladione (47)

Table 6:   Crystal data and structure refinement of hyaladione (**47**)

Empirical formula	$C_7 H_6 Cl N O_2 S$	
Formula weight	203.64	
Temperature	122(2) K	
Wavelength	0.71073 Å	
Crystal system	Monoclinic	
Space group	P2(1)/n	
Unit cell dimensions	a = 3.8875(8) Å	$\alpha = 90°$.
	b = 14.180(3) Å	$\beta = 94.808(11)°$
	c = 14.518(3) Å	$\sigma = 90°$.
Volume	797.5(3) $Å^3$	
Z	4	
Density (calculated)	1.696 Mg/m^3	
Absorption coefficient	0.692 mm^{-1}	
F(000)	416	
Crystal size	0.98 x 0.19 x 0.03 mm^3	
Theta range for data collection	2.01 to 41.83°.	
Index ranges	-7<=h<=7, -26<=k<=26, -27<=l<=27	
Reflections collected	18376	
Independent reflections	5432 [R(int) = 0.0309]	
Completeness to theta = 41.83°	98.2 %	
Max. and min. transmission	0.9769 and 0.5514	
Refinement method	Full-matrix least-squares on F^2	
Data / restraints / parameters	5432 / 0 / 133	
Goodness-of-fit on F^2	1.036	
Final R indices [I>2sigma(I)]	R1 = 0.0305, wR2 = 0.0739	
R indices (all data)	R1 = 0.0473, wR2 = 0.0812	
Largest diff. peak and hole	0.646 and -0.349 $e.Å^{-3}$	
Absorption correction	Multiscan	

Table 7:   Atomic coordinates (x 10^4) and equivalent isotropic displacement parameters (Å^2x 10^3) of hyaladione (**47**). U(eq) is defined as one third of the trace of the orthogonalized U^{ij} tensor.

	x	y	z	U(eq)
S	4734(1)	5820(1)	2400(1)	13(1)
Cl	7234(1)	8950(1)	4516(1)	16(1)
C(3)	4172(2)	7412(1)	5140(1)	12(1)
C(2)	5551(2)	7820(1)	4396(1)	12(1)
C(6)	4222(2)	6351(1)	3455(1)	11(1)
C(1)	5642(2)	7347(1)	3522(1)	12(1)
C(5)	2746(2)	5943(1)	4166(1)	13(1)
C(4)	2542(2)	6447(1)	5029(1)	12(1)
O(2)	1108(2)	6122(1)	5680(1)	18(1)
N(1)	4085(2)	7794(1)	5972(1)	17(1)
O(1)	6860(2)	7703(1)	2845(1)	18(1)
C(7)	3252(2)	4635(1)	2576(1)	15(1)

Table 8: Bond lengths [Å] and angles [°] of hyaladione (**47**). Symmetry transformations used to generate equivalent atoms.

S-C(6)	1.7340(8)
S-C(7)	1.8018(9)
Cl-C(2)	1.7350(8)
C(3)-N(1)	1.3277(10)
C(3)-C(2)	1.3717(10)
C(3)-C(4)	1.5112(10)
C(2)-C(1)	1.4391(11)
C(6)-C(5)	1.3522(10)
C(6)-C(1)	1.5171(10)
C(1)-O(1)	1.2327(9)
C(5)-C(4)	1.4505(11)
C(4)-O(2)	1.2268(9)
C(6)-S-C(7)	102.57(4)
N(1)-C(3)-C(2)	125.90(7)
N(1)-C(3)-C(4)	115.03(6)
C(2)-C(3)-C(4)	119.07(6)
C(3)-C(2)-C(1)	122.59(7)
C(3)-C(2)-Cl	118.65(6)
C(1)-C(2)-Cl	118.75(5)
C(5)-C(6)-C(1)	121.69(6)
C(5)-C(6)-S	125.19(6)
C(1)-C(6)-S	113.12(5)
O(1)-C(1)-C(2)	123.54(7)
O(1)-C(1)-C(6)	119.47(6)
C(2)-C(1)-C(6)	116.97(6)
C(6)-C(5)-C(4)	120.40(7)
O(2)-C(4)-C(5)	122.80(7)
O(2)-C(4)-C(3)	118.18(7)
C(5)-C(4)-C(3)	119.02(6)

Table 9: Anisotropic displacement parameters ($\text{Å}^2 \times 10^3$) of hyaladione (**47**). The anisotropic displacement factor exponent takes the form: $2\pi^2[\,h^2\,a^{*2}U^{11} + ... + 2\,h\,k\,a^*\,b^*\,U^{12}\,]$

	U^{11}	U^{22}	U^{33}	U^{23}	U^{13}	U^{12}
S	16(1)	13(1)	10(1)	-1(1)	3(1)	0(1)
Cl	21(1)	12(1)	16(1)	-1(1)	4(1)	-4(1)
C(3)	14(1)	12(1)	10(1)	0(1)	2(1)	0(1)
C(2)	15(1)	10(1)	11(1)	0(1)	3(1)	-1(1)
C(6)	13(1)	11(1)	10(1)	0(1)	2(1)	0(1)
C(1)	14(1)	11(1)	10(1)	1(1)	3(1)	0(1)
C(5)	16(1)	12(1)	11(1)	0(1)	3(1)	-2(1)
C(4)	15(1)	12(1)	10(1)	1(1)	2(1)	-1(1)
O(2)	24(1)	18(1)	12(1)	1(1)	7(1)	-5(1)
N(1)	25(1)	17(1)	11(1)	-3(1)	6(1)	-5(1)
O(1)	26(1)	16(1)	12(1)	1(1)	8(1)	-3(1)
C(7)	17(1)	13(1)	15(1)	-2(1)	3(1)	0(1)

Table 10: Hydrogen coordinates ($\times 10^4$) and isotropic displacement parameters ($\text{Å}^2 \times 10^3$) of hyaladione (**47**).

	x	y	z	U(eq)
H(1)	1710(30)	5344(10)	4138(8)	22(3)
H(3)	3100(40)	7479(12)	6381(12)	44(4)
H(2)	4960(40)	8302(11)	6087(10)	30(3)
H(5)	970(30)	4622(10)	2659(9)	24(3)
H(4)	4640(30)	4363(10)	3096(10)	25(3)
H(6)	3620(40)	4308(10)	2023(10)	30(3)

6.4 Spectra of hyafurones and hyapyrones

6.4.1 Spectra of hyafurone A1 (48)
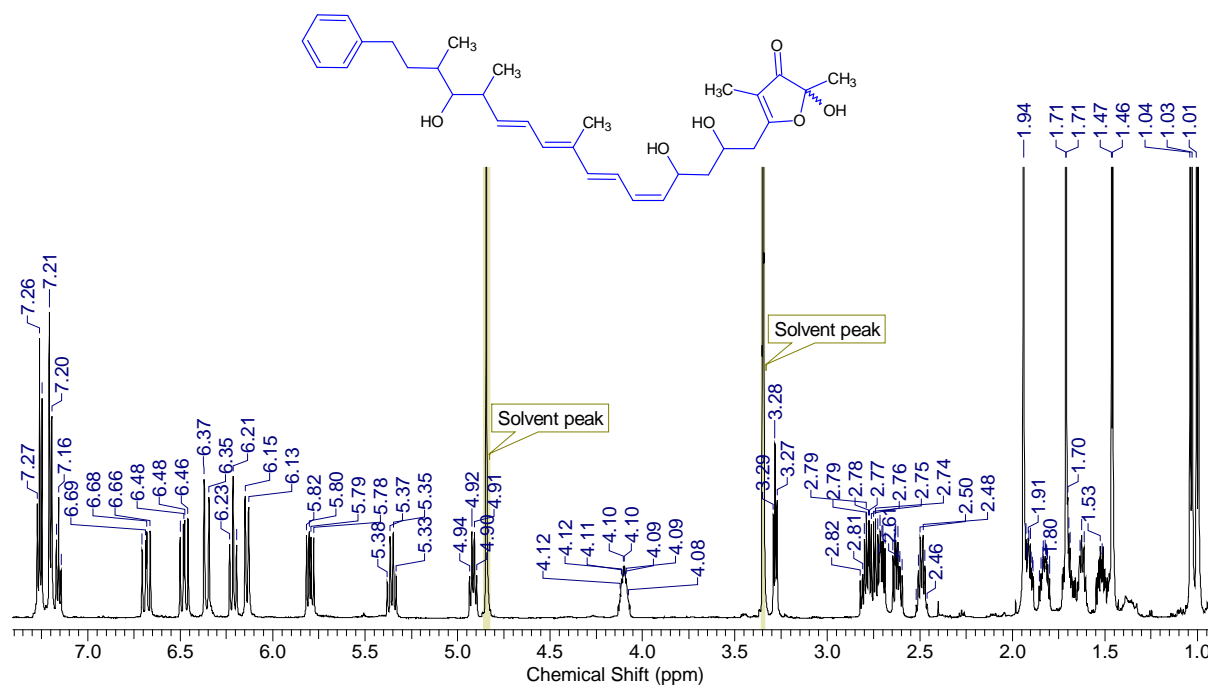
Spectrum 47: ^{1}H NMR spectrum of hyafurone A$_1$ (**48**) (^{1}H 600 MHz, CD$_3$OD).
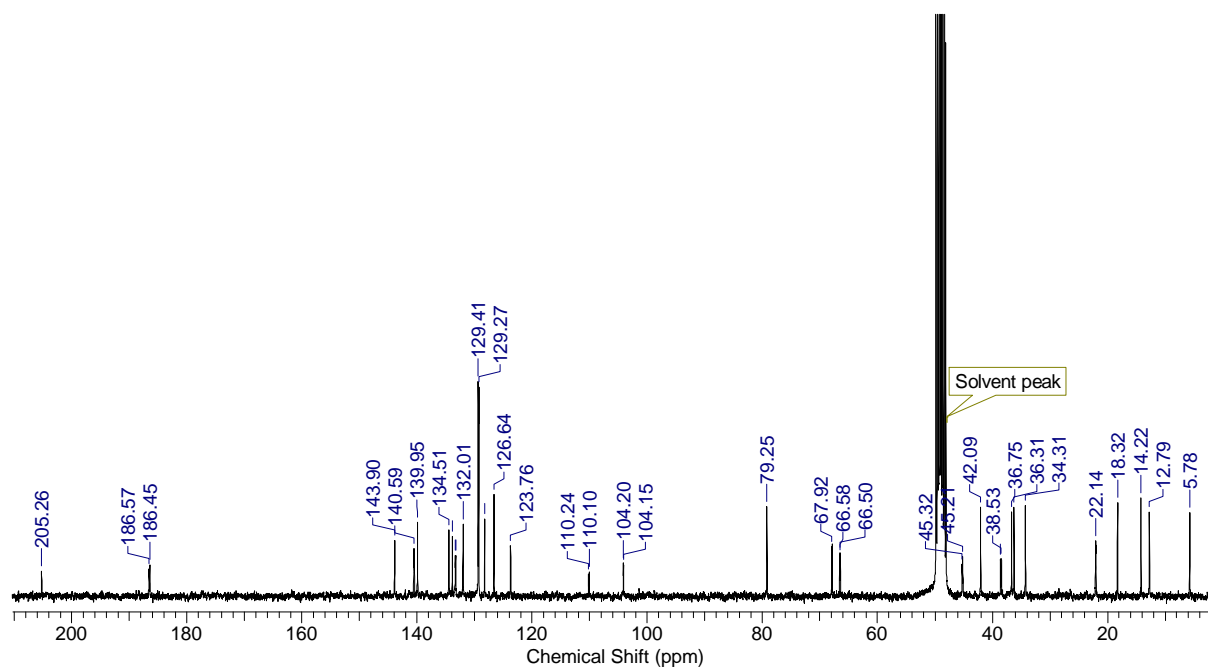
Spectrum 48: ^{13}C NMR spectrum of hyafurone A$_1$ (**48**) (^{13}C 150 MHz, CD$_3$OD).
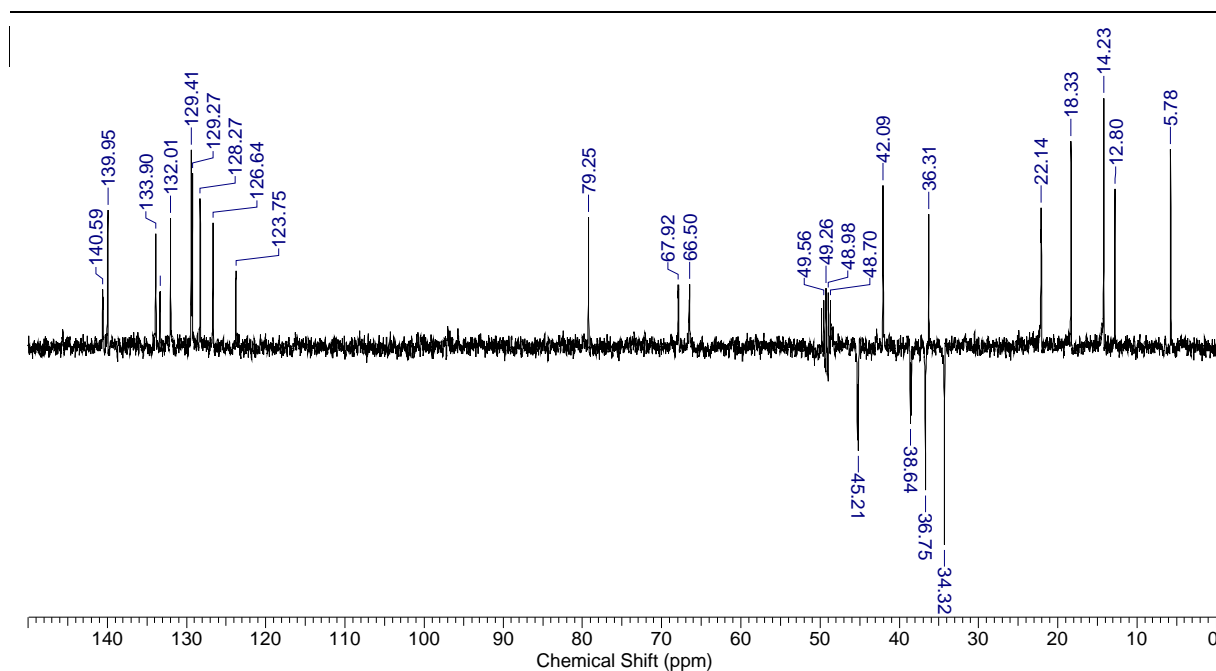
Spectrum 49: ^{13}C DEPT NMR spectrum of hyafurone A$_1$ (**48**) (^{13}C 150 MHz, CD$_3$OD).
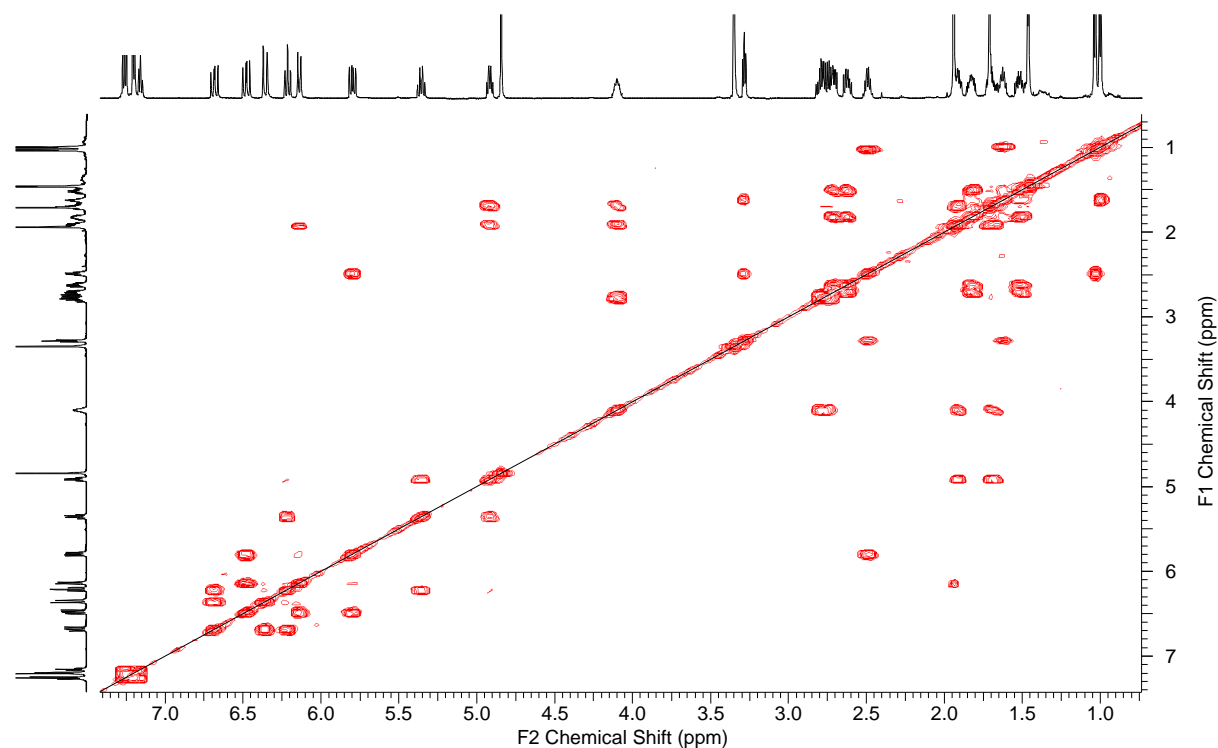
Spectrum 50: ^{1}H,^{1}H COSY NMR spectrum of hyafurone A$_1$ (**48**) (^{1}H 600 MHz, CD$_3$OD).
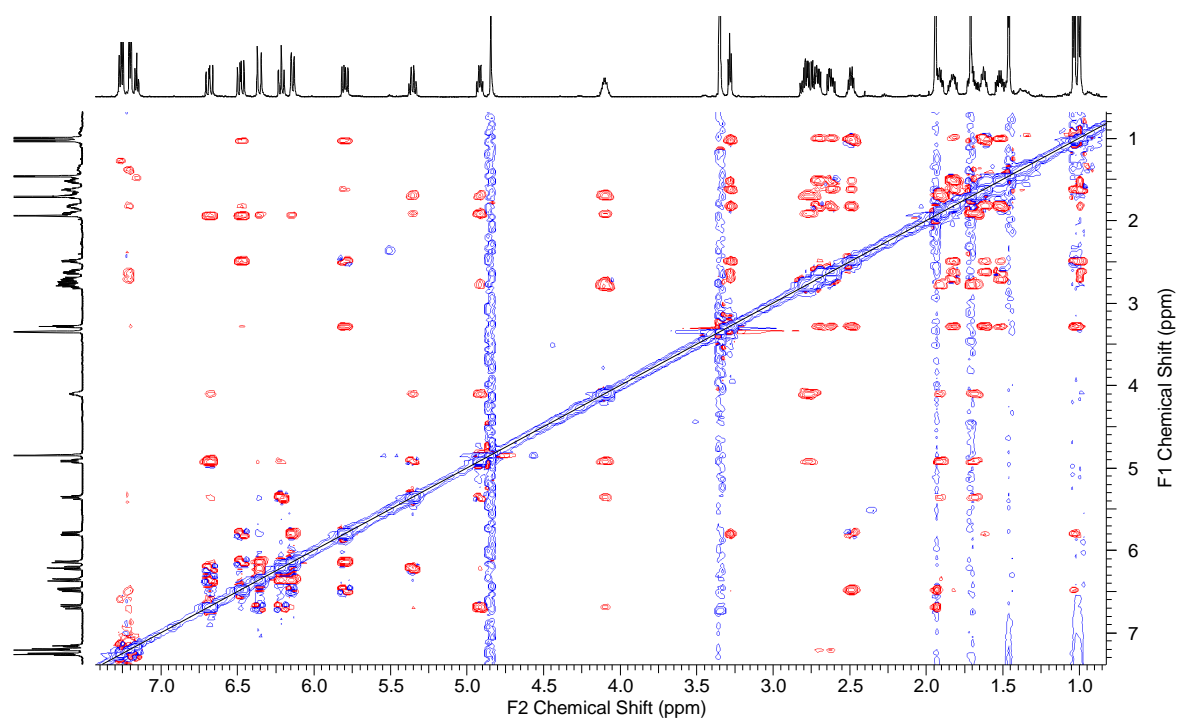
Spectrum 51: ^{1}H,^{1}H ROESY NMR spectrum of hyafurone A$_1$(**48**) (^{1}H 600 MHz, CD$_3$OD).
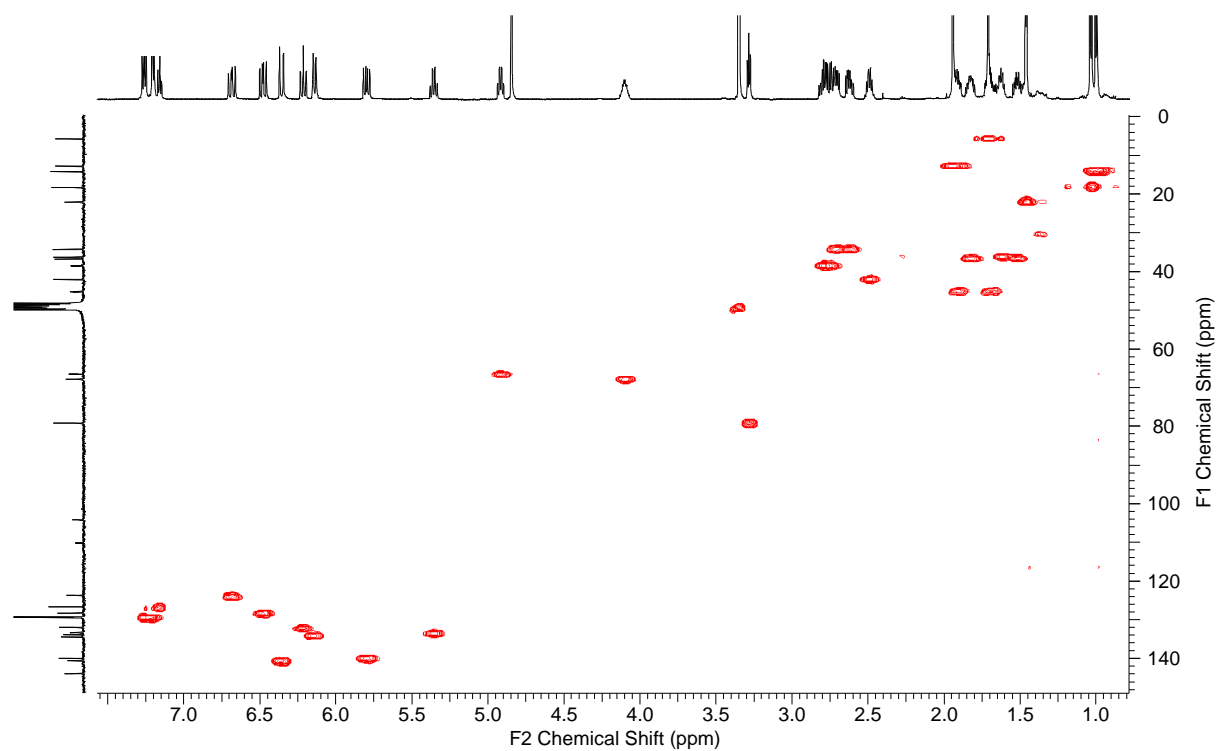
Spectrum 52: ^{1}H,^{13}C HMQC NMR spectrum of hyafurone A$_1$(**48**) (^{1}H 600 MHz, ^{13}C 150 MHz, CD$_3$OD).

137
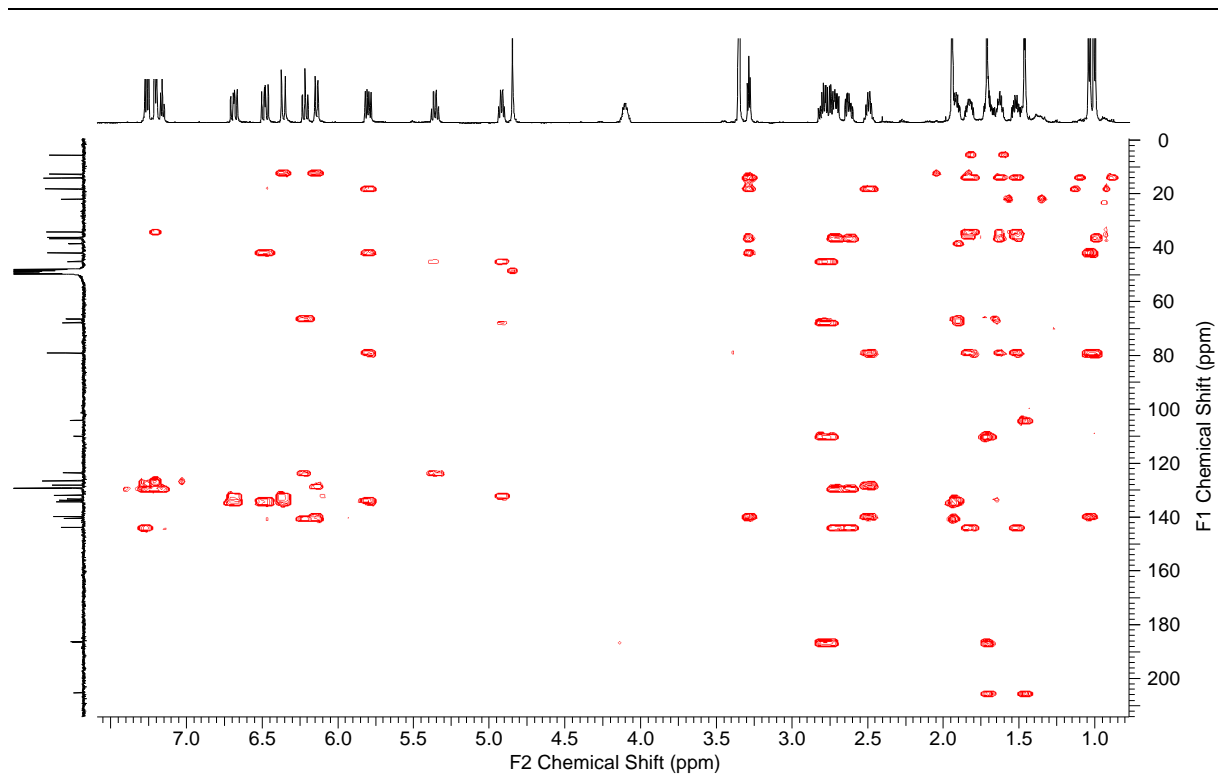
Spectrum 53: ^{1}H,^{13}C HMBC NMR spectrum of hyafurone A$_1$(**48**) (^{1}H 600 MHz, ^{13}C 150 MHz, CD$_3$OD).

6.4.2 Spectra of hyafurone A₂ (49)
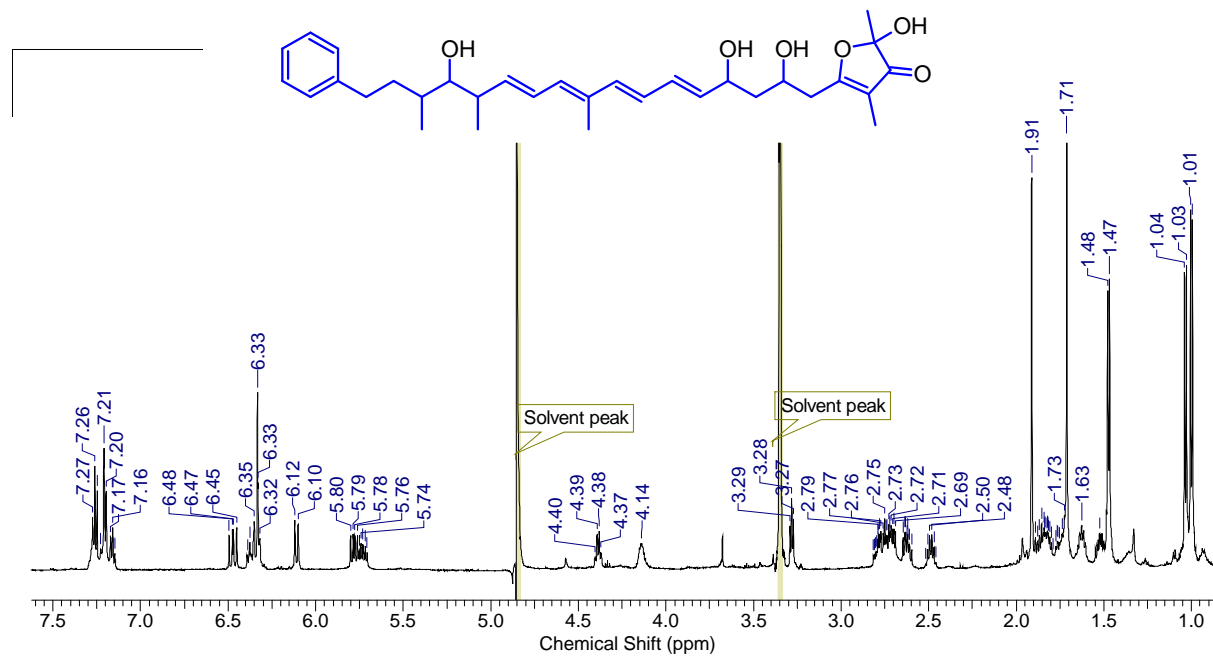
Spectrum 54: ¹H NMR spectrum of hyafurone A₂ (**49**) (¹H 600 MHz, CD₃OD).
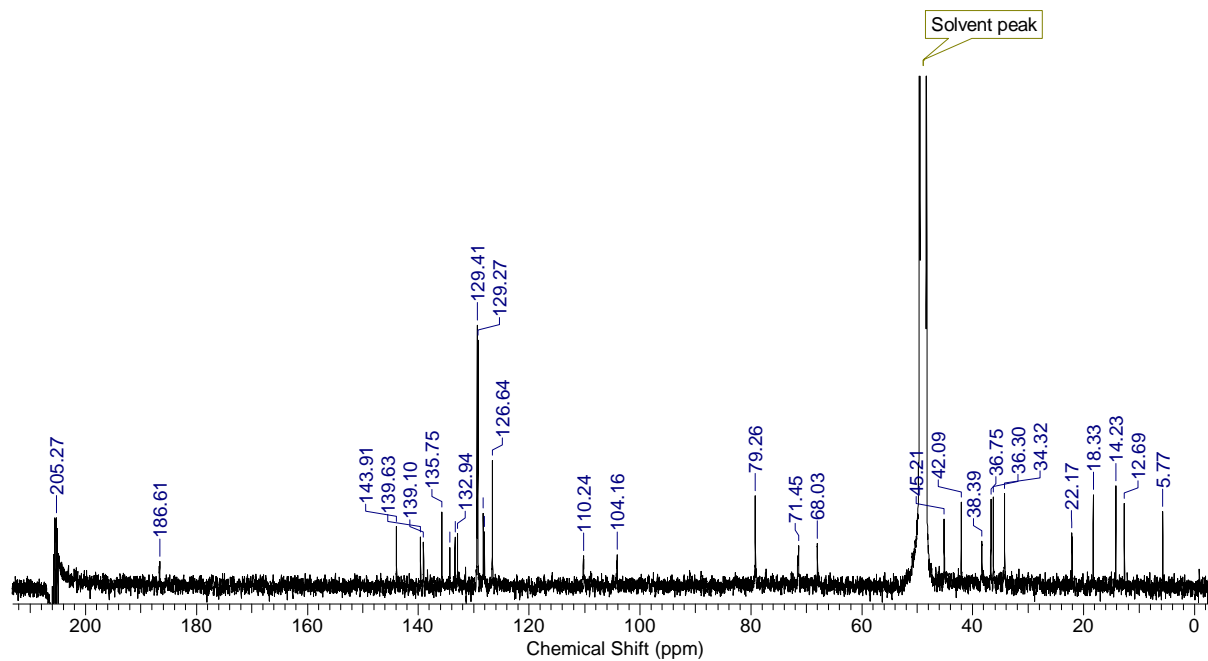
Spectrum 55: ¹³C NMR spectrum of hyafurone A₂ (**49**) (¹³C 150 MHz, CD₃OD).

139
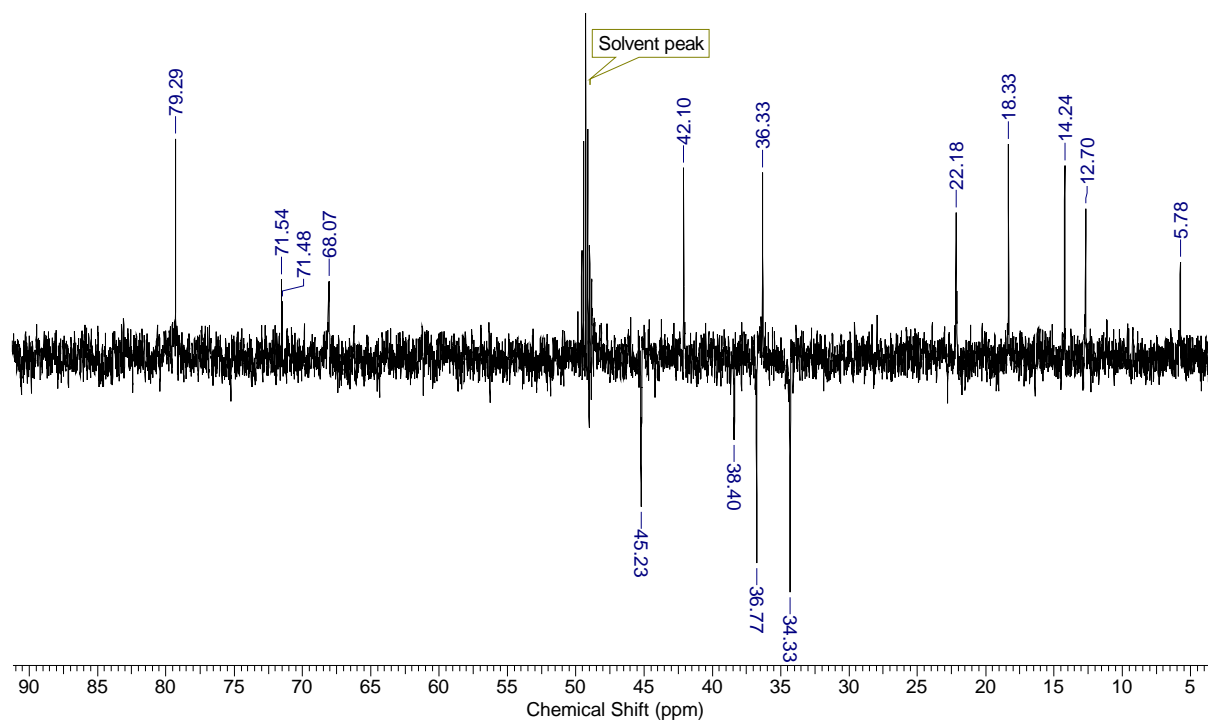
Spectrum 56: ^{13}C DEPT NMR spectrum of hyafurone A$_2$ (**49**) (^{13}C 150 MHz, CD$_3$OD).
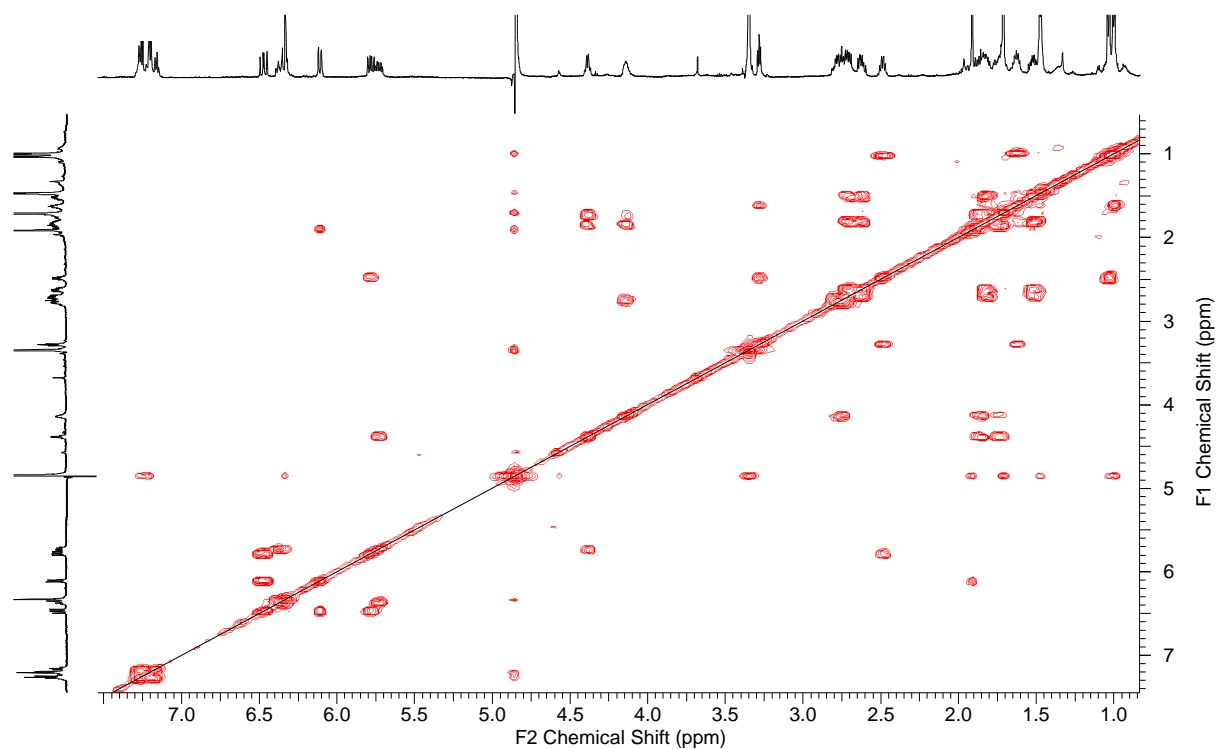
Spectrum 57: ^{1}H,^{1}H COSY NMR spectrum of hyafurone A$_2$ (**49**) (^{1}H 600 MHz, CD$_3$OD).
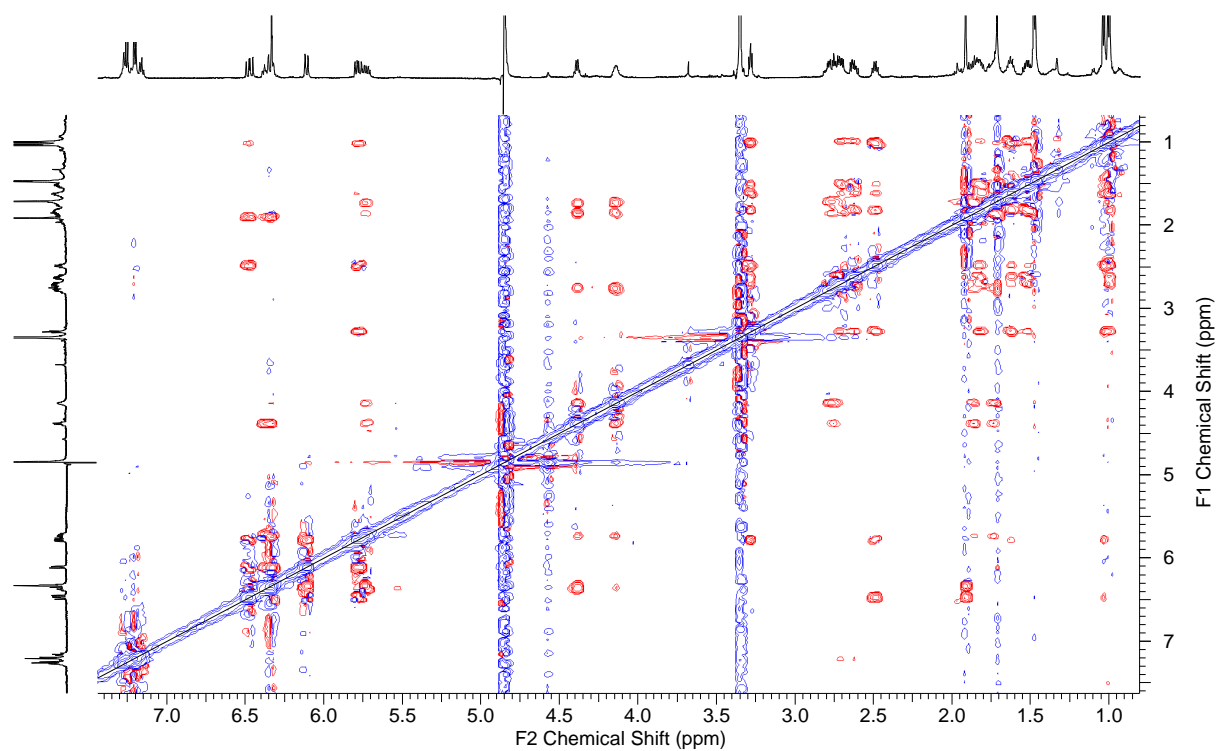
Spectrum 58: ^{1}H,^{1}H ROESY NMR spectrum of hyafurone A$_2$ (**49**) (^{1}H 600 MHz, CD$_3$OD).
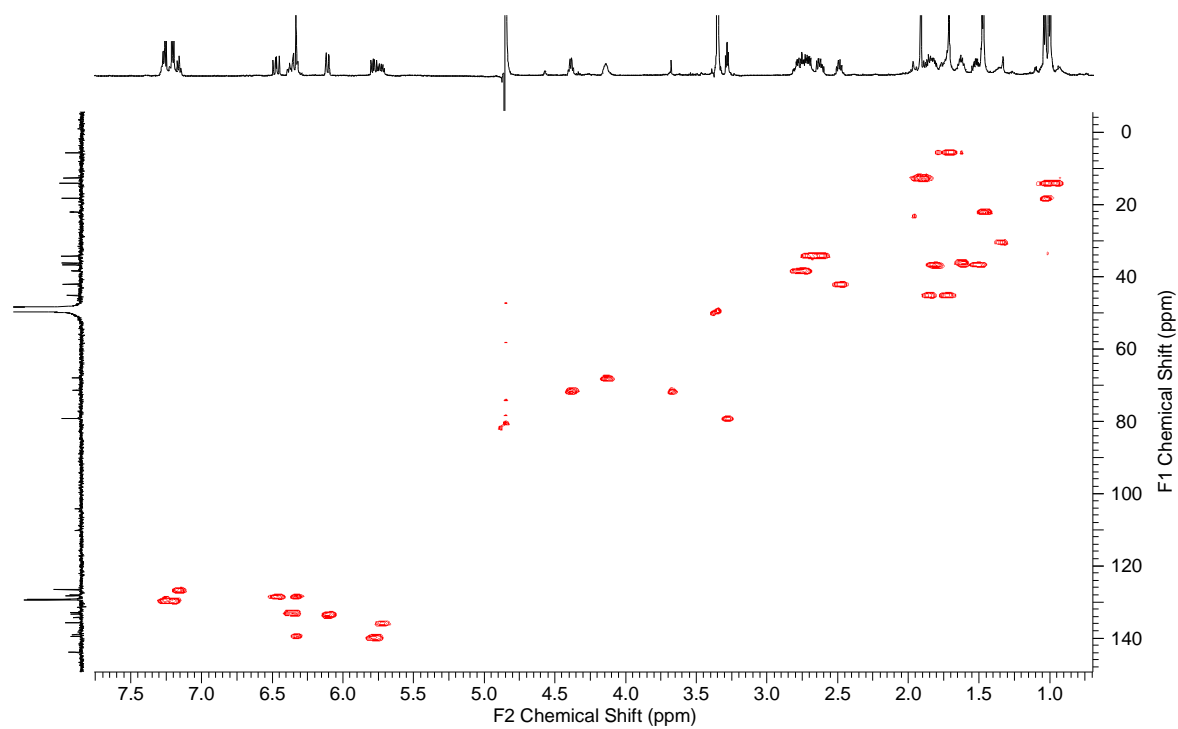
Spectrum 59: ^{1}H,^{13}C HMQC NMR spectrum of hyafurone A$_2$ (**49**) (^{1}H 600 MHz, ^{13}C 150 MHz, CD$_3$OD).
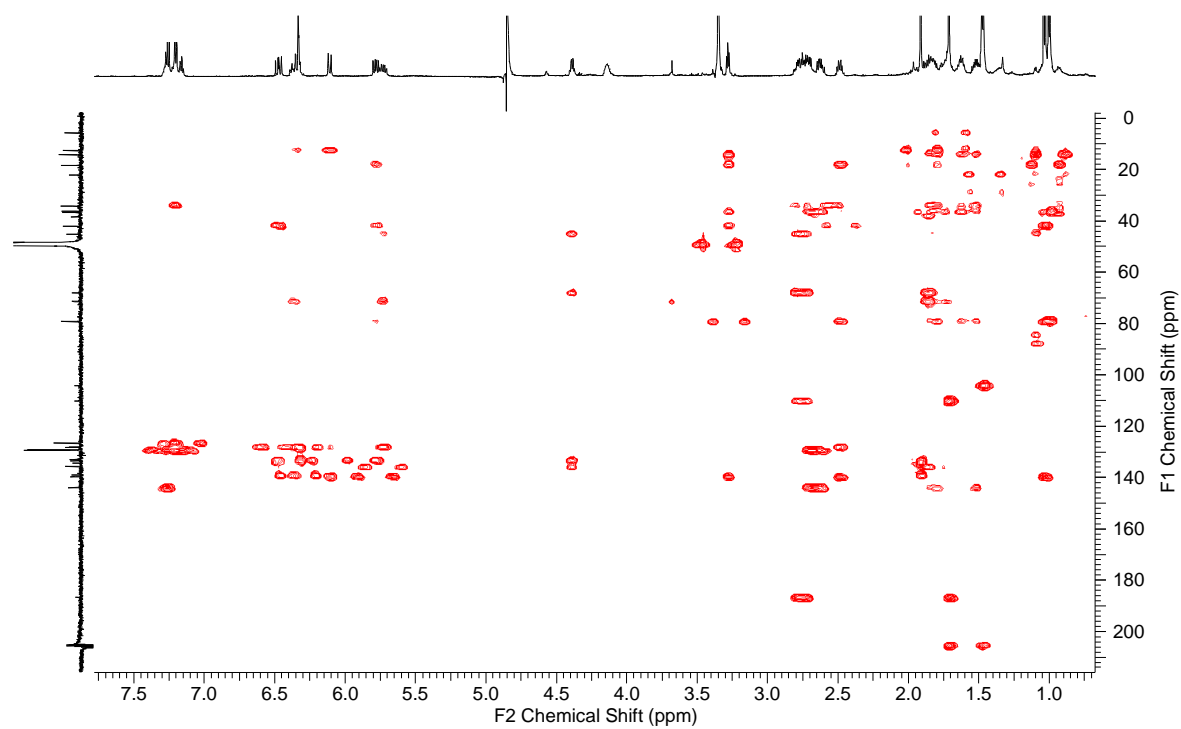
Spectrum 60: ^{1}H,^{13}C HMBC NMR spectrum of hyafurone A$_2$ (**49**) (^{1}H 600 MHz, ^{13}C 150 MHz, CD$_3$OD).

6.4.3 Spectra of hyafurone B (50)
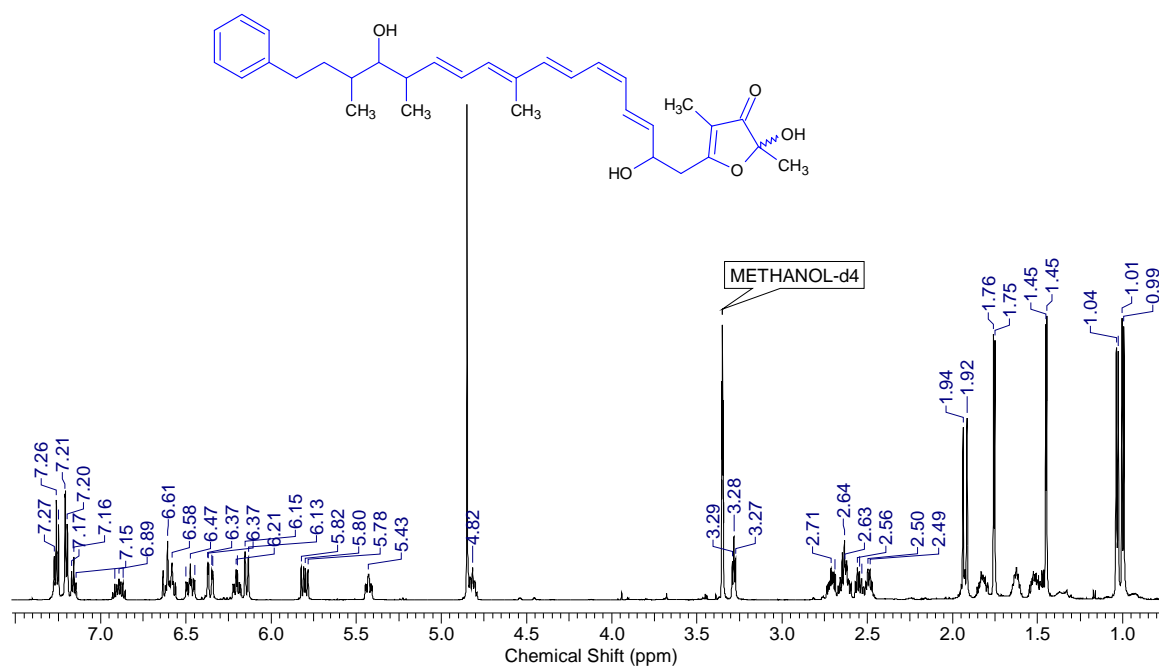
Spectrum 61: ^{1}H NMR spectrum of hyafurone B (**50**) (^{1}H 600 MHz, CD$_3$OD).
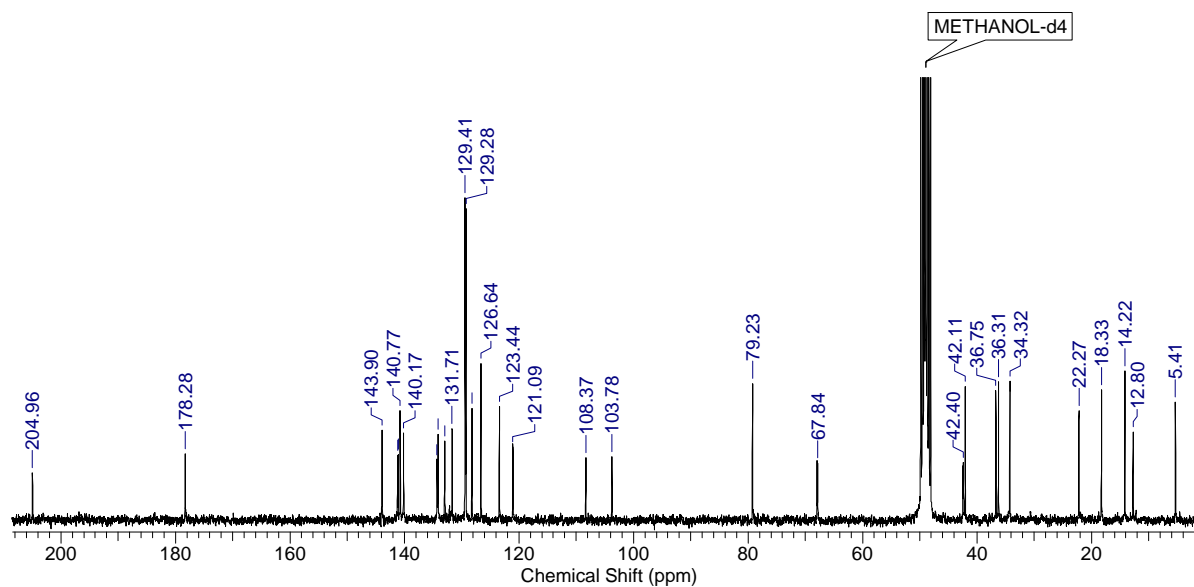
Spectrum 62: ^{13}C NMR spectrum of hyafurone B (**50**) (^{13}C 150 MHz, CD$_3$OD).
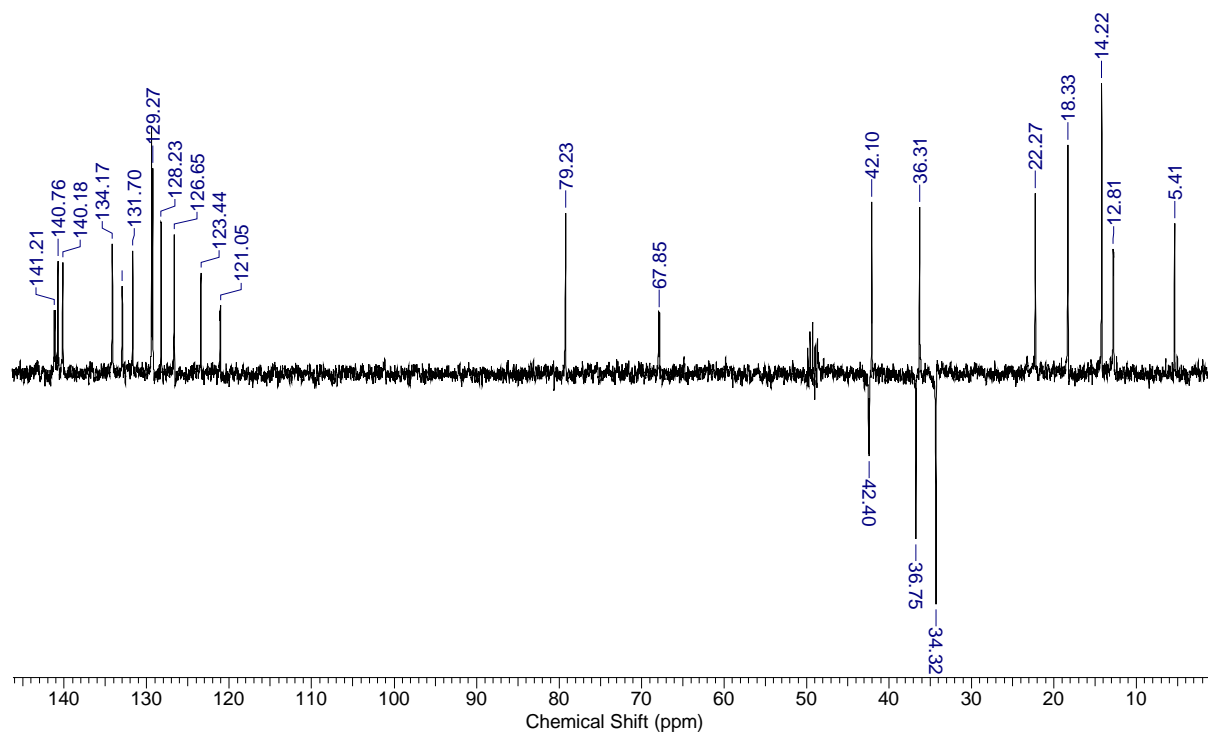
Spectrum 63: ^{13}C DEPT NMR spectrum of hyafurone B (**50**) (^{13}C 150 MHz, CD$_3$OD).
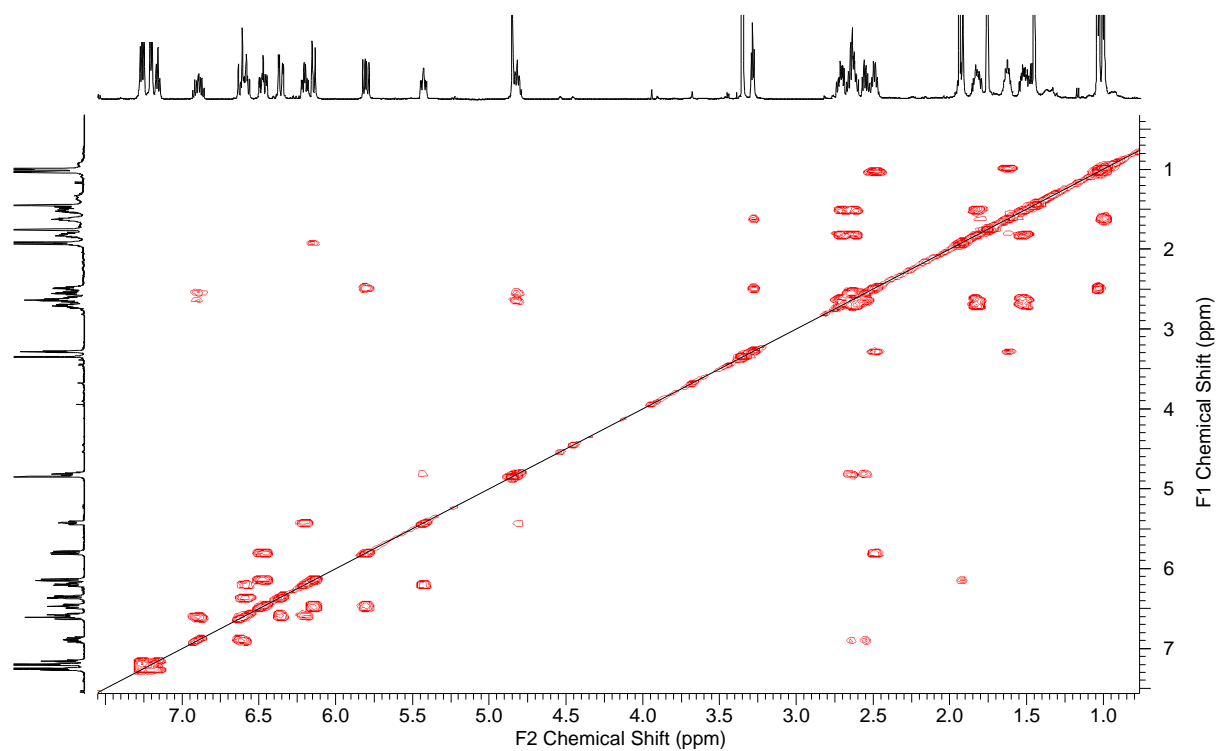
Spectrum 64: ^{1}H,^{1}H COSY NMR spectrum of hyafurone B (**50**) (^{1}H 600 MHz, CD$_3$OD).

144
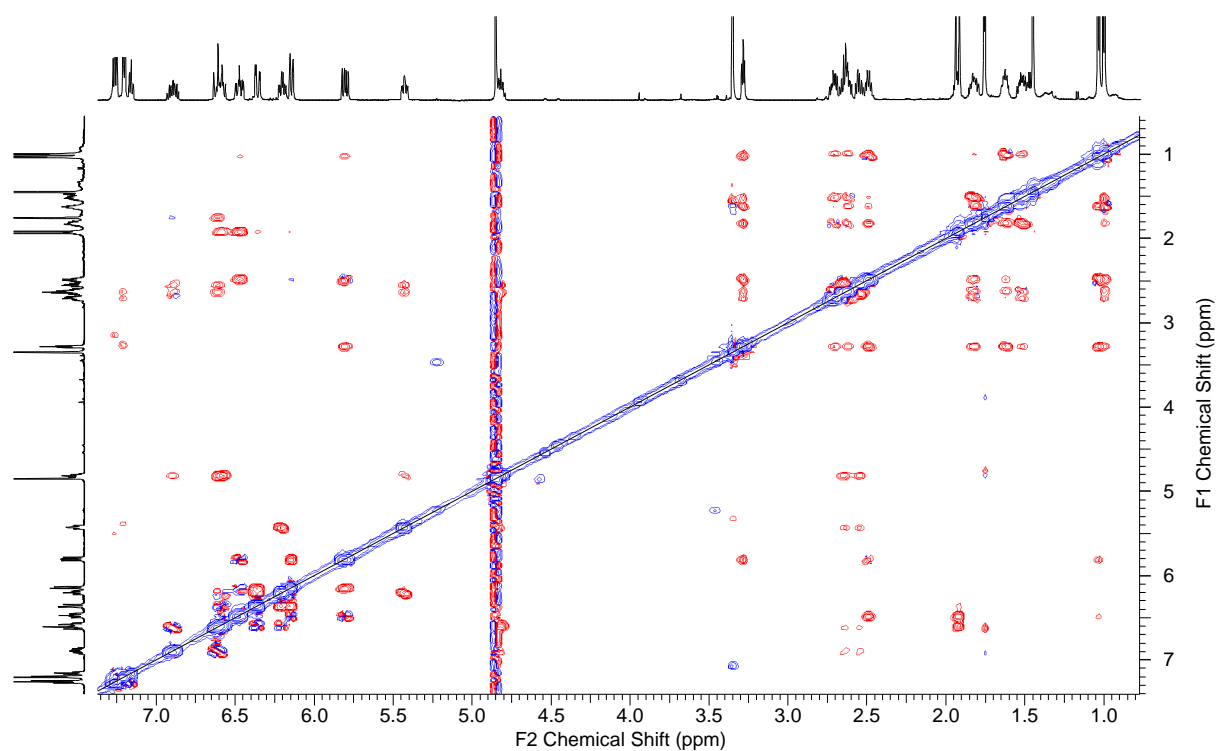
Spectrum 65: ^{1}H,^{1}H ROESY NMR spectrum of hyafurone B (**50**) (^{1}H 600 MHz, CD$_3$OD).
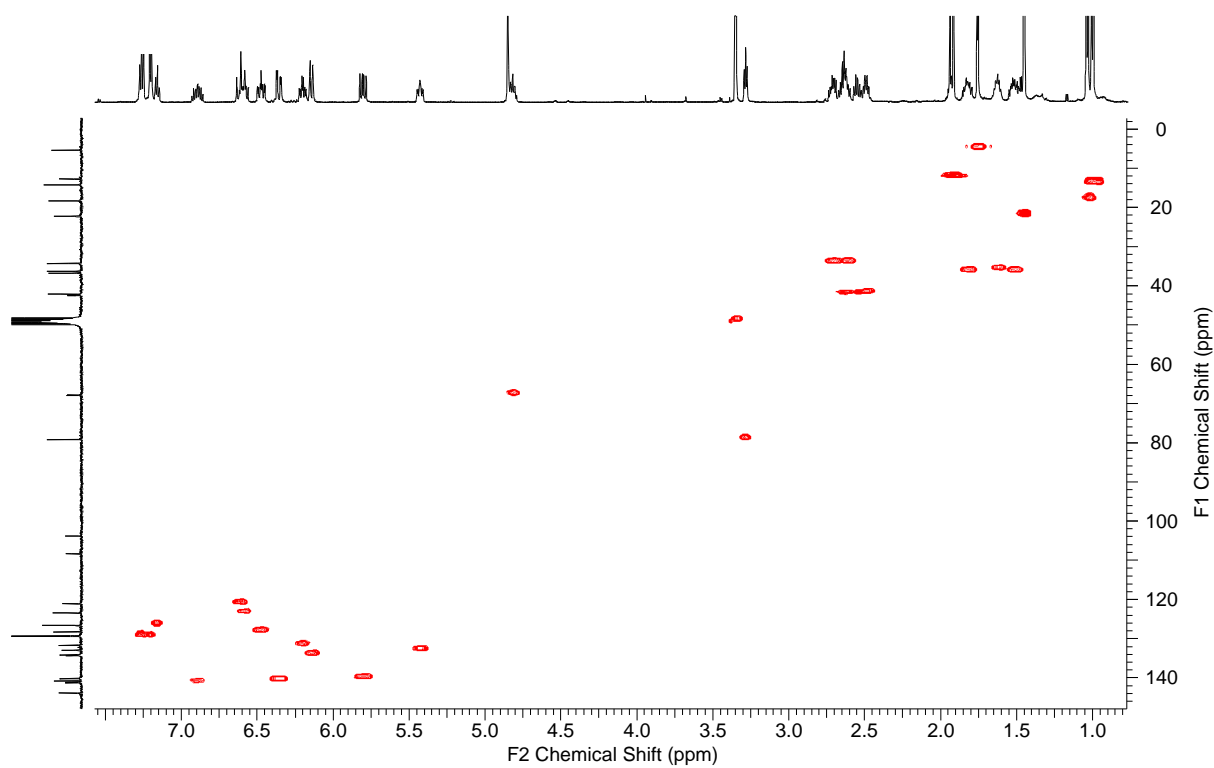
Spectrum 66: ^{1}H,^{13}C HMQC NMR spectrum of hyafurone B (**50**) (^{1}H 600 MHz, ^{13}C 150 MHz, CD$_3$OD).
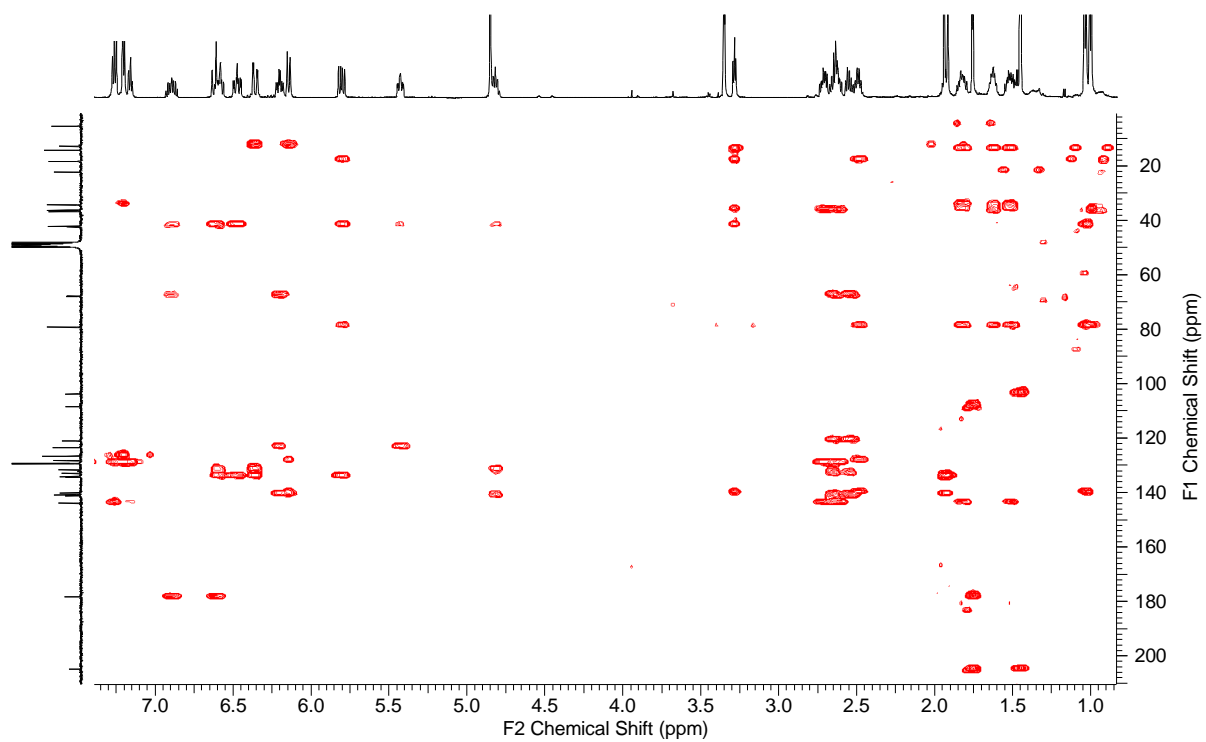
Spectrum 67: ^{1}H,^{13}C HMBC NMR spectrum of hyafurone B (**50**) (^{1}H 600 MHz, ^{13}C 150 MHz, CD$_3$OD).

6.4.4 Spectra of hyapyrone A
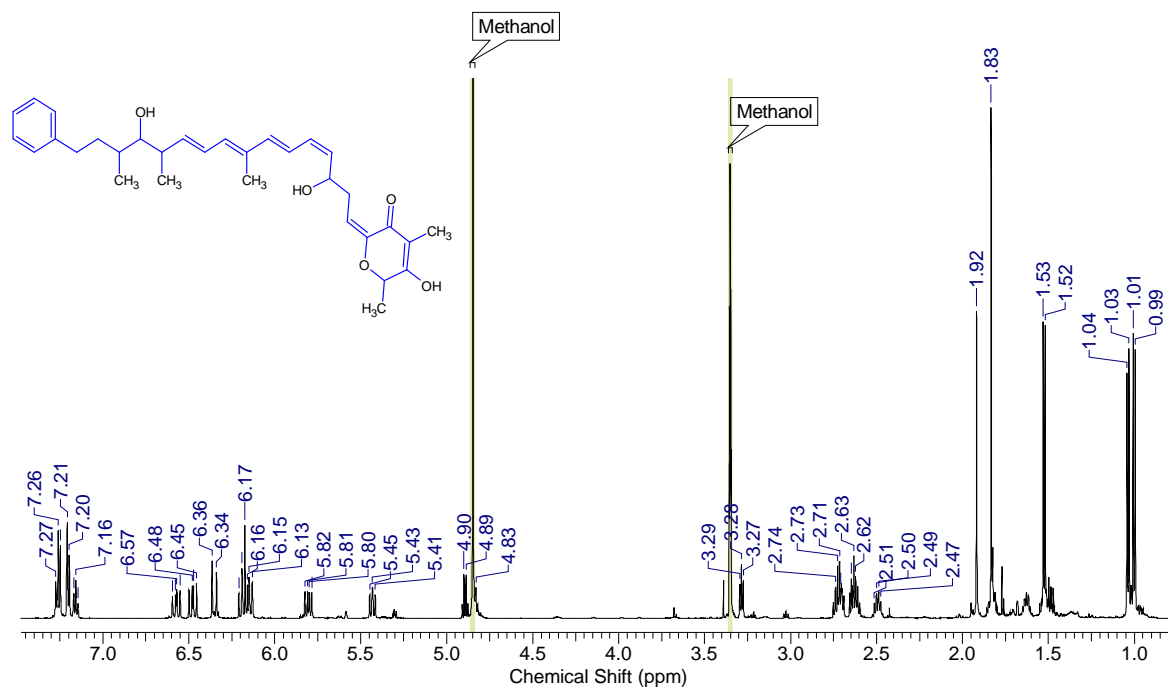
Spectrum 68: ^{1}H NMR spectrum of hyapyrone A (**51**) (^{1}H 600 MHz, CD$_3$OD).
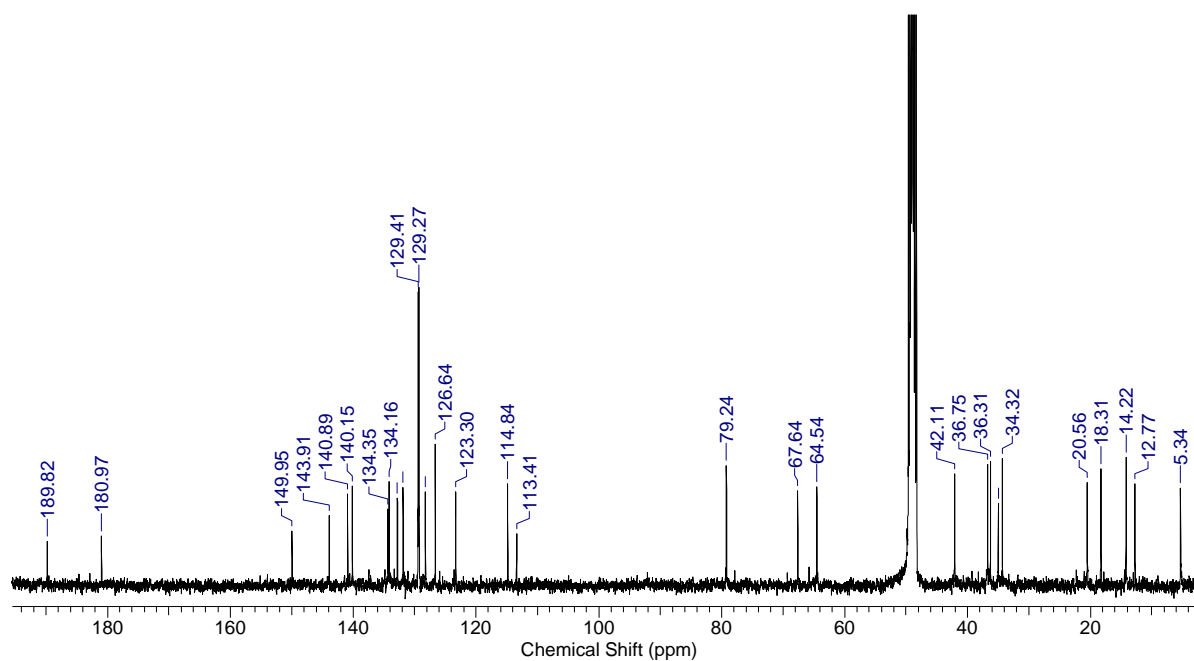
Spectrum 69: ^{13}C NMR spectrum of hyapyrone A (**51**) (^{13}C 150 MHz, CD$_3$OD).

147
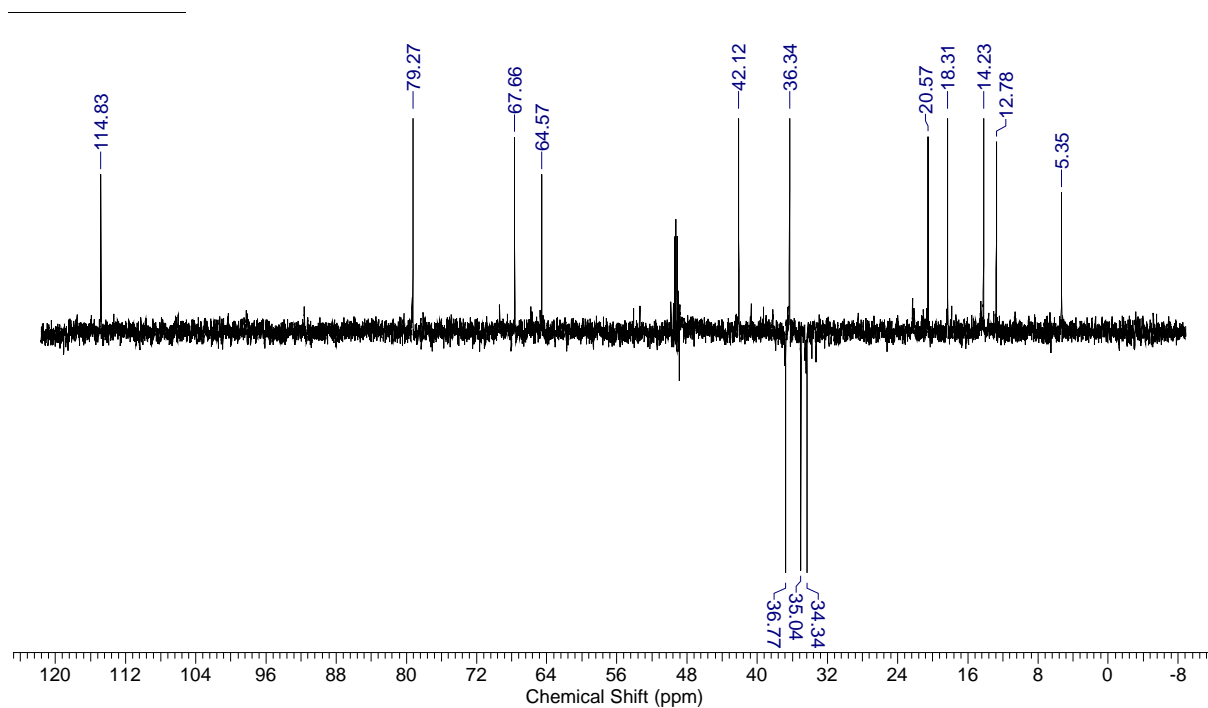
Spectrum 70: ^{13}C DEPT NMR spectrum of hyapyrone A (**51**) (^{13}C 150 MHz, CD$_3$OD).
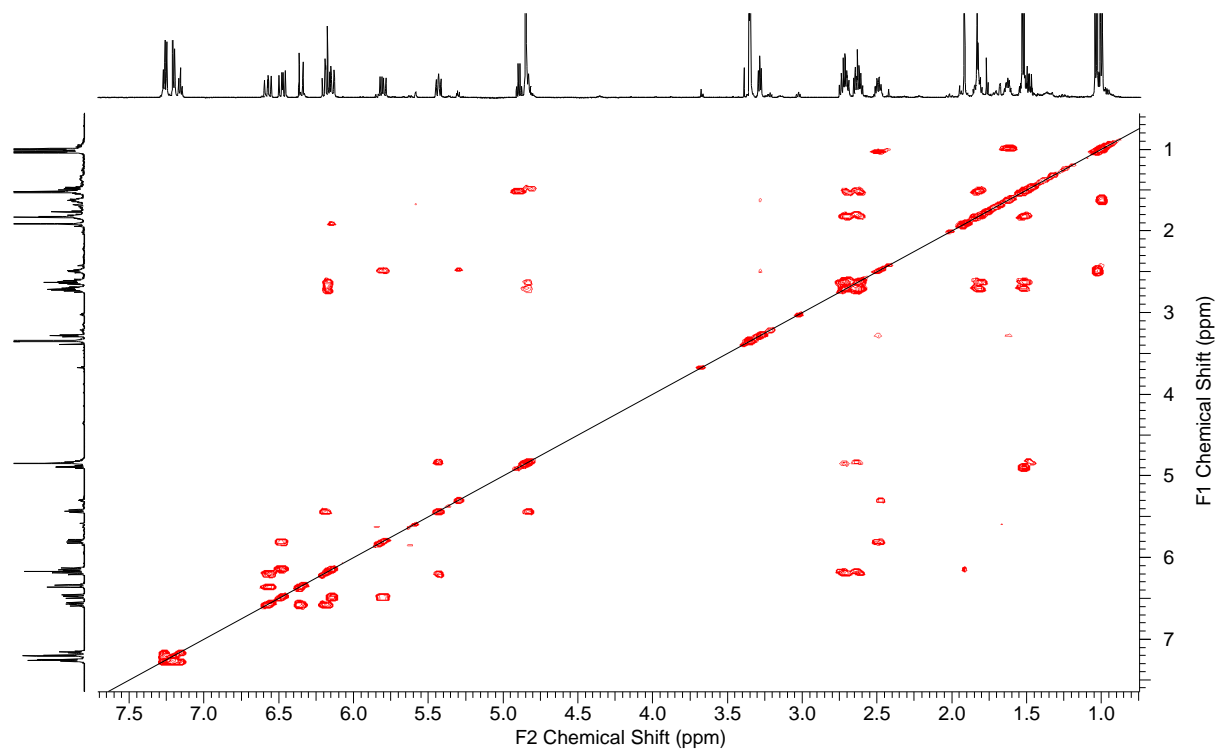
Spectrum 71: ^{1}H,^{1}H COSY NMR spectrum of hyapyrone A(**51**) (^{1}H 600 MHz, CD$_3$OD).
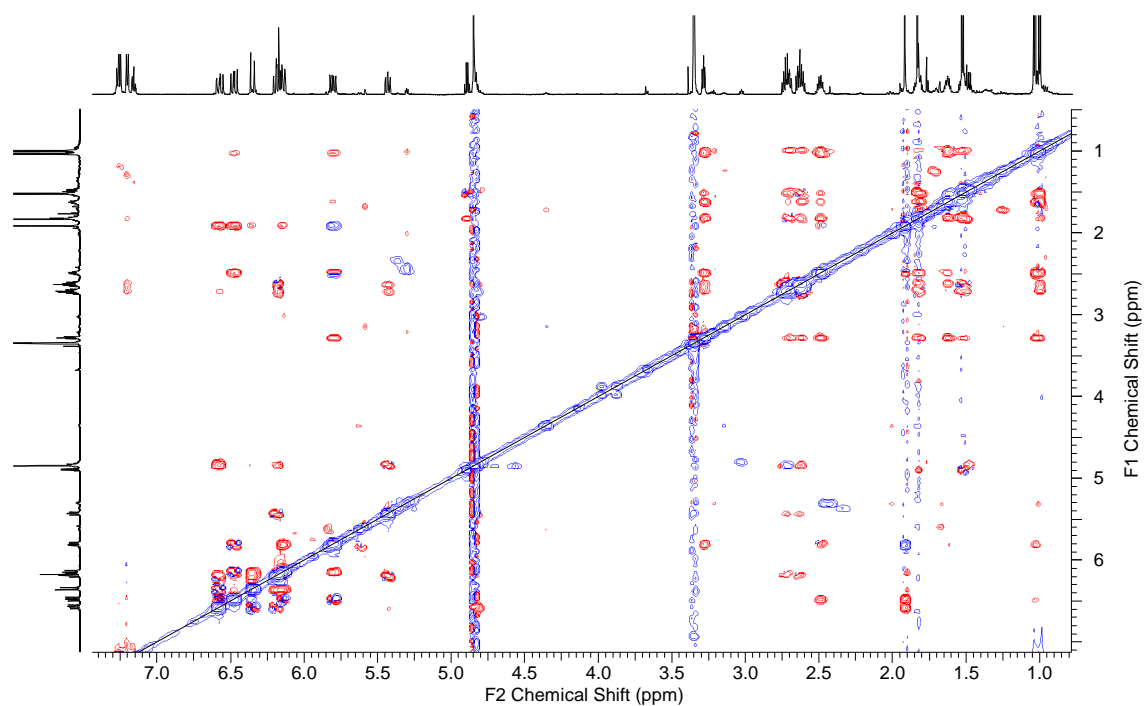
Spectrum 72: ^{1}H,^{1}H ROESY NMR spectrum of hyapyrone A (**51**) (^{1}H 600 MHz, CD$_3$OD).
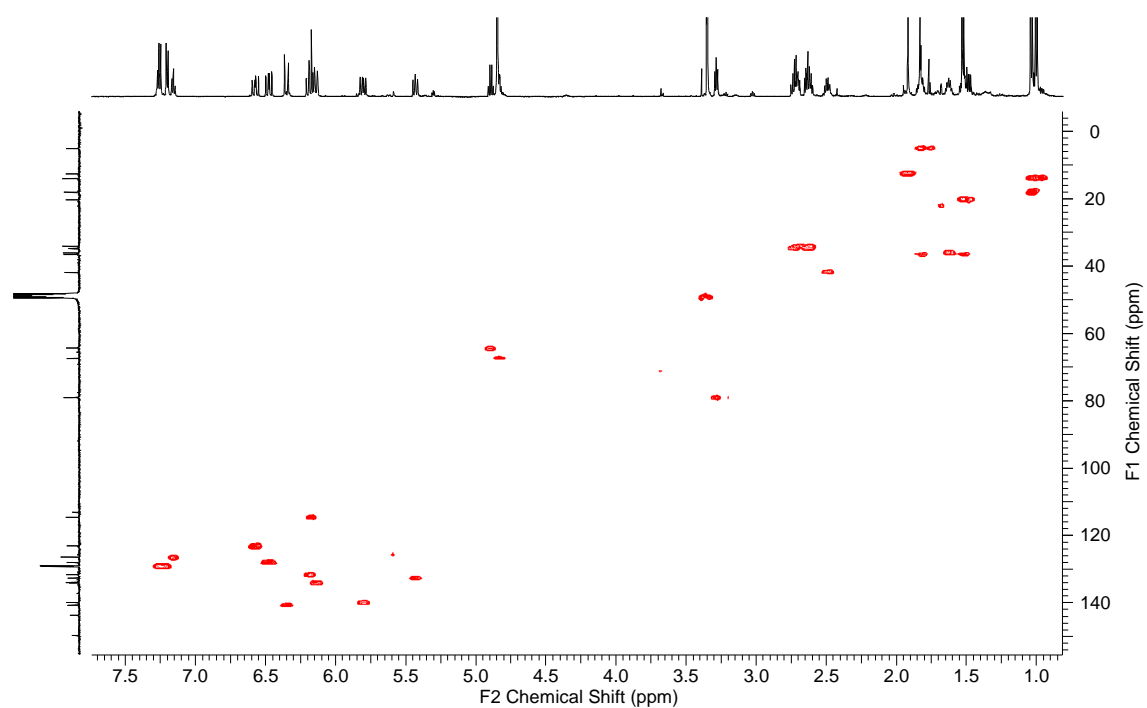
Spectrum 73: ^{1}H,^{13}C HMQC NMR spectrum of hyapyrone A (**51**) (^{1}H 600 MHz, ^{13}C 150MHz, CD$_3$OD).
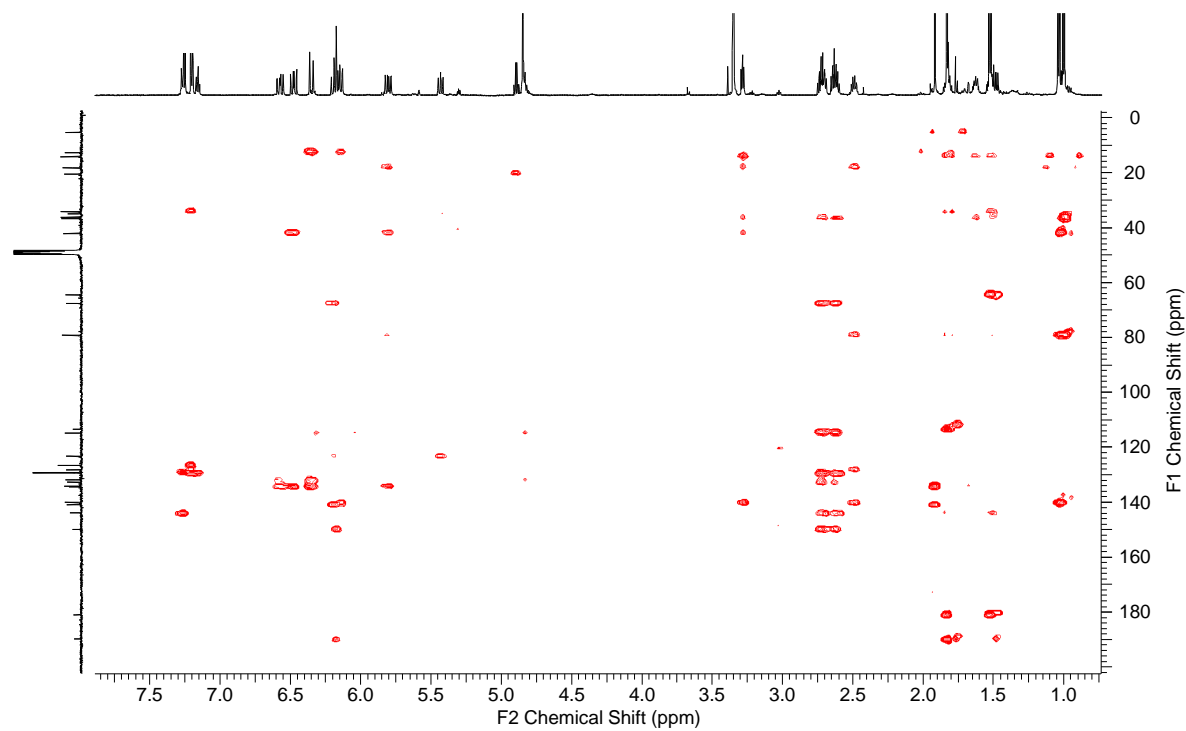
Spectrum 74: ^{1}H,^{13}C HMBC NMR spectrum of hyapyrone A (**51**) (^{1}H 600 MHz, ^{13}C 150 MHz, CD$_3$OD).

6.4.5 Spectra of hyafurone C (52)
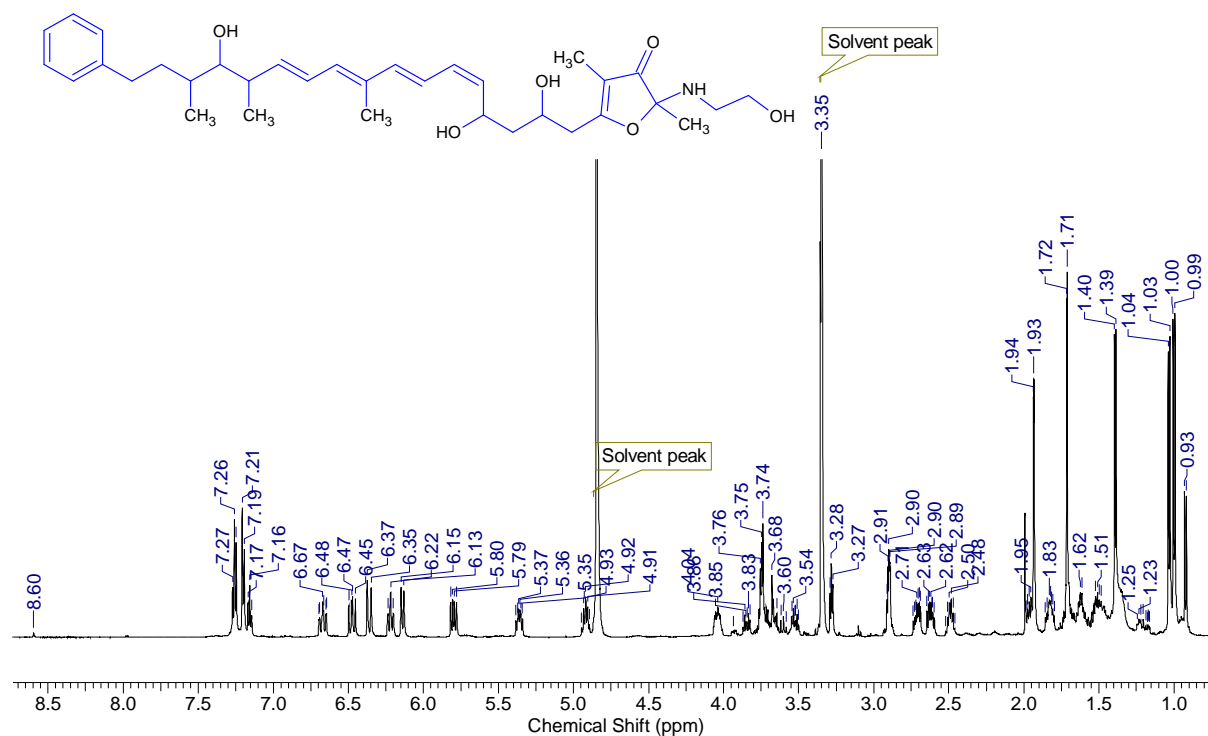
Spectrum 75: ^{1}H NMR spectrum of hyafurone C (**52**) (^{1}H 600 MHz, CD$_3$OD).
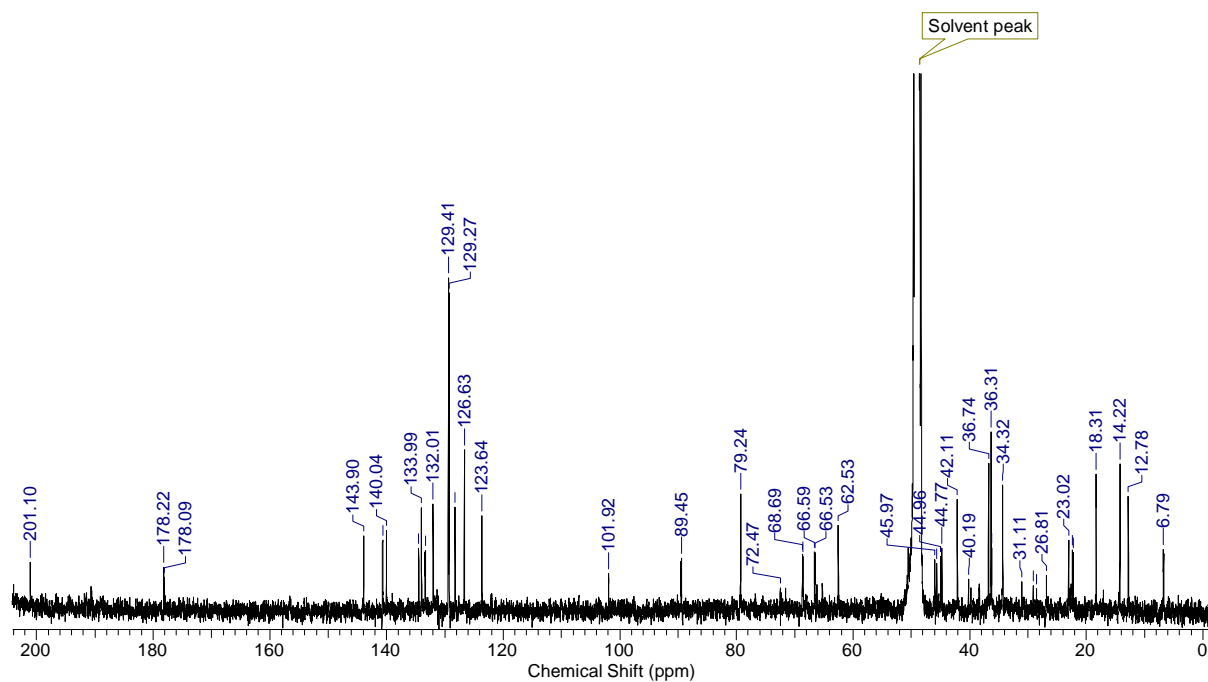
Spectrum 76: ^{13}C NMR spectrum of hyafurone C (**52**) (^{13}C 150 MHz, CD$_3$OD).
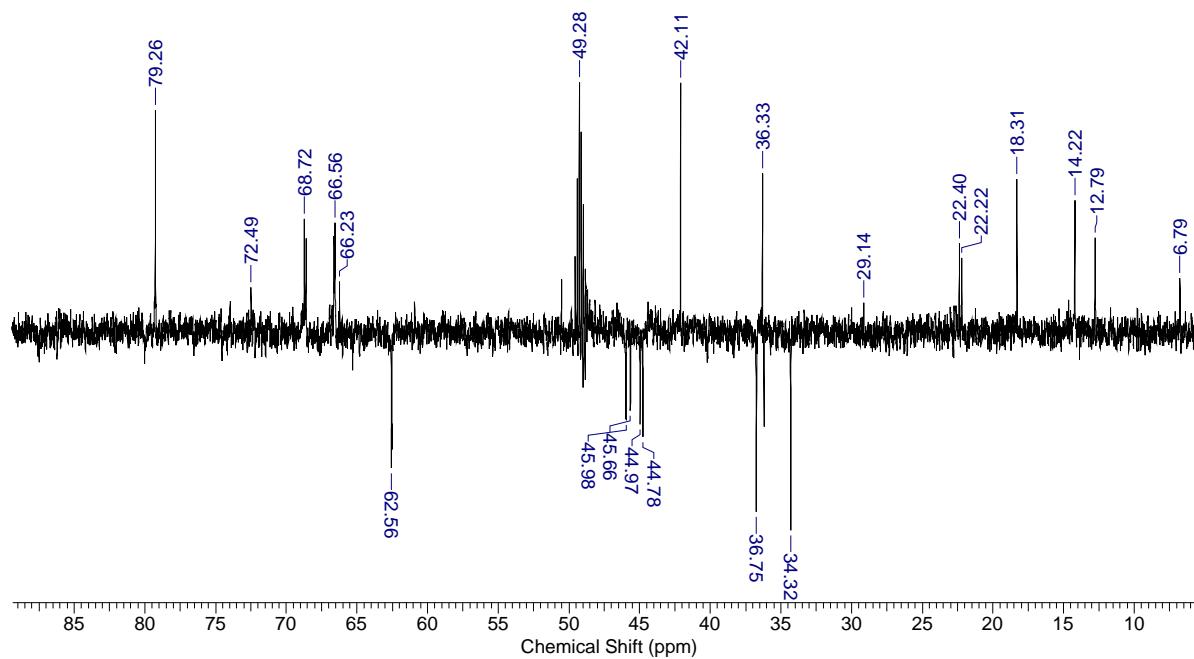
Spectrum 77: ^{13}C DEPT NMR spectrum of hyafurone C (**52**) (^{13}C 150 MHz, CD$_3$OD).
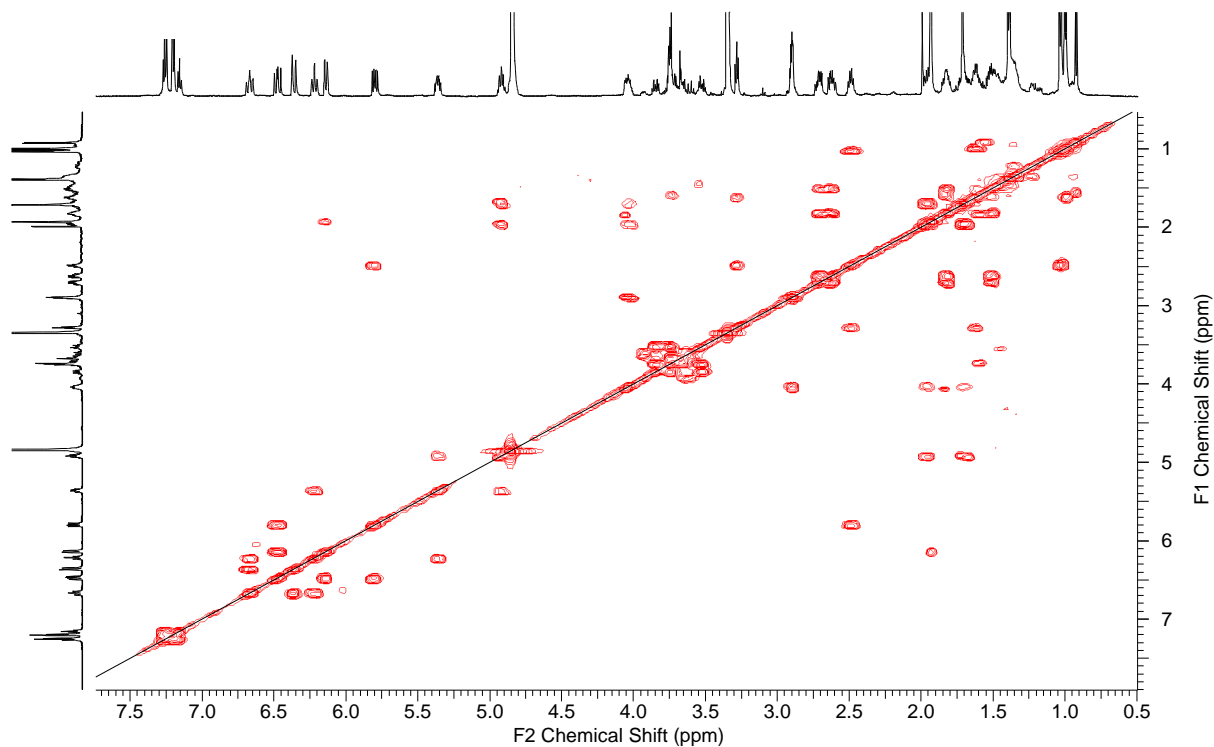
Spectrum 78: $^1H,^1H$ COSY NMR spectrum of hyafurone C (**52**) (^1H 600 MHz, CD$_3$OD).
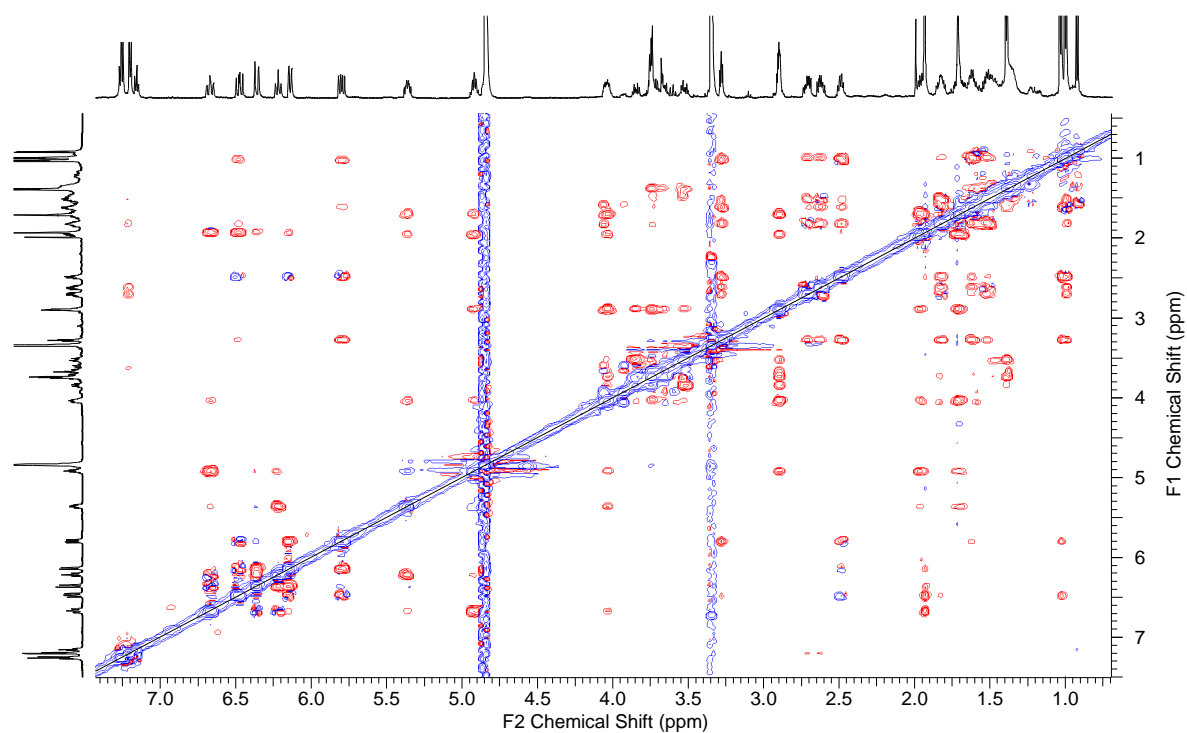
Spectrum 79: ^{1}H,^{1}H ROESY spectrum of hyafurone C (**52**) (^{1}H 600 MHz, CD$_3$OD).
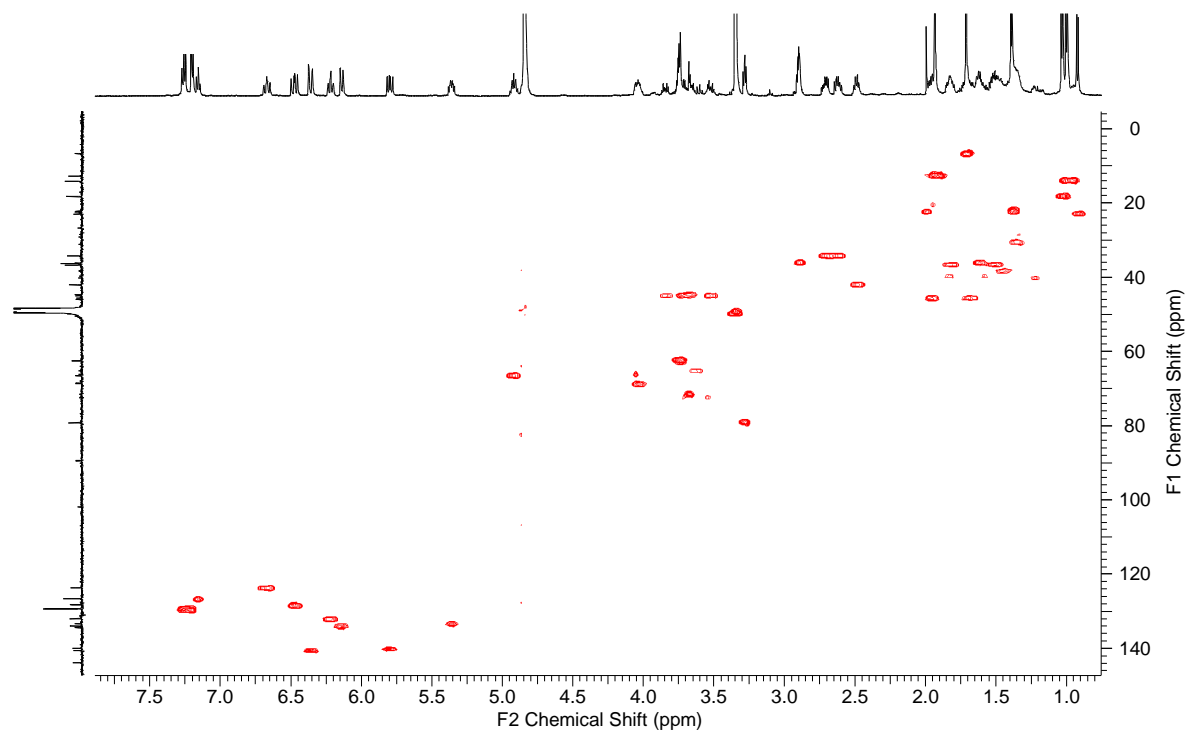
Spectrum 80: ^{1}H,^{13}C HMQC NMR spectrum of hyafurone C (**52**) (^{1}H 600 MHz, ^{13}C 150 MHz, CD$_3$OD).
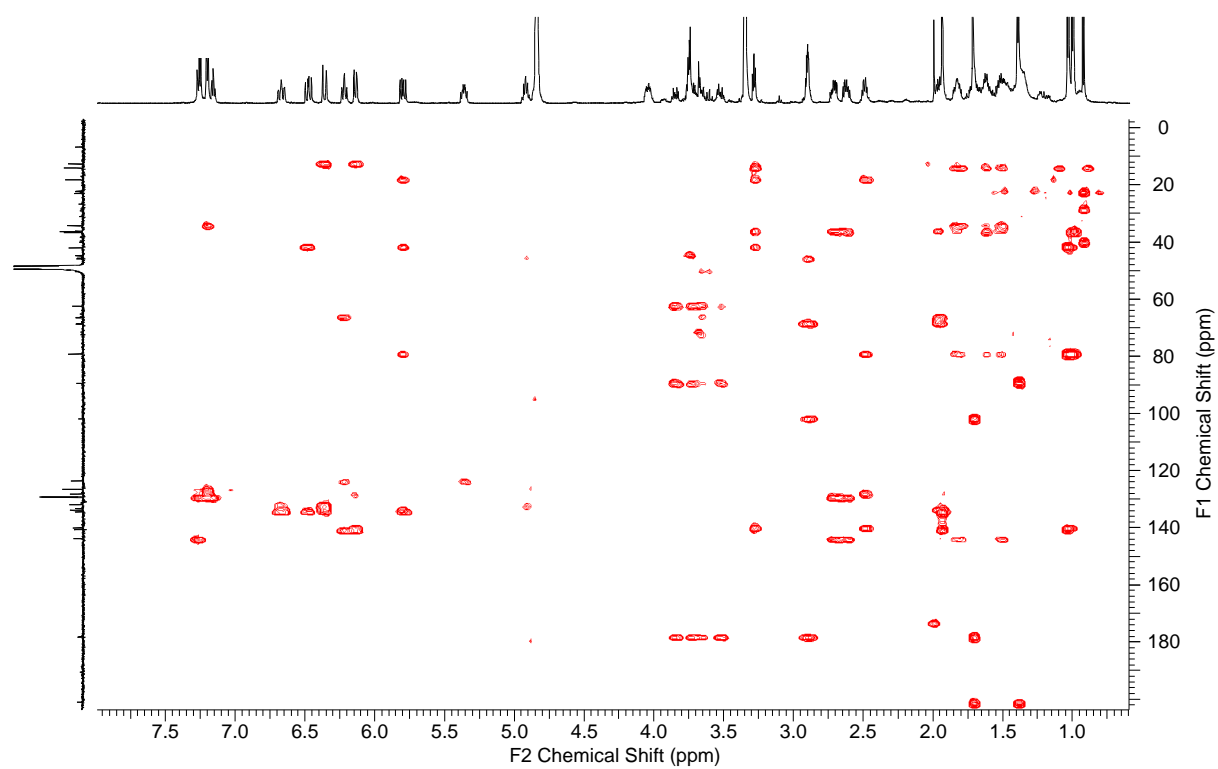
Spectrum 81: ^{1}H,^{13}C HMBC NMR spectrum of hyafurone C (**52**) (^{1}H 600 MHz, ^{13}C 150 MHz, CD$_3$OD).

6.4.6 Spectra of hyafurone D (53)
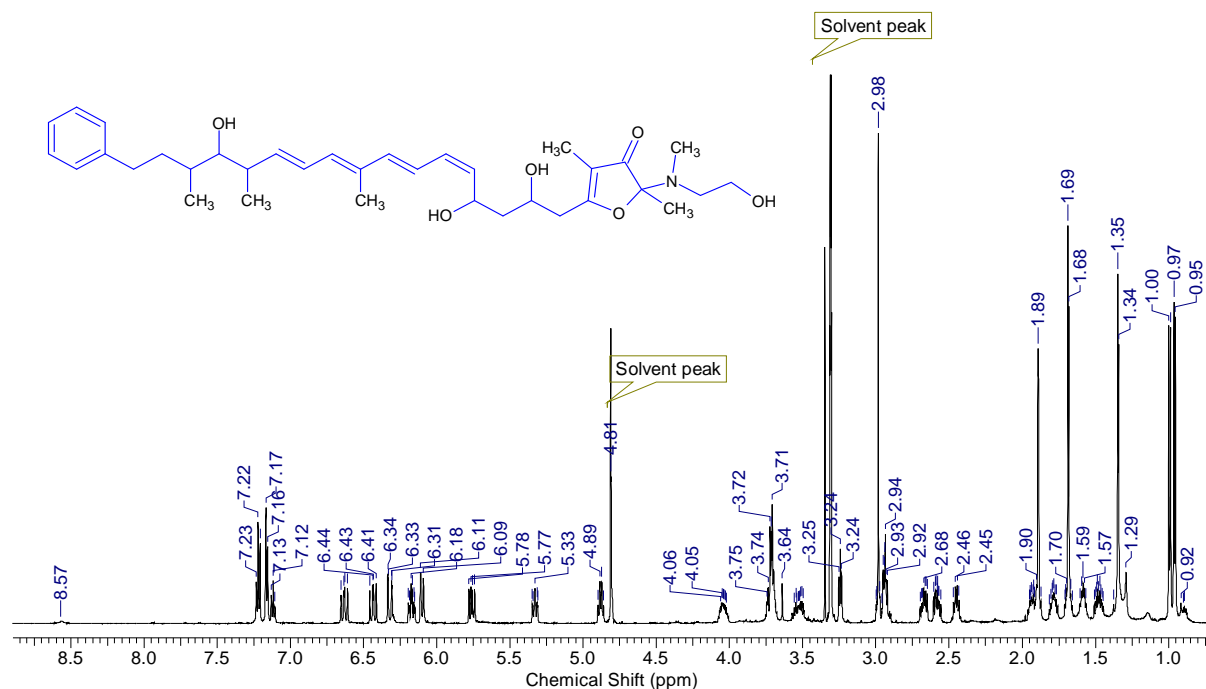
Spectrum 82: ^{1}H NMR spectrum of hyafurone D (**53**) (^{1}H 600 MHz, CD$_3$OD).
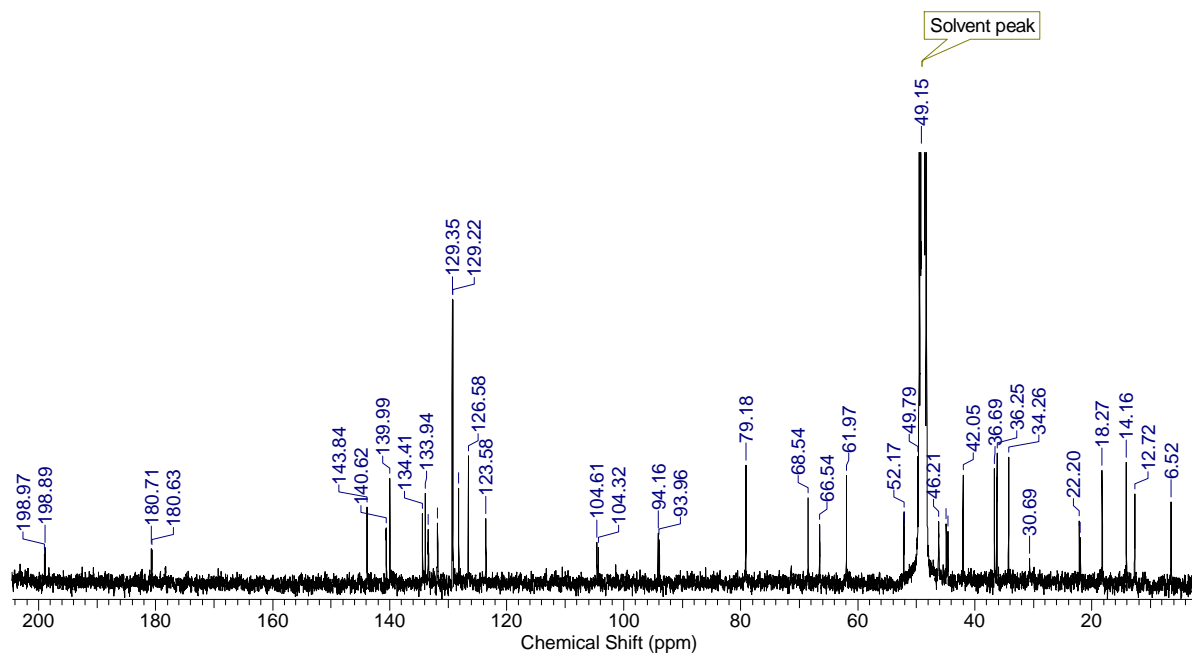
Spectrum 83: ^{13}C NMR spectrum of hyafurone D (**53**) (^{13}C 150 MHz, CD$_3$OD).
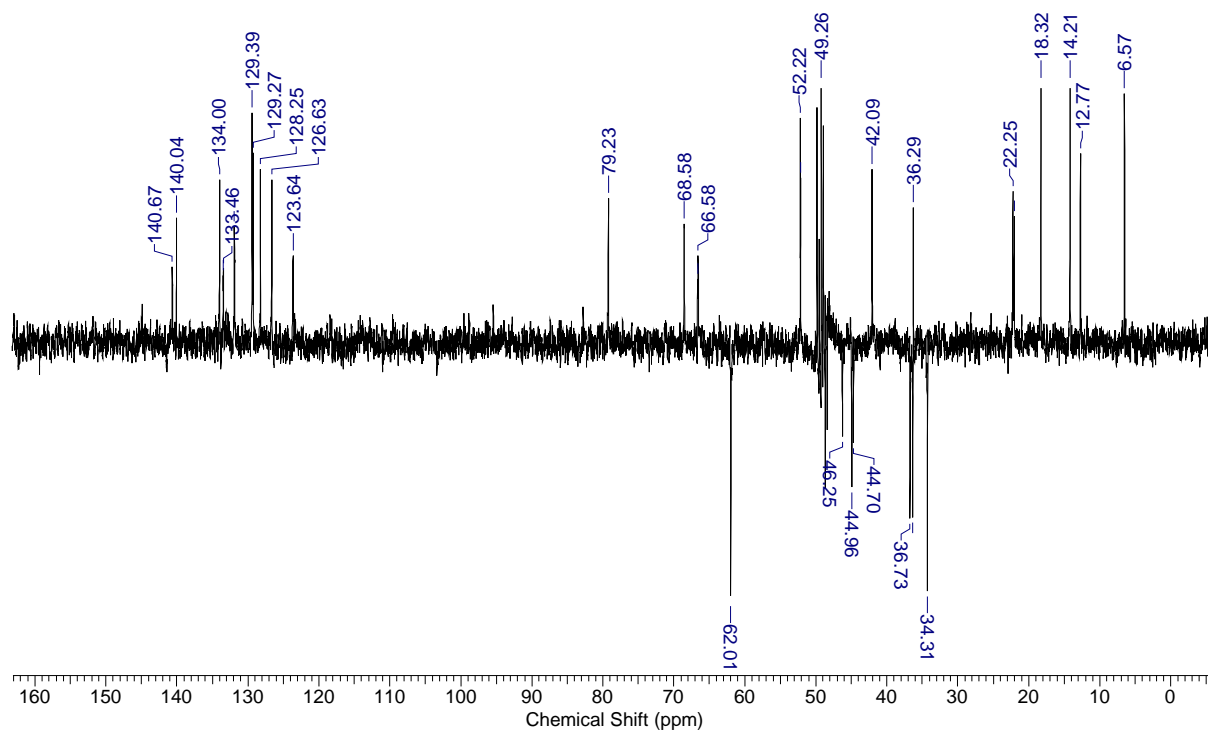
Spectrum 84: ^{13}C DEPT NMR spectrum of hyafurone D (**53**) (^{13}C 150 MHz, CD$_3$OD).
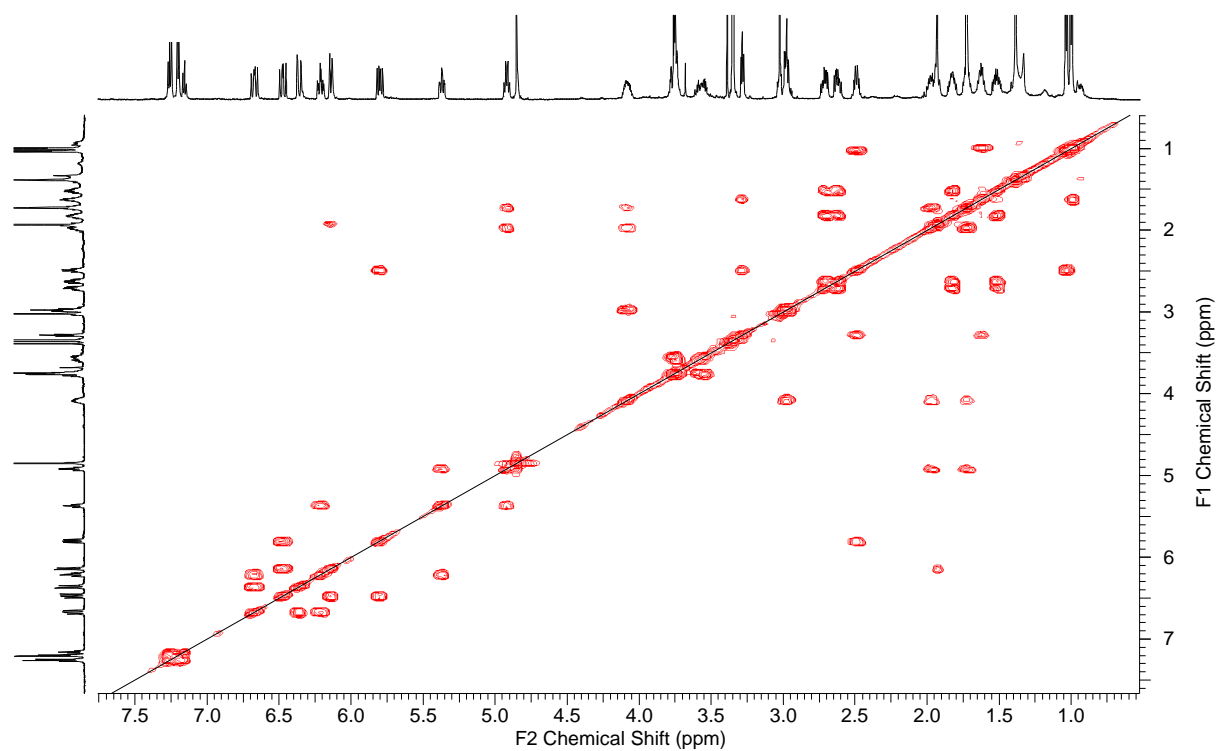
Spectrum 85: COSY NMR spectrum of hyafurone D (**53**) (^1H 600 MHz, CD$_3$OD).
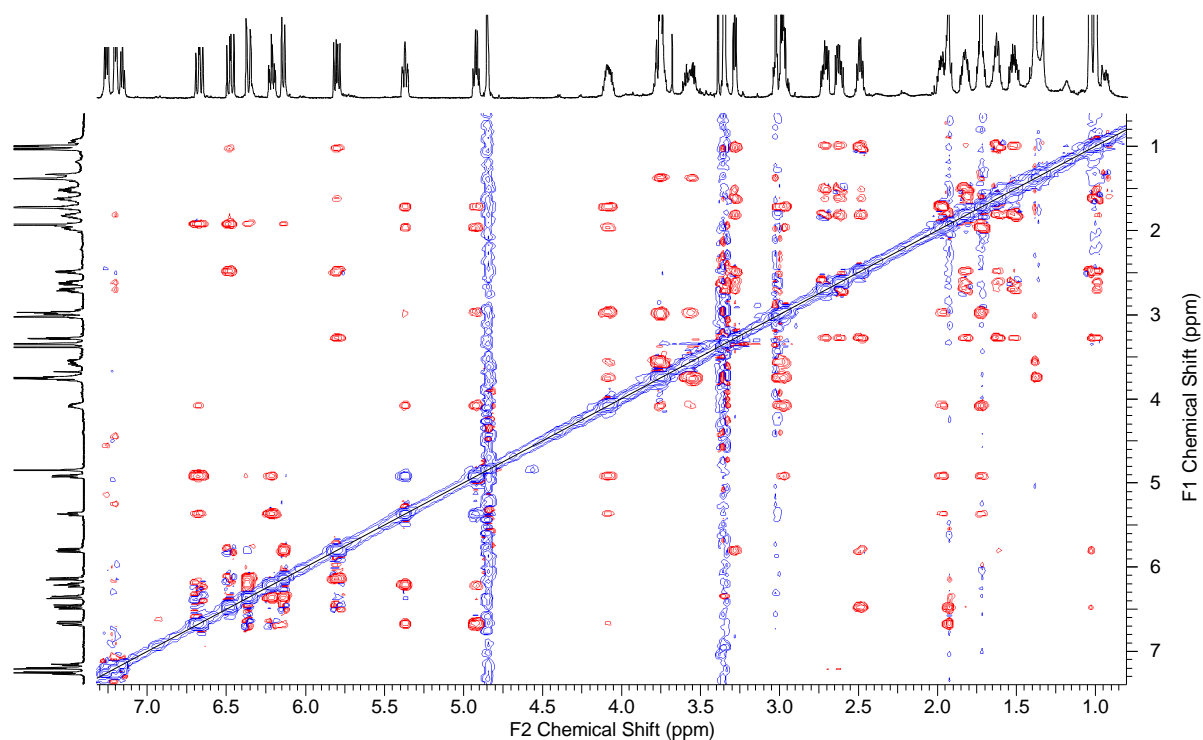
Spectrum 86: ^{1}H,^{1}H ROESY NMR spectrum of hyafurone D (**53**) (^{1}H 600 MHz, CD$_3$OD).
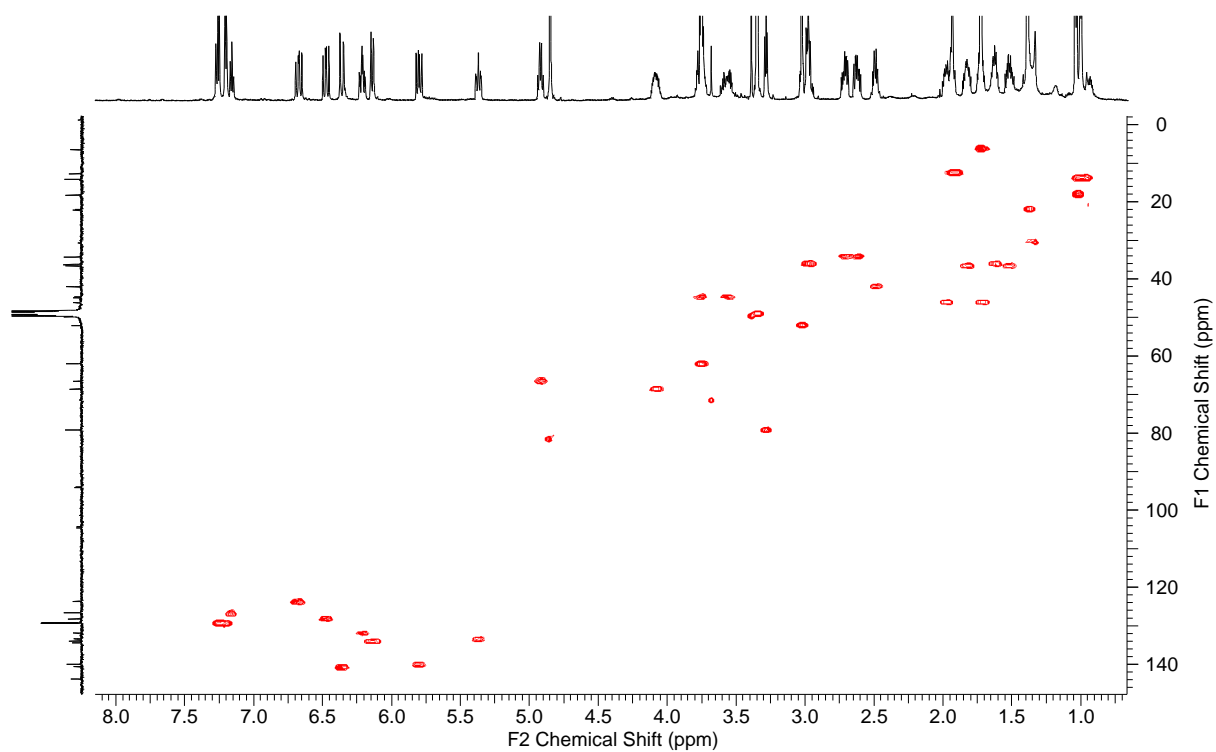
Spectrum 87: ^{1}H,^{13}C HMQC NMR spectrum of hyafurone D (**53**) (^{1}H 600 MHz, ^{13}C 150 MHz, CD$_3$OD).
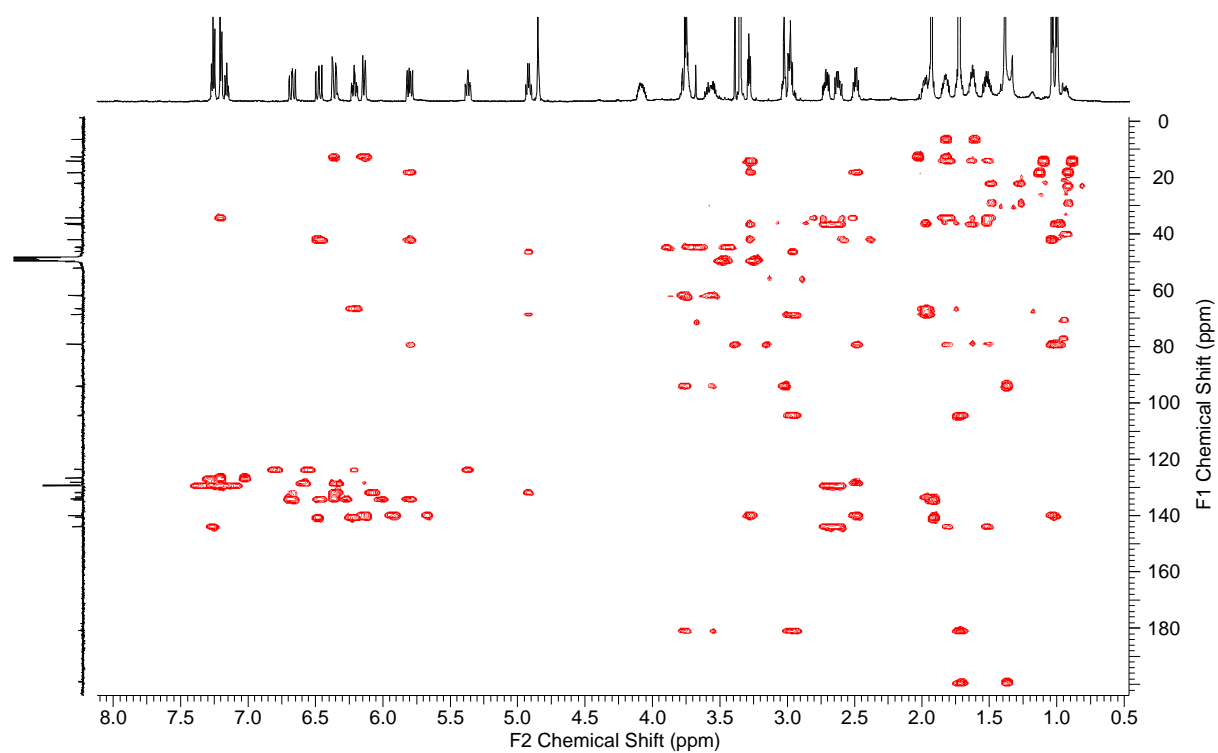
Spectrum 88: ^{1}H,^{13}C HMBC NMR spectrum of hyafurone D (**53**) (^{1}H 600 MHz, ^{13}C 150 MHz, CD$_3$OD).

6.4.7 Spectra of hyapyrone B (54)
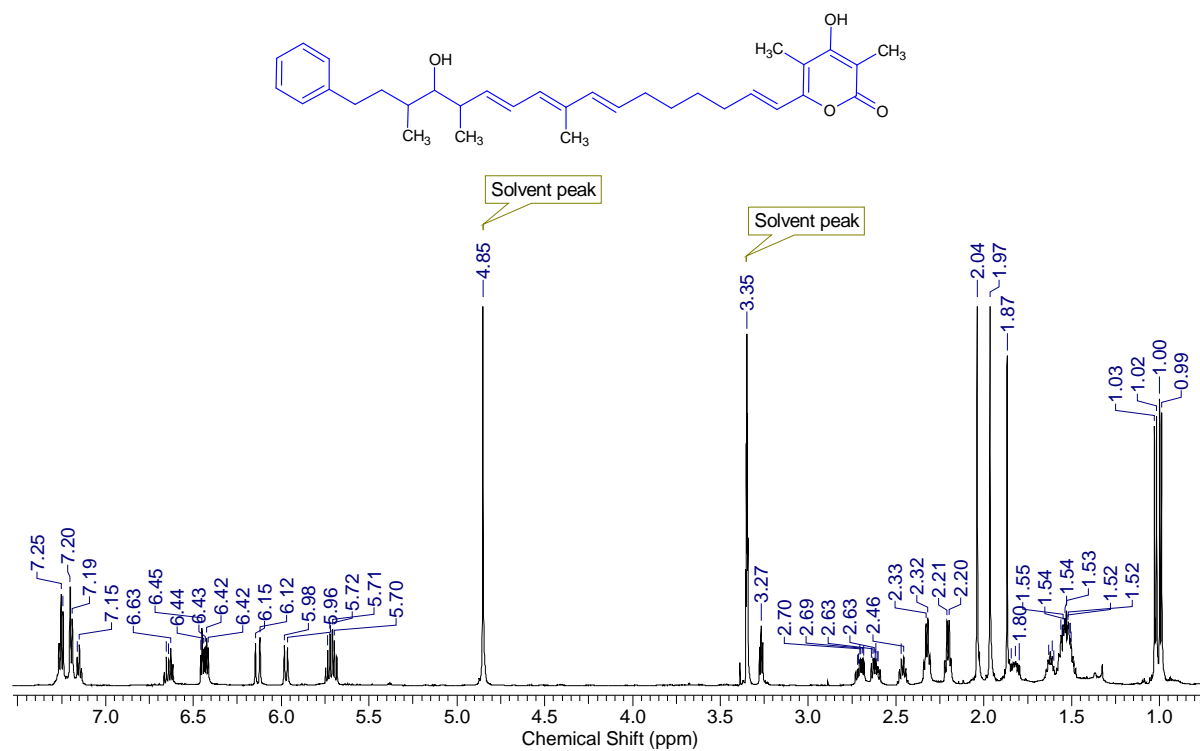
Spectrum 89: ^{1}H NMR spectrum of hyapyrone B (**54**) (^{1}H 600 MHz, CD$_3$OD).
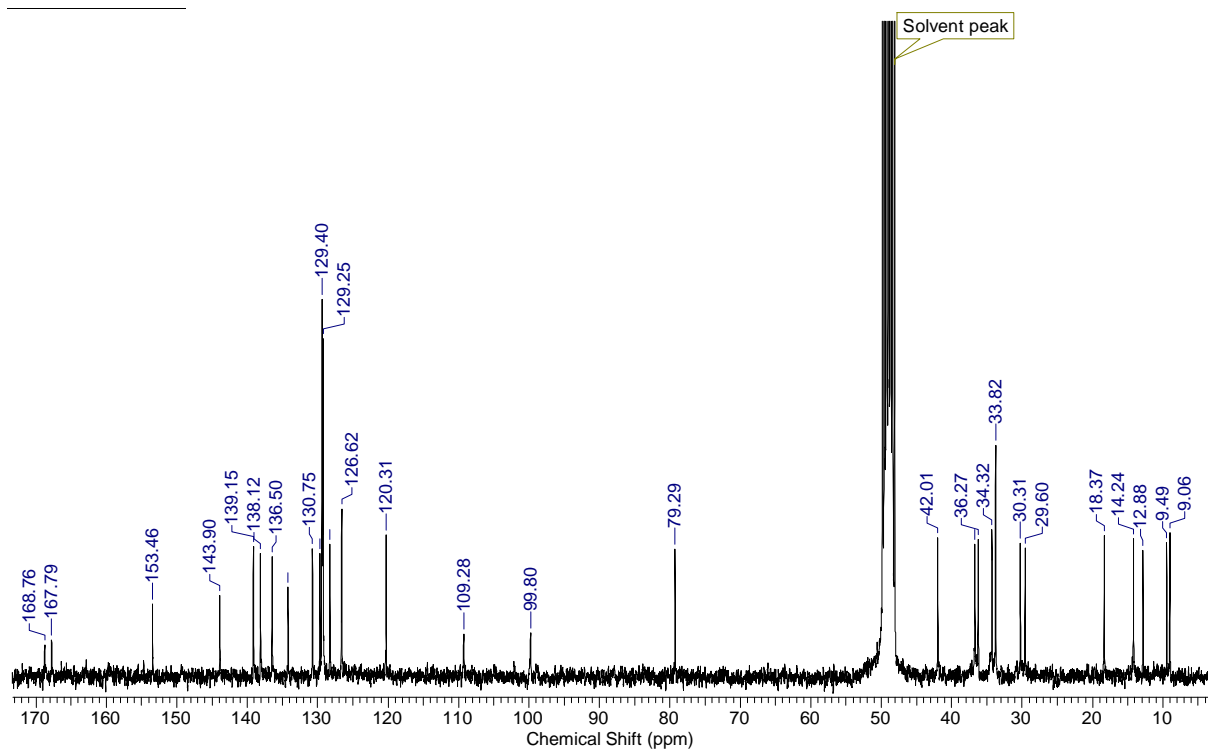
Spectrum 90: ^{13}C NMR spectrum of hyapyrone B (**54**) (^{13}C 150 MHz, CD$_3$OD).
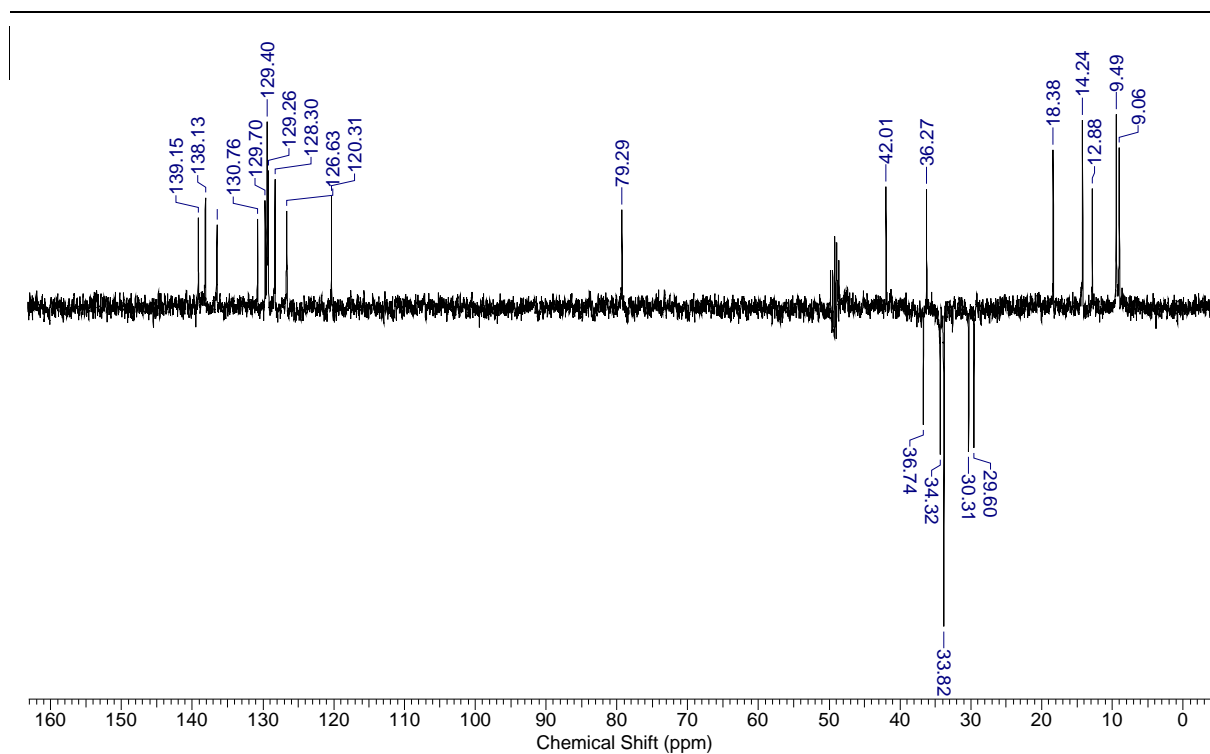
Spectrum 91: ^{13}C DEPT NMR spectrum of hyapyrone B (**54**) (^{13}C 150 MHz, CD$_3$OD).
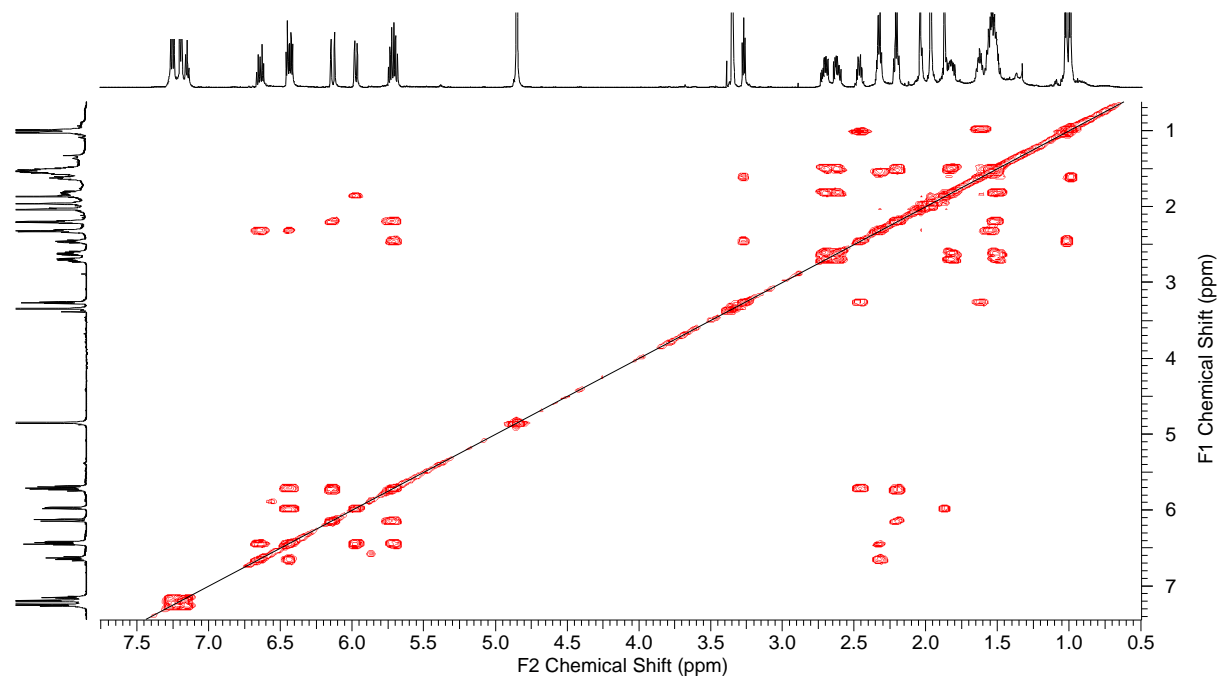
Spectrum 92: ^{1}H,^{1}H COSY NMR spectrum of hyapyrone B (**54**) (^{1}H 600 MHz, CD$_3$OD).
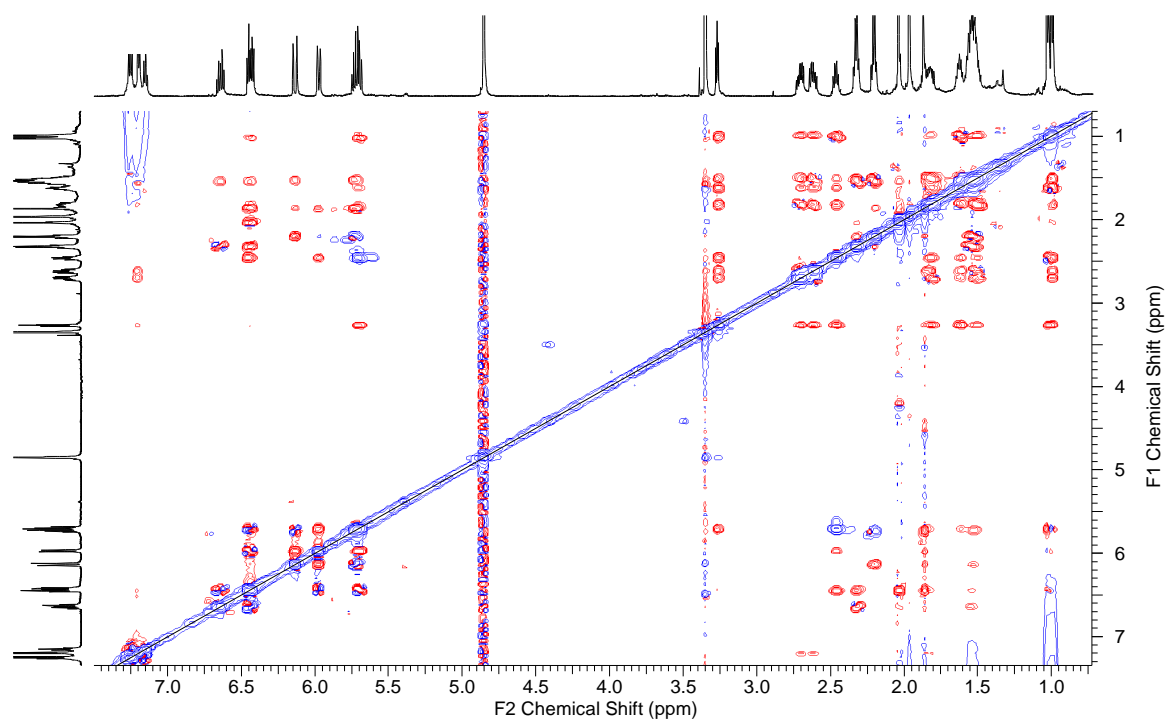
Spectrum 93: ^{1}H,^{1}H ROESY NMR spectrum of hyapyrone B (**54**) (^{1}H 600 MHz, CD$_3$OD).
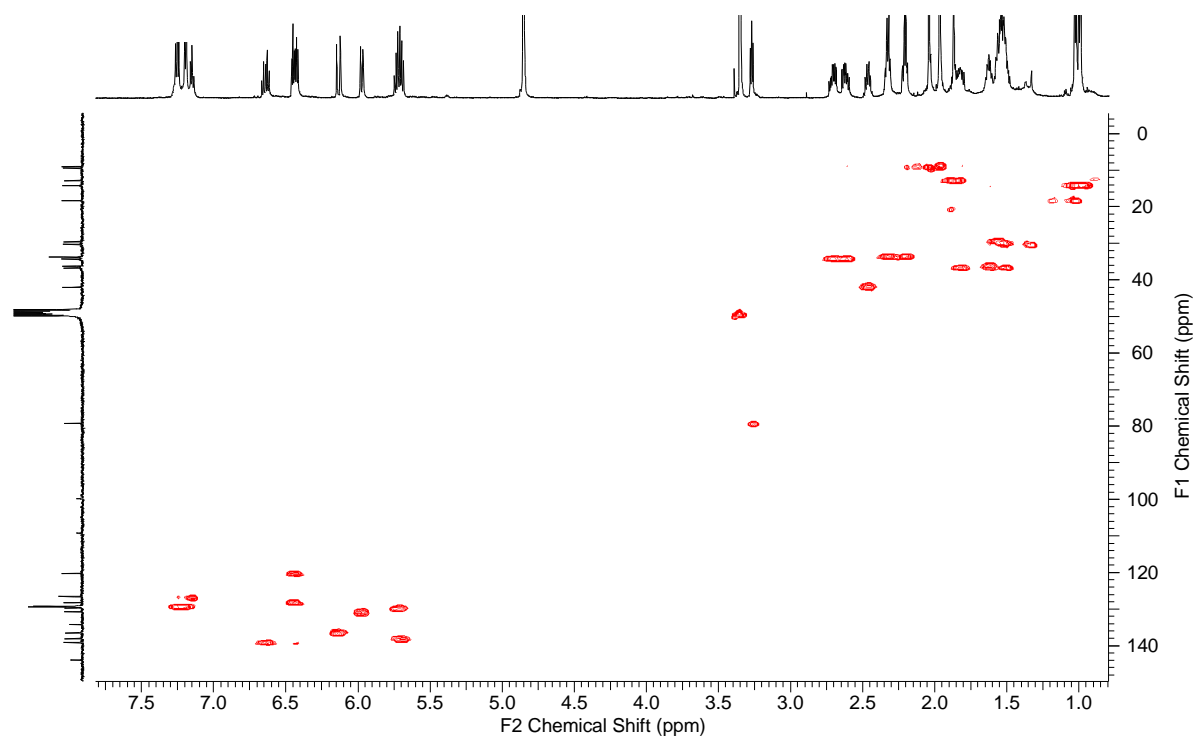
Spectrum 94: ^{1}H,^{13}C HMQC NMR spectrum of hyapyrone B (**54**) (^{1}H 600 MHz, ^{13}C 150 MHz, CD$_3$OD).
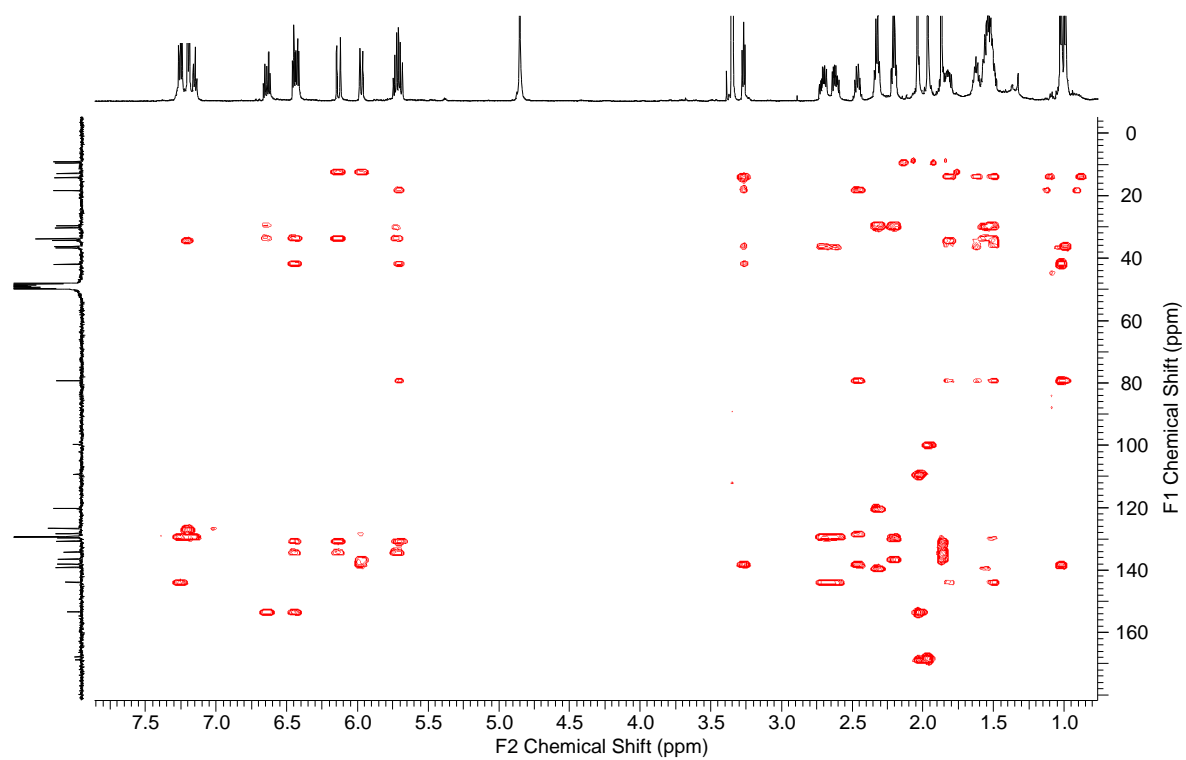
Spectrum 95: ^{1}H,^{13}C HMBC NMR spectrum of hyapyrone B (**54**) (^{1}H 600 MHz,^{13}C 150 MHz, CD$_3$OD).